

A COMPUTER BASED TREND SURFACE STUDY OF STRUCTURAL ANALYSIS: TEST CASE FROM LIPSON COVE, SOUTH AUSTRALIA

Vol. I

bу

Peter Haddon Cohen, B.Sc (Hons)

Department of Geology and Mineralogy
University of Adelaide

November, 1983

A Thesis submitted for the

Degree of Doctor of Philosophy

AMARDED 17th JUNE, 1986

TABLE OF CONTENTS

VOLUME I

	Page
TARLE OF CONTENTS	11
TABLE OF CONTENTS	ix
LIST OF TABLES	x
SUMMARY STATEMENT OF ORIGINALITY	xii
ACKNOWLEDGEMENTS	xiii
ACKNOWLEDGE-IEN 13	
CHAPTER 1 INTRODUCTION	
1.1 CLASSIFICATION OF STRUCTURAL GEOMETRY	1.1
1.1.1 Structural Geometry in Geometric Analysis	1.1
1.1.2 Classifying Fold Geometry in Fold Style	1.1
1.1.3 Limitations	1.2
1.2 A GENERAL CLASSIFICATION PROCEDURE	1.3
1.2.1 Trend Surface Analysis	1.4
1.2.1.1 Historical Usage	1.4
1.2.1.2 Problems	1.4
1.2.2 Statement of Aim 1	1.6
1.3 A GENERAL PURPOSE COMPUTER PACKAGE	1.6
1.3.1 Computer Technology in Structural Geology	1.6
1.3.2 Existing Computer Programs	1.7
1.3.2.1 Data Banks	1.7
1.3.2.2 Cartography	1.7
1.3.2.3 Spherical Projections	1.8
1.3.2.4 Structure Maps	1.9
1.3.2.5 Fold Classification	1.9
1.3.2.6 Microfabric Analysis	1.9
1.3.3 Graphical Displays	1.10
1.3.4 Statement of Aim 2	1.11
1.4 APPLICABILITY OF COMPUTER CLASSIFICATION	1.13
1.5 TERMINOLOGY	1.11
1.5.1 Geological	1.11
1.5.2 Computational and Mathematical	1.12
CHAPTER 2 SPATIAL ORIENTATION DISTRIBUTION ANALYSIS	
2.1 INTRODUCTION	2.1
2.1.1 Type I Trend Surfaces	2.1
2.1.2 Type II Trend Surfaces	2.2
2.2 PROPERTIES OF SPATIALLY DISTRIBUTED ORIENTATION DATA	2.2
2.2.1 Strike-lines and Isoclines	2.2

	2.2.2 The Formulation of New Properties for S.O.D.A.	2.3
	2.2.2.1 Orientation Values On A Single Surface	2.3
	2.2.2.2 Orientation Values in a Solid Body	2.4
	2.2.2.3 Rotated Planes of Reference	2.4
	2.2.2.4 Contour Nomenclature and Values	2.5
	2.2.2.5 Contours On Stereonets	2.5
	2.2.2.6 Use of Dip Vectors and Poles	2.6
	2.2.2.7 Density of Contours on a Profile Plane	2.7
	2.2.2.8 Radial Density of Contours	2.8
	2.2.2.9 A Description of Cylindricity	2.8
	2.2.2.10 Contours On Map Projections	2.8
	2.2.2.11 Behaviour of Contours	
	During Change in Geometry	2.9
2.3	TREND SURFACES	2.10
	2.3.1 Introduction	2.10
	2.3.2 Planar Surfaces	2.11
	2.3.3 Cylindrical Folds	2.11
	2.3.3.1 Upright Horizontal Rounded Folds	2.11
	2.3.3.2 Angular (Chevron or Kink) Folds	2.11
	2.3.3.3 Upright Rotated Folds	2.12
	2.3.3.4 Reclined Horizontal Folds	2.12
	2.3.3.5 Folds of any Other Orientation	2.13
	2.3.3.6 Fold Classification	2.13
	2.3.3.7 Transections Through Folds	2.14
	2.3.4 Non-cylindrical Folds	2.14
	2.3.4.1 Conical Folds	2.14
	2.3.4.2 Spheroidal Domes	2.15
	2.3.4.3 Ellipsoidal Domes	2.16
2.4	COMBINED GEOMETRIES	2.18
2.5		2.18
	DETECTION OF GEOLOGICAL DISCONTINUITIES	2.19
2.7	APPLICATION OF CONTOUR ANALYSIS TO REAL FOLDS	2.19
	2.7.1 <u>Introduction</u>	2.19
	2.7.2 Technique	2.20
	2.7.3 Unoriented Sample of a Conical Fold	2.21
	2.7.4 Orientated Specimen of an	2.22
	Approximately Cylindrical Fold	2.22
2.8	DISCUSSION	2.22

CHAPTER 3	A COMPREHENSIVE COMPUTER PACKAGE FOR	
	SPATIAL ORIENTATION DISTRIBUTION ANALYSIS (S.O.D.A.)	2.1
3.1	INTRODUCTION	3.1
3.2	PROCESSING SYSTEMS	3.2
	3.2.1 The Ideal System	3.2
	3.2.2 The S.O.D.A. System	3.3
3-3	3 COMPUTER EQUIPMENT	3.3
	3.3.1 Hewlett-Packard	3.3
	3.3.2 <u>Cyber</u>	3.3
	3.3.3 <u>Nova</u>	3.3
	3.3.3.1 Hardware	3.3
	3.3.3.2 Programming Raster Scan Displays	3.4
3.	4 DATA PREPARATION	3.5
	3.4.1 <u>Introduction</u>	3.5 3.6
	3.4.2 Field Data	
	3.4.3 Universal Stage Data	3.6
77	3.4.3.1 Single Axes	3.6
	3.4.3.2 Multiple Axes	3.6
	3.4.4 <u>Discussion</u>	3.6
3.		3.6
3•	6 STANDARD ANALYSIS PROGRAMS	3.7
3.	7 TYPE I TREND SURFACE ANALYSIS	3.7
	3.7.1 Existing Programs	3.7
	3.7.2 <u>Discussion</u>	-3.7
3.	.8 TYPE II TREND SURFACE ANALYSIS	3.8
	3.8.1 Cyber	3.8
	3.8.2 <u>Nova</u>	3.9
	3.8.2.1 Introduction	3.9
	3.8.2.2 Software	3.9
	3.8.2.3 Discussion	3.9
3	.9 DISCUSSIONS	3.10
	3.9.1 Advantages of the S.O.D.A. Technique	3.10
	3.9.2 Limitations of the S.O.D.A. Technique	3.10
	3.9.2.1 Introduction	3.10
	3.9.2.2 Equipment	3.11
	3.9.2.3 Technique	3.12
	3.9.2.4 Human Information Processing	3.12
	3.9.2.5 Overcoming Problems	3.13
3	.10 CONCLUSIONS	3.13

CHAPTER 4 GEOLOGICAL MODELS	
4.1 INTRODUCTION	4.1
4.2 CYLINDRICAL FOLDS	4.1
4.2.1 Data Generation	4.1
4.2.2 Upright Horizontal Folds	4.1
4.2.2.1 Fold Design	4.1
4.2.2.2 Display and Analysis	4.2
4.2.2.3 Discussion	4.2
4.2.3 Upright Rotated Folds	4.4
4.2.3.1 Fold Design	4.4
4.2.3.2 Display Method	4.4
4.2.3.3 Rotation of 0° (Horizontal)	4.5
4.2.3.4 Rotation of 10°	4.5
4.2.3.5 Rotation of 65°	4.5
4.2.3.6 Rotation of 90° (Vertical)	4.6
4.2.3.7 Conclusions	4.7 4.7
4.3 CLASSIFICATION OF SUBVERTICAL FOLDS	4.7
4.3.1 <u>Data Generation</u>	4.7
4.3.2 Display and Analysis	4.7
4.3.3 <u>Discussion</u>	4.8
4.4 DISLOCATIONS	4.8
4.4.1 <u>Data Generation</u>	4.8
4.4.2 <u>Display Methods</u>	4.8
4.4.3 Strike-slip Fault (Offsets)	4.8
4.4.4 Normal Fault	4.8
4.4.4.1 Change in Tightness	4.9
4.4.4.2 Change in Style	4.9
4.4.4.3 Minor Changes	4.9
4.4.4.4 Discussion	4.10
4.5 SPHERICAL DOMES	4.10
4.5.1 Data Generation	4.10
4.5.2 Display and Analysis	4.10
4.5.3 <u>Discussion</u>	4.10
4.6 PLANES	4.10
4.6.1 <u>Data Generation</u>	4.10
4.6.2 Display and Analysis	4.11
4.7 CONCLUSIONS	
CHAPTER 5 GEOLOGICAL TEST CASES	
CHALLER D GEOFOGICAT IEST CYORD	

5.1 INTRODUCTION

5.1

5	5.2	MACROSCALE	5.1
_		5.2.1 Llangedwyn-Dyffryn-Clwyd	5.1
		5.2.1.1 Display and Analysis	5.1
		5.2.1.2 Discussion	5.2
		5.2.2 Brockman Three Formation	5.3
		5.2.2.1 Domain f0	5.4
		5.2.2.2 Domain g0	5.4
		5.2.2.3 Domain h0	5.4
		5.2.2.4 Discussion on the structures	5.5
		5.2.2.5 Structural control on mineralisation	5.6
!	5.3	MESOSCALE	5.6
		5.3.1 Fold From Kanmantoo	5.6
		5.3.2 Fold From Enderby Land	5.6
	5.4	MICROSCALE	5.7
		5.4.1 Quartzite Microfabrics	5.7
		5.4.1.1 Introduction	5.7
		5.4.1.2 Random Fabrics	5.8
		5.4.1.3 Non-random Fabrics	5.8
		5.4.2 Amphibolite Microfabric	5.10
	5.5	CONCLUSIONS	5.10
CHAPTER	6 <u>I</u>	INTRODUCTION TO THE GEOLOGY OF THE LIPSON COVE AND ADJACENT	AREAS
	6.1	AIMS	6.1
	6.2	INTRODUCTION	6.1
		6.2.1 Location	6.1
		6.2.2 Topography	6.1
		6.2.3 Mapping Procedures	6.2
	6.3	LITHOLOGICAL DESCRIPTION	6.3
		6.3.1 <u>Introduction</u>	6.3
		6.3.2 Acid Gneisses	6.3
		6.3.2.1 Granitic Gneiss	
		6.3.2.2 Leucogranitic Gneiss	6.4
		6.3.3 Mafic Gneisses	6.4
		6.3.3.1 Amphibolite Gneiss	6.4
		6.3.3.2 Leucoamphibolite Gneiss	6.5
		6.3.3.3 Biotite Gneiss	6.5
		6.3.4 <u>Intrusions</u>	6.5
	6.4		6.6 6.6
		6.4.1 Tectonic History	
		6.4.2 Metamorphic Conditions	6.6

		6.4.3	Emplacement of the Lincoln Complex Rocks	6.7
	6.5	_	RAL ELEMENTS OF THE LIPSON COVE AREA	6.8
			The Lithological Layering	6.8
		6.5.2	Elements of D ₁	6.8
		6.5.3	Elements of D ₂	6.9
			Elements of D ₂	6.9
			Intersection Lineations	6.11
	6.6	STRUCTU	TRAL ANALYSIS	6.11
CHAPTER	7 G	EOMETRIC	ANALYSIS OF THE STRUCTURES OF THE LIPSON COVE AREA	
	7.1	INTRODU	CTION	7.1
		7.1.1	The Technique of Subarea Analysis	7.1
		7.1.2	Procedure Used for Applying Subarea Analysis	7.2
	7.2	A BRIE	DESCRIPTION OF THE STRUCTURES AT LIPSON COVE	7.3
	7.3	SUBMAP	M13	7.4
		7.3.1	Structural Description	7.4
		7.3.2	Subarea Analysis by the S.O.D.A. Technique	7.5
		7.3.3	Interpretation	7.7
	7.4	SUBMAP	M45	7.8
			Structural Description	7.8
		7.4.2	Subarea Analysis by the S.O.D.A. Technique	7.9
		7.4.3	Interpretation	7.11
	7.5	SUBMAP	M6AB	7.11
			Structural Description	7.11
		7.5.2	Subarea Analysis by the S.O.D.A. Technique	7.12
		7.5.3	Interpretation	7.13
	7.6	SUBMAP	м789	7.13
			Structural Description	7.13
		7.6.2	Subarea Analysis by the S.O.D.A. Technique	7.14
		7.6.3	Interpretation	7.15
	7.7	SUBMAR		7.18
		7.7.1	Structural Description	7.18
		7.7.2	Subarea Analysis by the S.O.D.A. Technique	7.18
		7.7.3	Interpretation	7.19
	7.8	DISCUS		7.21
		7.8.1	Interpretation of the Structures	7.21
		7.8.2	Usefulness of the S.O.D.A. Technique	7.23
011 + DMT	n 0	CIMMADY	SUGGESTIONS FOR FURTHER DEVELOPMENT, AND CONCLUSION	N

	8	1.1 Development		8.1
	8	.1.2 Testing		8.4
8.	2 7	HE STRUCTURAL HISTORY OF LIPSON	COVE	8.5
8.	3 1	JTURE LINE OF EXPANSION		8.5
	8	.3.1 Immediately Applicable		8.5
	8	.3.2 Long Range Projects		8.7
8.	4 (ONCLUSION		8.8
REFERENCES	CI'	ED		RC.1
APPENDIX A	i j	rogram CYBER		A.0
APPENDIX E	3	tereonet plotting on the Hewlet	t-Packard 9830A calculator	
APPENDIX C	2	oding geological descriptions o	f data stations	C.1
APPENDIX I) .	utomatic mapping on the Cyberl7	<u>3</u>	D.1
APPENDIX E	€ .	erivation of isodip lines for a	n ellipsoid	E.1
APPENDIX F	F,	raphics and utility routines fo	r the Nova2	F.1
APPENDIX (G ,	erminology for the Hierarchy of	Domains	
		in Subarea Analyses		G.1
APPENDIX I	H,	tereonet plotting and contouring	g program "CNTRFIN"	H.1
APPENDIX .	J	n efficient algorithm for sorti	ng line segments	J.1
APPENDIX I	K	ype I trend surface analysis pr	ogram package	K.1
APPENDIX	L	lgorithms for spherical project	ions of orientation data	L.1
APPENDIX I	M	utomatic contouring of irregula	rly distributed data	M.l
APPENDIX	N	Abstr.) Some Structural Aspects	of the Lincoln Complex	
		from Tumby Bay to Port Ne:	111	N.O
APPENDIX		eology of the Tumby Bay to Por		0.1
APPENDIX	P	A Geophysical Study of the Tumb	Bay to Port Neill Region	P.1
APPENDIX	Q	Polygon-fill routines for displa	ay on colour monitors	Q.1
APPENDIX	R	Description and use		
		of structural data analys		R.1
APPENDIX	S	(Abstr.) Application of interac		
		to the display and interp	retation of structural data	S.0
APPENDIX	U	(Abstr.) General fabric analysi	s techniques	
		with computer-aided S.O.D		U.0
APPENDIX	V	(Abstr.) Practical A.V.A. techn	ique applications	
		using computer-aided S.O.	D.A.	V.0
APPENDIX	X	Design and use of colour charts		
		for S.O.D.A. technique ap	plications	X.1
APPENDIX	Z	An efficient algorithm		_ 9
		to point count for contou	ring stereonets	Z.1
APPENDIX	CP	Colour plates		CP.1

LIST OF	TABLES	rage
6.1	Tectonic history of the Early Proterozoic rocks of	
	the Gawler Craton as derived by a number of researchers	6.12
B.1	List of stereonet plotting functions	B.4
B.2	List of variables for setting up stereographic nets	B.5
B.3	List of variables for plotting points	B.5
B.4	Types of data representing point	B.5
B.5	List of symbols for plotting points	B.6
B.6	Quadrant values used in Tables B.4 and B.8	B.6
B.7	List of variables for drawing planes	B.6
в.8	Types of data representing planes	B.6
B.9	List of lines for plotting planes	B.7
B.10	List of variables for drawing cones	B.7
B.11	List of variables for contouring data	B.7
B.12	List of variables for rotating data	B.7
B.13	List of variables for data storage and retrieval	B.8
B.14	List of variables for fitting circles to distributions	в.8
R.1	Console commands for cursor control	R.11
R.2	List of stereonet functions	R.12
R.3	Options for modifying current S.O.D.A. procedures	R.12
v i	Tables for defining references and colour charts	X.5

SUMMARY

A general analytical technique has been developed to unify and automate a number of methods employed in the analysis of structural orientation data. These methods have in the past been manually conducted and hence time consuming, which makes them unpopular as a general tool in the mineral and exploration industry.

The unified technique developed here is termed S.O.D.A. (Spatial-Orientation Distribution Analysis) and is an application of trend surface analysis to structural geology. Unlike standard trend surface analysis techniques which have known data heights with which to generate trend surfaces, no such height information is measured in structural orientation data. Consequently, height information must be generated. Two types of trend surface applications are defined (termed Types I & II). Type I produces surfaces that model geological surfaces, and Type II produces surfaces representing the properties of structural data. The former has been the subject of investigation by others and so only the latter is extensively developed here. It is more useful in that it encompasses the manual geometric analysis methods which are used to indirectly derive Type I surfaces.

For Type II trend surface analysis the mathematics needed to define basic geometrical shapes of surfaces from orientation data was formulated. It is manageable and displayable by computer. Two mathematical entities are defined to allow geometrical shapes to be classified; they are lines of equal trend and lines of equal plunge (isotrend and isodip contours respectively), relative to a reference plane. Trend surfaces can thus be subdivided if necessary, by domain (subarea) analysis, into simple geometries. The contours can be used to conduct axial distribution analyses (A.V.A.), classify fold profiles, and detect discontinuities.

Although individual methods of analysing data have recently been the subject of computer applications, developed here is a prototype interactive computer program package that performs the above structural data analysis in a non-statistical approach. The program package is fast, inexpensive, and versatile in displaying results. It was written on a Nova2 that had a peripheral colour graphics display processor and data tablet. The driving programs were written in FORTRAN IV and the bulk of the software in ASSEMBLY. Support programs were written or compiled on a Cyber173. A software link between the two was written for communication.

A number of models were generated to demonstrate the ability to

classify both fold surfaces in different orientations and fold profiles, and to recognize faults and dislocations.

Geological examples, from microfabrics to macroscopic structures, are examined to demonstrate the general usefulness of S.O.D.A. techniques.

Limitations of S.O.D.A. in its ability to analyse data, because of geological complexity, biased mapping, and usefulness of individual datum, were found by applying it to a test area that is complexly deformed. In testing the technique with a complex area (Lipson Cove) the structures at Lipson Cove were determined, analysed, and interpreted.

A well exposed coastal section of the Lincoln Complex extends in a north-northeasterly direction from Tumby Bay to Port Neill. This section cuts obliquely across the regional northeast structural trend and displays the complex morphology, geometry and history of the Kimban Orogeny (1800 to 1580 Ma). The Lincoln Complex is an interlayered sequence of granitic gneisses and minor amphibolites. Two geological scales are considered: a section 1.5 km long at Lipson Cove mapped in detail for structural analysis by S.O.D.A., and the general geology of the coast for its regional context.

Four periods of deformation are recognized. D_1 , a fabric-forming event, produced well-developed L-LS-S fabrics of varying intensity. The foliation (S_1) is mostly layer-parallel. D_2 was a fold-forming event which produced tight to isoclinal subhorizontal folds. D_3 was a major fold-forming event. Structures formed during D_3 control the regional northeast trend. D_m , a mylonite-forming event, appears to have been associated with D_3 . The shear zones are regionally parallel to D_3 structures. D_4 was a weak event that is only recognised by kink folds and crenulations at Port Neill.

The regional structures can be separated into three zones of differing D_3 deformational style. The Lipson Cove transition zone (Zone 2), which is an area of very complex strain variation and fold style, separates a southern zone (Zone 1) extending to Tumby Bay, from a northern zone (Zone 3) extending to Port Neill. In Zone 1, D_3 produced asymmetric, steep northerly plunging folds in S_1 , and local protomylonites. In Zone 3, D_3 folds plunge shallowly to the northeast and southwest, with less intensely deformed S_1 fabrics than Zone 1. Strain intensity increases towards the north and a mylonite zone forms the northern boundary at Port Neill.

The application of the S.O.D.A. technique to Lipson Cove enabled the recognition of structural domains noted during mapping, and of others that were necessary for the interpretation of the macroscopic structures.

This thesis contains no material which has been accepted for an award of any other degree or diploma in any University; nor does it contain, to the best of my knowledge and belief, any material previously published or written by another person, except where due reference is made in the text.

P.H. Cohen

ACKNOWLEDGEMENTS

There are a large number of people to whom I am indebted for their aid during the term of this study. In particular, I would like to thank Dr. Pat James for accepting the role of my supervisor, and to the Department of Geology and Mineralogy for supporting my studies, as well as the Department of Economic Geology for the use of their equipment and technical staff.

In the above department I would like to thank my colleagues Graham Mortimer and Mark Fanning for the discussions on their material, and Francis Ukaigwe and Prof. Boyd for their help with the geophysics. Thin sections were provided by Jeff Trevellyan, photographic plates by Rick Barrett, an introduction to Novas by John Stanley, and instructive explanations of machine level coding by John Willoughby. Thanks are also due to the other technical staff and colleagues whose numbers are too great to mention individually.

I am indebted to Prof. Bogner of the Electrical Engineering Department for free access to his computing equipment, and to Ray Nash for maintaining it in working order. I also thank fellow students Rob Clarke, Greg Bielby, Dave Fensom and Neil Clarke for providing software and instructive discussions.

Assistance was also gained from the Computer Centre and the Department of Applied Mathematics.

The thesis was critically read by Dr. P. James and Dr. P. Brooker.

Finally, I would like to thank Dr. M. Carabott for her encouragement and support throughout the tenure of this thesis, and my parents who encouraged me in all my endeavours.

CHAPTER 1

INTRODUCTION



1.1 CLASSIFICATION OF STRUCTURAL GEOMETRY

1.1.1 Structural Geometry in Geometric Analysis

The analysis of structural data (structural analysis) incorporates all types of analyses involved in the study of deformed rocks, particularly those produced by tectonic processes. Structural analysis incorporates a variety of techniques to analyse different facets of structural data, such as the geometrical relationships of structures (geometric analysis), their geometrical classification (descriptive geometry), strain analysis, and fabric analysis (microstructural analysis). None of these are independent from the others, and each can use results from the others to aid in reaching their respective objectives. The most important, and most general is geometric analysis (Turner and Weiss, 1963), which these, of incorporates those "methods used in field studies to establish the form, extent and arrangement of structures in a map area, together with the time sequence in which the structures developed." (Hobbs et al, 1976, p.347).

The "extent" of structures is determined principally by mapping. The "arrangement" of structures is the spatial and temporal relationship of structures and is determined by mapping and fabric analysis. The "form" of structures is a description of geometrical shapes and is derived qualitatively by mapping, and quantitatively by geometrical classification.

Mapping procedures form the basis of geometric analysis and have been well documented (e.g. Compton, 1962; Turner and Weiss, 1963). The description of structural geometry has not been as well documented, nor well coordinated. Consequently, there are a number of different methods for classifying different properties of the shapes of structures. (For example, folds can be classed as: cylindrical or non-cylindrical; angular or rounded; similar, concentric; open or tight; upright or inclined (Hobbs et al, op. cit.). As more precise descriptive procedures are derived, these descriptions can be modified so that folds can be classed (for example) according to: cylindricity (Charlesworth et al, 1976); curve shapes using parametric ratios of Fourier series (e.g. Hudleston, 1973a); and profile classification using dip isogons (Ramsay, 1967).)

Precise geometric descriptions (or "form") are not generally incorporated into geometric analyses because there is, to date, an inability to use it in conjunction with "extent" and "arrangement".

1.1.2 Classifying Fold Geometry in Fold Style

The description (e.g. Fleuty, 1964; Donath and Parker, 1964) and classification of the geometry of geological structures is important in

interpreting tectonic histories. Fold and deformation styles (i.e. fold shapes, fabrics and orientations - cf. Weiss, 1959; Turner and Weiss, 1963; Park, 1969; Burns et al, 1969) are often used in assigning structures to different deformation generations (e.g. Weiss, 1954; Weiss et al, 1955). It has been argued that this method may be inaccurate (Park, op. cit.; Williams, 1970) unless there is strict control on data consistency.

Cylindrical and noncylindrical folds (e.g. Mertie, 1959; Wilson, 1967; Williams and Chapman, 1979) can be described by a number of parameters, from profile shapes (Hudleston, 1973a; Stabler, 1968), to layer thickness variation (e.g. Ramsay, 1967), to the orientations of fold elements (Rickard, 1967; Wilson, op. cit.; Williams and Chapman, 1979). Interference folds have also been described in terms of their resultant patterns, and their component stress fields (e.g. Ramsay, 1967; Thiessen and Treagus, 1980; Watkinson, 1981).

Apart from the direct measurement of fold geometries taken from field exposures, attempts have also been made to interpret unexposed geometries (e.g. Dahlstrom, 1969; Charlesworth et al, 1976; Kelker and Langdenberg, 1976; Langdenberg et al, 1977).

In all, there have been many methods derived for describing fold geometries. Such descriptions are often restricted to cylindrical folds as they generally apply to only two dimensions of folds (generally the profile plane). Extension to three dimensions is mathematically feasible but generally impractical due to the very limited availability of data for all dimensions.

Use of dip isogons and their associated first and second derivatives (Ramsay, 1967) is a means of classifying fold profiles. The procedure is performed by manually constructing dip isogons from diagrams of fold profiles. This can be automated, using computers (e.g. Mancktelow, personal communication), operating on digitised profiles, or with a mechanical device (e.g. Marjoribanks, 1974).

Structural interpretations include analyses of orientations of structural elements by use of stereographic projections (e.g. Phillips, 1971). Techniques for analysing fold orientations are well documented (e.g. Vistelius, 1966; Ramsay, 1967; Ragan, 1973; Hobbs et al, 1976; Laing, 1977).

Orientation data are plotted on structure maps to form the basis of structural analyses involving the spatial distribution of data. Strikeline maps, vertical (cross-) sections, and block diagrams can be constructed from structure maps (e.g. Turner and Weiss, 1963; Ragan, 1973).

1.1.3 Limitations

To date, the main limitations in analyses of structural geometries

for geological interpretations are due to the inadequacy of programs for accurate and rapid processing of data. For expediency, measured data are generally representative of structures rather than comprehensive (i.e. random statistical sample), because of the discrete nature of exposed structures, inefficient methods of measurement (e.g. magnetic compass, universal stage), and inefficient methods of physically representing and manipulating data (manual plotting). This type of data is more difficult to process by automated means (computers) because of the high degree of mathematical sophistication required to obtain reasonable results.

Another limitation arises from the ad hoc nature of structural analyses: fold classification by dip isogons, structure maps, strike-line maps, and stereonet plots (stereoplots), among others. Although these are integrated to obtain results, they are generally viewed as separate entities, as there are no uniform underlying principles expounded. Sander (1970) has described a technique (Axial Distribution Analysis, or A.V.A.) that unifies the analysis of orientation and spatial data for micro structures. However, it is severely limited by the extreme inefficiency of manual processing. This is in contrast to the previously mentioned methods of structural analysis, which are generally easier to perform manually than automatically.

1.2 A GENERAL CLASSIFICATION PROCEDURE

Methods of classifications of geometries of structures are varied (§1.1.1) and uncoordinated. Because of the ad hoc nature of the derivation of geometrical descriptions, it is difficult to unite the various techniques, as they stand, with a comprehensive and universal mathematical foundation.

It is therefore necessary to reapproach the problem of classification and interpretation of structural geometry from the standpoint of a unified mathematical procedure that incorporates the orientation and spatial aspects of structural data. Specific descriptions of such a procedure do not exist, but can be adapted from previous techniques.

In a geometric analysis of a tectonically deformed area, two prime data types are <u>inter alia</u>, the orientations of structural elements and their geographic position, which are utilised in the methods described in \$1.1 to determine the shapes of lithologic (marker) horizons for layered rocks and theoretical marker horizons for non-layered rocks (Turner and Weiss, 1963). These horizons are morphologically equivalent to the trend surfaces of trend surface analysis, which is commonly used in other disciplines.

1.2.1 Trend Surface Analysis

Trend surface analysis is a technique that analyses the correlation of data values with spatial distribution. Trend surfaces are mathematical surfaces that are fitted to a distribution of points in three-dimensional space (which can be extended to higher dimensions if required). Two of the dimensions refer to the geographic coordinates of data points and the third to data values (Fig. 2.1).

1.2.1.1 Historical Usage

There have been numerous methods and procedures developed for the determination and presentation of trend surfaces in disciplines other than geology. Trend surfaces are used extensively in: meteorology (production of weather maps, e.g. Menmuir, 1975); height contour generation from spot heights, as in topographic maps (e.g. McClain, 1974), isopach maps (e.g. Cole, 1968); contouring of geophysical data (e.g. Krumbein, 1959; Crain, 1970; Holroyd and Bhattacharyya, 1970; Walters, 1969); and geochemistry (e.g. Dagbert, 1978). Techniques of deriving contours are reviewed by Crain (op. cit.).

Despite the advanced state of trend surface analysis, the only known attempt to use it in structural geology is by Yamamoto and Nishiwaki (1976). Their technique is limited to determining low angle lithologic surfaces (bedding planes) from ground-surface data which are assumed to be representative of the lithologic surface at depth. Hence, it is useful for the analysis of sedimentary basins, but not for the analysis of tectonic foliations.

Trend surface analysis techniques generally do not compute trend surfaces directly from irregularly distributed data, but first generate regular grids of values calculated from initial data (Walters, 1969). Several approaches are described by Lee and Kaula (1967), Junkins et al (1973), and Hardy (1971). A different approach is required for preparing gradient data. That of Yamamoto and Nishiwaki (op. cit., program SLINE) is mathematically simplistic (a least-squares best fit plane), which generally does not obtain a surface that either fits the initial data or the computed grid values (program RECON in Yamamoto and Nishiwaki, op. cit.). This contradicts standard trend surface analysis specifications, which attempt to minimize the discrepancy between computed surface values and the grid data.

1.2.1.2 Problems

There are a number of problems in applying standard trend surface analysis procedures to structural data.

1) Structural geological data consist <u>inter alia</u> of the orientations of a number of structural elements (e.g. surfaces and lineations) at

various locations. Orientation data represent gradient values (and are therefore height independent), and so the third dimension (height) for standard trend surface analysis is unknown. The consequences of this are (e.g. see Fig. 1.1): a) calculated heights of data points are dependent on all other points, hence b) there must be no "missing data", and c) standard mathematical procedures need to be modified to account for the different data form.

- 2) Structural surfaces are often of high relief, and so would require prohibitively large data sets for an accurate or comprehensive analysis. The problem is compounded as such surfaces may also be disrupted by discrete faults (dislocations). As orientation data are gradients and not heights, the existence of dislocations would be very difficult to detect by trend surface analysis unless they catastrophically alter the orientations of parts of the surfaces, for example, by rotation (hinge or scissor faults). Dislocations observed in the field could be incorporated into the computation of trend surfaces (cf. Shepard, 1968; Pouzet, 1980).
- 3) Availability of data is apt to be incomplete due to inadequate ground exposure, caused by ground cover (e.g. soil, water), variation in structural complexity, and erosion of structures that have high relief surfaces, (2) above. As compared to other disciplines, the distributions of data points in structural geology are commonly highly irregular, because the acquisition of structural data is more sensitive to the vagaries of nature for locations at which data can be obtained; is made only where there are significant changes in the values (for expediency, as geologic data measuring is relatively inefficient); and can only be made where structural surfaces have either not been eroded away or are not yet revealed from subsurface by erosion.
- at different locations. The only exceptions are where the structure surface is the ground surface, where all surfaces are identical, or where there is adequate bore-hole data. The first and last exceptions are not common and are generally limited in extent. The second exception requires folding to be of "similar" type (or a composite of Ramsay's (1967, Ch.7) types 1C and 3). As these exceptions are not the norm, at different locations data must be measured from different surfaces with slightly differing shapes.
- Data measured from subvertical surfaces (e.g. recumbent fold closures, upright tight to isoclinal folds, upright cleavages; see Fig. 1.2) must, by their very nature, be obtained from different surfaces. Trend surface analysis requires trend surfaces to have lateral extent.

But if strata is everywhere subvertical then trend surface analysis cannot account for the paradox of a subvertical layer having significant lateral extent.

- 6) Structural surface orientations may not be measurable at some locations although other structural elements (lineations, cleavages, fold vergence, younging) could be recorded that could aid in qualitative, if not quantitative, interpretations by inference or otherwise.
- 7) Structural surfaces may not always be single-valued. Trend surfaces that are overturned (i.e. more than one height for a point) are a problem not generally encountered by disciplines other than structural geology, except, perhaps, by geomorphologists encountering "caves" (Morse, 1969).

1.2.2 Statement of Aim 1

It is an aim of this thesis to develop a basis for a unified method of classifying structural geometry by adapting trend surface analysis techniques to structural data.

1.3 A GENERAL PURPOSE COMPUTER PACKAGE

1.3.1 Computer Technology in Structural Geology

Computers have been used less extensively in structural geology than in other branches of the discipline. Whereas other branches of geology have had frequent recourse to computers, particularly in data storage (§1.3.2.1), application of statistics (regression, discriminant, principal components, factor and cluster analyses), and data classification (see Sneath, 1977, and Tipper, 1979, for further references) their use in structural geology has generally been limited to relatively small and simple programs performing limited functions. The most notable exception is the use of finite-element analysis for the modelling of deformation processes, such as gravity structures (e.g. diapirs and salt domes - Stephansson and Berner, 1971; Stephansson, 1973), folds (e.g. Dieterich, 1969, 1970; Anthony and Wickham, 1978), amongst others (e.g. Voigt and Samuelson, 1969; Parish, 1973; DeBremaecker and Becker, 1977).

Computer usage in the past has been handicapped by the type of data involved combined with a paucity of powerful computing machinery. Unlike petrological, geochemical, or palaeontological data, structural data are generally incomplete in themselves, and so the programs required to manipulate structural data are far more complicated. With improved technology and an improved understanding of the role of structural data in geology, better use of computers can be made.

The extremely rapid expansion of computer technology, combined with an evergrowing understanding of the complexities of deformation processes, has opened a gap between geology and computer science that inhibits the practical application of computer technology to structural geology. Computer programmers become more specialised and less able to understand the intricacies of specific geological problems, and vice versa. This in effect opens a branch of geology that did not exist before.

1.3.2 Existing Computer Programs

1.3.2.1 Data Banks

The design and use of data banks are fundamental aspects of computing science (Sundgren, 1975; Chamberlin, 1976; Deen, 1977; Pfaltz, 1977; Ross, 1978), and hence occupy an important place in the consideration of computer applications (Low, 1976; Marble and Peuquet, 1978). The design, or structure, of data banks depends to some degree on the type of data to be stored, how it is to be stored (and retrieved), and how it is to be manipulated.

In the geological sciences, both general and particular geological data base systems (data banks) have been designed and implemented. The design and application of general purpose geological data base systems, including their merits and limitations, are described by, among others, Hutchison and Roddick (1968), Roddick and Hutchison (1972), Sharp (1972), Moshkin et al (1972), Moody (1972), Lea (1972), Haworth and Sparkes (1972), Berner et al (1972), Laurin et al (1972), Robinson (1972), Riva (1972), Bouillé (1976a), Jeffery and Gill (1976), Cruden (1978), Davidson and Moore (1978), and Davis and Levi de Lopez (1978). Design and implementation of specific purpose data bases in geology have been accomplished in a number of disciplines. Dall'Aglio and Gigli (1972), Shih and Heffler (1972), and Colonell et al (1972) discuss them for hydrological systems; Berry (1972) and Kent (1972) discuss palaeontological data; Longe et al (1978), Harrison et al (1972), and Le Maitre and Ferguson (1978) cover aspects and designs for mineralogical and petrological data systems.

Data banks designed solely for the storage and retrieval of orientation data have not been published, if they do exist. Many programs that analyse structural orientation data (e.g. stereonet plotting programs, \$1.3.2.3) read data from punched cards or facsimilies thereof (i.e. are not derived from data banks). This is a common procedure for data storage, and is expedient for the limited range and capabilities of available programs.

1.3.2.2 Cartography

Comprehensive systems for map production have been designed and used in the last decade (Bickmore, 1968; Bickmore and Kelk, 1972; Stutz, 1975; McCullagh, 1978), although it is only recently that systems have

become generally available (Teicholz and Dorfman, 1976).

There are a number of steps involved in the production of maps from initial data elements. They consist primarily of: a) digitisation of map and figure boundaries (Freeman, 1961; Bouillé, 1976b; Williams, 1979), which is a detailed, but purely technical, process; b) modification of raw data for efficient storage, i.e. data reduction (Freeman, 1969, 1974; Freeman and Glass, 1969; Montanari, 1970; Pfaltz and Rosenfeld, 1967; Douglas and Peucker, 1973; Andrew and Wheeler, 1978; Loudon et al, 1980a,b; and Dettori and Falcidieno, 1982); and c) the selection, projection (Melluish, 1931; Jancaitis and Junkins, 1973; Maling, 1973; Sen, 1976), and display of maps (Bengtsson and Nordbect, 1964; Hessdorfer, 1975).

A number of specific aspects of mapping procedures have been discussed in the literature: the computer science aspect of mapping is outlined by Palmer (1975); the usage of automation is noted by Lang (1969); and Clerici (1980) manipulates height contour data to obtain terrain information.

1.3.2.3 Spherical Projections

Noble and Eberly (1964) and Noll (1965) were among the first to consider the automation of stereonet plotting by computer. Tocher (1967) produced a program that used a direct encoding of a manual method (Ragan, 1973) for contouring plotted data, which is inaccurate, cumbersome, and underutilizes the abilities of computers. Consequently, Tocher (1978a,b and 1979) later published modifications and corrections. However, they still used a square grid for contouring. (The use of square grids is inferior to spherical ones.) Starkey's (1969, 1977) programs contained superior algorithms, which contoured on the sphere. Program ORIENT (Bridges and Etheridge, 1974) is an unpublished program for plotting contoured stereonets, by contouring on the sphere. It departed from the custom of using regular contour intervals by computing geometric intervals. Kalkani and von Frese (1979, 1980) use stereonet plotting and contouring programs that are mathematically correct (as used by program ORIENT, and Starkey, op. cit.). They offer two contouring grids based on spherical geometry, which are polar nets centred around a horizontal axis, instead of the vertical. However, they did introduce an accurate correction for the distortion of orthogonal grid lines on the sphere. The methods by which they draw their contour lines are unnecessarily complicated for most applications, although their results are precise.

The analysis of data distributions is related to the production of stereographic projections of orientation data. To some extent this includes the production of contoured stereonets, as there is contention about the methods used to determine counting circle size (Flinn, 1958; Kamb, 1959;

Bridges and Etheridge, op. cit.; and Starkey, 1977), and grid shape (Starkey, op. cit.). The description of the form of orientation data distributions (great and small circles, and points) is of immediate relevance to structural geology. Although descriptions can be made in terms of symmetry elements (Turner and Weiss, 1963; Paterson and Weiss, 1966; Woodcock, 1977), it is desirable to know the orientations of the individual Ramsay (1967) described a elements that form the fabric symmetry. mathematical procedure for fitting girdles, and finding averages, to data They proved to be unsound, being correct for only limited applications. (For example, the method of averaging data orientations (vectors), to find a mean, assumed that data is orientated, whereas data are almost universally measured unorientated, i.e. the upper hemisphere is not used.) Mardia (1972) and Mardia and Gadsen (1977) used a statistical approach to solving the problem attempted by Ramsay (op. cit.). Mancktelow (personal communication, 1979) used a technique after Ramsay (op. cit.) for fitting great circles, and linear programming for the others. Gray et al (1980) used a method of least-squares to fit great and small circles. Charlesworth et al (1976) used eigenvectors (i.e. the symmetry element description of Turner and Weiss, op. cit.).

1.3.2.4 Structure Maps

Strike-line maps, cross-sections, fold profiles, and others can be constructed from structure maps containing orientation data. (For example, Yamamoto and Nishiwaki (1976) have developed a program package for producing form surfaces of subhorizontal sedimentary horizons (Appendix K). Programs for producing sections through folds have been developed by Kelker and Langdenberg (1976) and Charlesworth et al (1976).) These programs are not complete packages, and many desirable functions are not yet automated.

1.3.2.5 Fold Classification

The classification of fold profiles as described by Ramsay (1967) has not been attempted by using orientation data. The classification of folds by using dip isogons can give rise to inconcise, not easily understood, and apparently meaningless results because fold classes can change from place to place within fold profiles. Mancktelow (personal communication) produced a program to classify fold profiles (using dip isogons) from digitised fold profile outlines (i.e. upper and lower bounding surfaces).

1.3.2.6 Microfabric Analysis

The A.V.A. technique (Sander, 1970) is a very useful method of analysing the spatial distribution of grain orientations in thin section. It is not generally used due to its extreme inefficiency when performed

manually. No known attempts have been made to automate it prior to this research.

1.3.3 Graphical Displays

The standard visual output of computer generated results are usually generated through printers and pen plotters (Sutherland, 1966). technology expanding rapidly and development With the computer-controlled graphic CRT (Cathode Ray Tube) displays this exciting and cost efficient method will soon be common enough for application to small scale usage. Interactive computer graphics were first put to use in scientific and engineering disciplines other than geology. They have been used in applications that can be collectively titled "Computer-Aided Design" (CAD). Applications of a variation of CAD to mapping are collectively titled "Computer-Augmented Mapping" (CAM). Many practical applications of these (particularly CAD) have been described by engineers (e.g. Atkinson, 1972), particularly in micro-electronics (Bracchi and Somalvico, 1970; Richardson and Oestreicher, 1969) and aeronautics (Gordon and Riesenfeld, 1974; Greiger, 1975); by architects (Newman, 1966; Patterson, 1974); and mathematicians (La Fata and Rosen, 1970; Gordon and Riesenfeld, 1974). CAD/CAM program packages and hardware facilities are extremely useful as they perform all routine processing (such as automatic draughting) many times faster than can be done manually.

Their use has so far been extremely limited in the geological sciences due to the general unavailablity of equipment and the lack of necessary expertise. Stingelin and Avis (1972), and Abrams et al (1977) were among the earliest to use CAD/CAM, for processing airborne and satellite remote-sensing data. Since then the geoscience industry (particularly in mining and exploration) has begun to make further use of graphic displays (e.g. Harris, 1977; Brady, 1978; Glass and Schowengerdt, 1979; Mooney et al, 1979; Daoust and Gelinas, 1981; Andrew and Linde, 1981).

One of the most powerful applications of interactive graphics (particularly colour) is the use of processing raster images, particularly for remote-sensing data in geology (e.g. Landsat Conferences in 1979, 1981). Its increased use has been so marked in geology, medicine and many other fields of science and engineering that complete hardware and software systems are now being marketed to suit every financial and physical requirement (e.g. refer to "Graphics Technology" magazine).

There is adequate literature available detailing the many algorithms and techniques involved in the process of converting data elements into a displayed form. General procedures for computer graphics are described in Fairman and Nievergelt (1969), Rosenfeld (1969), Andrews

(1970), Woodsford (1971), Pardow and Green (1971), Newman and Sproull (1973), Walker et al (1975), Rosenfeld and Kak (1976), Rogers and Adams (1976), and later by Giloi (1978). Some procedures applicable to CAD (apart from those above) are described in Newman (1966), Kilgour (1971), Prince (1971), Barnhill and Riesenfeld (1974), and Patterson (1974). This list does not include the multitude of mathematical techniques (particularly geometric, trigonometric and numeric) required for data element manipulation and display.

Modern computers that include interactive graphics devices also include graphics languages. Designs for a number of graphics languages are discussed in Kaneff (1970), Heindel and Roberto (1975), and Wyrill (1975).

1.3.4 Statement of Aim 2

It is an aim of this thesis to <u>develop a computer package that</u> makes the formulation of the general purpose classification technique for structural geometry (§1.2.2) a viable and practical procedure. The package must have a highly efficient means of interacting with users, and must be formulated in a way that allows for indefinite expansion.

1.4 APPLICABILITY OF COMPUTER CLASSIFICATION

In summary, it is the objective of this thesis to:

- Examine some of the problems in structural analysis (Chapter 1).
- Develop a general purpose classification technique, which may encompass existing methods (Chapter 2).
- Design an interactive program package to make the classification technique viable (Chapter 3).
- Test the program and classification technique. A general purpose classification technique (§1.2.2) and its implementation on an interactive computer (§1.3.4) requires thorough testing to determine its usefulness and its limitations. Many different types of examples are needed, from ideal models of various types of structural features (e.g. folds and faults, Chapter 4) to simple field examples (e.g. single folds and thin-sections, Chapter 5) to a full scale analysis of a structurally complex area (Chapters 6 and 7). Each of these help to determine the accuracy of the technique, its reliability, and its usefulness under varying conditions.
- Summarise the value of the developed technique, the programs, and the technology required (Chapter 8).

1.5 TERMINOLOGY

1.5.1 Geological

Geological terms and abbreviations are consistent with standard

practice, as defined in the geological dictionary (A.G.I., 1962); and used in Dennis (1972); Turner and Weiss (1963); Hobbs et al (1976). Abbreviations for structural elements are consistent with Bell and Duncan (1978) unless otherwise defined. Other terms are referenced as appropriate (e.g. Appendix G).

All stereoplots use the format of Fig. 1.3 (although layout may vary), and all angles, such as azimuth, dips, etc., are in degrees unless otherwise stated.

1.5.2 Compututational and Mathematical

The terminology used in this thesis is derived from a number of sources. Specific terms are defined or referenced in the text, general computational terms can be found in Queyssac (1976), and general mathematical terms and expressions can be found in Lanczos (1966); Cangelosi (1967); Kreyszig (1967); Maher (1968); Mase (1970); and Selby (1971).

CHAPTER 2

SPATIAL ORIENTATION DISTRIBUTION ANALYSIS

2.1 INTRODUCTION

Dip and strike measurements from a scatter of localities are the prime data used to interpret geometric shapes (form and style) of structural surfaces (layering and foliations). By plotting orientation data on a map (structure map), strike-line maps, cross-sections, block and isometric diagrams, and so forth, can be produced, usually by visual and Thus a three dimensional interpretation of structural manual means. surfaces can be made from an initial two dimensional representation. two controlling factors for any interpretation are orientation data and positional (spatial) data. The former is generally considered in terms of two variables (Fig. 3.5a), an azimuth (\emptyset) and an inclination* (θ); the latter, with two variables (X,Y) defining coordinates on some arbitrary or Grids are restricted to two dimensions (map surface) definitive grid. because a third dimension (height, Z) is associated with orientation data. Complications are introduced by topographic height data, which are therefore not considered in this thesis.

The interpretation of structural geometries from sets of scattered data is in fact the application of trend surface analysis to structural geology. There are two possible approaches that can be made, depending on the situation under analysis. The first is to compute mathematical surfaces that closely match measured structural surfaces, and the second is to compute trend surfaces of properties of data sets.

2.1.1 Type I Trend Surfaces

The first type of trend surface, designated here as <u>Type I</u>, models the geometric shape of a structural surface (Fig. 2.1a). Consequently, this surface must be a single curvi-planar surface, although it may contain discontinuities (e.g. faults contained within folded surfaces or sedimentary basins).

Manual methods of determining Type I surfaces incorporate the construction of strike-line maps and cross-sections (e.g. Hobbs et al, 1976). As strike-lines are identical to height contours, they are dependent on the two geographic coordinates and height. If strike-lines are

^{*} Although the term normally means the angle of dip upwards from the horizontal, structural geologists measure dip angles downwards, or declination. This last term is not used as it has a different meaning in geology (A.G.I., 1962). By mathematical convention, positive angles are measured as inclinations, but this aspect is not regarded here as otherwise the clockwise azimuthal angle would have to be considered negative.

constructed without regard to relative spacing (i.e. the relative height differences, ΔZ , between successive strike-lines are either unknown or inconsistent, in fact immaterial) then geometric shapes are qualitatively defined. If relative spacings between heights are considered, e.g. from cross-sections, then shapes are quantitatively defined.

Type I surfaces are only a particular type of a more general trend surface (below). They do not lend themselves to the development of a general classification scheme because of a number of problems outlined in §1.2.1.2.

2.1.2 Type II Trend Surfaces

Trend surfaces of properties of data sets are designated Type II
(Fig. 2.1b). These are more useful and versatile than type I as they are general surfaces. They have fewer problems than Type I surfaces as data sets need not belong to single curvi-planar surfaces (e.g. all three situations of Fig. 1.2 can be analysed by Type II surfaces). Furthermore, Type II trend surfaces can analyse any type of structural element (e.g. lineations, fold vergences and asymmetries, grain orientations, strain ellipsoids, etc.). It is also possible to determine type I trend surfaces from type II trend surfaces by analysing pertinent properties.

A comparable application to Type II trend surface analysis of geometrical shapes is dip slope analysis. Geomorphologists use it for many purposes, such as the analysis of surface energies, in regard to erosion and stream deposition. In all cases dip slope contour (isocline) maps are derived from elevation data (spot heights or topographic contours). The process has been automated (cf. Park et al, 1971; Grender, 1976; Clerici, 1980). This procedure is a reverse of the process to be developed here, i.e. finding topographic contours of the trend surface from isoclines.

2.2 PROPERTIES OF SPATIALLY DISTRIBUTED ORIENTATION DATA

2.2.1 Strike-lines and Isoclines

The only two properties of spatially distributed orientation data previously in use were strike-lines and isoclines. Strike-lines have the problem of being rigidly dependent on height. Although data sets supply geographic coordinates, they do not provide height. To determine height requires interpolation techniques, which have the problems faced by Type I trend surfaces. Lines orthogonal to strike-lines (dip slope lines), are less dependent on height. However not only do they contain less information, but they still require interpolation techniques similar to those for producing qualitative strike-lines. (Dip slope lines could be made to be more informative if they were contoured according to dip values, i.e. isoclines).

Interpolation and extrapolation techniques would need to be developed before these properties could be incorporated in a general classification scheme. These are inferential, or statistical, techniques. However, as a basis for analysis, it is more desirable to first develop a deterministic approach to defining trend surfaces, i.e. one by which each data point is considered as an entity throughout the analysis. (For an analogy, we can look at stereonet plots. The development of scatter plots was necessary before contoured data distributions could be developed.) Hence, it is desirable to find new properties that do not have this problem.

A technique that practically determines Type II trend surfaces (which may incorporate Type I trend surfaces) is named here as a Spatial Orientation Distribution Analysis technique (S.O.D.A.). In this thesis, S.O.D.A. will refer to the technique enlarged upon in the remainder of the chapter, and to the computer implementation described in Chapter 3 and the Appendices. However, it is open to expansion in that it can incorporate future developments that are impractical in this dissertation.

2.2.2 The Formulation of New Properties for S.O.D.A.

Although strike-lines and isoclines are not immediately applicable to the development of S.O.D.A. in this thesis, they are related to the two most important variables used in defining geometrical shapes, i.e. trend and plunge (synonymous with azimuth and dip). If the trend and plunge values of individual datum points are considered without attempting to infer other properties (such as height), then analytical methods can be simplified. The question then becomes one of whether the properties of trend and plunge alone are enough to unambiguously define geometrical shapes of trend surfaces.

2.2.2.1 Orientation Values On A Single Surface

For any single simple surface (e.g. Fig. 2.2a), the lines on the surface that join all points with the same dip direction (as opposed to strike directions that are bi-valued) are dip direction contours, which are here designated with the term, <u>isotrend lines</u>. Similarly, the lines joining all points with the same dip values are dip contours, which are designated with the term, <u>isodip lines</u>. The term isocline is not used because of its accepted topographic applications in geography, with its associated connotations.

Both the trend and dip values of a planar portion of a single geometric surface will be constant over the finite region of this planar portion. Hence contour lines for trend and dip will become surfaces. As planar geometric surfaces are reasonably common in structural geology (at suitable scales), it must be noted that contour lines (even if they are surfaces) will be termed <u>lines</u>, to avoid confusion with definitions

introduced in the next section. (The contour term, surface, will be used in applications to single geometric surfaces only when there is no likelihood of confusion, and even then only when a contour surface, as opposed to a contour line, is expected.)

2.2.2.2 Orientation Values in a Solid Body

Elements of a data set will rarely belong to a single structural Measured data is almost always made from a family of structural surface. This introduces complications as such surfaces will most surfaces. commonly differ from one another, and not necessarily by a gradual or smooth transition. It is important therefore that we consider how isotrend and isodip lines behave as they translocate from one surface to another. As a single (folded) geometric surface (upper surface, refer to Fig. 2.2b) is moved through space in the direction of the direction-of-movement vector to a second surface, all points on the contour lines will move parallel to all points on the hinge line, to give rise to corresponding contour lines on the second surface. Contour surfaces defined by moving curvi-linear contour lines in three-dimensional space are termed isotrend surfaces and depending on the type of contour. isodip surfaces, consideration, contour surfaces on single geometric surfaces will give rise to contour volumes. From the construction of contour surfaces, we observe that they have the following property: contour surfaces in a finitely thick folded layer are spatially orientated in relation to the fold axial surface (where the axial surface may have the standard definition(s) cylindrical folds and nonstandard definitions for conical folds and domes (e.g. see Fig. 2.13).

2.2.2.3 Rotated Planes Of Reference

Orientation values are measured with respect to the horizontal plane and a line (the North direction) contained within. This gives rise to a second point, namely that the values, and hence shapes, of contour surfaces are related to the horizontal. This can cause complications in the analysis of lines and surfaces when reference axial planes are not trivially related (parallel or orthogonal) to the reference horizontal plane.

It is desirable to have contour patterns that are dependent only on fold geometry, not its orientation. Accordingly, dip values for deriving isodip lines must be measured from a reference plane related to the fold geometry. A similar argument applies to trend values. Such a reference plane would be orthogonal to both the profile and axial planes.

The standard reference plane, the horizontal, applies when cylindrical folds are upright and horizontal, i.e. the direction-of-movement vector (or direction of tectonic transport, (Turner and Weiss,

1963, p.103)) is vertical. Any geometry not in the upright horizontal position (except for the trivial case of a planar feature) must use a rotated reference plane. Many of the problems associated with interpreting rotated geometries (e.g. §2.3.3.5) are obviated by this simple procedure.

Rotation of the reference plane causes isotrend and isodip values to change from direct functions of \emptyset and θ respectively, to functions of (\emptyset,θ) .

2.2.2.4 Contour Nomenclature and Values

The range of values encompassed by \emptyset and θ are $0 \le \emptyset < 360^{\circ}$ and $0 \le \theta \le 90^{\circ}$, respectively (Fig. 2.3a). Together, they uniquely define every non-directed orientation except the vertical, which is multiply defined. Isotrend and isodip contours defined from these ranges of values are termed uni-directional isotrends and bi-directional isodips, respectively. Alternatively, a range of \emptyset values, $0 \le \emptyset < 180^{\circ}$ (or equally well, $180^{\circ} \le \emptyset$ < 360°), combined with the θ range, $0 \le \theta \le 180$ °, (Figs. 2.3b,c) achieves the In this case, isotrend and isodip contours are termed same result. bi-directional isotrends and uni-directional isodips, respectively. For are designated u-isotrends and contours simplicity, uni-directional \underline{u} -isodips, and the bi-directional equivalents are designated \underline{b} -isotrends and b-isodips. Collectively, these contours are designated u-contours and b-contours, or just contours, as appropriate.

<u>Directed</u> orientations are covered by extending the range of values of isodip contours to include the negative equivalent of the positive values. The theoretical aspects of directed and non-directed data are equivalent. Directed data are rarely used in structural geology (e.g. Gray et al, 1980).

U-isotrends and b-isodips are used throughout the remainder of this thesis, unless otherwise stated. Where the term, contour, is used in conjunction with isotrends or isodips (e.g. isotrend contours), then no distinction is being made between the two different contour morphologies, lines and surfaces. Where the term contour is used without direct reference to either isotrends or isodips then both contour types are applicable.

2.2.2.5 Contours On Stereonets

Plotting structural data on stereonets has the effect of removing spatial information. Hence the shape of isotrend and isodip contours are lost. However, the quantity and values of these contours are still available.

Consider the case of a polar stereonet (e.g. Fig. 2.7). The radial lines represent contours of constant trend (isotrends), and the concentric small circles represent contours of constant dip (isodips). Therefore, the quantity and values of isotrends and isodips for structural

surfaces should be predictable, in stereonet plots (e.g. Fig. 2.17), from the intersections of data distributions and the lines of a polar net.

2.2.2.6 Use of Dip Vectors and Poles

(a) General Orientations. So far, dip values (i.e. of dip vectors, or lines "down-dip") have been mentioned in the computation and values of isodip contours. In the previous section poles (normals) to layering were assumed when referring to data distributions. Obviously, dip vectors and poles will give rise to complementary dip values for isodip contours, as well as opposing isotrend values. The advantages and disadvanges of both forms must be understood to make the best possible use of data analysis.

As dip vectors and poles have a strict geometrical relationship to each other there is no mathematical reason why both should be considered, as either one is quite sufficient. In the practicalities of application Both forms are illustrated in Fig. 2.4. are necessary. distribution of poles to layering of one limb of an upright horizontal fold, as it is rotated about the normal to the axial plane, is well behaved (i.e. its shape and position changes smoothly and predictably). corresponding dip vector distribution is not as well behaved (due to the transient, or unstable, nature of dip vectors). Despite the more complex mathematical description and behaviour of dip vectors, the generally larger spread of dip vector distributions at shallower dips make them more suitable for accurate analyses than the corresponding pole figures. At steeper dips, pole figures are generally more useful than dip vectors. That is, distributions that plot nearer the primitive are generally more suitable for analysis.

When rotated reference planes are used, the spread of plotted data does not change, but its usefulness in regard to contours does. (For example, isodip contours on the pole figure for the vertical fold (see Fig. 2.4a) can be improved by centering the polar net in the hinge point of the distribution, as is currently shown for the horizontal fold. Note that this can change the meaning of contours on S.O.D.A. plots - refer to Chap. 3 and program SHADEMAP, Appendix R.)

Although dip vectors are generally not suitable for manual stereonet analysis because of their complex behaviour, the geometry of structures can be discerned from dip vectors as well as from pole figures (cf. Ragan, 1973, p.115ff).

In \$2.2.2.4 it was stated that all orientations are uniquely defined by an isodip/isotrend pair, except the vertical. The ambiguity of the vertical gives rise to special cases of dip vectors and poles.

(b) <u>Vertical Poles</u>. When a plane is horizontal there is no one defined dip vector; instead the dip vector lies at all points of the compass. The

corresponding pole lies at the vertical where all trends meet at a single point. Consequently, the isotrend value of a horizontal plane is of all values simultaneously. This can be illustrated by noting that a plane can be given any desired dip direction by the smallest amount of rotation.

(c) Vertical Dip Vectors. When a plane is vertical the situation is quite different to the previous case although it appears identical. The pole lies at the horizontal where it can either be regarded as having two trend values simultaneously (180° apart), or as lying between these two possible trend values. (This can be envisaged if one of the two trends is imagined to be projected into the upper hemisphere so that the pole lies in the orientation between the two (colinear) trends.) In this case, the smallest rotation of the plane can either give the plane one of the two trend values (rotating about a horizontal axis), or place it between another pair of trend values (rotating about the vertical). The dip vector, on the other hand, lies at the junction of all trends, giving rise to what appears to be all points of the compass. This paradox is only an apparent one, and is resolved on further analysis. When the plane is rotated by a small amount in any direction, instead of all possible trend values being available, only the same limited trend variations as those experienced by the pole are obtainable. Therefore, although the vertical dip vector lies at the junction of all trends, only two are immediately available to it. It can be considered, then, that a vertical dip vector lies between all trends, not on all trends.

2.2.2.7 Density of Contours on a Profile Plane

The representation of geometric shapes by contours can be expressed as: the curvature of any portion of a curved surface is represented by the density of contours found in that region. Density as such is related to two factors, the angle of arc subtended by a curved surface and the radius of curvature. The roundness of a fold hinge can thus be expressed as a density value. A simple equation defining density would be:

density =
$$\rho_p$$
 = $\frac{\text{angle of arc}}{\text{arc length}}$ (2.1)

where arc length is measured in the <u>profile</u> plane. This requires data values to be relative to a rotatable reference plane. If rotation is not considered, i.e. field data is used as measured, then a second possible equation is:

density =
$$\rho_p$$
 = $\frac{\text{number of contour lines}}{\text{arc length}}$ (2.2)

for the portion of surface under consideration. This has limited practicality as the values obtained by (2.2) will vary as geometrical shapes change orientation.

For a flat plane, the angle of arc is zero and hence density is zero, causing contour lines to become contour surfaces*; whereas, for the hinge of a chevron fold, the arc length is zero, giving an infinite density value.

2.2.2.8 Radial Density of Contours

A second density measure can be defined when considering the variation in trend values of contours. For instance, with horizontal conical folds contour lines radiate away from high density (ρ_p) portions of hinges to low density portions. The radiating lines can be assigned density values, ρ_r , using the equation for ρ_p , i.e. (2.1), but substituting parameters measured in the reference plane.

2.2.2.9 A Description of Cylindricity

"Cylindrical" and "conical" are terms used to group fold shapes into two broad categories, as each category implies different stress and strain histories. There are two methods of deriving a quantitative measure of the degree of cylindricity of a fold. The simplest is to measure the half-apical angle of the best small-circle fit to a pole figure. A second method is to use ρ_r ; which involves more detailed computations. The use of S.O.D.A. maps (following chapters) gives a strong visual measure, provided care is taken in deriving the maps (following section).

A definition of cylindricity is described by Charlesworth et al, 1976. It is a statistical measure that gives a quantitative value computed from the eigenvalues of pole figure distributions. (Eigenvalues define data distributions in a similar fashion to symmetry elements (see Turner and Weiss, 1963, p.44). Woodcock (1977) discusses limitations of using eigenvalues for describing fabrics.)

The term "cylindricity" (and conversely "conicity"), as used throughout the remainder of the thesis does not refer to either measure explicitly but to the concept of the departure of a fold from, or its 'goodness-of-fit' to, a perfect cylinder.

2.2.2.10 Contours On Map Projections

The distortion due to the orthographic projection of contour lines (Fig. 2.5b) must be considered when analysing contour maps of structural models (e.g. Fig. 2.17). For example, isodip lines on the surface of a

^{*} A contour surface (see §2.2.2.1) on a geometric surface can be regarded as having a zero count if the section of arc under consideration is within the contour.)

sphere will show an exaggerated increase in \nearrow_p with increasing dip values (Fig. 2.17d). This is compounded by the fact that isotrend and isodip contours do not contain height information, which is implicit in other contour maps such as strike-line maps.

Field structural data measurements may be derived from a family of structure surfaces that make up one or more layers. The ground surface which exposes these surfaces can be represented diagrammatically as a plane transecting the geometry (e.g. Fig. 2.5a). The resulting pattern of isotrend and isodip contours will result from a combination of changes in structure with depth and extent. Therefore a map of contours from a field example may not match that expected for an ideal model produced by orthographic projection (above). This is further discussed in §2.3.3.7.

Contour lines for shallowly plunging folds can be used to indicate the curvature of folds by observing the line densities, ρ_p . High density hinge regions and low density limb regions indicate highly angular folds; uniform densities throughout indicate rounded folds; and low density hinges and high density limbs indicate flat hinges and rounded limbs (box folds). Note that such interpretations must take into consideration the way in which these patterns are derived (Fig. 2.5).

When folds have moderate to steep plunges the traces of contour lines on the ground express both the curvatures of folds and their cylindricity (Fig. 2.6b). That is, the traces represent dip isogons on the profile planes of folds. In this case, orthogonal projections and ground transections give rise to similar patterns, viz., those for profile planes.

2.2.2.11 Behaviour of Contours During Change in Geometry

As geometries change orientation, contours will shift their position if the reference plane is not rotated accordingly. Two different situations arise because of the two forms of data collection (§2.2.2.10).

(a) <u>Bodily Rotation</u>. With bodily rotation, contours move in a predictable fashion (e.g. as seen on a stereonet, Fig. 2.4). Either pole or dip vector diagrams can be used to demonstrate this as they give the same results.

The rate at which contours will move on rotation of the geometry depends on both the orientation of the geometry and on the contour density at each point of the profile plane shape. Subhorizontal portions of structures can have relatively large rates of change of isotrends (refer to Fig. 2.4b) compared to subvertical portions, whereas those portions with poles that sweep out a vertical plane during rotation (e.g. in the near vicinity of hinge lines of upright folds rotated around a horizontal axis) will experience the greatest rate of change in isodips. In regions of a structure that have relatively high densities due to small radii of curvature, contours move slowly. In low density regions the movement can

be very rapid. The <u>sensitivity</u> of the spatial position and orientation of isotrend and isodip contours to changes in the orientation of a geometry is a property that can be utilized in describing the roundness of portions of geometries.

The direction of movement of contours, and their appearance and disappearance can be observed from stereonets. Consider the pole figure for a horizontal fold (e.g. Fig. 2.4). As the fold is rotated, isodip contours enter at the extremity of the limbs (points of inflection), and move towards the hinge line, where they exit the fold. On the other hand, all isotrend contours are initially contained within the hinge line, and as the fold is rotated they move progressively outwards towards the limb extremities, where they exit the fold.

(b) Changes in Shape. As a structure changes shape with depth (such as a "non-similar" fold) the contours for each shape will change. Changes in profile shapes and cylindricity contribute to changes in contour patterns. The degree and rate of movement depends on the change in radii of curvature for the different parts, as discussed above and as shown by Ramsay (1967, p.359ff). This is given detailed consideration in §2.3.

2.3 TREND SURFACES

2.3.1 Introduction

Having defined the basic properties of orientation data, it is now necessary to examine their usefulness in performing trend surface analyses. To determine whether isotrend and isodip lines and surfaces are capable of unambiguously defining trend surfaces we need to: 1) define a set of basic geometrical models from which all practical trend surfaces can be constructed; and 2) determine the contour patterns that arise for each model, firstly for a single surface (contour lines) in an upright horizontal position; secondly for a finitely thick layer in an upright horizontal position; and thirdly for the model rotated into various orientations. In all cases, the reference plane is understood to be the horizontal plane. For a rotated reference plane, the models must be rotated until the reference plane becomes horizontal.

Any curvi-planar geometric surface can be considered in terms of its constituent primary shapes. For the practical purposes of structural geology, a number of simple shapes that are related to possible structure surfaces are defined. These consist of planes, cylindrical folds, conical folds, and spherical and elliptical domes, which are subsets of the mathematically ideal geometric shapes of planes, cylinders, cones, spheres and ellipsoids, respectively. The above shapes can be considered in the

following categories: planar/non-planar, cylindrical/non-cylindrical, and straight-hinged/curved-hinged.

With a purely mathematical definition of primary shapes, there are no possible ambiguities. However, strict definition is impractical for the purposes to which trend surface analysis is here applied. Approximations due to scaling factors need to be considered. (For example, an undulating plane may be regarded as a plane although it may be more correctly defined as a series of small amplitude domal folds of long wavelengths. Whether the plane or the constituent domes are of importance depends on the scale desired.)

2.3.2 Planar Surfaces

The plane (Fig. 2.17a) is the most trivial of geometric models. All points on a plane have the same trend and dip values. One isotrend surface and one isodip surface defines this geometric surface. A finitely thick layer is defined by corresponding isotrend and isodip volumes.

Truly planar features are rare in geology. Hence, geological planes may consist of a number of discontinuous contour lines with a limited range of values due to small scale perturbations. The patterns they form may be complex and highly irregular (for example, see the limb region of the fold in Fig. 2.22b).

2.3.3 Cylindrical Folds

2.3.3.1 Upright Horizontal Rounded Folds

A very open (rounded) fold can be produced by bending a horizontal plane. As soon as curvature is introduced, the isotrend surface representing the plane divides into two isotrend surfaces, one for each limb, whereas the initial isodip surface divides into a number of isodip lines (Fig. 2.7a), the number increasing the more the fold is bent.

The pole to the infinitesimally small area of the hinge line of the fold is plotted at the vertical on a pi diagram. As all radial isotrend lines on a polar net meet at this point, it has an indefinite isotrend value. From §2.2.2.6, the hinge line of this fold can be regarded as containing an infinite density of isotrend lines. Hence the fold in this position has the maximum number of isotrend lines possible.

2.3.3.2 Angular (Chevron or Kink) Folds

Two non-parallel planes intersect, giving rise to an overall geometry generally termed a kink or chevron fold. The line of intersection is termed the fold hinge. Accordingly, the fold is represented by two u-isodips and two u-isotrends. If either of the b-contours are used then fold orientations may be encountered where the two b-isotrends or two b-isodips become equivalent.

The discontinuity between the two limbs at the hinge may be

regarded in two ways, either as a discontinuity or as a continuous surface of infinitely small radius of curvature. Accepting the hinge as being a discontinuity requires that chevron folds be regarded as a special case, separate from hinges with a finite hinge region. This is unnecessary as the hinge can be regarded as being an infinitesimally narrow region of infinite contour density, containing contour values between those represented by the limbs, i.e. an extreme case of the phenomenon described in \$2.3.3.1.

2.3.3.3 Upright Rotated Folds

If the fold is rotated, but the axial plane kept upright (Figs. 2.7 and 2.17b) the number of contours changes, as can be seen in the changing number of intersections between the pole figure distribution and the isotrend and isodip contours of the polar net (see §2.2.2.5), and in the block diagrams (Fig. 2.7). At the extreme rotation, when the fold hinge is vertical, the number of isotrends is at the minimum possible, as is the number of isodips (just one, represented by an isodip volume. Two u-isodip volumes would appear if uni-directional isodips were used.)

2.3.3.4 Reclined Horizontal Folds

When the axial plane of a horizontal fold is rotated so that it is no longer vertical the contours will vary, in a similar fashion to that described in §2.3.3.3. The behaviour of the contours can again be examined by using stereonet plots.

In Fig. 2.8, profiles of a "similar" style fold in various degrees of inclination are presented with their appropriate stereonets. first four cases (Figs. 2.8a to d), the interlimb angle is less than 90°. In the first case, the standard situation of an upright horizontal fold (as for Fig. 2.7a) is given, i.e. two isotrend volumes with an infinite density of isotrend lines contained in the axial plane. During rotation, the two contour volumes move with respect to the geometry. In the third case (Fig. 2.8c), three isotrend volumes occur: two volumes identical in value separated by a third. One of the two identically-valued volumes represents the overturned portion of the middle volume. Note that only one of the boundaries between two adjacent volumes (arrowed) contains an infinite density of isotrend contours, while the other contains none density). These particular densities are discussed in §2.2.2.6. extreme case (Fig. 2.8d) the axial plane is horizontal. Again, only two volumes occur, one of which represents a completely overturned limb while the other remains upright. In this case there are no isotrend contours between the two volumes. The fifth case (Fig. 2.8e) is similar to the third except that the angle of arc is less than 90°. In this situation one limb does not achieve any horizontal dips, and the other limb does not attain vertical dips. The entire fold is then represented by one isotrend volume.

2.3.3.5 Folds of any Other Orientation

By applying the arguments and discussion presented in relation to rotated upright folds (Fig. 2.7) and horizontal reclined folds (Fig. 2.8), folds of any orientation are interpretable. By referring to a set of Fig. 2.9), stereonets covering the various orientations (e.g. understanding of the behaviour of contours can be reached. Parts (a)-(c) of Fig. 2.9 refer to Fig. 2.7, and parts (c), (e) and (f) refer to Fig. 2.8. Part (d) represents some combination of fold plunge and axial plane inclination which is derived by rotating (b) by (e) around (b)'s fold axis. That is, a fold with (b)'s fold axis orientation and an axial plane with (e)'s inclination, Fig. 2.9g. There is a restricted range of possible combinations of fold plunge and inclination, viz., the fold axis cannot plunge steeper than the dip of the axial plane (or, alternatively, the axial plane cannot dip more shallowly than the plunge of the fold axis).

2.3.3.6 Fold Classification

So far, finitely thick folds have been generated by considering two identical folded surfaces positioned such that they define the bounding surfaces of a thick (i.e. finitely thick) layer (Fig. 2.2). This type of fold, termed "similar" or class 2 of Ramsay (1967, fig. 7.24), has the simplistic property that all isodip and isotrend surfaces are planar and parallel, irrespective of their number or of the fold orientation. If however the two bounding surfaces are not identical then other classes of folds are created (Fig. 2.10). Ramsay (1967, p.365) defines three classes, depending on the relationships between adjacent dip isogons (or change in relative inclination of adjacent layers), i.e., convergent isogons are Class 1 ("a" are strongly convergent, "b" for 'parallel folds', and "c" are weakly convergent); parallel isogons are Class 2 ('similar folds', as for all models so far shown); and divergent isogons are Class 3. For all fold classes the contour surfaces (isotrend or isodip) are planar, and further, there is a simple relationship between adjacent contour surfaces.

The intersections of contour surfaces with profile planes give rise to patterns identical to the dip isogon patterns used by Ramsay (op. cit.) for classification. Consequently, the various complications that arise with real fold classifications (as discussed by Ramsay, op. cit.) apply. That is, the use of fold shape parameters (and first and second derivatives) plotted against dip isogon values often gives rise to different fold classes in different parts of the fold limbs. The values of

the dip isogons will depend on the orientation of the reference plane relative to the fold, and so is some function of trend and plunge. In standard procedures for deriving dip isogons the reference plane is always normal to the intersection of the axial and profile planes (§2.2.2.3).

2.3.3.7 Transections Through Folds

Patterns of isotrend and isodip contours (on a map derived from data collected on the earth's surface, i.e. the transection of a fold with an erosion surface*) result from a combination of fold cylindricity and profile shape. If, for instance, a fold is upright and horizontal, then profile shape has no effect and all contour lines will be parallel to the axial plane trace. On the other hand, an upright but plunging fold of class 1A gives rise to a diverging pattern, whilst a similarly orientated class 3 fold gives rise to a converging pattern (similar to the patterns for horizontal conical folds, shown in the isotrend and isodip columns of Fig. 2.17c and Fig. 2.6).

An understanding of the fold geometry of a three dimensionally exposed minor fold (e.g. in hand specimen) from the contour surfaces is relatively simple. However, the information, once it is restricted to a single transecting plane as is the case in major or mapped folds, is more limited, and may be ambiguous (see also §4.2). Nonetheless, an understanding of fold geometry can still be derived provided that the geometry being analysed reasonably approximates the ideal models shown in Fig. 2.10. For instance, a distinction can be made between conical folds and class 1A or class 3 cylindrical folds for a radiating contour pattern similar to that for isotrend contours of Fig. 2.17c by the fact that firstly, pole figures distinguish between conical and cylindrical folds (e.g. Fig. 2.17); and secondly, the direction in which contour lines converge in relation to the direction in which cylindrical folds plunge separates class 1A (or class 1B) from class 3 folds.

2.3.4 Non-cylindrical Folds

2.3.4.1 Conical Folds

The simplest non-cylindrical fold shape is a cone[#], of which circular cones are the basic form. As circular cones constitute a subset of the general class of elliptical cones, the following discussion is not restricted to any particular form. For an upright horizontal fold of a

^{*} In the following discussion it is assumed that the erosion surface is planar and horizontal, and so appropriate allowances must be made for ground surfaces with other than this configuration.

[#] Conical folds are defined here as being cone shaped, and therefore have straight fold hinges.

conical shape (Fig. 2.17c) the procedures described above (§2.3.3) can be repeated. A conical surface can be generated by changing the curvature of the fold profile along the (straight) fold hinge. This causes isodip lines to radiate outwards from the tighter curvature (from a high profile density region to a lower profile density region). The isotrend lines behave in a similar manner. From the pole figure of Fig. 2.17c and §2.3.3.1, there is an infinite density of isotrend lines in the hinge of the cone, as there is for upright horizontal folds.

Conical folds can exceed the maximum possible range of 180° for trend values in any one cylindrical fold, with a possible maximum of 360° for convoluted folds (e.g. in ptygmatic folds). For both types of folds, the possible values for the indefinite trend value of a vertical pole is defined as the limiting case as plunging folds approach the horizontal. For example, in Fig. 2.7, as the vertical fold is rotated towards the horizontal, the range of isotrend contour values increases from 110° towards 180°. That is, the range of isotrend values is a set of angles, [110°,180°), which is closed at 110° and open at 180°. When the fold becomes horizontal, the set closes at 180°. It is meaningless to introduce a catastrophic increase to 360°.

The various classes of folds (Ramsay, op. cit.) can be generated for conical folds as they were for cylindrical folds. However, apart from class 2 similar folds (Fig. 2.11a) contour surfaces are not planar (e.g. Fig. 2.11b). The bounding surfaces of non-similar folds must curve differently to each other. So, unless the rates of change of curvature along the direction-of-movement vector (see Fig. 2.2) are constant throughout the length of conical fold hinges, the vectors joining points on the upper surface (as for Fig. 2.2) to the corresponding points on the lower surface will be skew to their neighbours in the same contour. The resulting contour surfaces will therefore not be planar (Fig. 2.11b). Conical folds which have planar contour surfaces should rarely occur.

2.3.4.2 Spherical Domes

Real non-cylindrical folds tend to have curved fold hinges, which require an understanding of the next class of fold shapes, the ellipsoid. The ellipsoid is a general shape and will be easier to understand if the special ellipsoid, the sphere, is analyzed first.

A mathematically perfect spherical dome surface has no preferred orientation and hence no fold hinge (Fig. 2.17d). Isotrend lines radiate outwards from the centre of the dome with constant radial density, and isodip lines are concentric circles of constant profile density. However, on projection of the latter contours onto horizontal maps, such as

Fig. 2.17d, artificially high density values occur for isodips at higher dip angles (§2.2.2.10).

By the same methods employed earlier (Fig. 2.2), contour surfaces can be generated by moving a single dome surface in three dimensions (Fig. 2.12). In this case, the direction-of-movement vector is along the dome radius, originating from the point on the sphere's surface with a horizontal gradient, and directed towards the centre of the sphere. The various fold classes (Ramsay, op. cit.) can be generated for domes as they were for folds, by the same method of changing curvature. A class 2 dome is presented in Figs. 2.12a,b, and a class 3 dome isodip configuration is shown in Fig. 2.12c.

Two further cases are worthy of consideration, firstly when the ground surface is not horizontal, and secondly when the dome is asymmetric.

To appreciate a sloping ground surface, consider the concentric (class 1B) dome of Fig. 2.12d. Transecting the figure by a plane in any orientation will give rise to a set of radiating isotrend lines of varying density, and isodip lines forming a set of concentric ellipses, on the transecting plane (Fig. 2.12e). When projected onto the horizontal (e.g. for topographic maps), the isotrends attain an equal density distribution, and the isodips revert to circles, albeit not concentric (Fig. 2.12f). The isodip circles do share a common point where the isotrends meet.

Asymmetric domes can be generated in the same manner as symmetric domes, except the direction-of-movement vector is no longer directed at the centre of the sphere (Fig. 2.12g). Isotrend surfaces generated are the same as before except that they are bodily rotated so that the previously vertical line of intersection is now parallel to the inclined direction. Isodip surfaces form cones with elliptical cross-sections. A transecting horizontal plane gives rise to a set of radiating isotrends very much like that for Fig. 2.12e, and a set of concentric isodip circles (Fig. 2.12h).

Finally, transecting an asymmetric dome with a dipping plane will give rise to radiating isotrends of variable density, and non-concentric elliptical isodips. On projection to the horizontal, full symmetry will not quite be restored, with the final pattern still appearing as for the transecting plane, but with less departure from full symmetry. For subhorizontal transecting planes and approximately symmetric domes, the resulting isotrend and isodip maps for spherical domes of any fold style will always appear similar, the former a set of radiating lines of approximately equal density and the latter a set of nearly concentric, slightly elliptical circles.

2.3.4.3 Ellipsoidal Domes

Geological domes are generally not spherical, nor do non-

cylindrical folds generally have straight hinges as do conical folds. Folds with noticeably curved fold hinges are generally described as "double-plunging" folds, provided that they do not resemble spherical domes. They can be approximated by ellipsoids, although folds may also resemble portions of other conics, such as parabolas and hyperbolas, as well as ellipses and circles. As spherical domes are special types of ellipsoidal domes, many of the principles previously discussed apply here. With the x axis denoting the largest principal axis, y the intermediate axis, and z the shortest axis, the dome is designated to be horizontal if the x axis is horizontal, and upright if one of the principal planes containing the x axis is upright and the fold envelope is horizontal. Fig. 2.17e shows the contour patterns for an upright horizontal ellipsoidal dome. Parameters describing ellipsoidal dome geometry are given in Fig. 2.13.

It can be noted that maps (of either projection) of isodip lines (e.g. Fig. 2.17e) are not similar to strike-line maps, as they are for spherical domes and upright, horizontal cylindrical folds. vary in height (Appendix E; Fig. 2.14b), being highest where they cross the yz principal plane and lowest where they cross the axial plane. isodip line is horizontal everywhere and therefore is the only one which parallels a strike-line. Isotrend lines (Fig. 2.14a) radiate outwards from The density increases in the the centre, but not with uniform density. region of the fold hinge. For an upright horizontal dome, isodip lines are controlled by the ratio of the two horizontal principal axes (one of which will be the x axis). As the dome is rotated around a horizontal axis, all three principal axes contribute to the isotrend lines. (Fig. 2.15), if the axial plane of an upright horizontal ellipsoidal dome is the xy principal plane (so x and z are the two horizontal axes), then the isotrend lines have maximum possible density around the x axis, and minimum possible density around the z axis. As the ellipsoid is rotated around the normal to the axial plane (z axis) isotrend lines move away from Then y and z are the two the x axis until the ellipsoid is vertical. horizontal axes, with maximum density around the y axis (but less than previously) and minimum density around the z axis (but greater than before).

The departure of isodip lines from elliptical shapes depends on the ratio of the two horizontal axes, with greatest departure occurring when the x and z axes are horizontal and less so otherwise (Appendix E).

By using the same arguments as those for spherical domes, any subhorizontal plane transecting an ellipsoid of any orientation will give rise to radiating isotrend lines of non-uniform density, and an approximately elliptical pattern of isodip lines. The departure from

elliptical shapes for isodips becomes more pronounced as the ratio of the acting horizontal long axis to the acting short horizontal axis increases. As before, isotrend lines are independent of style, but isodips are dependent, provided the bounding surface ellipsoids do not change principal axes ratios. If they do change, then twisted contour surfaces can arise. Provided the change is not too great then the previously mentioned contour map patterns still hold. For real examples, this latter complication probably contributes more to the variability of contour map patterns than does fold style.

2.4 COMBINED GEOMETRIES

As individual models to classify real folds, the above ideal geometries will rarely be sufficient to analyse geological structures. Even simple folds may have to be modeled by using portions of different geometries. For example (Fig. 2.16), simple non-cylindrical folds may be constructed by using combinations of conical and ellipsoidal domes for fold hinge regions, and limbs constructed from ellipsoidal domes and planes. Other non-cylindrical folds may require changes in parameters describing conic sections along, and/or out from, their fold hinges (or even changes in type of conic sections, e.g. parabolic hyperbolas) to describe them accurately. As long as the basic patterns (Fig. 2.17) can be recognized, then judicious use of subarea analysis (Appendix S) will enable geological folds to be analytically dismantled into parts approximating ideal geometries.

2.5 SENSITIVITY OF ISOTREND AND ISODIP LINES

For those portions of structural surfaces where strike-lines are nearly straight, isotrend lines are very sensitive (§2.2.2.11). Any small perturbations in these strike-lines will result in large spatial shifts of the isotrend lines. The same applies to isodip lines in portions of structural surfaces where dips are nearly constant, i.e. the spacings between quantitative strike-lines, when projected onto maps, are constant. Hence, in places where isotrend and/or isodip lines are low in density, the lines can be very sensitive, and large spatial variation giving rise to complex patterns can be expected. The reverse is true for isotrend lines where strike-lines have small radii of curvature (i.e. densities of isotrend lines are high); as it is for areas containing high densities of isodip lines. Examples (Fig. 2.21b and 2.22b) demonstrating contour sensitivity can be seen in §2.7.

2.6 DETECTION OF GEOLOGICAL DISCONTINUITIES

Geological discontinuities (e.g. faults and erosion surfaces) may Movement isotrend/isodip contour maps. detected using be transcurrent faults will displace isodip and/or isotrend patterns, and movement on normal (or reverse) faults will juxtapose one geometry against another. Provided that enough orientation data is measured to detect such anomalies on a desired scale, then those discontinuities that can still be expected to avoid detection are ones that give rise to very similar contour patterns on both sides of discontinuities. These include planes, provided faults are non-rotational; cylindrical folds displaced by a multiple number of wavelengths, measured in a direction coplanar to their fold envelopes and normal to their fold axes; similar style folds displaced along their axial plane, with any amount of horizontal and vertical component; and minor faults parallel to fold hinges. In all these cases, the scales of these structures relative to their discontinuities must be such that in areas under analysis the geometries on either side of the discontinuities are equivalent (which depends on data density, i.e. the number measurements taken per unit area.) Other situations in which faults and erosion surfaces may go undetected are in those parts of the geometries which have sensitive isodip and isotrend contours patterns. In such cases, provided that contours are sensitive on both sides of discontinuities, then complex patterns may mask the existence of geological breaks.

2.7 APPLICATION OF CONTOUR ANALYSIS TO REAL FOLDS

2.7.1 Introduction

foregoing theory is dimensionless and so theoretically applicable to structures of all scales, from microscopic to megascopic. Although only a limited range of sizes are suitable in practice for analysis of data collected on a single structural surface, the range of sizes suitable for analysis of transections through structures are Single structural surfaces varying in size from microscopic to a few centimetres are physically too small to allow a large number of orientation readings to be taken over their surface without There are alternative methods for construction of a special device. describing structure morphology on such a small scale (e.g. Stone and Dugundji, 1965; Skjernaa, 1975). Hand specimens (up to approx. 100 kg) are manipulable and so suitable for contour applications. Larger mesoscopic structures can be measured in situ, but may not have 100% of their surface Structures larger than mesoscopic will generally only have transections available, rather than their geometrical surfaces. These are suitable for contour analysis, although interpretations will be different (§2.2.2.10). Some possible exceptions to this are large open structures (e.g. Shelton, 1966, p.84), and gneissic domes (e.g. Ollier and Pain, 1980). Any method of contour analysis which is applicable to sections can also be applied to thin sections whose grain (crystallographic) orientations have been measured.

Of the above scales, the one most easily subjected to contour analysis is the hand specimen. Larger scales are less readily analysed, but they constitute by far the greater proportion of structural problems (e.g. tectonic map analysis, basin studies, and orebody exploration), and are therefore considered more important in the present thesis than the development of a simple hand specimen classification system. Therefore, although at the scale of the hand specimen it would be possible to refine the theory of isotrend/isodip contours, in a similar manner to that of dip isogons, i.e., to develop fold surface classification procedures (an expansion of §2.3 and §2.4), and three-dimensional fold classification procedures for serially sectioned specimens, considered more important in this study to apply the theories and techniques developed here to more general problems in structural geology. However, a number of real hand specimen samples were analysed and the remainder of this chapter presents examples of contours on real fold surfaces to demonstrate the variations that may be expected between the mathematically perfect models described above and those real fold examples The following examples are demonstrative only; they are found in nature. not examples to confirm the accuracy of the foregoing models (§2.3).

2.7.2 Technique

There are a number of possible methods of finding the isodip and isotrend lines on the surface of a handspecimen sized structure. The method described here is fast and accurate. Strike-lines are first generated on the surface, and from this the isotrend lines are then derived. Isodip lines are directly generated on a structural surface by setting a clinometer to a dip value, and then tracking the loci of points to which the clinometer is tangential, and orthogonal to the strike-lines through the points.

An apparatus designed for this technique was developed in this study and is shown in Fig. 2.18a. A specimen is mounted on a levelled platform, on a trolley that is free to rotate and translate. A laboratory laser is mounted on a retort stand, with a clinometer attached so that the laser beam (reduced in intensity by filters for eye safety) can be set at any angle of declination.

Strike-lines are produced by tracing a horizontal laser beam on the surface (e.g. the solid lines in Fig. 2.19b). Once strike-lines are marked then the isodip lines are found by the above conditions (Fig. 2.18b, e.g. the dotted lines in Fig. 2.19b). The final stage is to produce a map of the lines by orthogonal projection (Fig. 2.5b). This can be done by photography (e.g. Fig. 2.19b) or by other means (e.g. Fig. 2.18c).

Isotrend lines are interpreted from maps of strike-lines by the simple procedure of joining points on the strike-lines with the same trend (tangential to the strike-lines at those points).

This procedure is applicable only to convex surfaces. Concave surfaces are not suitable unless both bounding surfaces of a specimen are similar, in which case the specimen could be inverted.

2.7.3 Unoriented Sample of a Conical Fold

The specimen (Fig. 2.19a) is a pelitic (mica) schist Kanmantoo, South Australia. It weighs approximately 100 kg, and represents the largest size that is readily manageable. The specimen was orientated with the hinge line of the antiform north-south (Fig. 2.2la), the axial plane vertical, and the hinge at the south end horizontal (i.e. the reference plane contains the fold axis and is perpendicular to the axial The fold surface, in the hinge region, is almost conical with the fold hinge only slightly curved. The limbs are reasonably planar. asymmetry of the limbs (Fig. 2.21b) can be seen from one side (east) being planar at the south end and very short at the north end (passing through the point of inflection very quickly to the adjacent synform). The reverse holds for the west limb. A mineral lineation on the surface displays a radiating pattern. The profiles of the fold ends (Fig. 2.21b) show a marked change in fold curvature from the tighter (south) end to the open (north) end. Due to the curved hinge, the north profile has a hade corresponding to the 12° plunge of the hinge (the dip values on these profiles are true dips, not necessarily matching dip isogons). resultant isodip and isotrend lines are close to the ideal discussed earlier, with only a small amount of discrepancy caused by procedural (approximation) errors and the fact that there was no single fold surface but rather a number of them, each a few millimetres thick. This latter problem causes horizontal displacement of the contour lines.

The small degree of hinge curvature causes the lower valued isodip lines to cross the hinge line (Fig. 2.2la), as expected for ellipsoidal domes and combinations thereof with conical folds (see Fig. 2.16). Isodip lines become irregular in orientation where the limbs are flat, due to high sensitivity.

The isotrend lines (Fig. 2.21a) show a similarly expected behaviour. The lines are very irregular in the flat limbs where strike-lines are nearly, but not quite, straight. In the hinge region they are

well behaved, and exemplify the patterns expected for conical folds.

This fold is further analysed using the computer package described in Chapter 3, and the results are presented in §5.3.1.

2.7.4 Orientated Specimen of an Approximately Cylindrical Fold

The specimen (Fig. 2.20a) is a small fold of granitic gneiss from Enderby Land (P. James, personal communication) which folds a gneissosity. Its surface forms a plunging, slightly conical fold with a weak to moderately curved fold hinge (18° of curvature). It was orientated as an upright plunging fold (25° towards 215°). The fold is rounded with an overall tight closure. The hinge region has a less marked change of fold curvature along the length of its axis, but is overall tighter at the south end than it is at the north end (Fig. 2.22b). The limb regions are relatively flat, as in the previous example. The fold surface, athough a gneissosity, still forms a reasonably consistent single surface.

The isodip map (Fig. 2.22a) shows a similar pattern to that of a combined ellipsoidal dome and conical fold (Fig. 2.20b), with isodip lines in the limb regions approximately parallel to the fold hinge, but close across the hinge. The western limb appears reasonably well behaved, showing some flatter and some more curved regions. The eastern limb shows a very sharp change in dip along a linear boundary that converges on the fold axis. Small flat areas (stippled) represent isodip surfaces.

The isotrend map (Fig. 2.22b) shows an overall geometry similar to that of Fig. 2.20a, i.e. an overall radiating pattern. The hinge region shows a markedly cylindrical pattern of parallel lines (compare with Fig. 2.7), reflecting the reasonably constant fold curvature in the hinge region mentioned above. Away from the hinge, the lines rapidly radiate outwards from the southern end of the fold, demonstrating the overall tighter southern end and more open northern end. The correspondence between the straightness of strike-lines (Fig. 2.22b) and the sensitivity of isotrends is well demonstrated in this example. In the eastern limb, where the strike-lines are particularly straight, the small perturbations cause quite complex isotrend patterns whereas in the hinge region, where the strike-lines are highly curved, the isotrends are well behaved. It is interesting to note that the strong linear feature in the isodip pattern does not appear in the isotrend map because of its linearity. A good correlation between the isodip and isotrend patterns is observed.

This fold is further analysed using the computer package described in Chapter 3, and the results are presented in §5.3.1.

2.8 DISCUSSION

This chapter has developed the foundation for the application of

trend surface analysis to structural geology. It has examined simple models of most types of structures to be found in geology and noted how the isotrend and isodip contours behave for each model. It has been shown that, although the models have unambiguous contour patterns, transected models can be ambiguous. However, it was also shown that the ambiguiuty can be resolved with the use of stereonets.

The theory is sufficiently developed to enable a practical application of the technique to be undertaken (following chapters). However, it is known that statistical techniques must be applied to structural data to increase the power of trend surface analysis to structural geology. For example, simple geometrical shapes with highly irregular surfaces on a small scale can be difficult to recognize due to the unnecessarily complex contour patterns that can arise (i.e. parts of structures with highly sensitive contours have very complex contour patterns for very simple shapes). In such cases, servo-analytical techniques, such as power spectrums, may be required to aid in interpreting results.

The dictum "near enough is good enough" is acceptable for many applications in this initial development of trend surface analysis in structural geology. However, future development of trend surface analysis in structural geology to the stage where statistical (inferential) mathematical techniques may be commonly applied, will necessitate a more rigorous, or mathematically correct, definition and categorisation of geometrical shapes, such as polynomial equations (Doornkamp and King, 1971; Evans, 1972) or Fourier Series (e.g. Stabler, 1968; Hudleston, 1973a).

CHAPTER 3

A COMPREHENSIVE COMPUTER PACKAGE FOR SPATIAL ORIENTATION DISTRIBUTION ANALYSIS (S.O.D.A.)

3.1 INTRODUCTION

It was outlined in §1.3.4 that a unified computer-aided approach would be the best means of processing, interpreting, and displaying of structural data. This chapter describes the computer implementation used to make the S.O.D.A. technique (previous chapter) a practical procedure. Not only does this include programs to produce and display isotrend and isodip contours, but also includes a number of support programs (e.g. domain analysis, structure maps (maps with structure symbols plotted), cross-sections, block diagrams and stereoplots), to form a comprehensive computer package suitable for general geometric analyses.

The procedure for deriving a geometric interpretation from a data set is a repetitive one, requiring much plotting and replotting of data on structure maps and stereoplots until a consistent result is derived. This is greatly aided by the use of domain analysis (Turner and Weiss, 1963). Domain boundaries are not immediately known but require repeated plotting and analysing (Appendix S).

Computer programs that perform repetitive processing under human control are best written for interactive use. An interactive program package provides a palette of functions (e.g. CAD/CAM) from which an interpreter may select to derive a solution. Thus the previously manual methods of selecting data subsets, plotting them on maps and stereoplots, and analysing them have been automated. To be successful the computation and display of results must be clear, accurate, unambiguous, and performed rapidly. Also, the more often a particular operation is required the faster it must be. Psychologically, delay times of even a few seconds can be inhibitive (Newman and Sproull, 1973) if such operations are required often enough, even if they are very much faster than all available alternatives.

Standard display peripherals (such as line printers and pen plotters) are acceptable for the simple display of data. However, for interactive computer processing, they are generally not suitable for the display of intermediate results. Interactive colour graphics is one of the most powerful mediates for user/program interaction and display.

The compilation of the program package was made from a number of existing programs and others written for the purpose. Existing programs are generally incompatible with each other because they were developed independently. However, only programs that needed to be developed or required extensive modification are described here and in the appendices.

3.2 PROCESSING SYSTEMS

3.2.1 The Ideal System

An optimum design for an interactive computer package must minimise the real-time retrieval and display of data, and effectively reduce the number of iterations necessary for achieving results. Such a computer package (Fig. 3.1) for converting raw field data into displays of completed analyses should have programs for:

- 1. standardisation of all data,
- 2. data bank creation and maintenance,
- extraction of data subsets,
- 4. analysis and display of orientation data,
- 5. analysis and display of structural and other geological maps,
- 6. analysis and display of orientation data in a spatial framework, and
- 7. production and display of three-dimensional diagrams (e.g. block diagrams) as well as other types of diagrams (e.g. graphs, digitized fold profiles).
- 1) A facility for standardisation and basic manipulation of data should be available and very easy to access and use.
- 2) Creation and maintenance of data files in a data bank is a large and involved area of computer applications in geology. Both general and specific systems have been devised for geologic use (§1.3.2.1). Although data banks need only store structural data for structural analyses, the capability to store other (pertinent) geological information enhances the capabilities of the system. For convenience of position and orientation, geographic data files (i.e. ground reference data) should also be available. Other data types (e.g. geophysical, geochemical) could be maintained to allow an open-ended expansion of the system.

Boehm et al (1980) describe a system whereby all structural maps are placed on file. Whereas they have merely catalogued the existence and description of maps, ideal structural data files should also contain digitised versions of them.

once a data bank is available then it should be a simple matter to extract a desired map for analysis. An extracted map may not necessarily be a particular source map, but a composite of a number of maps. Hence an efficient method of extracting the correct information is required. Determining which point data (e.g. data stations, bore-hole locations) are contained in a defined area for analysis does not pose problems as efficient methods for determining points in polygons exist (Alfred, 1972; Hall, 1975; Salomon, 1978). However, determining which portions of lines lie inside a map is computationally more involved. A further problem is that as the scale of a map becomes greater, small scale data references may

cease to be of significance (and even detrimental), as well as unnecessarily increasing computation times. This can be avoided by weighting all data items (§9.3.1).

Analysis of an extracted map may be conducted by a number of functions. So there is a need for all analytical programs to be able to access the same data files as well as one another and previously computed results. Analytical programs should consist of routines that can construct cross-sections and block diagrams, analyse orientation data and spatial distributions of orientations (geometrically and statistically), and produce trend surface analyses, among other functions.

Both rapid display of diagrams and high quality plotting equipment are desirable. For user interaction, high speed production of diagrams for modification and verification is required, as well as methods for rapidly entering data from the user. Detailed unambiguous plots of results are required for final presentation.

3.2.2 The S.O.D.A. System

The S.O.D.A. system developed here parallels the ideal in its structure (Fig. 3.2) but departs from it in content and usability. The system grew from an ad hoc collection of programs and was further complicated because the complete system could not be held by any one machine. The system further departed from the ideal as programs were written to specifically process thesis data (for expediency), as opposed to general data situations.

3.3 COMPUTER EQUIPMENT

3.3.1 Hewlett-Packard

A Hewlett-Packard desk-top calculator (see Appendix B) was used for easy-access simple data processing.

3.3.2 Cyber

The Cyber 173, and previously a CDC 6400, at the University of Adelaide were used for the larger programs requiring a powerful processor. These computers are very large and are fully equipped with standard peripherals (discs, magnetic and paper tapes, printers, plotters, and terminals). They are designed for processing many programs simultaneously, and so are unsuited to handle the detailed graphics processing required for interactive graphics. (That is, they are not suitable for dedicated computer programs.)

3.3.3 Nova

3.3.3.1 Hardware

The Nova2 (Fig. 3.3) is a minicomputer housed in the Department of Electrical Engineering of the University of Adelaide. It was retired at

the time of writing and had been extensively modified for research. It had 32K 16 bit words of central memory, of which the operating system used 11K words (1K=1024). Two 2Mbyte disc drives were available (although one was inoperational for the duration of this research). One nine track magnetic tape unit, and a paper tape read/punch unit were available. Two teletype (TTY) ports were supported by the system, one being the machine's console, while the second was shared between a Teletype (Model 43), a magnetic data tablet (Summagraphics Corporation, 1978), and the Cyber (see Appendix A). The central processor (CP) had access to a hardware multiply/divide, but not to floating point arithmetic. An HP pen plotter (as described in Appendix B) was the only hardcopy graphics device available. This machine was the only one available that supported interactive colour graphics.

Graphics are displayed on a colour monitor (BARCO CTVM 2/51) which is a raster type display with the refresh memory stored on a microcomputer, ULOS (Universal Lay-Out System; Davis, 1979). Interactive data input capability (stylus coordinates) is provided by the data tablet. A link between the Cyber and the Nova (via a terminal line) is available, and is managed by program CYBER (Appendix A).

The available hardware was slow in comparison to modern minicomputers, and also was prone to failure (machine stoppage) because of extensive experimental modifications. Consequently, these problems had to be considered when developing the programs (e.g. the programs had to be able to be restarted with limited loss of earlier results.)

The colour display consists of 512 x 512 3 bit pixels (one bit per colour: blue, green and red). With only one bit per colour per pixel, a maximum of eight colours (including black) can be displayed (Fig. X.3). As a consequence, software for producing variable colour tones had to be developed (Appendix X). ULOS was built to have a variety of plotting modes (monochrome, grey tones, see Davis, op. cit.) but most of these were unavailable.

3.3.3.2 Programming Raster Scan Displays

The display picture is stored in chip (MOSTEK MK4096) memory in ULOS (Davis, op. cit.). The display is refreshed from this rather than by the earlier methods of storing on disk (Lovercheck, 1972). Most of the literature (e.g. Giloi, 1978; Rogers and Adams, 1976; Newman and Sproull, 1973; Klinger et al, 1977) dealing with interactive graphics techniques assume that pictures are refreshed from a picture file maintained in central memory (CM) (Klinger et al, op. cit.; Walker et al, 1975), i.e. the picture is drawn using vector generators. The consequences following from differences between vector generated displays and raster displays are detailed below:-

- 1) Most importantly, a highly structured, efficient, compact picture file stored in CM is unnecessary. Inefficient disk files can be used to store data from which pictures can be generated. Hence graphics can be used quite readily without having to resort to special graphic languages (Kaneff, 1970; Lewin, 1975) and picture file maintenance routines.
- 2) Unlimited picture complexity is available with raster displays. Whereas screen flicker of vector generated displays was related to size and complexity of picture files (and machine speed), raster displays have removed this restriction (flicker is independent of picture complexity).
- There are two advantages of having this memory. (a) It can act as an extended central memory. When an unwanted colour is switched off, that colour's memory can be used as extended memory. ULOS has 16K 16 bit words per colour. Unfortunately, ULOS has a problem with random memory corruption. (b) It broadens the scope of practical graphical techniques. Because of inefficient FORTRAN compilers and slow machine speeds, many standard algorithms are prohibitively slow. For example, a point-in-polygon routine (Salomon, 1978) was impractical on the Nova. Given the ability to read display memory, an alternative technique could be developed (Appendix Q).
- 4) The repairing of pictures is generally more difficult with raster displays. When part of a picture is removed, remaining parts may be damaged. For instance, if one line of an intersecting pair is removed the remaining line is broken (in their common colours). For vector generated displays the picture is repaired on the next refresh cycle, but with raster displays, programs must be specifically directed to repair damaged pictures. If picture items are known to be temporary (cursors and "rubberband" lines) then they can be drawn in "inverse" mode (Appendix F). There is no conveniently reliable method for picture repair other than using a vector generated type display in the raster system. Consequently, a picture file must be maintained to refresh the display memory after an operation that causes damage is performed (R. Clarke, 1982).

3.4 DATA PREPARATION

3.4.1 Introduction

The initial step in computer aided structural analysis is to standardise all data, both in form and in orientation. This means converting all orientation data into one form, and rotating all orientations relative to the same reference plane (horizontal) and reference direction (true north).

3.4.2 Field Data

Structural readings are obtained in a number of forms (Compton, 1962) (e.g., "strike/dip", "pitch in a plane"), depending on particular recording preferences and necessity (Cruden and Charlesworth, 1976). These are standardised with program HPNET (Appendix B) using a desk top calculator (§3.3.1). This is a very easy and convenient stereonet plotting program is used to check for errors, obtain data consistency, and also enables a preliminary understanding of the data to be obtained.

3.4.3 Universal Stage Data

3.4.3.1 Single Axes

Orientations of single crystallographic (or optic) axes are directly convertable from Universal Stage axes readings (Turner and Weiss, 1963). Rotation of these orientations into their field orientations can be achieved by using program HPNET (above) or program CNTRFIN (Appendix H).

3.4.3.2 Multiple Axes

Calculation of the orientations of both biaxial mineral optic axes or of more than one crystallographic axis from universal stage axes requires more detailed computations (Turner and Weiss, op. cit.). Program HPHB (not described in this thesis) calculates the three crystallographic axes of (monoclinic) hornblendes for a four-axis universal stage. Programs for other minerals are not yet available. Rotation of data into field orientations are as described above in §3.4.3.1.

3.4.4 Discussion

The calculator lends itself very readily to simple programs for data preparation. Programs have only been developed as needed. Other structural analysis programs do exist (e.g. for finding finite strain ellipsoids from deformed pebbles, after Dunnet and Siddans, 1971), but are not described here.

3.5 DATA BANKS

Designs for the efficient use of data banks are dependent to some extent on the type of data. Two primary types of data considered were located orientation data and reference data (points and lines).

The creation, maintenance, and data extraction programs for data banks on the Cyber are described in Appendix D.

The creation, maintenance, and data extraction programs for data banks on the Nova are described in Appendix R (programs MAKEMAP and SUBMAP).

These programs were written only to the level required to make the aims of this thesis operational. There is much scope to improve the versatility and the sophistication of these programs.

3.6 STANDARD ANALYSIS PROGRAMS

Only two functions are considered here, i.e. mapping and stereonet analysis.

A program (PLTMAP) for the automatic plotting of structure maps is described in Appendix D.

Of the various published programs for plotting stereonets, the one chosen for use in this study was program ORIENT of Bridges and Etheridge (1974), firstly because it was already on the Cyber, and secondly because other programs (e.g. Noble and Eberly, 1964; Tocher, 1967; Cohen, 1975) available at the time were not as suitable for a number of reasons (see Appendix H). Even programs published later (e.g. Tocher, 1978b, 1979; Kalkani and von Frese, 1979; and Beasley, 1981) were still not considered suitable.

ORIENT, as it stood, suffered from a number of problems (Appendix H). This lead to a major rewrite of the program, with the new program called CNTRFIN. Only the subroutines that read in, standardised, and rotated data were kept. The program was restructured to work in overlays (Fig. H.9) so that extra functions, such as program FIT (Mancktelow, 1979), could be added with minimal modification and with no significant increase in central memory usage. Also, in this form there is little modification required to make the program part of a larger mapping and analysis package (Appendix D)

3.7 TYPE I TREND SURFACE

3.7.1 Existing Programs

Because of inherent problems caused by structural data (§1.2.1.2), trend surface analysis techniques commonly used in other disciplines can only be applied under rather limited situations (e.g. well exposed simple geometric surfaces, such as sedimentary basins).

The program package for determining structural surfaces, as described by Yamamoto and Nishiwaki (1976), was installed on the Cyber (Appendix K). Generally, the programs needed very large amounts of CM and CP time. The versions developed here require a fraction of that used by the originals, whilst extending their capabilities.

3.7.2 Discussion

The method employed by the above programs is not the only one that can be used to produce Type I trend surfaces, but was the only one available in print.

An alternative approach to the above smoothing method is to solve trend surfaces in such a way that each data point is considered throughout the analysis. By tessellating an area so that each data point is represented by one polygon, the structural surface is defined as a polyhedral surface consisting of a set of planar polygons with gradients as measured at the data points. A tessellated map then represents the orthographic projection of a three-dimensional polyhedral surface (Fig. 3.4). This approach is not simple, as the orthographic projection of planes with gradients measured at the data locations would not give the polygonal shapes (Thiessen polygons) that are derived from programs that tessellate maps. Part of the problem is caused by the fact that the relative heights of data points on the trend surfaces are unknown. Other reasons for mismatch are inaccuracies in measuring and positioning data, and the assumptions that all data belong to the one structural surface, that there are no discontinuities, and so on (§1.2.1.2).

Another approach would be to triangulate data sets (e.g. Appendix M). This again attempts to fit polyhedral surfaces to structural surfaces, but in this case, each face is a triangle with a data point at each vertex. Instead of each face being planar, a higher-ordered polynomial surface is fitted through each vertex. This approach suffers from the same problem as the others (§1.2.1.2, ¶1), i.e. two different paths to the same point may give two different results (Fig. 1.1).

If data smoothing is allowed (to overcome the problems of inaccuracy of data values and the paucity of data) then an approach described by Junkins et al (1973) provides an improved method for computing surface shapes. In this method, each unit area of the map is fitted with more than one surface, by incorporating different neighbouring unit areas, so that there is continuity throughout the map.

There are methods by which some of the problems described previously (§1.2.1.2) can be overcome. For example, overturned surfaces can be solved by dividing the map into subareas such that, with a suitable three-dimensional rotation of each subarea, all data become, or remain, upright. Each subarea can then be processed individually, and the results rotated back into their original orientations.

Only the first of the above alternatives was adopted, and is enlarged in the following sections.

3.8 TYPE II TREND SURFACE ANALYSIS

3.8.1 Cyber

A method to apply S.O.D.A. was tried on the Cyber by contouring a mathematical function, $f(\emptyset,\theta)$ (e.g. Fig. 3.5), of data orientations. By dividing the stereonet into ten regions with a function, $f(\emptyset,\theta)$ (trend: $0^{\circ} \le \emptyset < 360^{\circ}$, plunge: $0^{\circ} \le \theta \le 90^{\circ}$), then these regions can be delineated by nine contour levels, which can be unambiguously plotted on a map using five

colours (Appendix D and Appendix M).

Using program TRICON (Appendix M) to apply the S.O.D.A. technique is inefficient because the method of stereonet subdivision is crude and inflexible, and the turn-around time between program run and obtaining results is very slow compared to that achievable by other methods (below). As these problems are severe, the method was dropped and the S.O.D.A. technique transferred to the Nova (see next section).

The attempt demonstrated the unsuitability of available Cyber peripherals for the type of analysis represented by the S.O.D.A. technique, and the definite need for interactive graphics. Interactive graphics (such as Tectronix terminals) can be used on the Cyber, but those available do not have the colour facilities which have proved to be extremely useful.

3.8.2 Nova

3.8.2.1 Introduction

This section applies to the use of interactive graphics in the analysis of structural data (Appendix R). The sequence by which analyses are made using computer based S.O.D.A. techniques are described in Cohen and James, 1981; and Cohen, 1981b (Appendix S).

3.8.2.2 Software

Three types of software were developed: 1) graphics, 2) alternatives to slow FORTRAN routines (such as trigonometric functions), and 3) applications.

Most of the graphics for this thesis had to be developed because the existing graphics routines library (PLOT.LB, Bielby, personal communication) was extremely limited. Because of inefficiency of the FORTRAN compiler, and CP limitations, some slow FORTRAN routines had to be replaced with alternatives. With these two sets of software written (Appendix F), the application programs could be developed to operate at practical speeds. (For instance, the colour chart, Fig. CP.ld, took 20 minutes to produce when the programs were written in FORTRAN. With the alternative software and using ASSEMBLY language, it took 22 seconds.)

With the above routines available the analytical program package (Appendix R) could be developed to operate efficiently. Currently developed programs plot stereonets (program STEREO) and apply the S.O.D.A. technique (program SHADEMAP).

3.8.2.3 Discussion

Although the Nova system is relatively slow and has limited capacity, it has shown its value in the analysis of data by having an excellent user/machine interface, coupled with a high speed display of results. Lack of computer speed and memory is partially compensated by the fact that the machine is dedicated (to one user).

Many of the limitations imposed on the Nova system are due to the equipment itself. The display software routines (e.g. TITLE, GLINE and FLLA, Appendix F) account for a large proportion of CM and computing time. Modern minicomputers and display processors of equivalent price range would be many times faster, many times larger in memory, and more sophisticated to use. (For instance, displaying of text (TITLE), drawing of lines (GLINE), and shading of areas (FLLA) are now commonly included in display processors, freeing the computer for analytical programs.)

Modern machines incorporate hardware floating point arithmetic, which means that much faster, more accurate computations can be performed than those used in (For example, the raggedness of the colour charts shown in the colour plates (Appendix CP) would not only be abolished, but would also take only a fraction of the time to display.)

3.9 DISCUSSIONS

3.9.1 Advantages of the S.O.D.A. Technique

The S.O.D.A. technique has a number of advantages that make it superior to other methods used to date. It combines many standard manual methods into an integrated and related whole. It has been designed in a form that makes it suitable for rapid execution by semi-automated means, and on computing equipment that allows for rapid expansion and integration with other geological and geophysical data processing.

S.O.D.A. is a dimensionless technique, i.e., it is valid on all scales, from the analysis of thin sections through to continents.

The derivation of isotrend and isodip contours to express geometrical surfaces and volumes, to detect unconformities, and to define structural domains, are the same in each case although their meanings and conditions of use vary for the different functions.

The computer programs for S.O.D.A. are simple, relatively fast, and structured in such a way that data size is immaterial. Data sets of the size of national data archives are as easily processable as small data sets of a few elements. The size of required computer central memory is fixed (data independent) and the size of central processing time is a linear function of data size. However, the addition of statistical and other possible functions to improve the utility of S.O.D.A. (§8.3) may invalidate this current status.

3.9.2 Limitations of the S.O.D.A. Technique

3.9.2.1 Introduction

The previous chapters have demonstrated the usefulness and the power of the S.O.D.A. technique. The more serious problems encountered with this prototype are outlined below. Some of the problems are due to

limitations of both the computational and display equipment; some to the derivation of the technique; and some to limitations of human psychophysiology. These problems are interrelated, in that the limitations of equipment and technique will determine what human mental processes are required.

3.9.2.2 Equipment

Computational Two computers were used, a Nova and a Cyber. The Nova is an outmoded machine that suffered considerable hardware failures as a result of constant experimental modifications carried out by the Department of Electrical Engineering research students. The Cyber is an extremely powerful machine. The only link between the two is through a standard terminal line (see Appendix A), communicating only in ASCII because of the incompatibilty of internal data configurations between the two machines. The Cyber operating system is aimed at high-speed computation, and was not designed for efficient interactive programming. This meant that most programs were processed on the Nova at a relatively slow rate. The small size of this mini-computer also restricted the size and sophistication of programs, which meant that they were not protected from invalid data and approximations had to be used instead of computing accurate values.

The slowness of the programs means that there is a waiting time between a command being given and the results. Pyschologically, this small time lapse can be vexing, even inhibiting, although the total time spent in conducting analyses may be considerably shorter than that which would be experienced by any other available method of analysis (e.g. manual).

Display The display micro-processor (U.L.O.S.) was the main source of display problems. It allowed only three memory (colour) planes, which meant that picture regeneration was time-consuming as pictures could not be swapped in or out of display as desired. The memory was faulty (due to inadequate construction), resulting in picture corruption. The design of the micro-processor was such that some of its functions were inaccessible because they were incomplete or incompatible with the type of display desired. This meant that the only operable programming was relatively inefficient.

Other problems were: the signals from U.L.O.S. to drive the colour guns were not under software control, and so colour intensities were not programmable; and the colour monitor had a reasonably fast phosphor which did not adequately retain the image between refresh cycles, leading to an image "flicker" that causes eye strain.

A second source of display problems was the small size of the Nova, which had to combine both driving programs and display routines. A compromise between display sophistication and S.O.D.A. functions had to be made.

3.9.2.3 Technique

The S.O.D.A. technique assigns every data point with an equal weighting. This is not only undesirable at times, but it also leads to a severe bias in human information processing. To present every data point, the map must be tessellated into Thiessen polygons. Shapes and sizes of the polygons are solely defined by the distribution of data points. This results in unequal polygon sizes and thus unequal representation (weighting) on the display.

Deriving a tessellated map is computationally very slow, and so the same tessellated map is used repeatedly, even though only subsets of data may be under analysis (which would be better analysed with their own tessellation configuration). This would be particularly relevant if, and when, the tessellation procedure is not based solely on data point distribution (e.g. data weighting and/or data values).

3.9.2.4 Human Information Processing

No matter what information is displayed, the final real-world interpretation is dependent on psychophysiology, i.e. what happens to the information between display and interpretation. This includes the response of the eye to the display medium (Carterette and Friedman, 1975), the processing of the visual signal by the brain (data-driven processes, Lindsay and Norman, 1977), and the interpretation of the signal (conceptually-driven processes, Lindsay and Norman, op. cit.). increasing, but still novel, use of interactive colour graphics requires that the effects of this display medium be thoroughly understood. example, the change in intensity of light from one level to another is perceived in a non-linear manner (Cornsweet, 1970) and is affected by the interpretation of figure/ground relationships (Hurvich and Jameson, 1966; and Coren, 1969) and figure/figure relationships (e.g. Albers, 1963).) To be able to convey a meaningful change in data value by light intensity, the change in picture display signal strengths must be controlled by a non-linear function to correlate with an observer's response (Fangeras, 1979; and O'Callaghan, et al, 1981). To make a hard copy of the display (e.g. by colour photography) the response of photographic film to light must be considered (Eastman Kodak, 1972).)

Screen flicker will quickly fatigue an eye. The lack of eye distraction (all visual concentration being on the display monitor), coupled with high contrasts between bright picture elements and dark surrounds, add to this fatigue.

A problem mentioned above was the fact that all data points have a polygon that has its shape and size controlled by the distribution of neighbouring points. The shape of polygon boundaries may give rise to

linear trends which have no significance, being artificial by-products of the technique. This problem is minor compared to the major problem caused by size. The larger the size of a polygon, the more importance is psychologically attached to it, regardless of its true significance. This may be acceptable where data-collection methods have been chosen with the S.O.D.A. technique in mind, but may otherwise lead to problems of interpretation.

3.9.2.5 Overcoming Problems

Most of the problems described could be avoided by using the technology that has become readily available at the time of writing, and the promise of improvements in the near future. Problems due to technique could be largely overcome by the development of a more comprehensive package that takes a more sophisticated approach to performing analyses than the current empirical approach. (Analytical procedures would still be under user control, but the results would be more precise.) Solving these two classes of problems will solve the third, thus making the S.O.D.A. technique suitable for common, standard usage.

3.10 CONCLUSIONS

three computers required programming of the total The approximately 13,000 lines of code in FORTRAN, BASIC, and ASSEMBLY languages. The programs for the S.O.D.A. technique are truly interactive, Stereonet plotting is performed at around 30 with very fast performances. points per second, S.O.D.A. plots are produced at 1200 data stations per minute, and subareas can be created inside a minute. Colour charts can be displayed at 22 to 30 seconds per reference. Support programs on the Cyber are very fast, accurate, and require small demands on the machine. Highly complex contoured stereonets of very large data sets can be processed in 10 The slowest program is the generation of Thiessen polygons, the speed being proportional to the square of the number of points (600 points requires 5 minutes).

The usefulness of computers has been proved many times over. The Nova system is highly versatile and has proved much easier to use and faster in achieving results than the Cyber system. The Cyber proves itself to be useful mainly as a support system for processes that cannot be adequately managed by the Nova.

CHAPTER 4

GEOLOGICAL MODELS

4.1 INTRODUCTION

This chapter presents a few of the ideal geological examples previously described to demonstrate the capabilities of the theory of S.O.D.A. (Chap. 2) by the application of relatively modern computer technology (Chap. 3).

Of the five basic geometries, as well as their admix, only a few are needed to give an idea of S.O.D.A. practicalities. An exhaustive demonstration is not necessary. Once the new form of data display is understood and familiarised, even the more complex structures can be analysed with little difficulty.

The few models used here were generated from mathematically perfect models, which may or may not have included a random fluctuation to simulate natural variation in real geological data. Actual geological test cases presented in the next chapter can be interpreted by making use of the principles portrayed here.

4.2 CYLINDRICAL FOLDS

4.2.1 Data Generation

All data for cylindrical folds were generated by the orthographic projection (Fig. 2.5b) of randomly fluctuating gradient data on the surface of an upright horizontal folded layer of "similar" type (Class 2). Because a class 2 fold was chosen the data set produced could equally well have been derived from the real case of fold truncation by ground surface (Fig. 2.5a). This distinction is immaterial for type 2 folds but is very important when considering folds of any other class. Rotated folds were produced by rotating the data set for the upright horizontal fold. All data sets were divided into two populations, one on each side of an imaginary line that could be used as a line of discontinuity (see §4.4).

The locations of the data points were uniformly spaced with some degree of randomness incorporated.

4.2.2 Upright Horizontal Folds

4.2.2.1 Fold Design

Four different fold shapes were designed (Figs. 4.la to d) from four of the profiles in Hudleston's (1973a) figure 12. They are profiles "3B", "3D", "3F", and "1D" respectively. All fold geometries consist of a synform flanked on both sides by an antiform. They are all orientated with hinge lines north-south.

4.2.2.2 Display and Analysis

The first three folds (Figs. 4.1a,b,c) are displayed, using the S.O.D.A. technique on colour graphics, in Figs. CP.3a,c,e respectively. Each of the S.O.D.A. plots (Appendix R) is accompanied by a combined pole figure (red) and dip vector figure (green) (Figs. CP.3b,d,f respectively). (Yellow appears wherever green and red overlap, see Fig. X.3 and Appendix CP.) The S.O.D.A. plots are determined by plotting dip vectors on the standard colour chart (Fig. CP.3g, Appendix X), and colouring the area around the appropriate data station on a map with the colour determined from the colour chart (similar to the A.V.A. technique of Sander (1970), see Appendix S), which results in each plot being a composite of both isotrends (boundaries between hues) and isodips (boundaries between colour intensities). The following discussion on these figures can be compared to Figs. 2.7a and CP.5.

In all cases, only two isotrend surfaces are seen, west (cyan) and east (pink). Other colours are seen to occur in the hinges where any small undulations in the subhorizontal layering cause discrepant orientations (see $\S2.2.2.6$), i.e., there is an infinite density (ρ_p) in the hinges between isotrend surfaces.

Isodip lines are delineated by boundaries between colour intensities, which are 18° apart with the standard colour chart. As expected, they form lines that are reasonably straight and parallel to the fold hinges. The variation in positioning of the lines between the three plots are due solely to fold hinge roundness as all folds are of "similar" type. The most rounded fold (Fig. CP.3a) has the greatest spread of isodip lines. Because the hinge areas shrink as the folds become more angular, the isodip lines move towards the hinge lines (Fig. CP.3c). In the extreme case of chevron folds (Fig. CP.3e) the hinge area has been reduced to a line, where there is an infinite density of isodip lines.

The three profiles "3B", "3D", and "3F" achieve different maximum dip values, which can be seen in the S.O.D.A. plots. In the first profile, dips do not exceed 72°, and so no white areas occur. In the second, dip values readily exceed this isodip line value. In the third instance, the average dip is 65°, but semi-random fluctuation causes some areas to exceed the 72° isodip line. Areas of lower than average dip values can also be recognized by dips flatter than the 54° isodip line.

4.2.2.3 Discussion

Although the above displays and analyses appeared simple and unambiguous, this is only because of the a priori knowledge that the folds were of class 2 type. However, if this knowledge was not known, then an alternative explanation is available in the interpretation of the first two

profiles, while the third remains unambiguous. Two items of information are displayed by the S.O.D.A. plots which are not given by the stereonet plots: in going from Fig. CP.3a to Fig. CP.3c isotrend lines are noted to move towards the hinge lines and the maximum dip values decreased. If one assumes both folds to be of class 2 type, then the change between the two plots can be explained by a change in fold roundness. However, it is equally valid to keep the fold roundness constant but change the fold class (for example, from a class "IB" for the first profile to a class "IC" for the second). It is important to note that this applies to field data collection as portrayed in Fig. 2.5a. The lessening of maximum dip values from the first profile to the second is irrelevant except in the case when the folds are being related in terms of strain histories and/or deformation mechanisms.

From this it must be noted that not only does the level of the exposing ground surface affect the distribution of isodip lines but so do both fold angularity and fold class. Hence for the analysis of a single fold (or fold sequence of identical folds), unambiguous information cannot be derived about fold class from a S.O.D.A. plot when fold angularity is unknown, and vice versa. However, when comparing two or more folds of changing shape, class, ground level, or combination thereof, movement of isodip lines toward hinge lines signifies a tightening, or an increase in the angularity, of surfaces (imaginary or otherwise) which occur at ground level and are contained within, and folded with, the fold sequence. Hence, the more constraints that can be placed on fold shapes by extra information (e.g. stereonets, observed profiles) the better the analysis.

For example, suppose that the two folds above (Figs. CP.3a,c) are genetically related and it is desired to know how the two vary morphologically. Then by holding all constraints constant but one, show how the one variable effects the results, as follows:

- 1. Variation in ground level. To derive the second pattern from the first requires an increase in the angularity of an imaginary folded surface. Hence ground level must be lowered for class 1A, 1B, or 1C folds, is immaterial for class 2 folds, and must rise for class 3 folds. That is, ground level moves from the more open and/or rounded bounding surface to the more tighter and/or angular bounding surface of the folded layer. This would generally be accompanied by an increase in maximum dip values. As the reverse is in fact true, this line of argument is invalidated.
- Proceed as for (1) for all other possible variables.

A problem is encountered in the above example in that an increase in angularity should be accompanied by an increase in maximum dip values

due to an increase in fold tightening. To actually have a decrease in maximum dip suggests an opening of the second fold whilst increasing its angularity. This suggests a change in morphology due to other factors that have not yet been mentioned, such as layer thickness, changes in relative material strengths and rheologies, among others.

If maximum dip values had increased, not decreased, then wavelengths must also be considered in understanding the geological processes involved. Due to the inter-relation of the various factors discussed above, extra information appears to be a necessity if more than qualitative information is to be gained in the more ambiguous situations.

4.2.3 Upright Rotated Folds

4.2.3.1 Fold Design

The basic fold design for this demonstration is identical to those above, except that profile "ID" of Hudleston (op. cit.) is used. The orientation data was rotated about the normal to the axial plane by amounts of 0°, 10°, 65°, and 90° (Figs. 4.ld,e,f,g and Fig. 2.4) so that the folds plunged towards due north. The same geographic coordinates were kept for each rotated point, hence effectively changing the fold at each position. This can only be done for "similar" style folds. For any other class of fold, generation of orientation data by transection (Fig. 2.5a) must be used.

4.2.3.2 Display Method

Each data set (representing each stage of rotation) was displayed in an identical manner to that described above, viz. dip vectors were used to determine the colour and intensity of each element of the S.O.D.A. plots (Figs. CP.4a,b,c) by plotting on a standard colour chart (Fig. CP.4h). Poles to layering were used to produce plots for the vertical folds (Figs. CP.4d,e) as all dip vectors would appear white.

A composite (equal-area) stereonet plot of dip vectors of the data sets is presented in Fig. CP.4g (compare this to Fig. 2.4).

Due to the problem of separating hues from colour intensities, and thus recognizing and differentiating isodip and isotrend lines, each of the examples in this section are plotted twice, one portraying isodips (Figs. CP.5d,e,f,g) and the other isotrends (Figs. CP.5a,b,c). A u-isotrend colour chart (Fig. CP.5h) of 30° resolution was used to produce the isotrend contours, and a b-isodip chart (Fig. CP.5i) of 5° resolution for the isodips. The increased resolution of this b-isodip chart over that of the standard colour chart allows more isodip lines to be constructed, which allows a more accurate analysis of the geometry. Although much higher resolution can be achieved for both types of charts, it is desirable to select an optimum resolution for the scaling factor involved.

For the production of Fig. CP.5 S.O.D.A. plots, poles to layering were used. This complements the colours obtained for dip vectors (i.e. blue/yellow, red/cyan, etc.). Although intensity variation is incorporated in the b-isodip chart, adjacent intensity levels are separated, on the chart, by dips of 60° (12 x 5°).

4.2.3.3 Rotation of 0° (Horizontal)

The standard upright horizontal fold (Fig. 4.1d) is plotted in a similar manner to those in §4.2.2. Accordingly, the analyses and discussions of the latter pertain here. The isotrend patterns are identical, and isodip patterns similar. Because this fold profile is more open, fewer isodip lines occur.

Dip vectors are plotted on the stereonet (Fig. CP.4g) in cyan.

4.2.3.4 Rotation of 10°

The S.O.D.A. plot of Fig. 4.1e is presented in Fig. CP.4b, using the dip vector distribution (red points in Fig. CP.4g). The S.O.D.A. plot appears almost identical to the previous one except that an overall bluish cast in the colours appear because all points now have a north-trending component (see Fig. CP.1a). The fold is rotated by an amount sufficient to bring any southerly fluctuations in the horizontal position to a northerly orientation. If the colour chart were rotated identically then the resulting S.O.D.A. plot would be identical to the unrotated fold. For any "non-similar" style fold this would not be strictly true as fold profile shape would have a greater influence on the data values and their relative geographic positions (see §2.2.2.10 and §2.2.2.11).

Isotrends move away from the hinge lines to the point where they become visible (Fig. CP.5b). This can also be seen in the rapid shrinking of the pink and green-cyan areas of Fig. CP.5a to the small areas at the extreme "edges" (points of inflexion between antiforms and synforms) in Fig. CP.5b. Isodips, on the other hand, move towards the hinge lines, where they disappear (note the loss of yellow in Fig. CP.5d, and the movement of red towards the hinge lines).

4.2.3.5 Rotation of 65°

The S.O.D.A. plot of Fig. 4.1f is presented in Fig. CP.4c, using the dip vector distribution (magenta points in Fig. CP.4g). Because of the large amount of rotation from the previous position a large change can be noticed. The dip vectors now cluster quite closely, producing little variation in colour and intensity. As the cluster is predominantly close to due north the colours are very rich in blue. Also, as the cluster has little spread, intensity variation is quite small. In fact, only the small areas of large fluctuation register changes in intensity.

The isotrend contours of Fig. CP.5c are very similar to those of

the previous rotation. The red and green isotrends have moved "out" of the folds via the points of inflexion, with the light green and orange contours moving out to replace them. The hinge line yellow has also moved outwards.

The isodip contours of Fig. CP.5e have moved so much towards the hinge lines that most have disappeared, leaving red, orange, and pink to fill the plot. By this stage the pole figure girdle lies very close to the isodip contour small circle (see Fig. 2.4). Thus even small displacements of data points from the great circle girdle, anywhere along the girdle, can cause a shift from one side of a contour line to the other. This sensitivity to fluctuation causes the S.O.D.A. plot to lose its ability to adequately define isodip contours. The sensitivity varies along the girdle to some extent, and so resulting colour patterns will not be totally random. Consequently, hinge lines are still largely orange, and limbs near points of inflexion are still pink. The patterns still suggest the geometry of an open fold, but do not allow an analysis of fold classification.

The fold profile, as opposed to its cylindricity (see §2.2.2.10) contributes most to the data values. Hence the contour patterns derived will be controlled more by the former than the latter. The parallelism of the isotrend lines to the hinge lines is due to "similar" style folding. If the fold was of any other class then convergence or divergence of contours would have appeared (see Fig. 2.6).

4.2.3.6 Rotation of 90° (Vertical)

The S.O.D.A. plot of Fig. 4.1g is presented in Fig. CP.4d, using the pole figure distribution (yellow points [see (2) of Appendix CP] in Fig. CP.4g). The use of dip vectors would have caused the plot to appear totally white. All isodip contours have moved "out" of the folds via the hinge lines. As no dip value is less than 72° there is no intensity variation, and an isodip volume prevails.

The apparently haphazard colour pattern is still interpretable, and consistent with the geometry of the example. As the great circle girdle of the pole distribution lies parallel to the primitive, any minor and opposite fluctuations of two adjacent points will cause them to have opposing trend values, and hence opposing isotrend colours. It can be seen that in fact the S.O.D.A. plot contains parallel regions of randomly distributed colour complements (blue-cyan/orange = "west dipping"* limb; blue/yellow = hinge region; yellow-green/blue-magenta = "east dipping"* limb). The boundaries between the regions (b-isotrend contours) are still parallel to the hinge lines, suggesting a "similar" fold style.

^{*} Refers to those limbs of the horizontal fold equivalent.

Under these conditions, u-isotrend contours are not suitable for analysis, whereas b-isotrends are. The example is replotted (Fig. CP.4e) with a b-isotrend colour chart of 15° resolution (Fig. CP.4f).

The high resolution S.O.D.A. plot of isodip contours (Fig. CP.5g) shows the whole region to be defined by one b-isodip volume. (If u-isodips were used then the fold limbs could be separated by two volumes, resulting in a S.O.D.A. plot similar to that of Fig. CP.5a.) It can be noted that small departures from perfect fold cylindricity greater than 5° appear in fold hinges and points of inflexion.

4.2.3.7 Conclusions

The analysis of rotated folds is reasonably simple provided that fold class or style does not change radically, both in depth and length. The greater the change, the greater the number of points required in order to make an accurate analysis.

Class 1 folds are distinguishable from class 2 folds, as are class 3 folds. With further development of the mathematical relationships between contours and fold classes (for plunging folds and a horizontal reference plane), it should be possible to distinguish between the different class 1 folds. However, the intimate effects on S.O.D.A. patterns caused by roundness and ground level, among other factors, would make such distinctions difficult to make, particularly as fold profile must change with depth (hence length for rotated folds) due to the non-repeatability of all classes except class 2.

4.3 CLASSIFICATION OF SUBVERTICAL FOLDS

4.3.1 Data Generation

Data values were interpolated from diagrams of the five fold classes proposed by Ramsay (1967, Fig. 7.24). The geographic locations of the data points were the same for all classes. All dip values were set vertical.

4.3.2 Display and Analysis

The S.O.D.A. plots of the five fold classes are presented in Fig. CP.6. They were produced by plotting pole figures (e.g. for the class 1B "parallel" fold, Fig. CP.6g) on a b-isotrend colour chart of 15° resolution (Fig. CP.6f). The range of trend values for all classes of folds are identical (i.e. same range in hues). The analysis of the plots are simple and are identical to those discussed by Ramsay (1967, Ch. 7).

4.3.3 Discussion

Fold classification by S.O.D.A. requires a reasonably large data set per fold, or portions thereof, for a clear definition of dip isogons (about 300 points were used here). Only macroscopic folds are expected to

be analysed by this method as smaller folds can be accurately mapped and analysed by other methods (as currently practised, for example). scale folds tend to include dislocations, vergence folds, and other structures which all contribute to making complex macroscopic fold data sets. In such cases it is necessary to subdivide folds into smaller areas, which require relatively large and comprehensive sets of data.

4.4 DISLOCATIONS

4.4.1 Data Generation

Each data point generated for the cylindrical fold examples in §4.2 were geologically classified according to which side of an imaginary east-west fault line they were found. A fault could be made to appear by plotting the north side of one data set against the south side of another. The data sets for the examples discussed later (§4.5 and §4.6) were similarly classified and available for use. Only the data set for the strike-slip fault had to be especially devised for this analysis.

4.4.2 Display Methods

Four arrangements of faulting are used to demonstrate faults (Figs. CP.7a,c,e,g). (A further example can be found in §4.6.) S.O.D.A. plot is accompanied by a pole figure and/or dip vector figure on an equal-area stereonet. The two stereonets in Figs. CP.7b,d plot green for dip vectors and red for poles, for all data (yellow appears wherever green and red overlap, see Appendix CP); whereas the two stereonets in Fig. CP.7f,h plot dip vectors for the northern portions in green, and dip vectors for the southern portions in red. The S.O.D.A. plots were made by plotting dip vectors on a standard colour chart (refer to §4.2.2.2).

4.4.3 Strike-slip Fault (Offsets)

The model represents the open fold of Fig. 4.1d which has had the southern portion dextrally displaced by a quarter of a fold wavelength is dramatically portrayed The offset (Fig. 4.2a). Quite small offsets can be detected provided that enough (Fig. CP.7a). The high contrast in colours can be used to advantage data is available. to highlight features which could go unnoticed in an ordinary structure map.

4.4.4 Normal Fault

4.4.4.1 Change in Tightness

As folds generally change characteristics (such as wavelength and style) with depth, a normal fault can be simulated by aligning an open fold against a more closed fold. This was achieved by plotting the northern half of an open fold (Fig. 4.1d) against the southern half of a tighter one (Fig. 4.1b), to produce the model in Fig. 4.2b. The model departs from reality in that the fold wavelength does not change with depth, a

phenomenon not expected for the degree of flattening that the model attempts to portray.

The S.O.D.A. plot (Fig. CP.7c) demonstrates the change in tightness across the fault in terms of changes in isodip contours. The increase in both number and intensity highlights the existence of a discontinuity, despite the fact that the axial planes and hinge lines show no displacement.

4.4.4.2 Change in Style

A model for change in style across a fault was designed in a parallel fashion to the previous one, except that style rather than tightness was used. In this case the northern portion of Fig. 4.1b was faulted against the southern portion of the chevron fold in Fig. 4.1c. Again, the change in contour patterns when analysed by S.O.D.A. (Fig. CP.7g) is quite dramatic.

4.4.4.3 Minor Changes

Minor changes were modelled by using both changes in tightness and in style. The northern portion of Fig. 4.la was faulted against the southern part of Fig. 4.lb. As can be seen in the S.O.D.A. plot (Fig. CP.7e), small changes are not as readily detectable. However, as long as the changes are greater, or more consistent, than random fluctuations in the data (or "noise" caused by undulations in the layering), the discondances should be detectable by S.O.D.A.. In this model the small changes are still detectable due to small but consistent changes in the contour patterns.

4.4.4.4 Discussion

So far models of 100% exposure have been used. With scattered outcrops, uncertainties appear in the analyses due to lack of information. All models used in this chapter were designed to be able to incorporate data loss (or lack of data). Each geographic location was also geologically classified (see Appendix C) according to the percentage of outcrop in which it would appear. In this way all models could be analysed at various levels of exposure, from a few percent through to full exposure. The obvious conclusion which has been supported by this exercise is that the more complex an area, the more data that is required in each area of exposure.

Changes in wavelength with depth would improve the detection of faults as there would be offsets in the hinge lines, which were shown in §4.4.2.1 to be readily detectable.

The ease with which S.O.D.A. can highlight small changes in orientation data (both by value and position) would be extremely useful in those geological terrains where marker beds are not available (such as

massive sandstone units). Even small changes in tightness could be detected by suitable use of contours.

4.5 SPHERICAL DOMES

4.5.1 Data Generation

As for previous models, this model (Fig. 4.3) was generated by allowing data from an ideal dome model to randomly fluctuate within bounds. The data location coordinates (and geologic classification) of the cylindrical folds were used.

4.5.2 Display and Analysis

Two S.O.D.A. plots were produced, one for a u-isotrend plot and one for a b-isodip plot (Figs. CP.8a,b respectively). The isotrend plot was produced by plotting dip vectors (all points in Fig. CP.8j) onto a u-isotrend chart of 30° resolution (Fig. CP.8c), and the isodip plot was similarly produced by using an isodip chart of 3° resolution (Fig. CP.8d).

These plots closely match the patterns expected for the geometry of a dome (Fig. 2.17c). A very large data set would be required to detect asymmetric domes or obliquely transected domes (§2.3.4.2).

4.5.3 Discussion

Domes portrayed by this model achieve dips of up to 20°. However, many geological domes may have dips of no more than a few degrees. In these situations, the noise level may mask the structure (see next section), in which case it would be be necessary to conduct statistical analyses on data to remove the effects of the noise.

4.6 PLANES

4.6.1 Data Generation

The data set used for the dome (above) was rearranged to form an undulating plane which would approximate geologically planar features. The method of reassigning data values to point locations was as follows: first the data set was divided into two populations, one with an overall easterly dip, and the other containing the remainder (see Fig. CP.8j). A line of discontinuity was positioned in the locality map so as not to be interpretable as an axial plane trace. However, a large divergence between the discontinuity and a possible fold hinge was not wanted as it was desirable to examine how random undulations could cause misinterpretations or ambiguities. Data was then semi-randomly assigned, within each population, to the point locations in their respective area.

4.6.2 Display and Analysis

The stereonet plot of dip vectors is identical to that for the dome (Fig. CP.8j). The pole figure (Fig. CP.8e) shows a well defined point

maximum that resembles geological planes. A S.O.D.A. plot (Fig. CP.8f) was first produced by plotting dip vectors on a standard colour chart (Fig. CP.8h). By repeatedly using subarea analysis the two populations could be defined (separated by F-F in Figs. CP.8f,g). These are plotted on the stereonet (Fig. CP.8j) (see Appendix X) according to the two geographic subdomains. A colour chart (Fig. CP.8i) was devised from the two populations plotted in Fig. CP.8j, and a S.O.D.A. plot (Fig. CP.8g) was then generated using dip vectors on the new chart.

From the stereonet plot of the data the two subareas could represent a minor warp (very open fold) provided the axial plane trace trended west of north. Subarea analysis located the dislocation as occurring a few degrees east of north. The dislocation could then be better interpreted as a scissor fault (Fig. 4.4). The S.O.D.A. plot (Fig. CP.8g) based solely on the bi-polar orientations gives an ambiguous answer. It appears to have a possible axial plane trace in the correct orientation which is just as likely as the fault that was designed into the model. The trend variation between axial plane trace and fault line is sufficiently small to allow the random variation in plane undulation (+8°) to produce indefinite results.

4.7 CONCLUSIONS

The use of the few models described above provides a measure of the usefulness of the S.O.D.A. technique in the interpretation of field structures. The ambiguity in deriving quantitative estimates which concern the parameters of structural shapes making up the S.O.D.A. plots does tend to limit the technique. No further attempt is made to resolve these problems in this thesis because the technique developed is still being pioneered here, and so it is preferred to continue exploring the ground open to the technique rather than correct its shortcomings. However, the ability to highlight structural features, and to highlight differences between subareas of similar geometries, make this process extremely valuable; particularly as it is capable of processing very large data sets quickly and selectively.

No models of microfabric analysis were generated, as such analyses are best compared to work done by established authors (next chapter).

CHAPTER 5

GEOLOGICAL TEST CASES

5.1 INTRODUCTION

Geological examples of macroscopic, mesoscopic and microscopic structures were collected from a number of sources and the analyses of these by the S.O.D.A. technique are presented in this chapter.

The examples were chosen for demonstration purposes, and so the analyses derived here are not necessarily as detailed as those that could be obtained. As some examples were not generated by the author, additional information which could have produced better results was not available.

Terminology for domains in subarea analysis is defined in Appendix G.

5.2 MACROSCALE

5.2.1 Llangedwyn-Dyffryn-Clwyd

5.2.1.1 Display and Analysis

The data for the structural elements of a single macroscopic fold in layered rocks of unknown rock type were obtained from a teaching example (Department of Geology and Mineralogy, Univ. of Adelaide, P.R.James, personal communication). The composite stereo-plot (Fig. CP.9i) demonstrates an excellent geometry of a tight, moderately to steeply inclined cylindrical fold, with a fold plunge of 40° towards 171° and axial plane foliation 238°/66° (Fig. 5.1d).

The S.O.D.A. plot of isodips (Fig. CP.9a) derived by plotting poles to bedding, S_0 , on a b-isodip chart (Fig. CP.9b) demonstrates that the fold has a high concentration of contours in the hinge region, and has flat limbs. (A colour chart of increased resolution was used for producing greater detail in the limbs. It showed the limbs to be undulatory on the smaller scale (see Fig. 5.1a).) The pole figure demonstrates a cylindrical fold, but the contours show a radiating nature. Hence, the fold is in the Class 1 field of Ramsay's (1967) classification.

The S.O.D.A. plot of isotrends (Fig. CP.9c), derived by plotting bedding poles on a u-isotrend chart (Fig. CP.9d), shows two isotrend volumes, as is to be expected for cylindrical folds. The colour pattern also demonstrates the fold to be an antiform.

The S.O.D.A. plot for the axial plane cleavage, S₁, (Figs. CP.9e and 5.1c) was derived from plotting poles on a u-isotrend chart (Fig. CP.9f). The few data points available clearly demonstrate a convergent cleavage. In the hinge region, poles to cleavage define the best-fit axial plane girdle, and in the limbs the poles are grouped accordingly. There

are too few data to demonstrate how the contours are orientated, but there are sufficient data to show that the cleavage is steeper in the upright limb, and shallower in the overturned limb, consistent with the geometry described (above) so far.

The S.O.D.A. plot of L_1 lineations (Figs. CP.9g and 5.1b), derived from using a b-isodip chart (Fig. CP.9h), also demonstrates the fanning nature of the lineation, which is in accord with a fanning cleavage. However there are too few data available to allow the behaviour of the lineation contours to be precisely understood.

To further demonstrate the behaviour of contours for a cylindrical fold, a number of S.O.D.A. plots were produced using a variety of charts (Figs. 5.2a,b,c,d). In Figs. 5.2a,b, the reference plane was rotated to remove the effect of geometry orientation (see Chap. 2); whereas in Figs. 5.2c,d, the contours refer to a horizontal reference plane. In the former two diagrams, the location where layering is overturned is lost, but can be determined in the latter two diagrams (contour labelled "o"). Of the four diagrams, the only one that can, and does, accurately locate the hinge line is that which is contoured according to the hinge line geometry (Fig. 5.2a). Although it might be expected that isodip contours, using dip vectors measured from a rotated reference plane, would define the hinge region, this is not necessarily so. For this to be possible, the reference chart must either be a u-isodip chart (with the contours changing value across the axial plane) or the fold must be upright. In the case of Fig. 5.2b, a b-isodip chart was used (Fig. 5.2e). Such a chart cannot distinguish fold hinges of inclined folds as the contour of minimum plunge does not correspond to the fold hinge line.

5.2.1.2 Discussion

The S.O.D.A. plots of bedding poles (Figs. 5.1a and 5.2a) define a fold axial surface trace which does not tally with either the axial plane foliation (S₁) trace (Fig. 5.3a) or the apparent axial plane surface trace for the outcrop pattern (which lies very close to the axial plane foliation trace). The discrepancy between axial plane surface trace and the apparent axial plane surface is to be expected for inclined folds (Stauffer, 1973). The discrepancy between axial plane surface and axial plane trace is normal (Hobbs et al, 1976). Using the elliptical—arc method for constructing the trace of axial plane surfaces (Stauffer, op. cit.), it is found that the axial plane surface corresponds well to that determined by the S.O.D.A. plots (Fig. 5.3a).

Even with the few data points available, details of the fold geometry can be extracted quickly. (For example, the line of demarcation where bedding overturns, Figs. 5.2c,d, corresponds well with that

determined from the fold profile, Fig. 5.3a.) Further details could be obtained if more data were available, and if further analytical programs were developed (such as to determine more precisely the classification of the fold from a reconstructed fold profile, or to compute it from the mathematical equations that define contour lines. For example, it was shown in the previous section that the S.O.D.A. plot contours were for a Class 1 fold. The dip isogons for two of the folded layers on the profile plane, plotted on a to vary a plot (Fig. 5.3b), show that three of the four limbs are Class 1C and one limb is Class 1A. There is no reason why these cannot be computed from contours on the outcrop pattern provided enough data is available. In this example there are too few data.)

5.2.2 Brockman Three Formation

The data for this example came from a map (Fig. 5.4, which has most of the geologic data suppressed to protect its confidentiality) of an area in the Hamersley Ranges, Western Australia. The only structural data available were bedding orientations (measured to the nearest 5° of dip) and mapped fold hinge-line traces. Geologic data included rock formation, unit names, and the existence (or otherwise) and type of mineralisation occurring at each data station. The location of drill holes were also noted.

Domain analysis performed using the S.O.D.A. technique resulted in the definition of a number of primary, secondary and tertiary domains (Fig. 5.5). Data for these domains are presented in Fig. 5.6.

The overall geometry (domain a0) is approximated by an open cylindrical fold plunging 15° towards 312° with an axial plane orientation of 225°/80°. By plotting bedding poles on a standard chart (Fig. CP.10f) the S.O.D.A. map (Fig. CP.10e) is derived. From this map several domains can be recognized, some large and some small. Three primary domains are first defined (yellow outlines) by which the map could be divided for a more detailed analysis (see Fig. CP.11).

The u-isotrend contours on the S.O.D.A. map (Fig. CP.10a), derived by plotting poles on a u-isotrend chart (Fig. CP.10b), clearly delineate the three primary domains. The overall geometry derived from this map is that of a large synform/antiform pair (west and east respectively, corresponding to the mapped traces, see Fig. CP.10g). Within each domain, secondary, or subdomains, can be seen.

A S.O.D.A. map of isodips (Fig. CP.10c) derived from an isodip chart (Fig. CP.10d), shows the major folds to be angular, with flat (but undulating) limbs, which suggests that the structure is a megakink. The complexities that can be seen within the domains clearly contribute to the scatter in the pole figure.

The three primary domains have been separately analysed (Figs. 5.6 and 5.7).

5.2.2.1 Domain f0

Four secondary domains can be defined. The primary domain (f0), although forming a modal distribution on a pole figure (Fig. 5.7b), can be divided into four subdomains, f1, f2, f3, and f4 (Fig. 5.7c). Domain f4 represents the dominant limb orientation for the primary domain. Domains f1 and f4 (Fig. 5.7e) form an open horizontal fold trending towards 100°, with an axial plane inclined to the south. Domain f2 is a fold limb within the area of f4 which appears to be of the same generation as that of the primary structure. Domain f3 appears to be a tightening of f4. It occurs close to the primary synform hinge, and stratigraphically higher in the structure, suggesting that the synform is tightening upwards.

The isotrend contours marked on the pole figure for f4 (Fig. 5.6d) conform to the two minor structural trends observable in f0 (Fig. 5.8), which are demonstrated in pole figures for f1+f4 (Fig. 5.7e) and f3 (Fig. 5.6c). (For example, the northeasterly trend can be seen in Fig. CP.11a.). These minor trends contribute to the scatter in the pole figures. This is further discussed below.

5.2.2.2 Domain g0

This central zone is the one most affected by small folds. It can be divided into three secondary domains, gl, g4, and g5. The northern domain, gl, consists of two tertiary domains, g2 and g3. Together they define upright open folding, plunging 19° towards 331° (Fig. 5.6f). Domain gl is separated from g5 by a line of demarcation trending NNE (Fig. CP.10a).

Domain g5 can be divided into three tertiary domains, g6, g7, and g9. The first two are folds within the domain, g9, which is representative of the primary domain, g0.

Domain g4 broadly consists of two domains, g8 and g10. The pole figures for these domains (Figs. 5.7g,h) form a distribution that is approximated by a cone. The cyclographic trace separating the two orientation groups trends east of north, which does not match that observed on the map. The discrepancy is probably due to the fact that g4 consists of a number of small folds that should not be grouped together as they have in fact been. As seen from f0, there are a number of orientations for structural trends other than the dominant northwest, particularly a NNE and an east-west trend. In a number of small folds that may not conform to cylindricity, there are too few data to obtain precise information of the minor structures in this part of the map.

5.2.2.3 Domain h0

The overall geometry as defined by a contoured pole figure

(Fig. 5.7j) is close to that of cylindrical folding. This is due to the weighting of data towards the lesser plunge values in the north of the domain. The overall shape of the distribution is that of a cone (Fig. 5.7k and Fig. CP.11f). This domain can be segregated into two dominant secondary domains, h1+h2 and h5, and a lesser domain, h4. Domains h1 and h2 appear to be limbs of an angular, slightly conical fold; which is the tightest structure to be observed in the area. Domain h5 appears to consist of very open cylindrical folds with a tendency towards departure from cylindricity (conicity). Domain h4 contributes to the interpretation of domain h1+h2 as a conical rather than a cylindrical fold.

5.2.2.4 Discussion on the structures

The dominant trend of the structures (open, upright angular folds) is northwest with gentle plunges in that direction. Much weaker trends occur in NNE and east-west directions. Whether these trends are due to primary (sedimentary features) or to tectonic factors is not immediately noticeable from the data. However, cross-folding is observable in the area (Landsat scene: Edmund, (121,76), Scene 30169-01285*; and De la Hunty and Jones, 1964).

appears to have been more intense in the south of the area than in the north. There are two possible explanations: either the structures tighten in the stratigraphically lower parts of the structure (as opposed to that deduced in §5.2.2.1); or the hinge region of a cross-fold, at least covering the area shown by the map, occurs unobserved in the south in an east-west direction. As the former explanation clashes with an earlier observation, and the second is supported by mapped and delineated minor east-west structures, it is more likely that the second model applies. Increased deformation strains in the south also explain the tendency of the dominant northwest structures to depart from cylindricity.

The long curvilinear synform hinge that appears in g0 is probably a composite of the northwest and east-west fold trends.

Effects of topography have not been mentioned as they usually have little effect upon results. In this case, features can be observed that are due to topography. The exposed geology occurs in hills that rise out

An advantage of using interactive colour graphics equipment for displaying S.O.D.A. plots is that other related techniques using similar equipment can be incorporated into the analytical process (see §8.4). The Landsat scene referred to was actually displayed by using a Sygnetics 2650 microprocessor (Department of Economic Geology, Univ. of Adelaide) because ULOS did not have the necessary display capacity. (Normally 7 or 8 bits per pixel are required for the display of Landsat scenes, whereas ULOS only had 3 bits per pixel.)

of the colluvium. The straight river courses that can be observed in Fig. 5.4 form sharp shadows parallel to the regional trend of small faults (De la Hunty and Jones, 1964) on Landsat images. Hence inclined planes will give rise to curved traces on the maps (e.g. fold axial planes in the western portion of the map, such as the major synform which has its fold axial plane dipping southwest, cause the map trace to be concave in that direction for a positive surface relief); and upright planes show no effects (e.g. fold axial planes in the eastern portion of the map, such as the major antiform which has a straight fold trace).

5.2.2.5 Structural control on mineralisation

To examine how the structures may have controlled mineralisation, all mineralised data points were plotted in blue (Fig. CP.10g). This was produced by using an all blue colour chart, and screening for all types of mineralisation (Appendix C). Although there appears to be no correlation between the occurrence of mineralisation and the structures, it does appear that the grade of mineralisation may be controlled by the major structure, given that the location of drill holes can be used as an indicator of the more economic grades.

5.3 MESOSCALE

The folds used in §2.7.3. and §2.7.4 were analysed by the S.O.D.A. technique to compare the approximate computer-derived contour (S.O.D.A.) plots with the precision contours of the aforementioned sections. Orientations of the folded layering were measured over their upper surfaces and processed. The results are presented below.

5.3.1 Fold From Kanmantoo

The stereonet plots of poles to bedding are presented in Fig. 5.9a. The orientation distribution for the Kanmantoo ("KAN") specimen of \$2.7.3 is a small circle distribution, suggesting a conical fold. Most of the data occurs in two maxima that are coincident with an upright angular cylindrical fold. The isodip S.O.D.A. plot for the fold (Fig. 5.10a) shows contours that correlate well with that of Fig. 2.2la. The radiating isodip contours of a conical fold (Fig. 2.17c) are clearly displayed. The S.O.D.A. plot for the isotrend contours (Fig. 5.10c) also demonstrates a weak but definitely radiating contour pattern. The isotrend chart (Fig. 5.10d) is rotated 15° to that of the contours used in Fig. 2.2la, but this does not affect the results. The 090°-270° contours show some sensitivity due to the very flat limbs of this fold.

5.3.2 Fold From Enderby Land

The specimen from Enderby Land ("ENDL") was processed in an identical manner to that of the Kanmantoo specimen. The stereonet plot of

poles to bedding (Fig. 5.9b) also shows an orientation distribution of a small circle that is also approximated by a great circle. The isodip S.O.D.A. plot (Fig. 5.11a), based on the isodip chart of Fig. 5.10b, shows parallel contours except for those less than 30° in value, as was demonstrated in Fig. 2.22a. The isotrend S.O.D.A. plot (Fig. 5.11b) was based on the isotrend chart of Fig. 5.10d. Although fewer contours are used than in Fig. 2.22b, the pattern does not change significantly, delineating an approximately cylindrical fold hinge region and flat limbs with marked undulations. Deductions based on the accurate contours of Fig. 2.22 are also deduceable from the S.O.D.A. plots.

5.4 MICROSCALE

5.4.1 Quartzite Microfabrics

5.4.1.1 Introduction

A number of quartzite samples were prepared by Wilson (1973) for A.V.A. analyses (not published). The samples are from a prograde regional metamorphic sequence of pure quartzites at Mt. Isa, northwest Queensland, Australia. Two sets of A.V.A. plots are processed by S.O.D.A., one set containing two specimens with randomly distributed quartz c-axes, and the other of two thin sections with quartz c-axes forming crossed-girdles. microfabrics from the lowest metamorphic grade described by Wilson (op. cit.) are of detrital quartz grains (0.3 to 0.2mm) in a chlorite zone. data of this type of microfabric was available. The microfabrics show an apparent reduction in grain size, with the generation of new grains (0.05mm), in upper chlorite and the biotite zones. The quartzite fabrics then increase in grain size in the transition from biotite to biotitecordierite metamorphic zones, varying from 0.05mm to 0.15mm, whilst showing an increase in regularity of grain shape. In the biotite-cordierite zone, and perhaps also in the sillimanite zone, the quartz grains become polygonal in shape, with grain size varying from 0.25mm, where there is less than 10% mica, to 0.06mm with 20% mica. In this metamorphic grade, a similar microfabric may be found that contains abnormally large individual grains. These last two microfabrics are presented in §5.4.2. The highest metamorphic grade (sillimanite) quartzites have exaggerated grain growth, and two thin sections from the same specimen are presented in §5.4.3.

The data supplied for figures 9A,B and 11A,B of Wilson (op. cit.) (Figs. CP.12 and CP.13 respectively) were not field-orientated for the analysis here.

The total time taken to conduct the following analyses (excluding the initial digitisation of the thin sections and setting up of the orientation data) was on the order of thirty minutes. Such rapid

determination is essential if large numbers of specimens are involved (e.g. fabrics produced experimentally).

5.4.1.2 Random Fabrics

Display and Analysis

Fig. CP.12 contains two examples of random fabrics. In Fig. CP.12a four subareas may be observed (see Fig. 5.12a); two (domains b0 and c0) separated by a boundary crossing the figure from the northwest corner to the southeast corner, and a second pair (domains d0 and e0) by an east-west boundary at a position approximating that of the east-west bar on the north arrow. Stereo-plots of the individual subareas demonstrated random fabrics in all cases (Fig. 5.13). Likewise, in Fig. CP.12c the eastern portion appears to be predominantly purple compared to the western portion, and the central east-west portion appears more uniform in tone than the surrounding north and south regions (Fig. 5.12b). However, all show random fabrics when individually plotted on a stereonet (i.e. no significant groupings of orientations are observed).

Discussion

The striking visual methods of analysis highlight apparently heterogeneous distributions caused by the behaviour of random processes. In such analysis by visual perception, uniform distributions are easily confused with random ones. As a uniform distribution will show no colour or spatial groupings, it may be considered to be of no significance, whereas in fact a uniform distribution implies that the data has been subjected to homogenizing processes. Thus, in distributions of low orders of symmetry, it may be necessary to statistically demonstrate the significance of an apparently "random" distribution.

5.4.1.3 Non-random Fabrics

Display and Analysis

Two non-random fabrics were used (Wilson, op. cit., figs. 11A,B), which are reproduced in Fig. CP.13 and Appendix V.

Figure 11A: The stereonet (Figs. CP.13b and 5.14a) shows the distribution of c-axes of the grains, on first approximation, as two crossed girdles, 172°/79° and 061°/87°. However, the two distributions are neither great circles nor cones. The spatial relationship of these orientations (the S.O.D.A. (or A.V.A.) plot of Fig. CP.13a as coloured by the standard colour chart, Fig. CP.13c) is not very clear. The S.O.D.A. plot can be simply described as grains being divided into north-south orientated domains, the orientations within each domain lying either east or west of the north-south girdle. S.O.D.A. plots based on separation of the northern and southern regions using the east-west girdle did not show any obvious spatial arrangement.

Two general orientations of grain boundaries can be seen, one having a north-south direction parallel to the schistosity (parallel to the scale bar), and the other with a northwest-southeast trend approximately parallel to the distribution of the second girdle.

Figure 11B: The distributions, both in c-axis orientations (Figs. CP.13e and 5.14b) and grain distributions (Fig. CP.13d), are quite distinct from those in the previous example, although they are both from the same rock sample (but with different thin section orientations). The stereo-plot shows a strong northwest-southeast girdle, 026°/79°, containing distinct groupings (6°-153°, 60°-159°, 65°-335°, 30°-318°), and a possible weak cross-girdle, 271°/85°. Again, the distributions are not quite great circles nor cones. A grain boundary orientation of 030° is observable.

The marked grouping of orientations suggests the use of a S.O.D.A. plot (Fig. CP.13g) with a colour chart based on the groupings (Fig. CP.13f). A number of spatial groupings become clear.

The pink and blue areas show two separate domains with some interfingering, which demonstrates a rotation of orientation with position. The northwest boundary of the two groups combined has a northeast trend.

The dark red group shows two spatial domains, one dominating the northwest corner of the slide, and a smaller one showing a distinct linear trend in the direction of 030°.

The cyan group, meant to contain those orientations between blue and dark green, also includes a small portion of the dark green group. Two spatially distributed cyan groups appear. The first shows a possible spatial correlation with the smaller dark red group, and the second consists of randomly distributed grains in the north of the slide. The first group was extracted and was found to belong to the dark green group (in orientation). The second group has a distinct orientation but does not appear to convey a structural meaning.

The dark green group (including the cyan coloured grains that belong to it) has no spatial grouping; the grains appear to be randomly distributed.

The yellow group contains a few grains from both the red and dark green groups. This group has no structural significance.

The light green group contains only small, well scattered, grains which may or may not define a possible weak band with a northwest trend. However, if these are taken in conjunction with the light red grains, then the distribution appears random.

Discussion

The discrepancy in overall grain boundary orientation of 030° from

the direction of schistosity (north-south) is not explained by Wilson (personal communication). This trend is not so obvious in the second S.O.D.A. plot of figure 11B of Wilson (op. cit.) due to the optical effects of the colours. (The various dark colours, particularly blue and green, mask the grain boundaries rather than enhancing them. This can be overcome by rotating the colour chart so that the bright colours appear where the dark ones were; or by overlaying the grain boundaries in red or green.)

An observation to be made from the above examples is that some optical effects are attributable solely to the medium being used. For instance, a S.O.D.A. plot with grain boundaries drawn in red can give a markedly different impression from one with the grain boundaries in black. (The picture is imbued with an overall reddish tint. This tinting is recordable on film, although the effect is not as marked*). Other observable optical effects are apparent orientations due to colour contrast. It would therefore be useful to have a program available to analyse (e.g. by rose diagrams) the orientations of grain boundaries in order to detect significant orientations objectively.

In instances of well defined groupings on stereonet figures (e.g. Fig. CP.13e), it is desirable to subdivide the stereonet for S.O.D.A. analysis by drawing the boundary of each group with the stylus (refer to Appendix R) rather than by general stereonet geometry.

5.4.2 Amphibolite Microfabric

Crystallographic axes of hornblende grains in a sample collected from the hornblende gneiss shown in Fig.7.24b were measured on a universal stage and calculated using program HPHB (§3.4.3.2). This is described and analysed in Cohen (1982b) (reproduced in Appendix V, and supplemented with Figs. 5.15, 5.16, 5.17 and Figs. CP.14, CP.15).

From Fig. CP.15, where each of the three crystallographic axes were used to produce the S.O.D.A. (A.V.A.) plots, it is seen that each axis can differentiate the crenulation without referring to the grain shape. They all show orientations that are peculiar to specific regions within the crenulation, as well as those orientations that pervade the crenulation.

No further work is presented here because to proceed to an interpretation of the results is beyond the scope of this thesis.

5.5 CONCLUSIONS

The above examples have demonstrated the usefulness of the

^{*} This is probably because the film is least sensitive to red as contrasting colours tend to psychologically increase colour contrasts (green looks greener, etc.), not the reversed effects observed.

S.O.D.A. technique to geological examples on all scales. The interpretations derived are meaningful and consistent (both internally and with whatever other information was available).

A number of conclusions were derived in the above examples that were in agreement with results possible from standard manual techniques. However, the derived results were generally qualitative rather than quantitative, except for the derivation of orientations from structural domains. As was mentioned in §2.7.1, it would be possible to continue developing the S.O.D.A. technique to increase the ability of computing specific-valued results, but this is beyond the scope of the thesis. A program package with both an improved S.O.D.A. technique and automated standard techniques combined would be an extremely powerful and very rapid analytical tool. The incorporation of standard manual techniques into the S.O.D.A. technique is discussed in §8.3.

CHAPTER 6

INTRODUCTION TO THE GEOLOGY OF THE LIPSON COVE AND ADJACENT AREAS

6.1 AIMS

The technique for the analysis of structural orientation data (S.O.D.A.) was tested using simple models and geological test cases in the preceding chapters. The technique is now applied to a complicated geological area.

The type of geological environment observed at Lipson Cove is suitable for testing the usefulness of the S.O.D.A. technique in a geologically complex area as it has the following features: it is highly deformed, the form surface of its structures is not obvious, and the structures of the area have not been previously analysed and interpreted to a reasonable degree of completeness. A crystalline basement complex provides a far more severe test of the S.O.D.A. technique than a sedimentary (or metasedimentary) environment (such as an extension of the Hamersley Ranges example, see §5.2.2), where the form surfaces are generally accessible, because there are generally no marker horizons to indicate form surfaces.

An additional bonus would be the elucidation of the structural geometry of an area of interest not hitherto investigated. Consequently, this test case is divided into two chapters, the first (this chapter) describes the geology of the field area, and the second (Chap. 7) deals with the analysis of the structures.

6.2 INTRODUCTION

6.2.1 Location

The area under investigation lies on the coast between Tumby Bay and the Dutton River north of Port Neill on the southeast coast of Eyre Peninsula (Fig. 6.1), contained within the rectangle bounded by 136° 00', 34° 00' and 136° 30', 34° 23', and is covered by the half-mile topographic maps, Tumby A, Neill B and D (South Australian Department of Lands). Contained within this area is a small section of coastline that lies between Lipson Cove and Rodgers' Beach, and is bounded by the latitudes 34° 14' 40" and 34° 15' 20". It is in this small section that the geological investigations were made. The larger area was examined in less detail (Appendix O) to provide an understanding of the smaller area's relationship to the regional geology.

6.2.2 Topography

Outcrops investigated were restricted to the waterline along the length of the coast. They are generally on the order of 30 metres wide,

varying in nature from shore platforms to cliffs 20 metres high. In the vicinity of Lipson Cove, shore platforms were the only exposures. Inland from the high water line, the ground is either farmed or covered in sand dunes or marsh.

Outcrop is continuous, except for sandy and pebbly beaches. In the cliff regions, it is cut by joints that have been eroded out by the sea.

The coastline lies at a small angle to the regional structural trend, exposing geology more or less along strike, rather than generally more useful across-strike sections.

6.2.3 Mapping Procedures

The area around Lipson Cove is the only one which shows any fold structures in aerial photographs. Ground reconnaissance (Appendices O and N) also revealed this area to be structurally interesting and distinct from the area mapped by Clarke (1976). Ground surveying was considered the most suitable method for obtaining a base map because of the very small size of the area, and the very small lithologic units that revealed the structures. Plane tabling, although perhaps the optimal method available, was made impossible by continuous sea spray. A tape and compass survey was therefore chosen, mapping at a scale of 1:200.

The base map required 12 contiguous maps (numbered 1 to 12, from north to south), which are combined into four sheets (Figs. 6.1 and 6.2). For analytical purposes, these have been divided into five submaps (Chap. 7): M13 (maps 1 to 3), corresponding to most of Sheet 1; M45 (maps 4 and 5), corresponding to the northern portion of Sheet 2; M6AB (parts A and B of map 6), corresponding to the southern portion of Sheet 2; M789 (maps 7 to 9north), corresponding to most of Sheet 3; and M912 (maps 9south to 12), corresponding to Sheet 4. Locations within the base map are referenced by their grid coordinates (eastings, northings).

The larger field area was covered by a number of aerial photograph enlargements (1:1700). The air photographs used are (from north to south, using South Australian Dept. of Lands numbering): SVY 1507 SA, #13, 15, 32, 34, 38, 40, 53, 55, 59, 61, 78, 80, 81, 82; and SVY 1653 SA, #49 to 41.

The detailed and regional research area is wholly within the area previously mapped by Coin (1976) for his Ph.D. thesis and in turn the regional area contains Clarke's (1976) Honours thesis area. Both of these authors comprehensively describe the history of geological investigations in the area prior to 1976, although these did not include detailed or complete structural geological investigations.

6.3 LITHOLOGICAL DESCRIPTION

6.3.1 Introduction

The eastern side of southeast Eyre Peninsula is comprised of two suites of rocks, the metasedimentary Hutchison Group, described by Parker and Lemon (1982) as consisting of the basal Warrow Quartzite overlain by a sequence of schists, dolomites, banded iron formations, and local amphibolites, and the Lincoln Complex (known as the Flinders Group prior to 1979) consisting of acid and mafic gneisses and granulites. The two rock suites are separated by the Kalinjala mylonite zone (Fig. 6.1). The Lincoln Complex is never observed in direct contact with the Hutchison Group, but it is thought that the former is intrusive into the latter (Parker, 1980; Webb, 1980).

Although the research area is contained within the Lincoln Complex, geological investigations carried out in the Hutchison Group are noted because of the much greater clarity of the tectonic history that is revealed there, and as the two rock suites have had similar tectonic histories (Coin, op. cit.).

Detailed observations of the gneisses of the Lincoln Complex at Lipson Cove revealed compositional inhomogeneities even on small scales (metres). For mapping purposes the gneisses were grouped into general categories (Fig. 6.2). The two major categories were acidic (granitoid) gneisses and mafic (amphibolite) gneisses. The former was divided into two types: 1) a granitic gneiss, and 2) a leucogranitic gneiss; distinguished in the field largely by their colours (reflecting compositional differences). The amphibolites were divided into two types: 1) a dark amphibolite containing a smaller ratio of feldspar to hornblende than that of 2) a light coloured (leuco) amphibolite.

Other mappable lithologies were: 1) biotite schist/gneiss units containing quartz ribbons, 2) intimately mixed acidic/mafic gneiss units, and 3) pegmatites and granitic veins.

Only the clearly observable pegmatites and granitic veins were mapped (thin layer parallel veins were difficult to discern in the granitoids). Pegmatites that have been metamorphosed to a granitic gneiss in appearance (i.e. contain a foliation) have been mapped as granitic gneisses.

6.3.2 Acid Gneisses

6.3.2.1 Granitic Gneiss

These have a general granite composition of:

quartz + feldspar + biotite + hornblende + zircon + apatite + opaques

(magnetite + ilmenite).

The rock is generally coarse grained, although medium grained

units can be found. It contains 5% or more mafic minerals.

Augen gneisses are included in this category. The augen consist of feldspar, and they vary in size from one to several centimetres in diameter. They vary in shape from prolate to extreme oblate ellipsoids, of which the oblate form is most common, and can be folded.

Feldspars are mainly potassic (pink to white) although plagioclase (white) may abound locally. Perthites also occur. Partial alteration of the feldspars to sericite is common, and is associated with some alteration of biotite to chlorite.

Most gneiss units are relatively small (metres to centimetres wide), but can occur within larger semi-homogenous bodies decimetres wide and a hundred or more metres long, as well as within amphibolites (both large and small).

This gneiss is the "Augen Gneiss" unit described by Coin (op. cit.), and is similarly described by Clarke (op. cit.).

6.3.2.2 Leucogranitic Gneiss

The term refers to granitoid gneisses with mafic mineral constituents of less than 5%. Grain size can vary from medium to coarse.

Coin (op. cit.) described this gneiss unit as a "Quartzofeldspathic Gneiss", which Clarke (op. cit.) assigned to the feldspar-rich variety of the "Quartz-Feldspar- Hornblende Gneiss" unit.

6.3.3 Mafic Gneisses

6.3.3.1 Amphibolite Gneiss

The common mineral assemblage is:

hornblende + feldpsar + biotite + accessary sphene + apatite + zircon + epidote + chlorite + opaques (magnetite + ilmenite) + sericite.

Epidote is often found associated with biotite, as is zircon.

Feldspar can vary from fresh to highly sericitised, and is almost always plagioclase.

Hornblende can be seen to be replaced by biotite, which in turn is replaced by chlorite. All chlorite appears to be formed from biotite.

The opaques are generally fine-grained and are distributed in many parts of the amphibolites.

The gneisses often contain large amounts of quartz and migmatite veining (Fig. 6.3).

gneiss described amphibolite the (op. cit.) Coin "Porphyroblastic Amphibole Gneiss" because of the porphyroblasts of potash size. 1-30mm in from vary feldspar and amphibole which porphyroblasts do not occur in the amphibolite gneisses in the mapped Clarke (op. cit.) also described a similar type of amphibolite in the vicinity south of Port Neill.

6.3.3.2 Leucoamphibolite Gneiss

This rock type is light coloured in appearance because of the high ratio of feldspar to hornblende. It can be as light as, or even lighter than, some granitic gneisses, but because it contains no quartz and is always found with the dark amphibolites, it is included as an amphibolite.

Radiating fibrous sillimanite, which occurs in the feldspars, is an accessory found only in this unit.

6.3.3.3 Biotite Gneiss

This rock type occurs as small pods several metres in size contained mainly within the dark amphibolites. Thin layers (centimetres thick) can occur in the granitoid gneisses. They consist mainly of idioblastic biotite + quartz + accessory apatite + zircon.

The biotite gneisses occurring in the dark amphibolites have gradational boundaries which may include other minerals, mainly hornblende and plagioclase. The biotite gneisses in the dark amphibolites may also be associated with migmatite veins.

Quartz occurs both as ribbons and as grains within the matrix. The quartz grains in the ribbons show strain shadows and are generally larger than the matrix grains.

6.3.4 Intrusions

Only pegmatites and granitic veins are mapped as intrusions. Coin (op. cit.) included mafic and ultramafic materials, but none were found in the mapped area, although they occur to the north of the mapped area. This is because in the mapped area there is no overprinting evidence to show that any of the mafic material intruded the acidic material, or vice versa.

Several periods of pegmatite and granite intrusions can be recognized, but due to the intensity of early deformations and metamorphism, only intrusions occurring late in the tectonic history are easily recognizeable (Fig. 6.4). These veins are often emplaced parallel to S_{0-1} and the larger veins may approximate the S_3 orientation. They have a simple mineralogy consisting of:

quartz + microcline + plagioclase + biotite + opaques (magnetite + limonite) + zircon + myrmekite.

Post-tectonic intrusions are similar in mineralogy but tend to be coarser-grained. They may contain large amounts of magnetite and epidote.

South of Lipson Cove, these intrusions can include beryl, garnet, and small books of muscovite (Fig. 0.2c). Small veins with relatively large proportions of limonite, magnetite and epidote can also be found.

Coarse-grained opaques occur in two limited horizons (Fig. 6.5a) which cross-cut layering at small angles in both amphibolites (Fig. 6.5b) and granitic gneisses (Fig. 6.5c). They are recognizable by their large

size (up to one centimetre), and are often surrounded by feldspar and quartz (Fig. 6.5d). Late stage granitic and pegmatite veins may also contain large grains of opaques (Fig. 6.4c).

6.4 REGIONAL GEOLOGY

6.4.1 Tectonic History

Parker (1978) mapped and analysed the structural geometry and history of the Hutchison Group in the Cowell/Cleve area (Table 6.1). He interpreted four deformation episodes, the first (D_1) was a fabric-forming event producing rare folds, the second (D_2) was a fold and fabric forming event, the third (D_3) a fold-forming event, and the fourth (D_4) a crenulation event. The Kalinjala mylonite zone was thought to be synchronous with the third deformation (in agreement with Coin, op. cit.), but is regarded as a separate tectonic event (D_m) from the other four.

From whole rock and mineral radiometric dating procedures undertaken by the Department of Mines and Energy and the University of Adelaide, the tectonic sequence (Fig. 6.6) categorised by Parker's description is termed the Kimban Orogeny for the $\rm D_1$ to $\rm D_3$ (and $\rm D_m$) events (dating from approximately 1820 Ma to 1580 Ma (Webb, 1980)), whilst the $\rm D_4$ event is termed the Wartaken Event (Parker and Lemon, 1982).

In the vicinity of Port Neill, Clarke (op. cit.) conducted structural analyses of small outcrops contained wholly within the Lincoln Complex. He deduced three deformation episodes, of which the first produced a fabric and few folds; the second produced tight to isoclinal folds with a weak fabric in the fold hinges; and the third was a crenulation event comparable to the D_4 event described by both Coin and Parker.

Mortimer et al, (1980) observe the same deformation sequence in the Lincoln Complex as that described by Parker, as do Fanning et al, (1980) in the Sleafordian Complex, although there are variations in the intensity and orientations of each episode. Similar tectonic histories are noted by Pedler (1976), Golin (1976), and Richardson (1978) (Table 6.1) in possible equivalent rocks of the southern Yorke Peninsula. Again, the differences are in the relative intensities and orientations of the structural elements.

6.4.2 Metamorphic Conditions

The P-T conditions for the metamorphic episodes accompanying each of the deformation periods was not determined by Coin because of the wide stability fields of the quartzofeldspathic and granitic gneisses. He did however deduce from amphibole analyses, with comparisons to results of Leake (1971), Raase (1974), and Kostyuk and Sobolev (1969), that the

Lincoln Complex gneisses are of amphibolite-granulite facies formed at the low pressure of approximately 3kb; having been through two deformations during granulite facies conditions, followed by a retrogressive amphibolite facies metar morphism (local to the Tumby bay region) associated with D₃, and a retrogressive greenschist facies with the final deformation (Table 6.1). To the south of Tumby and to the north (Port Neill), some of the gneisses are of granulite facies (Mortimer et al, 1980; and Clarke). Bradley (1972) derived P-T conditions of 6 to 8 kbars at 750 to 900°C (granulite facies) for the Lincoln Complex in the vicinity of Tumby Bay, followed by amphibolite facies retrogression.

Pre- to syn-D₁ migmatisation can be seen in the amphibolites (Fig. 6.3a), and although they also occur in the granitoids they are very difficult to discern. Retrograde metamorphism in the amphibolites, as pyroxenes altered to hornblende, released quartz and magnetite (Sen and Ray, 1971; Mortimer, personal communication), which can be seen as ribbons and small veins of quartz (Fig. 6.3b), and disseminated magnetite. However, no trace of pyroxenes have been observed in the mapped area, and so it is possible that in the area of Lipson Cove the metamorphism never achieved granulite facies.

Retrogression of hornblende to biotite released excess silica, which accounted for the large amount of quartz in the biotite gneisses. Whether this second retrogression accounts for some of the quartz ribbons is unknown. The biotite gneisses show a structural history as complete as that of any other rock type, and so it is possible that the second retrogression occurred in the waning stages of the first retrogression, in those localities where the material was sufficiently hydrated and potash rich.

Parker (1978) concluded that the conditions of metamorphism for the Hutchison group rocks were at pressures of less than 10 kbars (around 5 to 7 kbars) and temperatures on the order of 750°C.

6.4.3 Emplacement of the Lincoln Complex Rocks

The rocks of the Lincoln Complex in the vicinity of Tumby Bay are summarised by Coin (op. cit., page x) as being: "... of a highly deformed complex of quartzofeldspathic and granitic gneisses with intrusions of dolerite, gabbro and an ultramafic as well as small granitic bodies."

The mafic intrusions occurred in two periods (Coin), one postdating D_1 and the other postdating D_2 . Flook (1975) also described two periods of mafic intrusions in the Lincoln Complex at Kirton Point. The first predated the Kimban Orogeny, and the second appeared to postdate D_1 . Cooper et al (1976) reinterpreted this locality, recognising that the second mafic intrusion event postdated D_2 . However, they interpreted

the structural history of the area to have only three deformations, with the third deformation corresponding to the Wartaken Event (D_{ij}) . Hence, the timing of the second dolerite intrusions is unresolved, and there are doubts on the timing of the first period of mafic intrusions.

Pretectonic granite intrusions are recognised. Flook (1975) determined the granite intrusion(s) to follow after the first mafic intrusion event, whereas Cooper et al (1976) obtained the reverse. Syntectonic granite intrusions are well documented (for examples see Coin; Parker, 1978; Thomson, 1980), and known to occur at all stages of the Kimban Orogeny. Pegmatite, granite and aplite veins were formed throughout the Kimban Orogeny, and occur spatially throughout the Complex.

6.5 STRUCTURAL ELEMENTS OF THE LIPSON COVE AREA

6.5.1 The Lithological Layering

Lithological layering (S_0) is defined by mineralogical differences. The layering can occur on all scales, from a thickness of a few millimetres (Fig. 6.7a) to metres (Fig. 7.23).

A pretectonic possibly igneous layering (Fig. 6.7a) occurs as banding in some of the amphibolites. The bands vary in width, up to a few centimetres thick, and are traceable over many metres. The bands are caused by varying ratios of hornblende, biotite and feldspar. Selvadges of biotite may occur on boundaries between hornblende rich and feldspar rich layers.

6.5.2 Elements of D_1

The first deformation event produced an LS fabric (S_1) , which is generally layer-parallel and is differently expressed in the different rock types. It can occur as a schistosity, defined by alignment of hornblende and biotite grains (e.g. Fig. V.1, Fig. 6.7d), or by large flattened augen of feldspar (e.g. Fig. 6.7b,c). The S_1 foliation is ubiquitous, and is the dominant foliation within the area (although it may be transposed into later foliations) and always appears to be orientated within a few degrees of S_0 , being mainly parallel to it. Accordingly, S_{0-1} refers to both S_0 and S_1 where it is unnecessary to distinguish them, and to any other layering produced by, or prior to, D_1 (e.g. M_1 , the first metamorphic event, which occurred synchronously with \mathbf{D}_{1} , migmatites, and pre- to $syn-D_{3}$ granitic veins - Fig. 6.3a). As S_{0-1} is the most intensely developed foliation it is an important structural element for the geometric analysis of the Lipson Cove area (Chap. 7). Furthermore, lineations are mostly measured on this surface, and most folds are formed by folding this surface.

 L_1^1 (abbreviated to L_1), the D_1 lineation on S_1 , is a

mineral elongation lineation occurring in localised regions throughout the mapped area but is not everywhere penetrative. It can vary from the orientation of augen (e.g. Fig. 7.38a) to alignments of biotite or quartz grains (e.g. Fig. 7.3b), and can be parallel or oblique to F_{2-3} folds.

Few, if any F_1 folds were produced during D_1 . All folds examined (e.g. Figs. 6.3c,d) that appeared to be F_1 , proved subsequently to be F_2 folds. There may be F_1 folds in early migmatites, e.g. Fig. 6.3a) and in the layered amphibolites (e.g. Fig. 7.16). F_1 folds are recognized elsewhere in the Gawler Craton (e.g. Pedler, 1976) and surrounds (e.g. Glen et al, 1976).

6.5.3 Elements of D2

The second deformation event produced a weak planar fabric (S_2) , a foliation occurring mainly in the finer grained units, such as amphibolites (Fig. 6.7d) and biotite schists. It is developed better where S_1 and/or S_3 are subparallel to it (e.g. Fig. 7.39). S_{1-2} refers to both the S_1 (or S_{0-1} if appropriate) and S_2 foliations when they are sub- parallel, or when S_2 is S_1 (S_{0-1}) transposed (Figs. 6.3c,d and 6.5b).

F₂ folds are tight to isoclinal, range from upright to recumbent, vary in size from a few centimetres (e.g. Fig. 6.7d) to decimetres (e.g. the folding in Fig. 6.2, Sheet 4, represented by Fig. 7.39), at times fold a lineation (L₁) (e.g. Fig. 7.3b), have a complex morphology over short distances (e.g. Figs. 7.5c,d), and are generally distinguished from F₃ folds by overprinting criteria (e.g. Fig. 7.3b). Style is not a suitable method for distinguishing between F₂ and F₃ folds. Fold plunges are generally shallow plunging, but they may have steep to vertical plunges. Some larger folds (measured in decimetres) are often recognized only by repetition of the thickness of rock units (e.g. in domain cl, Fig. 7.6), and/or because their asymmetric parasitic folds mismatch the F₃ fold limb senses on which they are found (e.g. Figs. 7.5a,b). The specific terms F₂⁰ and F₂¹ (Bell and Duncan, 1978) are not used as S₁ is everywhere parallel or subparallel to S₀.

6.5.4 Elements of Da

The third deformation event produced a weak LS fabric (S_3) , a schistosity similar to S_2 . It is easier to recognise when at a high angle to the previous foliations (Fig. 7.4). In the coarser units, the orientation of this foliation can be difficult to measure because of its anastomosing pattern around augen. Syn-D₃ pegmatites also exhibit this foliation (Fig. 6.4b).

S₃ can occur as a crenulation cleavage (Fig. 7.20c) or as axial

plane jointing (Fig. 7.4a). D_3 tends to intensify S_2 (rather than produce an S_3 foliation) when S_3 is subparallel to S_2 (Fig. 7.39). Thus the term S_{2-3} refers to both foliations when they are subparallel or indistinguishable. The S_3 schistosity, and the parallel F_3 fold axial planes, form a second important element in the structural analysis of the Lipson Cove area (Chap. 7).

 L_3^1 is a crenulation lineation, resulting from the crenulation of S_1 by D_3 (e.g. Fig. 7.20c). S_2 is insufficiently developed to be crenulated, or where it is well developed, it is subparallel to S_1 (i.e. S_1 a).

 L_3^3 (abbreviated to L_3) is an elongation lineation similar to L_1 , except that it is parallel to F_3 fold axes (e.g. Fig. 7.3a). It can occur as prolate augen or as alignment of biotite grains. Again, it only appears in localised areas and is not often penetrative (except in biotite gneisses). Hornblende grains may also be aligned parallel to this lineation, but such lineations are usually poorly developed.

 L_{2} is morphologically similar to L_{1} . However, the earlier lineation is not observed to be folded by steeply plunging F_3 folds (but are folded by subhorizontal F_{2-3} folds) and hence it appears that the two lineations may be the same. If this is so, then it can be deduced that the stress field for D_3 was such that L_1 was rotated into parallelism with F_3 where orientations were suitable (e.g. where the long axis of the D_3 strain ellipsoid was subparallel to the lineation, Fig. 6.8a) and $L_{\hat{l}}$ was obliterated by flattening where the orientations were unsuitable for rotation (e.g. when the long axis of the strain ellipsoid was approximately orthogonal to the lineation, Fig. 6.8b). The strain ellipsoid for D_{Q} was capable of producing LS fabrics, as shown by the biotite gneisses described elsewhere (e.g. Figs. 7.27b and 7.37c) which have an L_3 lineation defined by the long axis of biotite grains lying in an S_3 schistosity. Consequently, the two elongation lineations are regarded as separate entities, even if one may be shown in places to be the rotation of the other.

 F_3 folds vary in scale from microscopic (crenulations, e.g. Fig. 7.15) to decimetres (Geology Sheet 4), forming symmetric folds on small scales and asymmetric folds on all scales. As for the F_2 fold terminology, specific terms for F_3 will generally not be used. However, the F_3^2 term is used where the D_3 folding of F_2 fold axial planes and axial plane cleavages (S_2) need to be distinguished from D_3 folding of S_{0-1} foliations. F_{2-3} is used when a fold generation is in doubt because F_2 folds, particularly in the granitic gneisses, are difficult to differentiate from F_3 folds if overprinting criteria are not available.

 \mathbf{F}_3 folds and their associated lineations together form the third important element in the structural analysis of the Lipson Cove area.

The regional D_3 event had a stress field that produced macroscopic horizontal open folds with doubly plunging hinges (Fig. 6.6).

6.5.5 <u>Intersection Lineations</u>

The intersections of the tectonic foliations $(S_1, S_2 \text{ and } S_3)$ with S_0 , or the intersection of S_2 and S_3 with S_1 , produce intersection lineations which are collectively labelled in this study as L_1 . Intersection lineations are not common, mainly occurring in the finer grained units (e.g. Figs. 7.3c,d), and do not form a significant element in the analysis of the Lipson Cove area. Most L_1 could be specifically termed L_1^0 because S_1 is more intensely developed than S_2 or S_3 .

6.6 STRUCTURAL ANALYSIS

The vicinity of Lipson Cove was structurally analysed in Chap. 7. The most useful structural elements were the ones most readily recognised and common throughout the area. These were S_1 , S_3 (including the axial planes of F_3 folds), and F_3 fold hinges (including L_3). The geometric analysis of Lipson Cove included both the application of the S.O.D.A. technique and field observations.

After Parker, 1978 (Hutchison Gp.)		After Richardson, 1978	After Coin, 1976	
(Ma) 1450 D ₄ + M ₄	Cratonisation Minor east-west crenulations, kinks and fractures. Weaker conjugate set 150°/330°.	Upright open to close folding with a steep west or vertical plunge. Approx. E-W axial trace. S4 - none observed.	(Lincoln Complex) Large scale dextral warping and brittle fractures across mylonite zone. Local retrogressive green-schist facies along faults.	(Hutchison Group) Localised warping about axis approx. 60°-320°. Localised faulting across mylonite zone. Boudinaged layered amphibolites.
D ₃ + M ₃	Major fold deformation - tight upright folds of variable shallow plunge. S ₃ swings from 040°/220° to340°/160°. Local intense mylonitization (D _M).	Upright to steeply inclined open to tight folding on all scales. S ₃ - weak biotite.	Formation of S_3 and localised mylonite foliation S_m in mylonite zone. S_3 subparallel to S_2 . Regional amphibolite facies. Second series of dolerite and ultramafic intrusives. Some granitic emplacement.	Crenulations. Deformation as for D ₂ . Latter stage mylonitization. Mn rich outer zone of garnets, sillimanite continues to grow, staurolite unstable, second stage growth on some tremolites, andalusite.
D ₂ + M ₂	Major fold deformation - isoclinal, recumbent folds of shallow plunge trends 010° to 020°. Strong L-S fabric.	Upright to steeply inclined tight to isoclinal folds. Plunge to NW and SE. S2 - Weak to strongly developed biotite.	Folding of S ₁ . S ₂ subparallel to S ₁ . (?) Granulite facies. Pegmatite; first series of dolerite intrusives. (E ₂)	Fold forming event produces S2. L2 parallels fold axes. Initial growth of garnet, sillimanite, staurolite stable, first tremolite growth. Yunta Well Leucogranite.
D ₁ + M ₁	Major fabric forming deformation, folding not confirmed.	Tight to isoclinal folds. S1 - layer parallel fabric of strongly developed biotite and hornblende.	<pre>Layer parallel gneissosity, S₁. (?) Granulite facies. (?) Pegmatites and other acidic intrusives. (E₁)</pre>	Layer parallel foliation, S ₁ .
2120	Hutchison Group Sedimentation Lincoln Complex	Dolerite dyke intrusion ————————————————————————————————————	Indeterminate genesis.	Sedimentation in shallow, stable cratonic basin. Lincoln Complex.

CHAPTER 7

GEOMETRIC ANALYSIS OF THE STRUCTURES OF THE LIPSON COVE AREA

7.1 INTRODUCTION

7.1.1 The Technique of Subarea Analysis

Subarea analysis is the technique derived by Turner and Weiss (1963, p.145ff) as a useful procedure for conducting the geometric analysis of macroscopic structures. The term <u>domain</u> (Appendix G) was defined by Turner and Weiss (op. cit.) as an <u>area of structural homogeneity with respect to one or more structural elements (subfabrics). The classical procedure for using subarea analysis is to first collect a large amount of data from uniformly distributed locations, secondly define many domains of 20 to 50 data points each, based on the visual observations of plotted data, and thirdly analyse each domain separately, defining possible groupings of geometrically significant domains that adequately describe the macroscopic structure.</u>

In previous chapters, the S.O.D.A. technique was used to classify structures using isodip and isotrend contours of Type II trend surfaces to directly model Type I trend surfaces. These contours define domains as described in the previous paragraph, but the shapes of the domains for the dips and trends of data values were adequate to define the shapes of structures under analysis. However, the geological structures of the area of Lipson Cove have complexities that do not lend themselves to this method of analysis. The two main causes are (1) the mesoscopic structures are on such a small scale compared to the macroscopic structure that the collected data does not directly define the large scale structure, and (2) the outcrop is primarily one dimensional, i.e. not wide enough, and so the shapes of contours are not definable and hence the large scale structure cannot be determined from contour shapes.

The S.O.D.A. technique is therefore used here to define domains as commonly used in geometric analysis, i.e. Type II trend surfaces are used to analyse properties of the data, and so domains of structural homogeneity are thus defined between contour lines. The power of the S.O.D.A. technique enables the subarea analysis to be done directly and rapidly. That is, instead of using the classical mthod of having to break down the area into many small domains, analyse each, and then group them into meaningful domains, the S.O.D.A. technique allows the significant domains to be defined directly and then these can be subdivided into subdomains for more detailed geometric analyses, continuously, until the level of detail desired is reached (within the limits of the initial data set).

The method of defining domains and subdomains used in this chapter

elements. The structural element that shows the clearest domains is then used to define the approximate boundaries of the first level of domains. The exact position of the domain boundaries is then found by maximising the distinctiveness of the clusters of each of the fabric elements on a stereonet. Although this procedure may require several attempts to achieve satisfactory results, it only takes a few minutes. As an added bonus, by defining each domain based on all fabric elements, the number of domains required is kept to a minimum (instead of defining domains based on each element separately).

7.1.2 Procedure Used for Applying Subarea Analysis

In this chapter the structures to be found in the mapped area north of Lipson Cove (Figs. 6.1 and 6.2) are described subarea by subarea (see below). They are analysed using the S.O.D.A. technique and related field observations, and interpretations are attempted. As detailed investigations of all the structural elements are beyond the aims of this thesis, only the most common elements, S_1 , S_3 and F_3 (see §6.5), are analysed.

The mapped area was divided into five submaps (§6.2.3), which were determined by size and the availability of data. The area is conveniently divided into four geology sheets (Fig. 6.2) and the submaps were selected according to the continuity of data. Hence in geology sheets 1, 3, and 4 there is one submap per sheet (submaps M13, M789, and M912 respectively), extending for the length of outcrop where there is measured data (which may not be the full length of outcrop mapped). In geology sheet 2, most of the outcrop would have required very large amounts of data as compared to the other submaps, and so data collected for this sheet are spatially scattered. Because there is a region of no measured data between the north and south of the outcrop, the sheet was divided into two submaps (M45 and M6AB respectively).

The area of Lipson Cove has very large numbers of small-scale structures that make it necessary either to collect extremely large data sets to enable use of the S.O.D.A. technique alone, or to collect smaller amounts of data and use them in conjunction with field observations. The latter method was chosen as it is more efficient and accurate, given the complexity of the area and the absence of marker horizons. Therefore, in the ensuing analyses, the interpretations of the structures are based as much on the field observations as they are on the domain analyses.

At this point it is worth reiterating that the primary aim of this chapter is to test the usefulness of the S.O.D.A. technique in the structural analysis of a complexly deformed area consisting of crystalline

rocks, which requires interpretations of the structures to be based on the S.O.D.A. analyses. Accurate interpretations of the structures of such an area, based on all possible available methods normally used in structural analysis research, are secondary to this aim. In accordance with these goals, the interpretations of the structures in each submap are primarily derived from analyses by the S.O.D.A. technique with support from field observations. Because the field observations are of secondary importance in this chapter, and so not processed to the extent normally encountered in research work aimed at unravelling the structures of deformed rocks, interpretations made in each subarea may not be the only ones possible. Interesting mesoscopic structures are also discussed in the interpretations, but, like submaps in general, they are discussed mainly in the light of spatial-orientation distribution analyses and so models derived to portray them may not be comprehensive.

As a final introductory remark on the application of the S.O.D.A. technique in this chapter, it must be noted that there is a slight change in the use of domain labels (see Appendix G). In the analysis of Lipson Cove, it was impractical to label the whole mapped area of Lipson Cove (i.e. the map, see Appendix G for terminology) as 'a0' because it could not be displayed as a S.O.D.A. plot, in its entirety, and yield any useful information. Therefore the domain labels were associated with the next lower level of subdivision (i.e. submaps became 'a0', etc.), and the total map of Lipson Cove was not considered for processing by the computer programs, except to compile summary stereonet plots (Fig. 7.1) of the structural elements used in this chapter.

7.2 A BRIEF DESCRIPTION OF THE STRUCTURES AT LIPSON COVE*

The structures in the mapped area generally show a fairly simple folding history, until a close examination is made. At the smaller scales (hand specimen size) small layers of contrasting lithology reveal complex fold patterns that are highly variable over short distances (metres) and resemble sheath folds (e.g. Minnigh, 1979; Cobbold and Quiniquis, 1980). In other places in the mapped area, complex fold patterns are quite clear. Despite the complexity of the fold structures, the overall orientations for

Because of an oversight during the creation of the data files for the structural analysis of the area by the S.O.D.A. technique, i.e., orientation data were not corrected for magnetic inclination, all azimuthal orientations in this chapter are relative to magnetic north, which is approximately 7° east of true north (Fig. 6.2). Therefore, 7° must be added to all compass readings to obtain true directions. The oversight was not corrected because (1) the figures were already prepared, and (2) it has no affect on the aims of this part of the study.

the most common and recognisable structural elements $(S_1, S_3, and F_3)$, form simple distributions on stereonet plots (Fig. 7.1). These distributions define a strong NE-SW (040°-220°) structural trend, which is well-defined on aerial photographs for the entire coastal exposure from south of Lipson Cove to north of Port Neill. It is interesting to note that the best-fit great circle girdle containing F_3 fold hinges (and parallel L_3 lineations) is better defined by the mean S_1 (310°/86°) than the mean axial plane S_3 (317°/88°). (Although there are far fewer measurements of S_3 than there are for the other two elements, which are therefore less likely to represent the true mean orientations of S_3 , S_3 is more consistent in orientation and therefore requires fewer data points.)

7.3 SUBMAP M13

7.3.1 Structural Description

The geology of submap M13 as deduced by field mapping of structural elements (located in Fig. 7.2) is presented in geology sheet 1 (Fig. 6.2), which represents a sequence of interlayered granitic (augen) gneisses and amphibolite gneisses. The layering (S_0) and prominent foliation (S_1) have been folded into tight to isoclinal, generally subhorizontal, F_2 folds that are frequently not easily observed, and a series of open F_3 folds along the north shore with wavelengths and amplitudes of decimetres. S_0/S_1 remain relatively unfolded along the east shore. The F_3 folds steeply plunge to the southwest (Fig. 7.7c).

 \mathtt{S}_1 is layer-parallel with an elongation lineation, \mathtt{L}_1 (defined by prolate ellipsoidal augen and aligned hornblende grains). lineation does not occur in all folds but is often seen folded by the subhorizontal F_2 folds (e.g. Fig. 7.3b). A second elongation lineation (L_3) is parallel to the mesoscopic steeply-plunging fold hinges. In the $ar{ t L}_{ar{ t Q}}$ lineation becomes less intense as the fabric flattens to that of an oblate ellipsoid parallel to the dominant foliation. A weak axial plane cleavage (S_3) occurs in some folds, and is more intensely developed in the hinges than in the limbs. In other F_{γ} folds, an incipient axial plane cleavage is developed, which may be accompanied by joints that are parallel to the axial plane (e.g. Fig. The F_{γ} folds in the northwest of the submap are angular with straight limbs whilst to the east the folds become more rounded, where they change to open monoclines on the east shore. In the northwest and east the folds have sinistral asymmetry and the centrally positioned rounded folds are approximately symmetrical.

The presence of F_2 folds in parts of the submap is indicated by indirect evidence. Evidence for the recognition of the D_2 deformation

event include: 1) In the area represented by the northwest portion of the map the sequence of acid and mafic gneisses (folded by D₃) shows a pattern of thicknesses for the gneissic units that repeats itself. This suggests the presence of one or more tight to isoclinal folds of an earlier generation which are either subhorizontal or have their hinges transposed out (due to the lack of exposed fold hinges). These are most likely to be D₂ folds as they have the orientation of F₂ folds observed elsewhere at Lipson Cove. 2) Some asymmetric parasitic folds, highlighted by quartz and quartzofeldspathic veins, give an opposite to expected indication of fold vergence for some of the folded amphibolite gneisses in which they are found (e.g. Figs. 7.5a,b). These are primarily observed in the area represented in the northwestern half of the submap.

A summary of the structural history of submap M13 may therefore be stated as follows. Because the intrafolial folds fold the dominant foliation, the dominant foliation can be assigned to D_1 (S_1), the intrafolial folds to D_2 (F_2), and the mesoscopic folds to D_3 (F_3) with axial plane cleavage S_3 . No folds were found on any scale that had the dominant foliation as axial plane and no deformation effects were found to overprint D_3 . This summary also applies as a general rule to all other submaps of the mapped area, described in the rest of this chapter.

7.3.2 Subarea Analysis by the S.O.D.A. Technique

The structural data maps are presented in Fig. 7.2. Stereoplots for the structural domains (determined below) of submap M13 (Fig. 7.6) are presented in Fig. 7.7. The S.O.D.A. plots (Fig. CP.16) for each of the elements are based on their stereoplots (composite, Fig. CP.16b, comprised of parts (a)-(c) of Fig. 7.7A).

Poles to S_1 in the submap form a great circle girdle orientated at 036°/19°* (Fig. 7.7Aa). Data points are concentrated in the limbs because of the generally angular nature of mesoscopic F_3 folds.

S_l orientations around the great circle girdle correlate with their spatial positions on the map (Fig. CP.16a), which is more pronounced in the southern half of the submap and forms the basis for the primary subdivision of submap M13 into the two domains, c0 and d0 (Fig. 7.6). This same correlation between orientation and position in domain d0 forms the

Because of the variety of forms available for expressing orientations, planes will be given in the form xxx°/xx°Q (where Q is the quadrant of dip direction) for strike/dip and xxx°/xx° for dip direction and dip. Therefore, 135°/90° is a vertical plane with a strike of 045° (i.e. 045°/90°SE or 045°/90°NW). Lineations are given in the form xx°-xxx°, i.e. plunge towards plunge direction. Pitches, if any, will specify the quadrant of the strike from which the pitch angle was measured.

basis of the secondary domains dl, d2 and d3 (using isotrend contours, see Fig. CP.16a).

It is notable that the orientations of S_1 in the limbs of the smaller-scale asymmetric folds of domain c0 do not parallel the corresponding orientations of S_1 in the limbs of the larger-scale asymmetric folds of domain d0 (compare (d) with (g) of Fig. 7.7A).

Poles to S_3 in the submap form a modal distribution orientated at 0°-138° (Fig. 7.7Ab). As for S_1 , there is an observable correlation between orientation and spatial position. This correlation is not as close as for S_1 (Fig. CP.16c), but again it suggests that submap M13 could be subdivided into two domains, c0 and d0 (see (e) and (h) of Fig. 7.7), with southeast dips dominating domain d0, and northwest dips dominating domain c0. The rotation of the latter, relative to the former, through a few degrees of dip and strike explains why the smaller-scale asymmetric folds (in domain c0) do not parallel the larger-scale folds of domain d0.

 F_3 fold hinges in the submap (including the corresponding parallel elongation lineation, L_3) form a modal distribution plunging 73°-226° (Fig. 7.7c), with scatter along the axial plane girdle 135°/90°. The S.O.D.A. plot (Fig. CP.16e) was constructed by using a b-isodip chart (Fig. CP.16f) centred on the mode. The spread of colours suggests approximately uniform variations in orientation throughout the area, except for two small groups of anomalous values. Finer b-isodip charts were tried (with RES values from 1° to 4°), but these did not reveal patterns, in the corresponding S.O.D.A. plots, significantly different from before.

The primary subdivision of submap M13 (the boundary between domains c0 and d0) was made by taking F_3 data into account after an initial subdivision based on the S_1 S.O.D.A. plot (i.e. the separation of the corresponding F_3 orientation distributions were maximised after the location of the boundary was determined from the S.O.D.A. plots for the S_1 data). Domain c0 (Fig. 7.6) was divided into secondary domains c1 and c2, based on a combination of the S.O.D.A. plot for F_3 (to give the clearest distinction between the two F_3 orientation distributions) and the mesoscopic structures observed in the submap. The subdivision of d0 was based on the S.O.D.A. plot for S_1 (above).

Areas of anomalous values occur in the middle of domain d2 and on the boundary between domains c1 and c2. Both of these are associated with ${\rm F}_2$ folds that were initially mapped as ${\rm F}_3$ folds before this analysis.

An analysis of S₁ was conducted in order to demonstrate the care and purpose of design required in the construction of colour charts for use in the S.O.D.A. technique. A u-isotrend chart (Fig. CP.16h) was orientated so that the profile plane coincided with blue. The corresponding S.O.D.A.

plot (Fig. CP.16g) shows random variation from the profile plane throughout the area, except for a distinct area of anomalous colours. This anomaly is due more to the design of the chart than to the geology. Even so, it still indicates a high degree of ordering of S_1 orientations in that part of the map.

7.3.3 Interpretation

The S.O.D.A. plots of submap M13 are capable of delineating subareas by using the isodip and isotrend contours as domain boundaries. But because the S.O.D.A. plots are essentially one-dimensional, the contours cannot be used to deduce structure morphology in the same fashion described in previous chapters. Therefore, the interpretation of the structures requires the combined information from the S.O.D.A. plots and field observations. This procedure is used throughout the chapter.

Most F_3 folds observed in the submap have a sinistral asymmetry and both fold axes and axial planes show consistent orientations. From the mesoscopic structures observed in domain c2, it appears that the isoclinal F_2 folds are inclined to the southwest, causing F_3 fold hinges to have steep southwesterly plunges (Fig. 7.8a). Where F_2 folds are sufficiently open (and therefore no limbs are overturned), the F_3 folds can also plunge to the northeast (Fig. 7.8b). A block diagram of the structure is shown in Fig. 7.13a (which can be produced by the model shown in Fig. 7.10 - see later this section).

The area represented by domain c2 in geology sheet 1 (Fig. 6.2) shows Ramsay's type 3 interference fold patterns. Domain cl may also contain this type of interference pattern because of the inferred existence of horizontal F_2 folds (point (1) in §7.3.1). These structures (on the scale of metres) are observed in domain d0, but are generally only associated with thin veins and layers (apophyses(?)). Other types of interference patterns can be observed (e.g. type 2, see Fig. 7.5c) but these are also generally associated with the thinner layers (pre-D2 It can be concluded from the domains and the migmatite veins(?)). structures within that, provided that D_3 was caused by horizontal compressional stresses (Fig. 7.9a; as concluded by Parker (1978) in the Cowell/Cleve area, Fig. 6.6), F2 fold hinges have changed from subhorizontal and N-S in domain cl to moderate plunges NW-SE in domain c2 to subhorizontal N-S in domain d0 (Fig. 7.11), and that the macroscopic F₂ folds were inclined to steeply-inclined to the west (southwest in This variation in interference patterns among domains, for what should be essentially uniform deformation if both D_2 and D_3 homogeneous deformations, suggests that either D_2 and/or D_3 hetereogeneous or that there was a deformation event between D_{ρ} and D₃. The possibility of an intermediate independent deformation appears remote as such an event is not recorded elsewhere and because it is possible to explain the interpretations with the existing deformation Although D₂ may have been a heterogeneous deformation event, this conclusion is not necessary because D_3 appears to have had a two-part deformation sequence, as follows. The submap has an overall sinistral asymmetry corresponding to minor folds on the sinistral limb of a macroscopic F3 fold (Fig. 7.9b). From the study of folds as heterogenous structures, (e.g. see Kuenen and de Sitter, 1938; de Sitter, 1956; Turner and Weiss, 1963; among others) the sinistral limbs of buckle folds undergo shearing strains of sinistral rotation. So it can be concluded that the D_3 strains had a shearing (rotation) component. D_3 stresses also produced F_3 folds so it can be expected that D_3 would have had a flattening effect on the D_2 structures, i.e. D_3 strains had a flattening (irrotational) component. It appears that the F_2 folds may have been rotated in the vicinity of domain c2 by a significant amount prior to the compressional (buckling) component effectively producing small-scale interference patterns. In domain d0, S_{0-1} is on the limb of the submap-sized asymmetric F_3 fold, which, being subparallel to the original F2 orientation, shows very little effect of small-scale interference folding. Proceeding from domains d3 to d1, poles to S_1 progress around the F_3 profile plane (Figs. 7.7p,s,v) as would be expected for folds produced by only one deformation event.

7.4 SUBMAP M45

7.4.1 Structural Description

The geology of this submap (located in Fig. 7.12), as deduced by field mapping of structural elements, is presented in part of geology sheet 2 (Fig. 6.2). Unlike the structures described in submap M13, the mesoscopic structures are more complex, except in the north of the submap (north of the embayment) where the structures are reasonably similar to those observed in submap M13 (cf. Figs. 7.13a and 7.13b).

Proceeding southwards from the eastern shore represented in submap M13 into the area covered by submap M45, near-vertically plunging asymmetric (sinistral) F₃ folds (north of grid line 1900N) of decimetre wavelengths and amplitudes are encountered. The area grades into one of interference folds (varying between types 1 and 3) of smaller size (Fig. 7.14) over a short distance. On the NNW trending shore (the central area of sheet 2 between 1750N and the embayment), the structures have highly variable fold orientations (Fig. 7.15b) and asymmetric fold shapes, many of which are cuspate in appearance, but generally classifiable as a

form resembling a hybrid of Ramsay's type 1 and 3 interference figures (not discussed by Ramsay (1967) but occurs in the interference pattern volume of Thiessen and Transpas (1980)). The generation of each fold must be determined by overprinting criteria (e.g. Fig. 7.15a) because of the variability of the fold styles and orientations.

7.4.2 Subarea Analysis by the S.O.D.A. Technique

The analysis of this submap solely by the S.O.D.A. technique would require a very large data set (data points every square metre) because of the extreme complexity on all scales. But as the area is excellently exposed, an analysis using a selected data set and field notes was thought to be better. Consequently, only a small data set was collected for the S.O.D.A. technique.

The structural data maps are presented in Fig. 7.12. Stereoplots for the structural domains (determined below) of submap M45 (Fig. 7.17) are presented in Fig. 7.18. The S.O.D.A. plots (Fig. CP.17) for each of the elements are based on their stereoplots (composite, Fig. CP.17b, comprised of parts (a)-(c) of Fig. 7.18).

Poles to S_1 in the submap form a weak modal distribution around 0°-125°, with scatter around the near-equatorial plane 048°/04° (Fig. 7.18a). S_1 data show weak groupings into five regions (see S.O.D.A. plot Fig. CP.17a). They are: the extreme northern end containing steep southeasterly dips (green-cyan); followed by a region of northwesterly dips (red-pink); which forms an overlapping third region with the fourth region towards the south (green/green-cyan); and finally followed by a region at the southern end consisting of anomalous colours due to steep, generally northerly dips (warm colours, i.e., yellow, red, pink). The significance of these groups is very difficult to deduce because of the lack of two-dimensional information (i.e. width of outcrop).

In the interpretations below, the areas represented by the cool colours of the first four regions are grouped together, as are the areas represented by the warm colours, giving two domains (b3 and b2 respectively). The fifth region, domain bl (the southern most) remains separate.

Although too few data measurements of S_3 (Fig. CP.17c) were made to enable precise statements on their spatial relationships, the recording of this schistosity and axial plane was representative, and so the data are capable of being used in interpretations of the submap. In the north of the submap where the folds are larger and simpler (cyan/green-cyan), S_3 is constant. In the vicinity of the embayment it becomes more variable in orientation (blue-cyan/cyan/green-cyan), but stabilises its orientations south of the embayment (green-cyan). The warping in the general

orientation of S_3 is coincident with that region of S_1 data containing equal abundances of northwest and southeast dips (i.e. the southern portion of domains b2 and b3).

 ${\rm F_3}$ data of the submap has the distribution around the great circle 315°/90° (Fig. 7.18c) that was noted for submap M13, but there is a greater spread in the data, associated with an increased steepness in the average plunge (which corresponds to the shallower ${\rm S_1}$ pole girdle). Some of the shallower plunge values may represent ${\rm F_2}$ folds that were not correctly assigned at the time of mapping.

The S.O.D.A. plot for F_3 (Fig. CP.17e) was made using a b-isotrend chart (Fig. CP.17f), designed to divide the fold axis distribution into many parts. Four indistinct regions can be defined. From north to south they are: 1) a large area of subvertical folds, with an overall disposition towards the southwest (yellow/yellow-green); 2) a smaller area of markedly variable fold orientations and plunge (cool colours through to warm colours); 3) another, smaller, area similar to the first but spatially separated from the first two; and 4) an area containing variable orientations in the southern most portion of the submap. These groupings have a marked correlation to those regions noted for S_1 .

Domain b2 primarily consists of planar units with only small asymmetric (sinistral) vergence folds observed in the field. Hence poles to S_1 have a corresponding modal distribution representing a mean schistosity dipping steeply to the northwest (Fig. 7.18g). F_3 folds for this domain are constrained around the orientation 75° -239° (Fig. 7.18h). Domain b3 contains many folds, again sinistral, with S_1 steeply dipping to the southeast, but with a spread around the great circle girdle $016^{\circ}/14^{\circ}$ (Fig. 7.18i) caused by the more significant (larger) folds. F_3 data (Fig. 7.18k) have a greater spread at the steeper plunges, and a general rotation of the distribution towards east-west. Together, both domains have an S_3 trace $(063^{\circ}$, Fig. 7.18j) that is more east-west than the regional trend $(047^{\circ}$, Fig. 7.1).

In contrast, domain bl has a mean S_3 orientation with a more northerly trend (041°, Fig. 7.18e), and an F_3 distribution (Fig. 7.18f) around a great circle girdle markedly more north-south than the preceeding domains, with the average fold axis orientation plunging steeply to the northeast. The S_1 poles defining a southerly-dipping great circle girdle of $169^\circ/16^\circ$ (Fig. 7.18d) were measured from an F_{2-3} fold (Fig. 7.15b). However, the S_1 schistosity in this domain (data not presented) has a similar orientation to the other two domains, but with prevalently complex forms (more complex than those shown in Fig. 7.14).

7.4.3 <u>Interpretation</u>

The change in dip direction of S_1 between domains b2 and b3 suggests that the domains represent different limbs of a larger scale F_3 fold. The change in S_1 between domains b2+b3 and b1 suggests an overall change in plunge direction of the macroscopic F_2 folds from southwest (submap M13 and domains b2+b3) to northeast (if rotation effects of D_3 were to be removed - see discussion below). Supporting evidence is provided by the shift in the overall trend of F_3 from southwesterly to northeasterly.

The small but significant change in interference structures from the north to the south of the embayment, as mentioned previously in §7.4.1 suggests either a rotation of the macroscopic structures or a change in their morphology. As the distributions of all three significant structural elements (Fig. 7.18) show rotations across the bl/b3 boundary, it appears that rotation of the D_2 structures is the primary cause of the observed field data. Accordingly, submap M45 can be interpreted, continuing on from the interpretation of submap M13 (Fig. 7.11), as a series of westerly dipping subhorizontal F_2 folds as is shown by the F_2 axial trace envelopes on Fig. 7.19.

In this interpretation, F folds in this submap are spatially closer to the hinge of the macroscopic F_3 fold than those in domain dl of submap M13. In proceeding from the very north of submap M45 towards the embayment, the trend of the F_2 axial planes (N-S) lies at an angle to the outcrop, which exposes a progressive shallowing of these axial planes (i.e. ${f F}_2$ folds are subvertical in the north and becomes more inclined to reclined towards the embayment). Inclined to reclined F_2 folds (e.g. Fig. 7.15b) are folded by F_3 in the region of the embayment, which gives rise to highly variable fold plunges (particularly F_2). There were few data values measured at this locality because of the paucity of outcrop and the predominantly small-scale structures (as compared to structures in domain b3 to the north, see §3.9.2.3 and §8.3.1 for discussions on measurements from structures of different sizes). F2 fold hinge envelopes trend parallel to the coast in domain bl, which represents an anticlockwise (sinistral) rotation of approximately 25° to those F2 folds north of the embayment (from the rotation of F₃ folds in Figs. 7.18f,k). The tight folds that can be seen in Geology Sheet 2 are dominantly F_{3} , whereas the very tight to isoclinal closures are F2.

7.5 SUBMAP M6AB

7.5.1 Structural Description

The geology, as deduced by field mapping of structural elements,

of this submap (located in Fig. 7.12) is presented in part of geology sheet 2 (Fig. 6.2). The structures appear much simpler than in the previous submap because the units are generally coarser and massive (Fig. 7.20a), and because there is a lack of distinguishing marker layers (such as the amphibolite gneisses) to highlight the structures. Where small contrasting lithologies occur, the structures (Fig. 7.20c and location (1270,1650) of geology sheet 2) appear as complex as those observed elsewhere.

In the north of the area (north of 1700N) the folds show some indications of refolding with some small folded folds and unusually shaped isolated occurrences of amphibolite gneiss enclosed within granitic gneisses. The large folds have decimetre amplitudes and small interlimb angles. Small units of biotite gneiss (e.g. Fig. 7.20c) contain an L_3^1 lineation and S_3 foliation.

7.5.2 Subarea Analysis by the S.O.D.A. Technique

The structural data maps are presented in Fig. 7.12. Stereoplots for the structural domains (determined below) of submap M6AB (Fig. 7.17) are presented in Fig. 7.21. The S.O.D.A. plots (Fig. CP.18) for each of the elements are based on their stereoplots (composite Fig. CP.18d, comprised of (a)-(c) of Fig. 7.21).

Poles to S_1 in the submap have a modal distribution around the mean 7°-127° and a small spread around the great circle girdle 101°/8° (Fig. 7.21a). A S.O.D.A. plot of S_1 data (Fig. CP.18a) shows a predominance of dips to the northwest (warm colours, see also Figs. 7.21f,h) throughout the area, except for a small region of southeasterly dips (visible in Fig. 7.20a) (i.e. represented by the cool colours, which defines domain bl, see Figs. 7.17 and 7.21d). F3 folds in domain bl have consistent plunges around 78°-217° (Fig. 7.21e). Fold variation is due to an upright, subhorizontal ellipsoidal dome (double-plunging antiform, Fig. 7.20a). There are too few data for the dome to be derived by the S.O.D.A. technique. The small red bands of the S.O.D.A. plot (Fig. CP.18a) correspond to one of the limbs of upright vertically-plunging folds that The details of the structures in this area are abound in the area. difficult to observe clearly in the field because the rocks consist almost entirely of massive, coarse grained granitic gneisses.

Poles to S₃ (Fig. 7.21b) are constant and are nearly parallel to the regional trend. The data are representative, and are therefore constant over the submap. There are too few data to derive accurate interpretations (i.e. detect subtleties in the structures) from the S.O.D.A. plot (Fig. CP.18b). This problem does not detract from either the S.O.D.A. technique or the thesis as it is beyond the scope of this research to collect the very large data sets required to derive small refinements on the

interpretations of the structures.

 F_3 folds are generally subvertical, with some spread around the axial plane girdle 305°/87° (Fig. 7.21c). Anomalous shallow plunges define a second domain, b3. The mean orientation of F_3 is 10°-220° (Fig. 7.21g), which is in contrast to L^1_3 observed in Fig. 7.20c which plunges steeply to the northeast. There are too few measured data to reproduce the details of the structural variation that can be observed in the field.

The few data points in this domain can be given either a great circle or a small circle distribution (Fig. 7.21g). The small circle distribution probably has little significance (if any) because the data measurements were made from a number of fold hinges, rather than from the same folded hinge, and because there is variability in the structures over short distances (§7.5.1) (i.e. it is not reasonable to interpret the distribution in the same way as for folded lineations).

The remainder of the submap (domain b5) contains a consistent \mathbf{S}_{0-1} foliation dipping steeply to the northwest and subvertically plunging \mathbf{F}_3 folds.

7.5.3 Interpretation

There is some resemblance between this submap and the previous one (M45). Whereas in the latter there was a sinistral rotation of structural elements from domain b2+b3 to bl (Fig. 7.18), in this submap there is a dextral rotation from domain b5 to b1+b3 (Fig. 7.21). This is matched by a dextral asymmetric fold that can be seen in geology sheet 3, near the boundary between b5 and b1+b3. The dextral rotation suggests that the D2 structures are restored to an orientation similar to that in the north of submap M45. The dextral fold indicates possible type 1 interference folding in the region, which would indicate a steeply-inclined to upright subhorizontal F_2 macroscopic fold structure refolded by D_3 (Fig. This interpretation is supported by the double-plunging fold structures which can be recognised to the south of submap M6AB (see §7.5.1, and similar to Fig. 7.20a). (The area to the south of this submap has not been mapped in detail, but in the field several doubly-plunging structures have been detected by the alternating changes in steep northeast and southwest fold plunges, while S_{0-1} continues to dominate dips to the southeast and northwest.)

7.6 SUBMAP M789

7.6.1 Structural Description

The geology, as deduced by field mapping of structural elements, of this submap (located in Fig. 7.22) is presented in geology sheet 3

(Fig. 6.2). It is poorly exposed compared to the other submaps. north of the area the outcrop changes from massive granitic gneisses, obscured by a cover of boulders, to a massive amphibolite gneiss which is represented by the centre of the submap. Detailed observations within these bodies reveal that portions of them are massive (e.g. Fig. 7.23) whereas other portions have been thickened by numerous refolding (e.g. Figs. 7.25a and 7.26a). In the south of the area there is a well-exposed outcrop that demonstrates interference folds on a larger scale. contacts between the three outcrops are not exposed. Apart from the southern outcrop, the rest of the subarea has an overall simplicity similar to that observed in the southeastern portion of submap M13. However, small-scale structures demonstrate complexities, as have been observed elsewhere. For example, the body of simple leucogranitic gneiss at (1090, 1490) shows extreme internal complexities (Fig. 7.26). This gneiss contains both L_{i} and L_{3} lineations (Fig. 7.3d). Similar complexities can be seen in migmatitic veins in the amphibolite gneisses (e.g. Fig. 6.3a).

The structures in the southern portion of the submap have outcrop patterns reminiscent of the type 2 and type 3 interference patterns classified by Ramsay (1967, p.520ff). The dominant foliation (S_1) is everywhere parallel to layering. A biotite gneiss containing excellent examples of interference structures (Fig. 7.27) occurs in the amphibolites. Despite the apparent increase in complexity as compared to those previously described, the small scale structures do not appear to show more than two fold generations (e.g. Fig. 7.24).

7.6.2 Subarea Analysis by the S.O.D.A. Technique

The structural data maps are presented in Fig. 7.22. Stereoplots for the structural domains (determined below) of submap M789 (Fig. 7.28) are presented in Fig. 7.29. The S.O.D.A. plots (Fig. CP.18) for each of the elements are based on their stereoplots (composite, Fig. CP.18e, comprised of (a)-(c) of Fig. 7.29A).

Poles to S_1 in the submap are distributed around the near-equatorial great circle girdle 078°/04°, with a mean orientation of 2°-130° (Fig. 7.29Aa). The S.O.D.A. plot of S_1 shows many small domains of easterly (greens) and westerly (pinks) dips, with some northerly dips (yellows) corresponding to larger F_2 fold hinge regions.

Poles to S_3 in the submap define a great circle girdle of 018°/06°, with a mean orientation of 2°-312° (Fig. 7.29Ab). The S.O.D.A. plot of S_3 also shows reasonably well-defined domains, although there are too few data to delineate them precisely. However, as has been stated for previous submaps, the data are representative where applicable. Therefore,

in the centre and north of the submap the data are representative, whereas in the south many more data were required because of variability of orientation over short distances.

 $\rm F_3$ fold plunges lie on the vertical plane with trend 042°, and a mean plunge of 82°-218° (Fig. 7.29Ac). Many of the $\rm F_3$ (and $\rm F_2$) folds have curved hinges (up to 180°, e.g. Fig. 7.25c). The S.O.D.A. plot of $\rm F_3$ folds (Fig. CP.18h) demonstrates that there are domains characterised by areas of reasonably consistent fold plunge and areas of more variable fold plunge.

The submap was divided into three primary domains, c0, d0, and e0 (Fig. 7.28 and Fig. 7.29A). These domains were based primarily on F_3 data, but with some contribution from $S_{\hat{1}}$ data in order to position the boundaries accurately. Again, domain boundaries were chosen to maximise the differences between the orientation distributions for adjacent F_3 folds show a shift of mean plunge from 62°-220° in domain c0 (Fig. 7.29Af) to 79°-200° in domain d0 (Fig. 7.29Ai) to 83°-025° in domain e0 (Fig. 7.29Al). The two northern domains also have reasonably planar F_3 distributions, whereas the southern domain (e0) has a small circle S_1 and S_3 data distributions are also significantly distribution. Each of the primary domains were further different between domains. subdivided into secondary domains (Fig. 7.28 and Fig. 7.29B,C), based on the same criteria as the primary domains. Domain c0 is divided into secondary domains cl and c2 (which are divided into tertiary domains c3 and $\underline{c4}$ for domain cl (based on the S₁ S.O.D.A. plot, Fig. CP.18f), and c5 through to c8 for domain c2 (based on the F2-3 S.O.D.A. plots, Fig. CP.18h)); domain d0 is divided into secondary domains d1, d2, and d3; and domain e0 into secondary domains el, e2, and e3, based on a similar criterion as the primary domains.

7.6.3 <u>Interpretation</u>

In many respects, there are similarities in the geology maps between domains c0+d0 and submaps M45+M6AB. The northeastern end of domain c0 is similar to submap M6AB, and the remainder of domain c0 is similar to domain bl of submap M45. Domain d0 is similar to domains b2+b3 of submap M45. Hence we can interpret the macrostructures as being morphologically similar. Although domain c0 has secondary and tertiary domains, there are too few data to know the significance of them, or even if these subdomains represent actual differences in the structures.

Domain e0 presents a different structure from the forgoing. It demonstrates a structural form resembling a type 2 interference pattern overprinted by a later fold (Fig. 7.30). This is the first indication that there may have been three fold-forming events. Three possible explanations

- are available and are more fully described below as models. (a) Either F_1 is unambiguously expressed on a mesoscopic scale, or (b) D_4 (the Wartaken event) is locally expressed, or (c) one of the fold-forming events (i.e. D_2 or D_3) had a heterogeneous strain history.
- (a) The first model appears unlikely as nowhere was S_1 seen to be axial planar to any folds, i.e. S_1 remained layer-parallel throughout. However, this model may still be correct as in many of the areas where F_1 hinges would be expected, the outcrop was not clear. Furthermore, it is in this region that such highly deformed migmatitic veins (e.g. Fig. 6.3a) can be found.
- (b) The second model is unlikely as D_{μ} effects are not only limited to this small outcrop, but the structural elements associated with this deformation have orientations parallel to those of D_{3} in other parts of the mapped area. Where D_{μ} structures have been described elsewhere (e.g. Parker, 1978; the D_{3} event of Clarke, 1976; and the dextral offset of the mylonite zone as described by Coin, 1976) they had orientations markedly different from the preceding deformations.

The third model requires that either i) $^{\rm D}{}_{\rm 2},$ or ii) $^{\rm D}{}_{\rm 3},$ refolded folds produced earlier in the same generation.

- (i) For D₂ to have produced two fold events resulting in a type 2 interference pattern, it must first have produced reclined to recumbent folds and then have horizontally compressed these folds. This is unlikely as the mechanisms which produce reclined to recumbent folds will tend to move the folds out of the stress field (e.g. Marjoribanks et al, 1980). Hence, recumbent folds would not be expected to remain in a location capable of being compressed by the same deformation. Despite this argument it may be possible for the model to be applicable, because on the small scales dealt with here, local heterogeneous strains may very well arise and thus cause the refolding of recumbent folds in the same deformation generation.
- (b) Interpretations of the effects of D_3 on the earlier structures described so far in this chapter have indicated that the D_3 stress had both a compression component and a shearing component (§7.3.3), producing tight F_3 folds of sinistral asymmetry (Fig. 7.9b). So far in this chapter, D_2 structures have been interpreted as being approximately upright, and so the compression component of D_3 would have had the effect of tightening and reorientating the D_2 structures as well as combining with the shear component to refold them (Fig. 7.10). In domain e0 it appears that the D_2 structures must have been reclined or recumbent, and so the compression component of D_3 would then have produced the type 2 interference noted above. The

effects of the shearing component while S_{0-1} was subhorizontal (e.g. Figs. 7.3la,b) was to shear the type 2 interference pattern out of symmetry, and at the same time rotate the whole geometry in an anticlockwise direction (as demonstrated by Fig. 7.30) (i.e. D_3 structures produced early in the deformation would no longer be coaxial with later D_3 stress fields). As S_{0-1} rotated into steeper dips with increasing strain, the ongoing D_3 deformation then folded the preceeding geometry to give a more intense second overprinting effect (Figs. 7.3lc,d).

The anticlockwise rotation can be seen in the stereoplots of S_3 for the subdomains of e0 and d0, the stereoplots for F_3 for the subdomains of e0, and geology sheet 3. The reverse (clockwise) rotation of S_3 in domains e2 and d1 from the mean orientation (047°, Fig. 7.1b) is caused by the limited (localised) effectiveness of the shearing component. (That is, the shearing component was incapable of rotating both domains as a single unit, but it could rotate a part of it. Accordingly, the anticlockwise rotation of a central portion of an S_3 axial plane (see Fig. 7.32), without a significant rotation and therefore translation of those parts at a distance from the central portion, would cause parts of the S_3 plane to have an apparent clockwise rotation from the mean orientation.)

A problem common to all three models is that domains c0 and d0 were compared to structures elsewhere that had \mathbf{D}_{2} upright prior to the D_3 deformation. In going from the central portion of submap M789 to the southern portion, the pre-D₃ structure has gone from upright to recumbent. This phenomenon was also observed in the northern part (domain b2+b3) of submap M45 where F_2 was interpreted as being steeply-inclined to upright in the extreme north, changing rapidly to reclined further to the south. However, details in domains dO and cO are difficult to obtain because the uniform grain size and colour of the amphibolite body makes it extremely difficult to map its internal structure. No structures that were observed unambiguously demonstrated either a reclined or an upright pre-D3 structure. Internal structures of the northern areas represented in the submap were also very difficult to map because of marine growth and the prolific boulder cover. It can be noted that the complexity and intensity of the structures internal to the unit shown in Figs. 7.25c and 7.26a demonstrate a structural geometry that is too complex to analyse here.

The interpreted structures for submap M789 are presented in Fig. 7.33, based on the stereonet plots of Fig. 7.29 and the geology presented in Geology Sheet 3. Other possibilities for the structures in domain e0 are possible from the discussion of the above models, but it is immaterial

to the thesis to attempt to present a comprehensive and detailed analysis of all the models mentioned above. The structures appear quite simple considering the complexity of the mesoscopic structures observed in outcrop, but they are consistent with each other, and this is further discussed in §7.8.1.

7.7 SUBMAP M912

7.7.1 Structural Description

The geology, as deduced by field mapping of structural elements, of this submap (located in Fig. 7.34) is presented in geology sheet 4 (Fig. 6.2). The northern shoreline consists of massive granitic gneisses, as does the northeast headland. Between the two occurs an interlayering of amphibolite and granitic gneisses. These interlayers can be traced for most of the submap. It can be seen that many, if not all, amphibolite layers are the same layer repeated by folding.

fold plunges vary from horizontal to moderate (Figs. 7.35b,c). Fold interference patterns are common but are best observed in the interlayering because of the colour contrast. They vary in different parts of the submap. In the north, type 3 (Fig. 7.35a) are common; dome and basins (type 1) occur north of, and following around, the embayment; type 3 interference folds again occur on the shoreline south of the embayment, which pass into a type 2 interference fold at the southeast headland where the interlayering crosses the coastline; and complex structures of hybrid interference patterns occur in the south of the submap (e.g. Fig. 7.35d and Fig. 7.36). Common to these mesoscopic structures is the variability of the visible fold plunges (e.g. Figs. 7.35b,c and Fig. 7.37; and in the vicinity of (1070,1130) folds may vary from vertical (e.g. Fig. 7.3a) to horizontal (Fig. 7.38a)).

 $\rm S_2$ is relatively well-developed in the shoreline area containing the type 1 folds (location of Fig. 7.39). It is not as well-developed elsewhere (e.g. Fig. 6.7d).

7.7.2 Subarea Analysis by the S.O.D.A. Technique

The structural data maps are presented in Fig. 7.34. Stereoplots for the structural domains (determined below) of submap M912 (Fig. 7.40) are presented in Fig. 7.41. The S.O.D.A. plots (Fig. CP.19) for each of the elements are based on their stereoplots (composite, Fig. CP.19e, comprised of parts (a)-(c) of Fig. 7.41A).

Poles to S_1 form a modal distribution (Fig. 7.41Aa) centred at 6°-136°, and have a small spread in the plane 159°/06°. The S.O.D.A. plot of S_1 (Fig. CP.19f) delineates tenuous structural domains, which generally match the limbs and hinge regions of the larger fold structures.

Poles to S_3 form a modal distribution (Fig. 7.41Ab) with mean S_3 orientation of 046°/83°NW, which is close to the regional orientation of 047°/88°NW (Fig. 7.1b). The S.O.D.A. plot of S_3 (Fig. CP.19h) contains small domains of northwesterly dips within an overall southeasterly-dipping distribution. Because of the small number of readings compared to the total number of data points, the polygons are quite small, and so even though the measured S_3 data are representative of S_3 orientations everywhere, they do not demonstrate the domains as well as they would if the polygons were to be enlarged to fill the map space.

 F_3 data form a well-defined great circle girdle of 311°/86°, which differs from the mean S_3 by only a few degrees. This discrepancy is in fact significant because in the region of the type 1 interference folds, D_3 is nearly coaxial with D_2 (§7.7.1 and Fig. 7.39), and so at the time of mapping these folds were classified as F_3 folds. These folds are now believed to be F_2 modified by D_3 .

A b-isodip chart (Fig. CP.19b) was first used to analyse F₃ folds (Fig. CP.19a) by separating differing fold plunge values, but it does not provide information about the azimuthal orientation. (U-isodip charts would do so, but they were not incorporated into the computer program package at the time of this research*.) However, it is possible to delineate domains more clearly (Fig. CP.19c) by using a b-isotrend chart (Fig. CP.19d). The variation of data orientations between the domains suggests double-plunging folds.

Based on the S.O.D.A. plots for F_3 , the submap is divided into two primary domains, c0 and d0. These are further divided into the secondary domains c1 and c3, and d1 to d4 (Fig. 7.40), based mainly on F_3 data but with some refinement of the boundaries using S_1 data.

The primary domains define two regions of differing overall plunge orientations, with the northern portion (domain d0) having predominantly southwesterly plunges (Fig. 7.41Ai) and the southern portion having predominantly northeasterly plunges (Fig. 7.41Af).

7.7.3 Interpretation

The four subdomains of domain d0 clearly delineate substructures. Domains d1 and d2 are similar, with $\rm S_1$ values (Figs. 7.41Bg,j) showing a few degrees variation in orientation which match the small variation in the

^{*} Analytical functions were added to the programs only as they were required because of machine limitations (§3.3.3.1). The limitation of program size had been reached before the need for u-isodip charts became apparent. This problem can be overcome by restructuring the programs but the effort was not warranted here.

 S_3 values (Figs. 7.41Bh,k). However, the F_3 values are markedly different, with those for domain dl (Fig. 7.41Bi) being subhorizontal and those for domain d2 (Fig. 7.41Bl) having steep plunges. It is probable that the folds in domain dl are in fact F_2 folds (there are no overprinting characteristics discernible in the granitic gneiss units). On the other hand, the structural elements of domains d3 and d4 have sinistrally-rotated away from the orientations for domains dl and d2. Poles to S₁ in domain d3 (Fig. 7.41Bm) define a great circle girdle of 046°/80°, which has a pi orientation approximating that of the mean F_{γ} (Fig. 7.41Bo). The great circle distribution of F_{γ} corresponds well with the mean S_3 orientation (Fig. 7.41Bn). The S_1 and F_3 elements of domain d4 (Figs. 7.41Bp,r) have been rotated anticlockwise to those of domain d3. The S_1 distribution can be divided into two separate distributions, each defining a great circle girdle which represents separate limbs of F_2 folds (Fig. 7.42a). (That is, the northwest and southeast distributions of S_1 in Fig. 7.41Bm represent two limbs of F_2 folds (e.g. Fig. 7.39) with shallowly-plunging, gently curved fold hinges to the southwest (25°-225°). As the F_2 folds approach the hinge of the macroscopic F_3 fold east of the embayment, the type 1 interference folds become more pronounced, and so the relatively planar F_2 limbs become more curved, giving rise to an increased separation of F2 fold hinges into two populations, Fig. 7.42b.) Although F_3 folds (as mapped) define a single girdle, the distribution of data can be divided into two groups, each with a mean that approximates to the poles of the S_1 girdles. Therefore, these ${}^{t}F_{3}$ folds are in actuality probably D_{2} folds. In contrast, S3, apart from becoming steeper, has kept its trend constant. It appears that the more northerly trend of S_3 in domains d3 and d4 was caused by the preferred increased development of S_2 (i.e. S_{2-3}) rather than the separate development of S_3 at a small angle to S_2 . The rotation of structural element orientations from domain d3 to d4 was caused by the larger macroscopic folding of F_2 by D_3 (F_3^2) in the vicinity of the S_{2-3} was not rotated because of the constraints of S_3 . However, in the hinge of the macroscopic fold, S2 is at a higher angle to S_3 and so S_2 again is axial plane to F_2 folds (trending approximately north-south) and S_3 reverts to an orientation approximating its regional trend (see domain c0 below).

Domain c0 is divided into two subdomains based on the plunge direction of F_3 , with domain c1 having folds predominantly plunging northeast (Fig. 7.41Bc) and domain c3 having folds predominantly plunging southwest (Fig. 7.41Bf). In correspondence to these fold plunges, poles to S_1 in domain c1 tenuously define a girdle with its pole trending

northeast $(71^{\circ}-016^{\circ})$ and those for domain c3 tenuously define a girdle with its pole trending southwest $(80^{\circ}-276^{\circ})$. S₃, however, is constant throughout and corresponds to the regional orientation.

From the foregoing analysis and accompanying field observations, the structures for the submap can be deduced as forming a single sinistral \mathbf{F}_3 fold (in the middle of the submap) that folds a steeply inclined (to the west) \mathbf{S}_2 foliation (Fig. 7.43). In progressing around the fold, from north to south, \mathbf{S}_2 changes from steeply-inclined westerly, to vertical to moderately-inclined to the northeast and finally becoming subvertical in the south. Domain d0 contains a mixture of types 1 and 3 interference patterns, reflecting changes in \mathbf{F}_2 fold hinge inclination. Domain c0 contains types 2 and 3 in the north, reflecting changes in both \mathbf{F}_2 fold hinge inclinations and axial plane inclinations; and mostly type 1 with some effect of types 2 and 3 in the south.

From the interpretations it is clear that much of the mesoscopic folding are \mathbf{F}_2 folds modified by \mathbf{D}_3 (rotated and flattened, giving rise to variable \mathbf{F}_2 fold hinges and axial planes no longer orientated N-S).

7.8 DISCUSSION

7.8.1 Interpretation of the Structures

The structures interpreted in the five submaps are summarised in Fig. 7.44, which is of one or more macroscopic \mathbf{F}_2 folds that are steeply-to shallowly-inclined to the west with subhorizontal hinges trending N-S, overprinted by subhorizontal upright \mathbf{F}_3 folds of sinistral asymmetry trending NE-SW.

It was observed (Appendix 0) that between localities A and B_0 on Fig. 0.1 the structure and geology is a mirror image of submap M13, i.e. the F_3 folds are dextral. The major difference to be noted is that the L₃ elongation lineation is more intensely developed than in the mapped area. Because the asymmetric folds change sense along strike, it appears that they are minor folds on the same limb of a macroscopic F_3 fold. As it is reasonable to assume that the F_3 fold hinge plunges in the same direction as the L_3 lineation (although the fold envelope remains axial planes (S_2) because the F, fold and horizontal), predominantly inclined to the west, then it follows that the coastline from the mapped area south (localities C_1 to A) is on the sinistral limb (looking southwest) of a macroscopic F_3 synform (Fig. 7.44). interference pattern arising from the overprinting of moderately- to steeply-inclined subhorizontal folds by upright horizontal folds trending at 45° to the first folds, is Ramsay's type 1 ('dome-and-basin'). In the mapped area, type 3 interference patterns are quite common, which requires

the first fold hinges (F2) to be skew (non-coplanar) to F3 hinges.

The observed structures in the mapped area correlate reasonably well with the first three deformation events in the tectonic schemes of Parker (1978) and Richardson (1978) (Table 6.1). The fourth (Wartaken) deformation event is not expressed. However, whereas F_2 is steeply inclined in the mapped area, D_2 fold structures are described by Parker (1978) (Fig. 6.6) as being recumbent prior to overprinting by D_3 folds similar to those determined for the mapped area. Evidence for recumbent F_2 folds are also found in the surrounding area. At two localities north of Lipson Cove, Cape Burr and Cape Hardy, that are far enough away from the shear zones (Fig. 0.1) to be unaffected by them, S_{0-1} is moderately inclined (45° or less) to the west. At Waterfall Creek (locality W, Fig. 0.1) recumbent F_2 folds can be observed (Fig. 0.8). It appears possible that in the region between Tumby Bay and Port Neill macroscopic F_2 folds are recumbent, but this is not observed at Lipson Cove because that area is on the flank of an upright macropscopic F_3 fold.

Small complex regions within the mapped area (e.g. domain e0 of submap M789), where F_2 is shallowly-reclined to recumbent, may be due to a number of factors based on the above discussion. They may, for instance, represent areas of parasitic folds on the macroscopic F_2 folds, or regions where F_1 folds significantly affect the outcrop pattern. Other possible causes can be found if heterogeneous strain histories are considered.

The marked variation in strain (Appendix N) from south to north of locality D (Fig. 0.1) was explained (Appendix P) as being caused by upthrusting of the south side relative to the north side. As it is expected for rocks to be more ductile at deeper levels in the crust, rock fabric and folding is more pronounced south of locality D, which represents a deeper level in the crust, than it is to the north, which represents a shallower level in the crust. Hence the number of small shear zones (Fig. 0.1) and boudins to the north of locality D translate into folding at depth.

The structures interpreted from the mapped area and observations of the surrounding geology (Appendix O) appear to form part of variably-plunging structures similar to those described elsewhere in the Gawler Craton (e.g. Jones, 1968; Parker, 1978; Parker and Lemon, 1982). Although no D_{ij} effects are observed in the mapped area, this is not unusual as they are not common to the south or north. In fact, D_{ij} (the D_{ij} event of Clarke, 1976) was not observed south of Port Neill, except for the large E-W dextral shear (Fig. 0.1).

7.8.2 Usefulness of the S.O.D.A. Technique

Isodip and isotrend contours of the S.O.D.A. technique were not used in the interpretation of Lipson Cove structures in the same way as they were used in previous chapters. Instead, the contours were used to There are a number of reasons why this was so. delineate subdomains. Firstly, the map was a one-dimensional traverse through the larger-scale structures (submap to macroscopic sizes) and hence contour lines can be detected but their relationships to each other are unknown; secondly, the prolific number of small-scale structures (on the order of metres) cause confusion on the S.O.D.A. plots as it is not always possible to make measurements of fold envelopes, but only the visible structures; which is related to the third reason, viz. it can be extremely difficult to relate structures from one point to the next because of the lack of marker horizons; and fourthly, data measurements were made before the structural history had been ascertained, and hence structural data may be incorrectly labelled (particulaly from submap M6AB southwards).

However, it must be noted that <u>none of this detracts from the S.O.D.A.</u> technique because in effect the technique was used in a different mode to that of the previous chapters. Whereas the (Type II) trend surface contours of previous chapters were used to determine structural geometries by approximating Type I trend surfaces (e.g. strike-lines) by analogy, in this example the practice is not possible and so the structural geometries must be deduced from Type II trend surfaces that are trend surfaces of the properties of the data (e.g. delineating regions of different dip values, trend directions, etc.).

Once the maps had been digitised and the data files created, the S.O.D.A. technique enabled the domains for all subareas to be defined in one working day and the stereonet plots produced with girdle and mode distributions fitted. (There was actually a time lapse of several days because the computer could only be used for a few hours of each day, which had to include machine failure, down-loading and storage of files on magnetic tape, photographing, transference of data between the Cyber and Nova at low speeds (300 BAUD), and waiting in plotter queues for penplotter output.)

Although the S.O.D.A. technique was extremely useful for defining domains, it must be noted that some of those domains appeared to have little, if any, significance, and that much of the interpretations were based on the structures observed in the field (compare this to its ability to interpret the Brockman Three example, \$5.2.2). It is not known how much of this drawback is related to the fact that the Lipson Cove area was mapped before the details of the S.O.D.A. technique had been formulated

(and hence data was not collected in an appropriate manner), or that perhaps this area was not entirely suitable for testing the S.O.D.A. technique in its prototype form.

CHAPTER 8

SUMMARY, SUGGESTIONS FOR FURTHER DEVELOPMENT, AND CONCLUSION

8.1 SUMMARY OF THE S.O.D.A. TECHNIQUE

8.1.1 Development

The advent of high-powered, low-cost computing facilities with high quality, very fast display peripherals has made possible the modernisation of analytical procedures used in structural geology, particularly those that are slow and/or those requiring iterative processing of data. Not only are existing procedures and manually impractical techniques candidates for modernising, but entirely new ones have been made possible.

Of the many aspects of structural geology that were considered suitable for computer implementation, the ones chosen for this thesis were those that are extensively used in geometric analysis (the technique employed to interpret the structural geometry and history of an area from These included stereonet plotting, mapping of collected field data). structural elements, cross-sections and block diagrams, and analysis. Although all of these are necessary for geometric analysis, computerisation of all but the last is primarily a technical problem. Modernisation of subarea analysis is the only one that qualified for original research. This enabled a specific goal for the thesis to be defined, and that was to develop an analytical technique for determining the geometry of geological structures from spatially distributed This led to two aims: (1) to formulate a method that orientation data. could visually display data in such a way as to unambiguously express the geometry of geological structures, or the geometry of properties of structural data (trend surface analysis), and (2) to computerise the method so that it becomes a practical analytical procedure in structural geology.

To achieve the goal of the thesis it was first necessary to determine what type of geological structures were to be analysed. As all types of foliations may be used, and not just bedding, a number of problems were unearthed that made it difficult, if not impossible, to compute a block diagram of the geometry of some types of geological structures. To overcome these problems, the structures have to be interpreted and displayed in an alternative mode, which led to the use of trend surface analysis. Two types of geometries could then be defined: (1) those where trend surfaces can replicate actual geometrical shapes (Type I trend surfaces), and (2) those where trend surfaces imply specific geometrical shapes (Type II trend surfaces). Type I trend surfaces have been the subject of previous research (Yamamoto and Nishiwaki, 1976), although

limited to that paper. Type II trend surfaces show more promise, as they can be used not only to imply all types of geometrical shapes (including those modelled by Type I trend surfaces), but also to analyse the properties of structural elements that do not define geometrical shapes (e.g. lineations). Hence, only Type II trend surfaces were considered for research.

To achieve the first aim two possible methods of analysing data were considered, a statistical one and an empirical one. The writer thought it more prudent at the initiating stages of development that an empirical method be tried, which has the advantage of leaving control of the analytical procedure, and hence the results, to the expertise of the geologist.

The most commonly collected field data, and one that is basic to structural geology, is orientation data. Hence a method was formulated to consider orientation data and their spatial positioning. This method was Spatial-Orientation Distribution called the appropriately (S.O.D.A.) technique. The principle of the technique is almost identical to the manually impractical A.V.A. technique of Sander (1970), except that grain boundaries of grains in thin-section are replaced by Thiessen polygons on a map of structural elements (see Appendix S). (When the surfaces trend analyse the used to S.O.D.A. technique is crystallographic or optic axes of grains in thin-section, it becomes the A.V.A. technique).

The S.O.D.A. technique appeared feasible as it uses a variant of the general, and popular, trend surface analysis technique. remained the problem of choosing the variables (or functions of variables) from orientation data that would generate trend surfaces that unambiguously represented geometric shapes (for cases where structural elements had trend surface strictly Type II geometric shapes). For applications (i.e. analysing lineations, etc.), choosing variables did not Five basic geometric shapes that would commonly be pose a problem. referred to in geometric analysis were defined, and it was shown that trend surfaces defined by contours of dip values (isodip lines) and contours of trend values (isotrend lines) could in most cases unambiguously define these geometric shapes. When orientation distributions on stereonets were also considered, then all basic shapes could be unambiguously defined.

The behaviour of isodip and isotrend lines for various shapes in different configurations were examined. It was found that when data was derived from a plane cut through a basic shape, it was not necessarily possible to define all parameters of the shape unambiguously (i.e. more than one type of fold profile could give the same trend surfaces).

The sophistication of the method at this point satisfied the first part of the goal of this thesis, and it would have been detrimental to the second part of the goal if the formulation of the S.O.D.A. technique had been continued.

The second aim, to computerise the S.O.D.A. technique and make it a practical tool in structural geology, required both the amalgamation and modification of existing computer software and the generation of many new programs to cover the variety of applications for which the S.O.D.A. technique could be used.

Inherent in the basic techniques used in geometric analysis (see earlier this section) are a number of procedures, such as data library creation, maintenance, and access; stereonet plotting and the statistical analysis of spherical (orientation) data; and map and perspective diagram production. All of these procedures had been computerised separately by a number of people in a variety of ways over the last ten to fifteen years (refer to \$1.3). At the start of this research, no known attempt had been made to group these computerised procedures into a working program package. During the tenure of this thesis, the only notable publication that approached the lines of this research was that by (Cooper and Nuttall, 1981), and they did not achieve the same level of applicability as reached in this thesis.

Many of the computerised procedures were obtained from the literature and elsewhere and those that were practical for a computer package were adopted. In almost all cases, this required extensive modifications to the original programs, such as correcting fundamental errors; improving (where possible) the efficiency of the algorithms or otherwise replacing them with alternative methods; and adding functions to improve their capabilities. These programs formed a program library on a Cyber 173, and they performed high quality, high precision data processing and displaying. However, they were not suitable for computerising that part of geometric analysis requiring iterative, and hence interactive, processing, which was that part of the S.O.D.A. technique whereby trend surfaces are subdivided into single geometric shapes, i.e. subarea Because the Cyber did not support the peripheral equipment required for the rapid display of results, another computer, a Nova2, was This machine was completely dissimilar to the Cyber, and very It was therefore mandatory that a suite of inferior in computing power. new programs be written for the Nova. The new programs performed most of the functions of the old ones, but to increase their speed and reduce their sizes, the algorithms were simplified and much of the programming code was Accordingly, the precision of the results was written in ASSEMBLY.

reduced. This is not a serious problem as once the final results are determined, the data can be recomputed to high precision with the programs on the Cyber.

The Nova became an independent processing system, and so an extra suite of programs was written, including a program to create data files by digitising maps with a data tablet, and programs that allow interactive definition of subareas on a map and that create data files for those subareas from the data library.

8.1.2 Testing

The program package for performing the S.O.D.A. technique was extensively tested to find the advantages and disadvantages of the technique and to refine the computer package to a practical level. The more detailed advantages and disadvantages are presented in §3.9.

Ideal models of cylindrical folds, domes, and dislocations were analysed and the results came up to full expectations. The technique also demonstrated its capability to perform dip isogon classification of fold profiles of subvertical folds.

Geological examples of folded layered stratigraphy proved to be very good geological environments for analysis by the S.O.D.A. technique. Hand specimen sized structures could also be analysed by the technique and gave results that correlated well with results produced from isodip and isotrend contours generated by analogue methods (see §2.7). The results of applying the technique to thin-sections (the A.V.A. technique) are also notably good. In this case, the S.O.D.A. technique does not attempt to determine geometric shapes; it generates Type II trend surfaces, the interpretations of which are fully dependent on the skills of the geologist conducting the analysis. Interpretations of the examples were not attempted in this thesis.

As a final test, the technique was applied to a structural analysis of a complexly deformed crystalline basement terrain. The area had excellent continuous outcrop, but suffered from a problem in that the outcrop was restricted to a very narrow coastal strip. The technique was extremely useful in rapidly defining a number of relevant structural domains (subarea analysis). Other domains were also defined by the technique but their significance was not determined. Although the analysis was scaled down, there was a wealth of information in the data collected, too much for a complete structural analysis in this research. Instead, sufficient structures were analysed by the S.O.D.A. technique to determine the usefulness of the technique in such terrains. Emphasis was placed on the analysis of the data by the S.O.D.A. technique, and so, as for the earlier examples, less importance was given to the interpretations.

However, in this final test example, a subsidiary aim was to gain an understanding of the structures and the structural history of Lipson Cove. Consequently, the area was thoroughly mapped and some interpretations attempted (§8.2).

It was discovered that the technique was more suited to geologic terrains where the stratigraphy is well defined (earlier this section) because in complexly deformed terrains, only key localities are measured for data, and interpretations based on these depend mainly on the skills of the geologist. As with most analytical programs, the more data measured the better they perform.

8.2 THE STRUCTURAL HISTORY OF LIPSON COVE

The area of Lipson Cove was examined and it was found that three deformation episodes are expressed, which correspond to the first three deformation events described by Parker and Lemon (1982). These structures are summarised in Appendix N and the SUMMARY to this thesis. The structural analysis of Lipson Cove was not complete, with many interesting mesoscopic structures left unexamined. Likewise, not all possible explanations for the structures and structural data were discussed. As the structural data did not show any obvious deviations from the structural history of the Lincoln Complex, the data was interpreted in the light of this history. Because of the small scale of the area, many anomalous features would be expected from locally heterogeneous strains, which appears to be the case.

The coastline north and south of Lipson Cove was examined geologically, as were low-level aeromagnetic data for the same area. A number of NE-SW shear zones were detected, as well as ENE-WSW faults that had apparently appreciable movements. These faults are interpreted from the geology examined to have caused the area of Lipson Cove to be on the northern end of an upthrusted crustal block, which is a possible explanation for the zones of differing deformation style mentioned in Appendix N.

8.3 FUTURE LINE OF EXPANSION

8.3.1 <u>Immediately Applicable</u>

The system is open to expansion by the incorporation of additional programs and extension of existing ones. Because the data files are uniform and the user is able to switch from one program to another, extra programs can be incorporated very easily.

Data bank creation. Geological data banks similar to those described in the literature (see \$1.3.2.1), but with structural data included, could be

implemented. By using a table of geological mnemonics (as discussed in Appendix C), data banks could be created directly from field data cards and/or by technicians (Fig. 3.1). Map reference data could be created and processed by the methods described by Williams (1979) and Bouillé (1976a). Each map contributing to a data bank would be transformed by affine transformations (e.g. Loudon et al, 1980b; and program PLTMAP), so that data banks have only one scale and one coordinate system (Doyle, 1981).

Data banks need not be restricted to one structural and one reference data file, but could consist of several reference files such as geological, geographical, topological, and Landsat files (Doyle, op. cit.). They could also contain geochemical and petrological data, as these are also suitable for analysis by the S.O.D.A. technique - where instead of colouring according to orientation (which is not applicable to chemical data) colouring would be dependent on elemental or mineral concentrations.

Map extraction. Maps to be analysed could be extracted from data banks by an extraction program similar to SUBMAP. The outlines of all maps in a data bank would be displayed (Boehm et al, 1980) and then a process similar to program SUBMAP used to delineate the initial map to be analysed. The extraction program would then create all necessary analysis data files (XY, RF and PY files, see Appendix R).

Map display. Structure map production for pen plotting (program PLTMAP) or display could be extended. Plotting all data may be undesirable because of cluttering and insignificance at the plot scale. Hence capabilities for data selection and optional labelling are required. Below are two ways to select data, and a program should incorporate both.

- a) Weighting function. All reference items in data banks must be weighted (according to symbol size or line thickness). The weights would then be adjusted by the plot scale, and items whose weights become less than a predefined minimum would not be plotted. The plotted size of items would depend on some function of their weights.
- b) User selection. Data and reference files, and three light buttons ("REJECT", "NAME" and "PLOT") would be displayed (see Appendix R). The stylus then assumes the function of the last selected light button. With "NAME", selected items will be named on the map; with "REJECT", selected items will not appear; and "PLOT" signifies all remaining items to be plotted.

By extending the menu, extra capabilities for designing the map layout could be added (legend design, scale, orientation, grid, placement of stereonets, etc.).

Subarea comparison. As it is a part of subarea analysis to make comparisons between stereonet plots of different subareas (by using STEREO

picture files (Appendix R), display menus and the data tablet), tables of annotated picture files could be designed, displayed and/or plotted.

Generating cross-sections. The positions of cross-sections are first drawn on maps displayed by SUBMAP or SHADEMAP. By triangulating XY maps (e.g. program TRICON, Appendix M), or using PY files, data points along cross-section traces can be chosen for cross-section generation. Simple methods of cross-section construction are straightforward (e.g. after manual techniques described by, inter alia, Stockwell (1950) and Ragan (1973); and using algorithms described, for example, by Rogers and Adams, 1976, p.100.).

However, such methods do not take into account the rheological properties of lithologies under stress. (For instance, the behaviour of a sandstone will be markedly different from that of a schist.) The results of relating fold shapes with strain variation, determined by strain markers within folds (Hobbs and Talbot, 1966; Dunnet, 1969; Elliot, 1970; Hobbs, 1971; Tan, 1973; Mathews et al, 1974), for example, Gay (1969), or using overall deformation strain (Borradaile, 1974; Lisle, 1977), can be integrated with Fourier analysis methods (e.g. Stabler, 1968) to predict fold shapes at depth. As the results of experimental fold forming procedures under various conditions are refined, they can be incorporated. These include the following: (strain rate: Dieterich and Onat, 1969; Cheeney, 1971; Donath and Fruth, 1971; Shimamoto, 1974: rheology variation: - Biot, 1964a,b,c; Ramberg, 1964; Chapple, 1969; Donath, 1972; Fletcher and Groshong, 1973; Caprariis, 1974; Johnson and Ellen, 1974; Johnson and Honea, 1975; Gay and Jaeger, 1975a,b: shear and strain type:-Biot, 1961; Ramberg, 1961, 1970, 1971; Norris, 1963; Ghosh, 1966; Gay, 1968; Ramberg and Strömgard, 1971; Hobbs, 1972; Ghosh and Sengupta, 1973; Reed and Tryggvason, 1974: strain distribution within folds:- Ramberg, 1963; Mukhopadhyay and Sengupta, 1966).

Block diagrams. Perspective views of block diagrams (with hidden lines suppressed) can be generated (Maxwell, 1946; Galimberti and Montanari, 1969; Bouknight, 1970; Loikow et al, 1971; and Yoeli, 1976; among others). A matrix of heights, or Digital Terrain Model (DTM) is required. As the process for generating surfaces (program MRECON) is far too large for the Nova, a possible alternative is to use a section-generating program (above). A series of cross-sections through the map will construct the necessary data matrix. This process can be simplified as perspective programs fit curves through the points (e.g. Forrest, 1972).

8.3.2 Long Range Projects

These are too numerous and diverse to describe here, but are summarily mentioned in the closing section below.

The amount of data required for any analysis will depend on the

usefulness of the data measured. Detailed analysis can be made with few data points provided that the data are carefully selected to contain the required information. This is usually not the case and so large data sets are required in order to achieve accurate interpretations by statistical analyses. For this to be practical, data must be rapidly gathered and recorded. Compared to some other geological and geophysical data-collection procedures, structural data measurement is slow and tedious. Two applications that are suitable for modification to take advantage of the microelectronic industry are the compass and the universal stage. The former could be electronic and the latter could be measured directly by machine. Research is currently being undertaken in both these fields (Huntington, personal communication; Price, 1973,1978; Lister, personal communication).

8.4 CONCLUSION

The S.O.D.A. technique is an attempt at an empirical approach to the analysis of structural geological data. It was the desire of the writer to build a system whereby the interpeter maintained control over the analytical procedings. The interpretation of data by statistical methods are currently being attempted by geologists in Canada (Huntington, personal communication). It is understood that the statistical analysis of data is essential for more accurate, unbiased interpretations that avoid some of the shortcomings experienced by S.O.D.A. However, the writer is of the opinion that the foundations for analytical procedures of any given set of data must be understood, and the procedures controlled. Otherwise the results of a statistical analysis may not be meaningful. (For example, if a structural map consists of mixed areas of detailed and cursory (or representative) data measurements, then these areas must be segregated, or in some way homogenised, before applying statistical methods.) This thesis has adequately defined a basis on which a comprehensive integrated computer package for the analysis of structural geological information can be built.

The foundations that this thesis has laid does not stop at structural information. As the technique is based on image-processing graphics equipment, it is eminently suitable for integration with other geological and geophysical information. Geochemical data can be analysed by identical means as that for structural data; and can include the many computer programs that have already been developed in the past. Likewise, and very importantly, the ability to interpret structural information in a form compatible with geophysical and remote-sensing data (e.g. Landsat and Gravsat) means that the latter data can be interpreted within realistic controls. This has important implications for the exploration industry, both in minerals and petroleum.

REFERENCES CITED

- ABRAMS, M.J., SIEGAL, B.S., GOETZ, A.F.H., and GILLESPIE, A.R., 1977:

 Computer image processing techniques applied to geologic problems.

 In (R.V. Ramani, ed.): 14th APCOM., p.843-853.
- ADAMS, J.A., 1974: A comparison of methods for cubic spline curve fitting. Computer Aided Design, 6:1-9.
- A.G.I., 1962: Dictionary of Geological Terms. Dolphin Books, New York, 545pp
- AHLBERG, J.H., NILSEN, E.N., and WALSH, J.L., 1967: The Theory of Splines and Their Applications. Academic Press, New York, 284 pp.
- AHUJA, D.V., 1968: An algorithm for generating spline-like curves. IBM Systems Jounal, 7,3 and 4:206-217.
- ALBERS, J., 1963: Interaction of Colour. Yale Univ. Press, New Haven, 81pp.
- ALFRED, B.K., 1972: Points in polygon algorithms. UKSC-0025, U.K. Scientific Centre, IBM United Kingdom Ltd., Peterlee, County Durham, England, 31pp.
- ANDREW, A.S., and LINDE, J., 1981: PRP: a FORTRAN IV interactive plotting program. Computers & Geosciences, 7(1):3-20.
- ANDREW, K.P., and WHEELER, J.F., 1978: Preprocessing programs for digitized line data on an IBM 1130. Computer Appl. Rep. IGS/CAR/78/1, Inst. Geol. Sciences, London, England, 28pp.
- ANDREWS, H.C., 1970: Computer Techniques in Image Processing.
 Academic Press, New York, 187 pp.
- ANTHONY, M., and WICKHAM, J., 1978: Finite-element simulation of asymmetric folding. Tectonophysics, 47:1-14.
- ARMBRUST, C.A., 1968: A contour generator. Paper presented at SWAP-14 Conf., April.
- ATKINSON, P., 1972: Computer-aided design of closed loop control systems. Comp. Aided Design, 4:120-128.
- BADGLEY, P.C., 1959: Structural Methods for the Exploration Geologist. Harper & Row, New York, 280pp.
- BARNHILL, R.E., and RIESENFELD, R.F., 1974: Computer Aided Geometric Design. Academic Press, New York, 326 pp.
- BAYLY, M.B., 1969: Viscosity and anisotropy estimates from measurements on chevron folds. Tectonophysics, 9:459-474.
- BAYLY, M.B., 1974: An energy calculation concerning the roundness of folds. Tectonophysics, 24:271-316.
- BEASLEY, A.J., 1981: A computer program for printing geometrically accurate structural fabric diagrams. Computers & Geosciences, 7(3):215-228.

- BELL, J.S., 1978: A Computer-Controlled Colour Graphical Display. M.Eng. thesis (Unpubl.), Dept. Electrical Engineering, Univ. of Adelaide.
- BELL, T.H., and DUNCAN, A.C., 1978: A rationalized and unified shorthand terminology for lineation and fold axes in tectonites.

 Tectonophysics, 47:T1-T5.
- BENGTSSON, B., and NORDBECT, S., 1964: The construction of isarithms and isarithmic maps by computer. B.I.T., 4:87-105.
- BERNER, H., EKSTRÖM, T., LILLJEQUIST, R., STEPHANSSON, O., and WIKSTRÖM, A., 1972: GEOMAP a data system for geological mapping. 24th I.G.C., Sect. 16:3-11.
- BERRY, W.B.N., 1972: An automated system for paleontologic data retrieval a case history. 24th I.G.C., Sect. 16:92-96.
- BHATTACHARYYA, B.K., 1969: Bicubic spline interpolation as a method for treatment of potential field data. Geophysics, 34:402-423.
- BICKMORE, D.P., 1968: Maps for the computer age. Geographical Magazine, 41(3):221-226.
- BICKMORE, D.P., and KELK, B., 1972: Production of a multi-colour geological map by automated means. 24th I.G.C., Sect. 16:121-127.
- BIOT, M.A., 1961: Theory of folding of stratified viscoelastic media and its implications in tectonics and orogenesis. Geol. Soc. Am. Bull., 72:1595-1620.
- BIOT, M.A., 1964a: Theory of internal buckling of a confined multilayer structure. Geol. Soc. Am. Bull., 75:563-568.
- BIOT, M.A., 1964b: Theory of viscous buckling of multilayered fluids undergoing finite strain. Phys. Fluids, 7:855-861.
- BIOT, M.A., 1964c: Theory of stability of periodic multilayered continua. Q. J. Mech. Apl. Math., 17:217-224.
- BOEHM, S., FRENKEL, Y., and GILL, D., 1980: Computerized catalog of geological maps of Israel. Computers & Geosciences, 6(4):451-462.
- BORRADAILE, G.J., 1974: Bulk finite tectonic strain estimates from the deformation of neptunian dykes. Tectonophysics, 22:127-139.
- BOUILLE, F., 1976a: A model of scientific data bank and its application to geological data. Computers & Geosciences, 2(3):279-292.
- BOUILLE, F., 1976b: Graph theory and digitization of geologic maps. J. Math. Geol., 8(4):375-393.
- BOUKNIGHT, W.J., 1970: A procedure for generation of three-dimensional halftone computer graphics representation. Assoc. Comp. Mach. Comm., 13(9):527-536.
- BRACCHI, G., and SOMALVICO, M., 1970: An interactive software system for computer aided design: an application to circuit project. Assoc. Comp. Mach. Comm., 13(9):537-545.

- BRADLEY, G.M., 1972: The Geochemistry of a Medium Pressure Granulite Terrain at Southern Eyre Peninsula, Australia. Ph.D. dissertation, Dept. of Geol. & Miner., Univ. of Adelaide, South Australia, (Unpubl.).
- BRADY, J.B., 1978: SYMMETRY: an interactive graphics computer program to teach symmetry recognition. Computers & Geosciences, 4(2):179-188.
- BRASSEL, K., 1974: A model for automatic hill-shading. The American Cartographer, 1(1):15-27.
- BRIDGES, M.C., and ETHERIDGE, M.A., 1974: A computer program to contour orientation densities. Dept. of Geol. and Mineral., Univ. of Adelaide, Unpubl. report.
- BRIGGS, I., 1981: Integration of elevation data with remotely sensed data.

 Proc. 2nd Aust. Remote Sensing Conf., Canberra, 1981.
- BULLER, J.V., 1972: Development of the Saskatchewan computerized well information system, 1964-1971. 24th I.G.C., Sect. 16:97-102.
- BURNS, K.L., MARSHALL, B., and GEE, R.D., 1969:

 Computer-assisted geological mapping. Proc. Aust. Inst. Min.

 Met., 232:41-47.
- BURTON, W., 1977: Representation of many-sided polygons and polygonal lines for rapid processing. Assoc. Comp. Mach. Comm., 20 (3): 166-171.
- BUSK, H.G., 1929: Earth Flexures. Cambridge Univ. Press, London, 106 pp.
- CANGELOSI, V.E., 1967: Compound Statements and Mathematical Logic. Charles E Merrill Books, Ohio, 114 pp.
- CAPRARIIS, P. de., 1974: Stress-induced viscosity changes and the existence of dominant wavelengths in folds. Tectonophysics, 23:139-148.
- CARTERETTE, E.C., and FRIEDMAN, M.P., (eds) 1975: Handbook of Perception. Volume 5, Seeing. Academic Press, New York, 527 pp.
- CHAMBERLIN, D.D., 1976: Relational data-base management systems. Computing Surveys, 8(1):43-66.
- CHAPPLE, W.M., 1969: Fold shape and rheology: the folding of an isolated viscous-plastic layer. Tectonophysics, 7:97-116.
- CHARLESWORTH, H.A.K., LANGDENBERG, C.W., and RAMSDEN, J., 1976:

 Determining axes, axialplanes, and sections of macroscopic cylindrical folds using computer-based methods. Can. J. Earth Sci., 13:54-65.
- CHEENEY, R.F., 1971: Strain-rates, folding and cleavage. Scot. J. Geol., 7:345-348.
- CHENG, R.T., and HODGE, D.S., 1976: Finite-element method in modeling geologic transport processes. Math. Geol., 8(1):43-56.
- C.I.E., 1978: Recommendations on uniform colour spaces, colour difference equations, psychometric colour terms. Supplement No.2, C.I.E. Publ. No.15 (E-1.3.1)1971/(TC-1.3).

- CLARKE, N.G., 1976: Structural Analysis of the Port Neill Mylonite Zone and its Country Rocks, Pt. Neill, S. Australia. B.Sc. Hons. thesis, Dept. of Geol. & Miner., Univ. Of Adelaide, South Australia, (Unpubl.).
- CLARKE, R.J, 1982: Stand Alone Interactive Graphics Systems for Integrated Circuit Mask Layout. Ph.D. dissertation, Dept. of Electrical Engineering, Univ. of Adelaide, South Australia, (Unpubl.).
- CLERICI, A., 1980: A method for drawing slope maps from contour maps by automatic data aquisition and processing. Computers & Geosciences, 6:289-297.
- COBBOLD, P.R., and QUINIQUIS, H., 1980: Development of sheath folds in shear regimes. J. Struct. Geol., 2:119-126.
- COHEN, P.H., 1975: A Study of Lineation Distributions and Fold Mechanisms in the Barron River Metamorphics, Gillies Highway. B.Sc. Hons. thesis, James Cook University North Queensland, (Unpubl.).
- COHEN, P.H., 1981a: Application of interactive colour graphics to the display and interpretation of structural data. (Abstr.) Int. Conf. on Deformation Processes in Tectonics, Alice Springs, Aust.
- COHEN, P.H., 1981b: Program CYBER: a software link between the Nova2 and the Cyber, for use on the Nova2. Unpubl. report, Dept. of Elec. Eng., Univ. of Adelaide, South Australia.
- COHEN, P.H., 1982a: General fabric analysis techniques with computer-aided S.O.D.A. . (Abstr.) Int. Conf. on Planar and Linear Fabrics of Deformed Rocks, Zürich, Switzerland.
- COHEN, P.H., 1982b: Practical A.V.A. technique applications using computeraided S.O.D.A. . (Abstr.) Int. Conf. on Planar and Linear Fabrics of Deformed Rocks, Zürich, Switzerland.
- COHEN, P.H., and JAMES, P.R., 1980: Some structural aspects of the Lincoln Complex from Tumby Bay to Port Neill. <u>In</u>: A.J. Parker (ed.): Symposium on the Gawler Craton, ll December 1979. J. Geol. Soc. Aust., 27:51 (Abstr.).
- COHEN, P.H. and JAMES, P.R., 1981: Report on the structural analysis of Brockman Three using interactive colour graphics of the ULOS computer system. Unpubl. Report, Univ. of Adelaide, 20pp.
- COIN, C.D.A., 1976: A Study of the PreCambrian Rocks of Southern Eyre Peninsula in the Vicinity of Tumby Bay, South Australia. Ph.D. dissertation, Dept. of Geol. & Miner., Univ. of Adelaide, South Australia, (Unpubl.).
- COLE, A.J., 1968: Algorithm for the production of contour maps from scattered data. Nature, 220:92-94.
- COLONELL, J.M., GOLDSMITH, V., and TURBIDE, P.N., 1972:

 Development of a coastal data bank for the northeastern United States. 24th I.G.C., Sect. 16:12-21.
- COMPTON, R.R., 1962: Manual of Field Geology. J. Wiley, New York, 378pp.
- CONTROL DATA CORPORATION, 1977: Sort/Merge Reference Manual. C.D.C. Publ. No. 60343900.

- CONTROL DATA CORPORATION, 1978: FORTRAN Extended Version 4 Reference Manual. C.D.C. Publ. No. 60305600.
- COOPER, J.A., FANNING, C.M., FLOOK, M.M., and OLIVER, R.L., 1976:

 Archaean and Proterozoic metamorphic rocks on southern Eyre
 Peninsula, South Australia. J. Geol. Soc. Aust., 23:287-292.
- COOPER, M.A., and NUTTALL, D.J.H., 1981: GODPP: programs for the presentation and analysis of structural data. Computers & Geosciences, 7(3):267-286.
- COREN, S., 1969: Brightness contrast as a function of figure-ground relations. J. Experimental Psychology, 80:517-524.
- CORNSWEET, T.N., 1970: Visual Perception. Academic Press, New York, 475pp.
- CRAIN, I.K., 1970: Computer interpolation and contouring of two-dimensional data: a review. Geoexploration, 8:71-86.
- CRAIN, I.K., 1978: The Monte-Carlo generation of random polygons. Computers & Geosciences, 4:131-141.
- CRUDEN, D.M., 1978: A computer-based system for rock mass description.

 Proc. 3rd Int. Congr., Int. Assoc. Eng. Geol., Special Session
 A, p.155.
- CRUDEN, D.M., and CHARLESWORTH, H.A.K., 1976: Errors in strike and dip measurements. Geol. Soc. Am. Bull., 87:977-980.
- DAGBERT, M., 1978: The use of simulated spatially distributed data in geology. Computers & Geosciences, 6:175-192.
- DAHLSTROM, C.D.A., 1969: The upper detachment in concentric folding. Can. Petrol. Geol. Bull., 17:326-346.
- DALL'AGLIO, M., and GIGLI, C., 1972: Storage and automatic processing of hydrogeochemical data. 24th I.G.C., Sect. 16:49-59.
- DAOUST, G., and GELINAS, L., 1981: TELECINO: an interactive petrological and geochemical diagrams generator. Computers & Geosciences, 7(1):21-36.
- DATA GENERAL CORPORATION, 1970a: How to use the Nova computers. Publ. No. 015-000009.
- DATA GENERAL CORPORATION, 1970b: Relocatable Math Library File. Publ. No. 093-000041.
- DAVIDSON, A., and MOORE, J.M. Jr., 1978: Omo River Project data-management system: an appraisal. Computers & Geosciences, 4(1):101-113.
- DAVIS, A., 1979: U.L.O.S. Universal LayOut System. Unpubl. document, Dept. Electrical Engineering, Univ. of Adelaide, April, 193pp.
- DAVIS, J.C., and LEVI De LOPEZ, S., 1978: Computer Mapping for Resource Analysis. Int. Conf., Instituto de Geografia, Univ. of Mexico.
- DAYHOFF, M.O., 1963: A contour-map program for X-ray crystallography. Assoc. Comp. Mach. Comm., 6(10):620-622.
- DeBOOR, C., 1972: On calculating with B-Splines. J. Approx. Theory, 6:50-62.

- DeBREMAECKER, J.C., and BECKER, E.B., 1977: Some applications of the finite element method in tectonophysics. Trans., Am. Geophys. Union, 58:497 (Abstr.).
- DEEN, S.M., 1977: Fundamentals of Data Base Systems. The Macmillan Press Ltd., London, 219pp.
- De La HUNTY, L.E., and JONES, W.R., 1964: 1:250,000 Geological Map of Mt. Bruce, Western Australia, Sheet SF 50-11. W. Aust. Geol. Surv., Perth.
- DENNIS, J.G., 1972: Structural Geology. Ronald Press Co., New York, 532pp.
- De SITTER, L.U., 1956: Structural Geology. McGraw-Hill, 552pp.
- DETTORI,G., and FALCIDIENO,B., 1982: An algorithm for selecting main points on a line. Computers and Geosciences, 8(1):3-10.
- DIETERICH, J.H., 1969: Origin of cleavage in folded rocks. Am J. Sci., 267:155-165.
- DIETERICH, J.H., 1970: Computer experiments on mechanics of finite amplitude folds. Can. J. Earth Sci., 7:467-476.
- DIETERICH, J.H., and ONAT, T., 1969: Slow finite deformations of viscous solids. J. Geophys. Res., 74:2081-2088.
- DIXON, J.M., 1974: A new method of determining finite strain in models of geological structures. Tectonophysics, 24:99-114.
- DONATH, F.A., 1972: Effects of cohesion and granularity on deformational behaviour of anisotropic rock. Geol. Soc. Am. Mem., 135:95-128.
- DONATH, F.A. and FRUTH, L.S. Jr., 1971: Dependence of strain-rate effects on deformation mechanism and rock type. J. Geol., 79:347-371.
- DONATH, F.A. and PARKER, R.B., 1964: Folds and folding. Geol. Soc. Am. Bull., 75:45-62.
- DOORNKAMP, J.C., and KING, C.A.M., 1971:

 Numerical Analysis in Geomorphology. Edward Arnold, London, 372pp.
- DOUGLAS, D., and PEUCKER, T., 1973: Algorithms for the reduction of the number of points required to represent a digitized line or its caricature. The Canadian Cartographer, 10(2):112-122.
- DOUGLAS, J., 1980: South Australia From Space. (MacFarlane, W.V., ed.), Rigby, Australia, 104pp.
- DOYLE, F.J., 1981: Digital cartographic data base. Proc. 2nd Aust. Remote Sensing Conf., Canberra, 1981.
- DUEKER, K.J., 1972: A framework for encoding spatial data. Geographical Analysis, 4(1):98-105.
- DUNNET, D., 1969: A technique of finite strain analysis using elliptical particles. Tectonophysics, 7:117-136.
- DUNNET, D., and SIDDANS, A.W.B., 1971: Non-random sedimentary fabrics and modification by strain. Tectonophysics, 12:307-325.

- EASTMAN, C.M., 1977: The concise structuring of geometric data for computer aided design. In (A. Klinger, K.S. Fu, and T.L. Kunii, eds.):

 Data Structures, Computer Graphics, and Pattern Recognition.

 Academic Press, New York, 498pp.
- EASTMAN KODAK, 1972: Color as Seen and Photographed. Kodak Publ. E-74.
- EKSTRÖM, T.K., WIRSTAM, A., and LARSSON, L.E., 1975: COREMAP A data system for drill cores and boreholes. Econ. Geol., 70:359-368.
- ELLIOT, D., 1968: Interpretation of fold geometry from isogonic maps. J. Geol., 76:171-190.
- ELLIOT, D., 1970: Determination of finite strain and initial shape from deformed elliptical objects. Geol. Soc. Am. Bull., 81:2221-2236.
- EVANS, I.S., 1972: General geomorphometry, derivatives of altitude, and descriptive statistics. in (Chorley, J.R., ed.): Spatial Analysis in Geomorphology, Harper & Row, London: p.17-90.
- FAIRMAN, M., and NIEVERGELT, J., (eds.), 1969: Pertinent Concepts in Computer Graphics. Univ. of Illinois Press, 439 pp.
- FANGERAS, O.D., 1979: Digital colour image processing within the framework of a human visual model. IEEE Trans. on Acoustics, Speech and Signal Processing, 27(4):380-393.
- FANNING, C.M., OLIVER, R.L., and COOPER, J.A., 1980:

 The Carnot Gneisses, a metamorphosed Archaean supracrustal sequence in southern Eyre Peninsula. <u>In</u>: A.J. Parker (ed.):

 Symposium on the Gawler Craton, 11 December 1979. J. Geol. Soc.

 Aust., 27:47 (Abstr.).
- FANNING, C.M., in prep.: Ph.D. dissertation, Geology Dept., Univ. of Adelaide, South Australia.
- FINLAYSON, D.M., 1973: Isomagnetic maps of the Australian region for epoch 1970.0. BMR. Geol. Geophys. Rept. 159.
- FLETCHER, R. and GROSHONG, R., 1973: Rock rheology from wavelength selection in folding. Trans., Am. Geophys. Union, 94:456 (Abstr.).
- FLEUTY, M.J., 1964: The description of folds. Geol. Assoc. Proc., 75:461-492.
- FLINN, D., 1958: On tests of significance of preferred orientation in three-dimensional fabric diagrams. J. Geol., 66:526-539.
- FLOOK, M.M., 1975: The Geology and Geochronology of High Grade Metamorphic Rocks at Kirton Point and Cape Donnington, Southern Eyre Peninsula. B.Sc. (Hons.) thesis, University of Adelaide, (Unpubl.).
- FOLEY, J.D., 1971: An approach to the optimum design of computer graphics systems. Assoc. Comp. Mach. Comm., 14(6):380-390.
- FORREST, A.R., 1972: On Coons and other methods for the representation of curved surfaces. Comp. Graphics and Image Processing, 1:341-359.
- FREEMAN, H., 1961: On the encoding of arbitrary geometric configurations. IRE Trans. on Electronic Computers, EC-10:260-268.

- FREEMAN, H., 1969: A review of relevant problems in the processing of line-drawing data. In (A. Grasselli, ed.): Automatic Interpretation and Classification of Images. A NATO Advanced Study Institute, Academic Press, p.155-174.
- FREEMAN, H., 1974: Computer processing of line-drawing images. Computer Surveys, 6:57-97.
- FREEMAN, H., and GLASS, J.M., 1969: On the quantization of line drawing data. IEEE Trans. SSC-5, 1:70-79.
- GALIMBERTI, R., and MONTANARI, U., 1969: An algorithm for hidden line elimination. Assoc. Comp. Mach. Comm., 12:206-211.
- GAY, N.C., 1968: Pure shear and simple shear deformation of inhomogeneous viscous fluids. I. Theory. Tectonophysics, 5:211-234.
- GAY, N.C., 1969: The analysis of strain in the Barberton Mountain Land, eastern Transvaal, using deformed pebbles. J. Geol., 77:377-396.
- GAY, N.C., and JAEGER, J.C., 1975a: Cataclastic deformation of geological materials in matrices of differing composition: I. Pebbles and conglomerates. Tectonophysics, 27:303-322.
- GAY, N.C., and JAEGER, J.C., 1975b: Cataclastic deformation of geological materials in matrices of differing composition: II. Boudinage. Tectonophysics, 27:323-331.
- GHOSH, S.K., 1966: Experimental tests of buckling folds in relation to strain ellipsoid in simple shear deformations. Tectonophysics, 3:169-185.
- GHOSH, S.K., and SENGUPTA, S., 1973: Compression and simple shear of test models with rigid and deformable inclusions. Tectonophysics, 17:133-175.
- GILOI, W.K., 1978: Interactive Computer Graphics. Prentice-Hall Inc., 354pp.
- GLASS, C.E., and SCHOWENGERDT, R.A., 1979: Application of digital image analysis to mined land reclamation. <u>In</u> (T.J. O'Neil, ed.): 16th APCOM, p.16-24.
- GLEN, R.A., LAING, W.P., PARKER, A.J., and RUTLAND, R.W.R., 1976:

 Tectonic relationships between the Proterozoic Gawler and Willyama
 Orogenic Domains, Australia. J. Geol. Soc. Aust., 24:125-150.
- GOLIN, V.L., 1976: Structural Analysis and Microfabric Development of the Gneisses East of Marion Bay, Southern Yorke Peninsula. B.Sc. (Hons.) thesis, University of Adelaide, (Unpubl.).
- GORDON, W.J., and RIESENFELD, R.F., 1974: Berstein-Bezier methods for the computer-aided design of freeform curves and surfaces. Assoc. Comp. Mach. J., 21(2):293-310.
- GORNY, P., 1975: A symbol handling system for CAD utilizing menu techniques and CRT. In (D.W. Lewin, ed.): The European Computing Conf. on Interactive Systems, London, 1975. Online Conferences Ltd., England, p.187-199.
- GRENDER, G.C., 1976: TOPO III: a FORTRAN program for terrain analysis. Computers & Geosciences, 2(2):195-209.

- GRAY, N.H., GEISER, P.A., and GEISER, J.R., 1980: On the least-squares fit of small and great circles to spherically projected orientation data. J. Math. Geol., 12(3):173-184.
- GRIEGER, I., 1975: Computer aided design by means of finite elements.

 In (D.W. Lewin, ed.): Interactive Systems. Online Conferences
 Ltd., p.155-170.
- HALL, J.K., 1975: PTLOC a FORTRAN subroutine for determining the position of a point relative to a closed boundary. J. Math. Geol., 7(1):75-79.
- HAMILTON, W.C., 1961: On the least-squares plane through a set of points. Acta Cryst., 14:185-189.
- HARBAUGH, J.W., and MERRIAM, D.F., 1968: Computer Applications in Stratigraphic Analysis. J. Wiley, New York, 282pp.
- HARDY, R.L., 1971: Multiquadric equations of topography and other irregular surfaces. J. Geophys. Res., 76(8):1905-1915.
- HARRINGTON, H.J., SIMPSON, C.J., and MOORE, R.F., 1982:

 Analysis of continental structures using a digital terrain model

 (DTM) of Australia. J. BMR. Aust. Geol. & Geophys., 7(1):68-72.
- HARRIS, R.A., 1977: A brief description of the Kidd Creek Mine engineering system. <u>In</u> (R.V. Ramani, ed.): 14th APCOM.. p.781-791.
- HARRISON, R.K., LAWSON, R.I., HAWKES, J.R., and DANGERFIELD, J., 1972:

 Data storage retrieval problems and pilot-scale computer studies in mineralogy and petrography. 24th I.G.C., Sect. 16:141-151.
- HAUGH, I., BRISBIN, W.C., and TUREK, A., 1967: A computer-orientated field sheet for structural data. Can. J. Earth Sci., 4:657-662.
- HAWORTH, R.T., and SPARKES, R., 1972: Computerized system for storage and retrieval of geologic data. 24th I.G.C., Sect. 16:155-160.
- HEINDEL, L.E., and ROBERTO, T.J., 1975: An Interactive Language Design System. American Elsevier, New York.
- HENNESSY, J., 1979: Interactive computer programs for instrumental neutron activation analysis. Computers & Geosciences, 5(3/4):281-288.
- HESSDORFER, R.W., 1975: CAMS: computer augmented mapping system.

 In (D.W. Lewin, ed.): European Computing Conference on Interactive Systems, London, 1975. Online Conferences Ltd., England, p.535-556.
- HOBBS, B.E., 1971: The analysis of strain in folded layers. Tectonophysics, 11:329-375.
- HOBBS, B.E., 1972: Deformation of non-newtonian material in simple shear. Geophys. Monograph Ses., 16:243-258.
- HOBBS, B.E., MEANS, W.D., and WILLIAMS, P.F., 1976:
 An Outline of Structural Geology, Wiley, New York, 571 pp.
- HOBBS, B.E., and TALBOT, J.L., 1966: The analysis of strain in deformed rocks. J. Geol., 74:500-513.

- HOLROYD, M.T., and BHATTACHARYYA, B.K., 1970: Automatic contouring of geophysical data using bicubic spline interpolation. Geol. Surv. Canada, Paper No. 70-55.
- HORN, B.K.P., 1981: Hill shading and the reflectance map. Proc. IEEE., 69(1):14-47.
- HUDLESTON, P.J., 1973a: Fold morphology and some geometrical implications of theories of fold development. Tectonophysics, 16:1-46.
- HUDLESTON, P.J., 1973b: An analysis of 'single-layer' folds developed experimentally in viscous media. Tectonophysics, 16:189-214.
- HUDLESTON, P.J., 1973c: The analysis and interpretation of minor folds developed in the Moine rocks of Monar, Scotland. Tectonophysics, 17:89-132.
- HUDLESTON, P.J., and STEPHANSSON, O., 1973: Layer shortening and fold shape development in the buckling of single layers. Tectonophysics, 17:299-321.
- HURVICH, L.M., and JAMESON, D., 1966: The Perception of Brightness and Darkness. Allyn & Bacon, Rockleigh, N.J.
- HUTCHISON, W.W., and RODDICK, J.A., 1968: Machine retrieval and processing for recording geological data. Western Miner, 41:39-43.
- JANCAITIS, J.R., and JUNKINS, J.L., 1973: Mathematical Techniques for Cartography. Final contract report for U.S. Army Eng. Topographic Lab., Fort Belvoir, Virginia, Contract No. DAAK02-72-C-0256, p.15-20.
- JEFFERY, K.G., and GILL, E.M., 1976: The design philosophy of the G-Exec System. Computers & Geosciences, 2(3):345-346.
- JOHNSON, A.M., 1977: Styles of Folding. Elsevier, Amsterdam, 406 pp.
- JOHNSON, A.M., and ELLEN, S.D., 1974: A theory of concentric, kink, and sinusoidal folding and of monoclinal flexuring of compressible, elastic multilayers. I. Introduction. Tectonophysics, 21:301-339.
- JOHNSON, A.M., and HONEA, E., 1975: A theory of concentric, kink, and sinusoidal folding and of monoclinal flexuring of compressible, elastic multilayers. II. Initial stress and nonlinear equations of equilibrium. Tectonophysics, 25:261-280.
- JONES, M.T., 1968: Structural Geology of the South Middleback Range. B.Sc. (Hons) thesis, University of Adelaide, (Unpubl.).
- JUNKINS, J.K., MILLER, G.M., and JANCAITUS, J.R., 1973:

 A weighting function approach to modelling of irregular surfaces.

 J. Geophys. Res., 78(11):1794-1803.
- KALKANI, E.C., and Von FRESE, R.R.B., 1979: An efficient construction of equal-area fabric diagrams. Computers & Geosciences, 5(3/4):301-312.
- KALKANI, E.C., and Von FRESE, R.R.B., 1980: Computer construction of equalangle fabric diagrams and program comparisons. Computers & Geosciences, 6:279-288.

- KAMB, W.B., 1959: Ice petrofabric observations from Blue Glacier, washington, in relation to theory and experiment. J. Geophys. Res., 64:1891-1909.
- KANEFF, S., (ed.), 1970: Picture Language Machines. Proc. of Conf. at ANU, Canberra, Academic Press, 425pp.
- KELKER, D., and LANGDENBERG, C.W., 1976: A mathematical model for orientation data from macroscopic cylindrical folds. J. Math. Geol., 8:549-559.
- KENDALL, D., 1971: Construction of maps from odd bits of information. Nature, 231:158-159.
- KENT, H.C., 1972: Computer-based information bank for Foraminiferal data, Western interior region, North America. 24th I.G.C., Sect. 16:112-118.
- KERNIGHAM, B.W., and PLAUGER, P.J., 1978: The Elements of Programming Style. 2nd Edition, McGraw-Hill Book Co., New York, 168pp.
- KILBY, W.E., and CHARLESWORTH, H.A.K., 1980: Computerized downplunge projection and the analysis of low-angle thrust-faults in the Rocky Mountain foothills of Alberta, Canada. Tectonophysics, 66(1-3):287-299.
- KILGOUR, A.C., 1971: Computer graphics applied to computer aided design. Computer Bull., 15(7):18-23.
- KLINGER, A., FU, K.S., and KUNII, T.L., (eds.), 1977: Data Structures, Computer Graphics, and Pattern Recognition. Academic Press, 498pp.
- KOSTYUK, Y.A., and SOBOLEV, V.S., 1969: Paragenetic types of amphibolites of the hornblende-actinolite series in metamorphic rocks. Dokl. Akad. Nank., U.S.S.R., 164:155-158.
- KREYSZIG, E., 1967: Advanced Engineering Mathematics. 2nd Edition, John Wiley, New York, 899pp.
- KRUMBEIN, W.C., 1959: Trend surface analysis of contour-type maps with irregular control point spacing. J. Geophys. Res., 64(7):823-834.
- KEUNEN, Ph.H., and De SITTER, L.U., 1938: Experimental investigation into the mechanism of folding. Leidsche Geol. Med., 10:271-340.
- KULSRUD, H.E., 1968: A general purpose graphic language. Assoc. Comp.
 Mach. Comm., 11(4):247-254.
- LaFATA, P., and ROSEN, J.B., 1970: An interactive display for approximation of Linear Programming. Assoc. Comp. Mach. Comm., 13(11):651-659.
- LAING, W.P., 1977: Structural interpretation of drill core from folded and cleaved rocks. Econ. Geol., 72:671-685.
- LANCZOS, C., 1966: Discourse on Fourier Series. Oliver & Boyd, Edinburgh, 255pp.
- LANG, T., 1969: Rules for robot draughtsmen. Geographical Magazine, 42(1):50-51.

- LANGDENBERG, C.W., RONDEEL, H.E., and CHARLESWORTH, H.A.K., 1977:

 A structural study in the Belgian Ardennes with sections constructed using computer-based methods. Geol. Mijnbouw, 56:145-154.
- LAURIN, A.-F., SHARMA, K.N.M., WYNNE-EDWARDS, H.R., and FRANCONI, A., 1972:

 Application of data processing techniques in the Grenville Province, Quebec, Canada. 24th I.G.C., Sect. 16:22-35.
- LEA, G., 1972: GEO-ARCHIVE: an information retrieval system for geoscience. 24th I.G.C., Sect. 16:204-211.
- LEAKE, B.E., 1971: On aluminous and edenitic hornblendes. Mineral. Mag., 38:389-407.
- LEE, W.H.K., and KAULA, W.M., 1967: A spherical harmonic analysis of the earth's topography. J. Geophys. Res., 72(2):753-758.
- LeMAITRE, R.W., and FERGUSON, A.K., 1978: The CLAIR data system. Computers & Geosciences, 4(1):65-76.
- LEWIN, D., (ed.), 1975: Interactive Systems. The European Computing Conf. on Interactive Systems, London, Sept., 1975. Online Conferences Ltd., England.
- LINDSAY, P.H. and NORMAN, D.A., 1977: Human Information Processing.
 Academic Press, New York, 777 pp.
- LISLE, R.J., 1974: Deformed lineations as finite-strain structures. Tectonophysics, 21:165-179.
- LISLE, R.J., 1977: Estimation of the tectonic strain ratio from the mean shape of deformed elliptical markers. Geol. Mijnbouw, 56:140-144.
- LOIKOW, J.D., STEVENS, J.D., and WITTICK, R.I., 1971:

 Perspective views and block diagrams drawn on the CALCOMP plotter.

 Technical Report 71-5, Computer Institute for Social Science
 Research, Michigan State Univ., April, pp.5-7.
- LONGE, R.V., BURKE, C.F., DUGAS, J., EWING, K.A., FERGUSON, S.A., SUTTERLIN, P.G., and WILLIAMS, G.D., 1978: Computer-based files on mineral deposits; guidelines and recommended standards for data content. Geol. Soc. Canada Paper 78-26.
- LOUDON, T.V., WHEELER, J.F., and ANDREW, K.P., 1980a:
 A computer system for handling digitized line data from geologic maps. Computers & Geosciences, 6:299-308.
- LOUDON, T.V., WHEELER, J.F., and ANDREW, K.P., 1980b:
 Affine transformations for digitized spatial data in geology.
 Computers & Geosciences, 6(4):397-412.
- LOVERCHECK, L.R., 1972: Raster scan technique provides multicolour graphics displays. Electronics, 45(12):111-116.
- LOW, J.R., 1976: Automatic Coding: Choice of Data Structures. Interdisciplinary Systems Research: 16, Birkhäuser Verlag Basel, 108pp.

- LOW, P.S., 1980: Dust Fallout Study In The Vicinity Of Stonyfell, Greenhill and Riverview Quarries, South Australia. M.Sc. thesis, Dept. of Environmental Studies, Univ. of Adelaide, S. Australia, (Unpubl.).
- LOWE, K.E., 1946: A graphic solution for certain problems of linear structure. Amer. Miner., 31:425-34.
- MAHER, L.P. Jr., 1968: Finite Sets: Theory, Counting, and Applications. Merril Publ. Co., Ohio, 110pp.
- MALING, D., 1973: Coordinate Systems and Map Projections. G. Philip, London, 255 pp.
- MANCKTELOW, N.S., 1979: The Structure and Metamorphism of the Southern Adelaide Fold Belt. Ph.D. dissertation, Dept. of Geol. & Miner., Univ. of Adelaide, South Australia, (Unpubl.).
- MARBLE, D.F., 1981: Some problems in the integration of remote sensing and geophysical information systems. Proc. 2nd Aust. Remote Sensing Conf., Canberra, 1981.
- MARBLE, D.F., and PEUQUET, D.J., 1978: Problems in the storage and manipulation of large data sets. <u>In</u> (J.C. Davis and M.J. McCullagh, eds.): Computer Mapping for Resource Analysis. Int. Conf., Instituto de Geografia, Univ. of Mexico, 1978.
- MARDIA, K.V., 1972: Statistics of Direction Data. Academic Press, London, 357pp.
- MARDIA, K.V., and GADSEN, R.J., 1977: A small circle of best fit for spherical data and areas of vulcanism. Appl. Stat., 26:238-245.
- MARJORIBANKS, R.W., 1974: An instrument for measuring dip isogons and fold layer shape parameters. J. Geol. Educ., 22(2):62-64.
- MARJORIBANKS, R.W., RUTLAND, R.W.R., GLEN, R.A., and LAING, W.P., 1980:

 The structure and tectonic evolution of the Broken Hill region,
 Australia. Precambrian Res., 13:209-240.
- MASE, G.E., 1970: Theory and Problems of Continuum Mechanics. Schaum's Outline Series, McGraw-Hill, New York, 221pp.
- MATTHEWS, P.E., BOND, R.A.B., and van den BERG, J.J., 1974: An algebraic method of strain analysis using elliptical markers. Tectonophysics, 24:31-67.
- MAXWELL, E.A., 1946: Methods of Plane Perspective Geometry Based on the Use of General Homogenous Coordinates. Cambridge Univ. Press, Cambridge, 230 pp.
- McCULLAGH, M.J., 1978: The potential of minicomputer systems for mapping resources. In (J.C. Davis and M.J. McCullagh, eds.): Computer Mapping for Resource Analysis. Int. Conf., Instituto de Geografia, Univ. of Mexico, 1978.
- McLAIN, D.H., 1974: Drawing contours from arbitrary data points. Computer J., 17(4):318-324.
- MEANS, W.D., HOBBS, B.E., LISTER, G.S., and WILLIAMS, P.F., 1980:

 Vorticity and non-coaxiality in progressive deformations. J. of

 Struct. Geol., 2(3):371-378.

- MELLUISH, R., 1931: An Introduction to the Mathematics of Map Projections. Cambridge Univ. Press, Cambridge.
- MENMUIR, P., 1975: The automatic production of weather maps. The Cartographic Journal, 11:12-18.
- MERTIE, J.B., Jr., 1959: Classification, delineation and measurement of non-parallel folds. U.S. Geol. Surv., Prof. Papers, 314-E: 91-124.
- MINNIGH, L.D., 1979: Structural analysis of sheath-folds in a metachert from the Western Italian Alps. J. Struct. Geol., 1(4):275-282.
- MONTANARI, U., 1970: A note on minimal length polygon approximation to a digitized contour. Assoc. Comp. Mach. Comm., 13(1):41-47.
- MOODY, D.W., 1972: Applications of generalized information systems to the storage and retrieval of geological and geographic information. 24th I.G.C., Sect. 16:161-168.
- MOONEY, E.L., GIBSON, D.F., and LEHMAN, T.E., 1979: Mine planning and evaluation with a dedicated computer graphics system. <u>In</u> (T.J. O'Neil, ed.): 16th APCOM., p.269-278.
- MOORE, R.F., and SIMPSON, C.J., 1982: Computer manipulation of a digital terrain model (DTM) of Australia. J. BMR. Aust. Geol. & Geophys., 7(1):63-67.
- MORSE, S.P., 1969: Concepts of use in contour map processing. Assoc. Comp. Mach. Comm., 12(3):147-152.
- MORTIMER, G.E., in prep.: Ph.D. dissertation, Geology Dept., Univ. of Adelaide, South Australia.
- MORTIMER, G.E., COOPER, J.A., and OLIVER, R.O., 1980:

 Petrological and petrochemical evolution of the 1.82 b.y.

 Donington Granitoid Suite of the southeast Eyre Peninsula. <u>In:</u>

 A.J. Parker (ed.): Symposium on the Gawler Craton, 11 December 1979. J. Geol. Soc. Aust., 27:50 (Abstr.).
- MOSHKIN, V.N., BOGUSLAVSKY, I.S., BULKIN, G.A., DVORKINA, B.D., ZHITENEVA, V.V., KIZAEV, M.M., KOLOTUSHKINA, T.F., MOSKALENKO, Z.D., TIULENEV, A.E., MUSTAFAEV, I.A., NILOVA, N.V., POZDNIAKOVA, T.N., and STARIKOVA, M.D., 1972: A computer based descriptor-type information retrieval system for geology. 24th I.G.C., Sect. 16:169-172.
- MUCKHOPADYAY, D, and SENGUPTA, S., 1966: Strain distribution in flexure folds. Bhu-Vidya, 27:88-101.
- NETTLETON, L.L., 1971: Elementary Gravity and Magnetics for Geologists and Seismologists. Monograph Series 1, (P.C. Wuenschel, ed.), Society of Explor. Geophys., 121 pp.
- NEWMAN, W.M., 1966: An experimental program for architectural design. Computer J., 9(1):21-26.
- NEWMAN, W.M., 1968: A graphical technique for numerical input. Computer J., 11:63-64.
- NEWMAN, W.M., 1971: Display procedures. Assoc. Comp. Mach. Comm., 14(10):651-660.

- NEWMAN, W.M., and SPROULL, R.F., 1973: Principles of Interactive Computer Graphics. McGraw-Hill Book Co., New York, 607pp.
- NOBLE, D.C., and EBERLY, S.W., 1964: A digital computer procedure for preparing beta diagrams. Am. Jour. Sci., 262(9):1124-1129.
- NOLL, A.M., 1965: Stereographic projections by computer. Computers and Automation, May: 32-34.
- NOLL, A.M., 1971: Scanned-display computer graphics. Assoc. Comp. Mach. Comm., 14(3):143.
- NORRIS, D.K., 1963: Shearing strains in simple folds in layered media. Geol. Surv. Can. Pap., 63:26-27.
- NUTBOURNE, A.W., 1973: A cubic spline package part 2 the mathematics. Computer Aided Design, 5(1):7-13.
- O'CALLAGHAN, J.F., ROBERTSON, P.K., and FRASER, D., 1981:

 Colour image display it's not that simple. Proc. 2nd Aust.

 Remote Sensing Conf., Canberra, 1981, paper 6.8.
- OLLIER, C.D. and PAIN, C.F., 1980: Actively rising surficial gneiss domes in Papua New Guinea. J. Geol. Soc. Aust., 27(1):33-44.
- PAIMER, J., 1975: Computer science aspects of the mapping problem.

 In (J. Davis and M. McCullagh, eds.): Display and Analysis of Spatial Data. J. Wiley, New york, p.155-172.
- PARASNIS, D.S., 1979: Principles of Applied Geophysics. Chapman and Hall, 3rd edition, 275 pp.
- PARK, C.M., LEE, Y.H., and SCHEPS, B.B., 1971: Slope measurement from contour maps. Photogrammetric Engineering, 37(3):277-283.
- PARK, R.G., 1969: Structural correlation in metamorphic belts. Tectonophysics, 7:323-338.
- PARKER, A.J., 1978: Structural, Stratigraphic and Metamorphic Geology of Lower Proterozoic Rocks in the Cowell/Cleve District, Eastern Eyre Peninsula. Ph.D. dissertation, Dept. of Geol. and Miner., Univ. of Adelaide, South Australia, (Unpubl.).
- PARKER, A.J., 1980: Symposium on the Gawler Craton, 11 December 1979. J. Geol. Soc. Aust., 27:45-54.
- PARKER, A.J., and LEMON, N., 1982: Reconstruction of the Early Proterozoic stratigraphy of the Gawler Craton, South Australia. J. Geol. Soc. Aust., 29:221-238.
- PARRISH, D., 1973: A non-linear finite-element fold model. Am. J. Sci. 273:318-334.
- PARSLOW, R.D., and GREEN, R.E., (eds.), 1971: Advanced Computer Graphics: Economics, Techniques, and Applications. Plenum Press, London, 1230 pp.
- PATERSON, M.S., and WEISS, L.E., 1966: Experimental deformation and folding in phyllite. Geol. Soc. Am. Bull., 77:343-373.

- PATTERSON, J., 1974: An integrated c.a.d. system for an architect's department. Comp. Aided Design, 6(1):25-32.
- PEDLER, A.D., 1976: The Geology and Geochronology of High Grade Metamorphic Rocks Between Point Yorke and Meteor Bay, Southern Yorke Peninsula. B.Sc. (Hons.) thesis, University of Adelaide, (Unpubl.).
- PEUCKER, T.K., and CHRISMAN, N., 1975: Cartographic data structures.

 The American Cartographer, 2(1):55-69.
- PFALTZ, J.L., 1977: Computer Data Structures. McGraw-Hill Book Co., 446pp.
- PFALTZ, J.L., and ROSENFELD, A., 1967: Computer representation of planar regions by their skeletons. Assoc. Comp. Mach. Comm., 10(2):119-122,125.
- PHILLIPS, F.C., 1971: The Use of Stereographic Projection in Structural Geology. 3rd edition., Edward Arnold (Publishers) Ltd., 90pp.
- POUZET, J., 1980: Estimation of a surface with known discontinuities for automatic contouring purposes. J. Math. Geol., 12(6):559-575.
- PRICE, G.P., 1973: The photometric method in microstructural analysis. Am. J. Sci., 273:523-537.
- PRICE, G.P., 1978: Study of heterogeneous fabric and texture within a quartz-feldspar mylonite using the photometric method. Geol. Soc. Am. Bull., 89(9):1359-1372.
- PRINCE, M.D., 1971: Interactive Graphics for Computer Aided Design.
 Addison-Wesley, Reading, Mass., 301 pp.
- QUEYSSAC, D., Ed., 1976: Understanding Microprocessors. Unwin Brothers, Surrey, 113 pp.
- PRO-LOG CORPORATION, 1979: Microprocessor User's Guide. 77pp.
- RAASE, P., 1974: Al and Ti contents of hornblende, indicators of pressure and temperature of regional metamorphics. Contr. Miner. and Petrol., 45:231-236.
- RAGAN, D.M., 1973: Structural Geology. 2nd Ed., Wiley, New York, 222pp.
- RAMBERG, H., 1961: Relationship between concentric longitudinal strain and concentric shearing strain during folding of homogenous sheets of rock. Am. J. Sci., 259:382-390.
- RAMBERG, H., 1963: Fluid dynamics of viscous buckling applicable to folding of layered rocks. Am. Assoc. Pet. Geol. Bull., 47:484-515.
- RAMBERG, H., 1964: Selective buckling of composite layers with contrasted rheological properties, a theory for the formation of several orders of folds. Tectonophysics, 1:307-341.
- RAMBERG, H., 1970: Folding of laterally compressed multilayers in the field of gravity. I. Phys. Earth Planet. Inter., 2:203-232.
- RAMBERG, H., 1971: Folding of laterally compressed multilayers in the field of gravity. II. Numerical examples. Phys. Earth Planet. Inter., 2:203-232.

- RAMBERG, H., and STRÖMGARD, K.E., 1971: Experimental tests of modern buckling theory applied to multilayered media. Tectonophysics, 11:461-472.
- RAMSAY, J.G., 1960: The deformation of early linear structures in areas of repeated folding. J. Geol., 68:75-93.
- RAMSAY, J.G., 1967: Folding and Fracturing of Rocks. McGraw-Hill, 568pp.
- RAMSDEN, J., and CRUDEN, D.M., 1979: Estimating densities in contoured orientation diagrams. Geol. Soc. Am. Bull., 90:229-231.
- REED, L.J., and TRYGGVASON, E., 1974: Preferred orientations of rigid particles in a viscous matrix deformed by pure shear and simple shear. Tectonophysics, 24:85-98.
- RHYNSBURGER, D., 1973: Analytic delineation of Thiessen polygons. Geographical Analysis, 5(2):133-144.
- RICHARDSON, F.K., and OESTREICHER, D.R., 1969: Computer assisted integrated circuit photomask layout. <u>In</u> (M. Fairman and J. Nievergelt, eds.): Pertinent Concepts in Computer Graphics. Univ of Illinois Press.
- RICHARDSON, S.M., 1978: Structural Analysis of the Gneisses at Corny Point, Southern Yorke Peninsula. B.Sc. (Hons.) thesis, University of Adelaide, (Unpubl.).
- RICKARD, M.J., 1971: A classification diagram for fold orientations. Geol. Mag., 108:23-26.
- RIVA, J.P. Jr., 1972: Computerized indexing and retrieval of information regarding on-going geological research. 24th I.G.C., Sect. 16:213-217.
- ROBINSON, J.E., 1972: Economic use of geological data files in exploration. 24th I.G.C., Sect. 16:173-180.
- ROBINSON, J.E., CHARLESWORTH, H.A.K., and ELLIS, M.J., 1969:
 Structural analysis using spatial filtering in interior plains of
 South-Central Alberta. Am. Assoc. Petrol. Geologists,
 53(11):2341-2367.
- ROBINSON, J.E., MERRIAM, D.F., and BURROUGHS, W., 1978: A quantitative technique to determine relation of oil production to geologic structure in Graham County, Kansas. <u>In</u> (J.C. Davis and M.J. McCullagh, eds.): Computer Mapping for Resource Analysis. Int. Conf., Instituto de Geografia, Univ. of Mexico.
- RODDICK, J.A., and HUTCHISON, W.W., 1972: A computer-based system for geological field data on the Coast Mountains Project, British Columbia, Canada. 24th I.G.C., Sect. 16:36-46.
- ROGERS, D.F., and ADAMS, J.A., 1976: Mathematical Elements for Computer Graphics. McGraw-Hill Book Co., New York, 239pp.
- ROONEY, T.P., RIECKER, R.E., and GAVASCI, A.T., 1975:
 Hornblende deformation features. Geology, 3:364-366.
- ROSENFELD, A., 1969: Picture Processing by Computer. Academic Press, New York, 196 pp.

- ROSENFELD, A., and KAK, A.C., 1976: Digital Picture Processing. Academic Press, New York.
- ROSS, R.G., 1978: Data Base Systems Design, Implementation, and Management. AMACOM, 239pp.
- SALOMON, K.B., 1978: An efficient point-in-polygon algorithm. Computers & Geosciences, 4:173-178.
- SANDER, B.H.M., 1970: An Introduction to the Study of Fabrics of Geologic Bodies. Authorised translation by F.C. Phillips and G. Windsor, Oxford Pergammon Press, 641pp.
- SANTOYO, A.L., 1978: Structural relief interpretation through profile analysis. In (J.C. Davis and M.J. McCullagh, eds.): Computer Mapping for Resource Analysis. Int. Conf., Instituto de Geografia, Univ. of Mexico.
- SCHWERDTNER, W.M., 1970: Hornblende lineations in the Trout Lake area, Lac la Range map sheet, Saskatchewan. Can. J. Earth Sci., 7:884-899.
- SCHWERDTNER, W.M., BENNETT, P.J., and JAMES, T.W., 1977:

 Application of L-S fabric scheme to structural mapping and paleostrain analysis. Can. J. Earth Sci., 14(5):1021-1032.
- SELBY, S.M., Ed., 1971: Standard Mathematical Tables. 19th Edition, C.R.C., 710pp.
- SEN, A.K., 1976: On a class of map transformation. Geographical Analysis, 8(1):23-37.
- SEN, S.K., and RAY, S., 1971: Breakdown reactions for natural hornblendes. in granulite facies. N. Jb. Miner. Abh., 114(3):301-319.
- SHANLEY, R.J., and MAHTAB, M.A., 1976: Delineation and analysis of clusters in orientation data. Math. Geol., 8(1): 9-23.
- SHARP, D.A., 1972: The Canadian system for geoscience data. 24th I.G.C., Sect. 16:196-203.
- SHAW, A.C., 1969: A formal picture definition scheme as a basis for picture processing systems. Information and Control, 14(1):938-947.
- SHELTON, J.S., 1966: Geology Illustrated. Freeman & Co., 434pp.
- SHEPARD, D., 1968: A two-dimensional interpolation function for irregularly spaced data. Proc. 23rd Nat. Conf. of Assoc. Computing Machining, p.517-524.
- SHIH, K.G., and HEFFLER, D.E., 1972: Bedford Institute geographically ordered marine geophysical data storage and retrieval system. 24th I.G.C., Sect. 16:76-81.
- SHIMAMOTO, T., 1974: Application of the Pi-theorem to the similarity criteria of slow deformation of inhomogenous viscous fluids. Tectonophysics, 22:253-263.
- SIMPSON, C.J., 1978: LANDSAT: developing techniques and applications in mineral and petrologum exploration. BMR J. Aust. Geol. & Geophys., 3:181-191.

- SKJERNAA, L., 1975: Experiments on superimposed buckle folding. Tectonophysics, 27:255-270.
- SMITH, L.B., 1971: Drawing ellipses, hyperbolas or parabolas with a fixed number of points and maximum inscribed area. Comput. J., 14: 81-86.
- SMITH, N.I., 1980: The GASP utility package incorporating the Fast Fourier Transform. Unpubl. report, Dept. Elec. Eng., Univ. Adelaide, June 1980, 16pp.
- SNEATH, P.H.A., 1977: A method for testing distinctness of clusters: a test of the disjunction of two clusters in Euclidean space as measured by their overlap. J. Math. Geol., 9(2):123-143.
- STABLER, C.L., 1968: Simplified Fourier Analysis of fold shapes. Tectonophysics, 6:343-350.
- STARKEY, J., 1969: A computer programme to prepare orientation diagrams.

 In (P. Paulitsch, ed.): Experimental and Natural Rock
 Deformation. Springer, New York, p.51-74.
- STARKEY, J., 1977: The contouring of orientation data represented in spherical projection. Can. J. Earth Sci., 14(2):268-277.
- STAUFFER, M.R., 1973: New method for mapping fold axial surfaces. Geol. Soc. Am. Bull., 84:2307-2318.
- STAUFT, D.L., 1972: Evolution of data systems in oil exploration. 24th I.G.C., Sect. 16:181-188.
- STEPHANSSON, O., 1973: The solution of some problems in structural geology by means of the finite-element tectonique. Geol. För. Stockholm Förh., 95:51-59.
- STEPHANSSON, O., and BERNER, H., 1971: The finite element method in tectonic processes. Phy. Earth Planet Interiors, 4:301-321.
- STINGELIN, R.W., and AVIS, G.B., 1972: Digital processing of airborne infrared imaging signals. 24th I.G.C., Sect. 16:82-88.
- STOCKWELL, C.H., 1950: The use of plunge in the construction of crosssections of folds. Geol. Assoc. Canada Proc., 3:97-121.
- STONE, R.O. and DUGUNDJI, J., 1965: A study of microrelief its mapping, classification, and quantification by means of a Fourier analysis. Eng. Geol., 1(2):89-187.
- STUTZ, F.P., 1975: Interactive computer cartography. The Cartographic Journal, 12(1):17-21.
- SUMMAGRAPHICS CORPORATION, 1978: BITPAD Users Manual, 17pp.
- SUNDGREN, B., 1975: Theory of Data Bases. Mason/Charter Publ. Inc., 244pp.
- SUTHERLAND, I.E., 1966: Computer inputs and outputs. Scientific American, Sept., 1966.
- TAN, B.K., 1973: Determination of strain ellipses from deformed Ammonoids. Tectonophysics, 16:89-101.

- TAPLEY, I., and HORWITZ, R.C., 1981: Interference folding in the Hamersley Basin of Western Australia. Proc. 2nd Aust. Remote Sensing Conf., Canberra, 1981.
- TEICHOLZ, E.D., and DORFMAN, J., 1976: Computer Cartography: World Wide Technology and Markets. Int. Technology Marketing, 430pp.
- TELFORD, W.M., GELDART, L.P., SHERIFF, R.E., and KEYS, D.A., 1976:
 Applied Geophysics. Cambridge University Press, 860 pp.
- THIESSEN, R.L. and TREAGUS, J.E., 1980: Classification of fold interference patterns: a reexamination. J. of Struct. Geol., 2(3):311-316.
- THOME, P.G., 1981: NASA's resource observations program in the 1980's. Proc. 2nd Aust. Remote Sensing Conf., Canberra, 1981.
- THOMSON, 1980: 1:1,000,000 Geological Map of South Australia. S. Aust., Geol. Surv., Adelaide.
- TIPPER, J.C., 1979: An ALGOL program for dissimilarity analysis: a diverseomnithetic clustering technique. Computers & Geosciences, 5:1-14.
- TOCHER, F.E., 1967: A point counting computer programme for petrofabric analysis of uniaxial mineral orientations. Min. Mag., 36(279):456-457.
- TOCHER, F.E., 1978a: Some modifications of a point-counting computer program for fabric analysis of uniaxial orientations. Computers & Geosciences, 4(1):1-4.
- TOCHER, F.E., 1978b: Petrofabric point-counting program fabric (FORTRAN IV). Computers & Geosciences, 4(1):5-22.
- TOCHER, F.E., 1979: The computer contouring of fabric diagrams. Computers & Geosciences, 5(1):73-126.
- TURNER, F.J., and WEISS, L.E., 1963: Structural Analysis of Metamorphic Tectonites. McGraw-Hill, U.S.A., 545pp.
- VISTELIUS, A.B., 1966: Structural Diagrams. Pergamon Press, Oxford, 178pp.
- VOIGT, W., and SAMUELSON, I., 1969: On the application of finite-element technique to problems concerning potential distribution and stress analysis in the earth sciences. Pure and Applied Geophysics, 76:40-55.
- WALKER, B.S., GURD, J.R., and DRAWNEEK, E.A., (eds.), 1975: Interactive Computer Graphics. Computer Systems Engineering Series: Crane, Russack & Co., Inc., 160pp.
- WALTERS, R.F., 1969: Contouring by machine: a user's guide. Am. Assoc. Petroleum Geologists Bull., 53(11):2324-2340.
- WATKINSON, A.J., 1981: Patterns of fold interference: influence of early fold shapes. J. of Struct. Geol., 3(1):19-24.
- WATKINSON, A.J., and COBBOLD, P.R., 1978: Localization of minor folds by major folds. Geol. Soc. Am. Bull., 89:448-450.
- WATSON, D.F., 1982: ACORD: automatic contouring of raw data. Computers & Geosciences, 8(1):97-101.

- WEBB, A.W., 1980: A geochronological investigation of the tectono-magmatic history of the Gawler Craton. <u>In</u>: A.J. Parker (ed.): Symposium on the Gawler Craton, 11 December 1979. J. Geol. Soc. Aust., 27:45 (Abstr.).
- WEISS, L.E., 1954: A study of tectonic style: structural investigation of a marble-quartzite complex in southern California. Univ. of California Publ. in Geological Sciences, 30:1-102.
- WEISS, L.E., 1959: Geometry of superimposed folding. Geol. Soc. Am. Bull., 20:91-106.
- WEISS, L.E., McINTYRE, D.B., and KÜRSTEN, M., 1955:

 Contrasted styles of folding in the rocks of Ord Ban Mid Strathspey. Geol. Mag., 92:21-36.
- WHITTEN, E.H.T. and THOMAS, J.J., 1965: Geometry of folds portrayed by contoured maps: a new method for representing the geographical variability of folds. Geol. Soc. Am. Spec. Pap., 87:186.
- WILLIAMS, C.M., 1979: Scanning digitizers: automating the input of drawings. Computer Aided Design, 11:227-230.
- WILLIAMS, G.D. and CHAPMAN, T.J., 1979: The geometrical classification of noncylindrical folds. J. of Struct. Geol., 1(3):181-186.
- WILLIAMS, P.F., 1970: A criticism of the use of style in the study of deformed rocks. Geol. Soc. Am. Bull., 81:3282-3296.
- WILLIAMS, R., 1971: A survey of data structures for computing graphics systems. Computing Surveys, 3(1):1-21.
- WILSON, C.J.L., 1973: The prograde microfabric in a deformed quartzite sequence, Mount Isa, Australia. Tectonophysics, 19:39-81.
- WILSON, G., 1967: The geometry of cylindrical and conical folds. Proc. Geol. Assoc. Engl., 78:179-210.
- WITTICK, R.I., 1976: A geographic computer system for the analysis and graphic representation of spatial point data. Geographical Analysis, 8(3):319-328.
- WOOD, D.S., OERTAL, G., SINGH, Jr., and BENNETT, H.F., 1976:
 Strain and anisotropy in rocks. Phil. Trans. R. Soc. London,
 Ser. A, 283:27-42.
- WOODCOCK, N.H., 1977: Specification of fabric shapes using an eigenvalue method. Geol. Soc. Am. Bull., 83:1231-1236.
- WOODSFORD, P.A., 1971: The design and implementation of the GINO 3D graphics software package. Software Practice and Experience, 1(4):335-365.
- WYRILL, G., 1975: Pictorial description language. <u>In</u> (D.W. Lewin, ed.): Interactive Systems. The European Computing Conf. on Interactive Systems, London, Sept., 1975. Online Conferences Ltd., England, p.511-525.
- YAMAMOTO, K., and NISHIWAKI, N., 1975: FORTRAN program of preparing contour maps for geologic use. Memoirs of Faculty of Science, Kyoto Univ., Series of Geol. and Miner., 41(1):34pp.

- YAMAMOTO, K., and NISHIWAKI, N., 1976: Automatic analysis of geologic structure from dip-strike data. Computers & Geosciences, 1:309-323.
- YOELI, P., 1976: Computer-aided relief representation by traces of inclined planes. The American Cartographer, 3(1):75-85.



APPENDIX A

Program CYBER

A report of a program contributed to the Department of Flectrical Engineering, University of Adelaide

(Program listing is excluded here as it is 1345 cards long of ASSEMBLY language code.)

APPENDIX A

Program CYBER

Written by P.H. Cohen, Geology Department, February 1981

Program to transfer ASCII data between the Electrical Engineering NOVA2 and the University CYBER 173, for use on the NOVA2.

Symbols and Abbreviations

CR 7	Carriage return
^=	CONTROL- (e.g., A = CONTROL-A)
BOF	Beginning of file
EOF	End of file
BS	Backspace
LF	Linefeed
ESC	Escape
Ø	Zero
RO	Rubout (Delete)

Connections

Connection is made between a CYBER port and the NOVA second-I/O port.

Purpose

The program was written to enable the transfer of ASCII files* between the NOVA and the CYBER through a standard CYBER terminal line. Because of its design, it can also be used to concurrently work on both computers from the one terminal (NOVA console).

Description

The program consists of two modes.

- treats the NOVA console as a terminal for the CYBER. This allows Mode 1 the user to set up the CYBER ready for transmission/reception.
- is made up of three parts: Mode 2

Part I: allows the user to set flags for transfer control,

Part II: opens a NOVA disk file for reception/transmission, and

Part III: transfers the file, with user interruption available.

Special Characters

Certain control characters are used to control the flow of the program: - the system interrupt characters are always available,

^{*} A file is any data transmitted between the start and end of transmission.

- causes immediate switching from one mode to the other, and is always available,
- esc closes all NOVA files and channels and exits from the program. It is not available when the console is under system control (indicated in the text below).

Assumptions

The program was written for the use of these two particular machines and so there are certain assumptions that may not pertain to other machines.

- 1. The program is independent of transfer rates (110 9600 BAUD).
- The program assumes an echo from the CYBER.
- A real-time clock (RTC) of 10Hz is used.
- 4. The program uses llK_{Ω} words of central memory.
- 5. The CYBER suspends transmission when a character is sent to it, and repeats the line before continuing transmission when a CR is received by it.
- Operator messages have ".**," in columns 11 14.
- 7. The CYBER sends at least one null character after a LF.
- 8. Horizontal tab (^I) is interpreted as blank-filling to the next modulo 8 column.

Usage

The program is invoked by giving the command: "CYBER" to the CLI (Command Language Interpreter). The program enters Mode 1, which is indicated by the message: "[CYBER]" appearing on the console. (If rubbish appears (due to a faulty interface board), exit program and try again.) The program does not need the system to be bootstrapped before using.

The user is now interacting with INTECOM on the CYBER.

When the CYBER is ready for transmitting (COPYSBF is probably the best method) or receiving (EDITOR is better than EDNA for large files), use ^Z to terminate the CYBER command rather than a CR. This causes the program to send a CR to complete the command as it enters Mode 2, indicated by the message:

CYBER TO NOVA(Ø), NOVA TO CYBER(1), ELSE NOT?

e.g. COMMAND- CONNECT, NOVA ?

COMMAND- COPYSBF, 1fn, NOVA^Z

CYBER TO NOVA(Ø), NOVA TO CYBER(1), ELSE NOT?

User response to the above query is under system control and so normal editing features (RO, /) are available, but ESC becomes unavailable. A CR

is used to end the response. If the first character is not a zero or one then the program returns to Mode 1, otherwise the message:

REQUIREMENTS? f=.s. ...

is displayed, where f is a flag and s is the state of that flag. The state of a flag is changed by typing its name (i.e., A,E,M, or T - see below), and the new state is echoed. Unrecognized flags are ignored. User response to this query is finished with a CR (although not under system control).

From this stage onwards, until the program is returned to Mode 1, there are several minor procedural differences between a file transmitted by the CYBER and by the NOVA. So they are dealt with separately.

Transmitting CYBER to NOVA

Although any flag can be changed, only those pertaining to this direction of movement are considered here.

Flags currently available are:

- E Empty lines are ignored if E=.F., else accepted.
- ${\tt M}$ Operator messages (described above) are only ignored if M=.T. CR is typed to finish the flag specifications.

FILENAME?

is then displayed. The user types in the disk filename that is to receive the CYBER file. The console is under system control for this response.

Use a CR for the filename if it is desired to append the incoming data to the last opened disk file. Otherwise the program assumes that a new disk file is to be created. If the disk file already exists, the message:

BOF(Ø), PREV(1), ELSE NOT?

is displayed. Response to this is again under system control. If zero then the existing file is deleted and a new one created; if one then the file is opened at EOF; otherwise another filename is requested.

Data transmission automatically starts once the file is opened.

Suspending transmission: The file is echoed on the console as it is being received by the NOVA. The user can temporarily stop transmission by striking any key (except a special character). Typing a CR will resume transmission. Note: anything typed after transmission is suspended, is sent to the CYBER. The suspended (partial) line is ignored.

End of transmission: Typing ^Z will reject the partial line (if any), close the disk file and return the program to Mode 1. ESC will also achieve this except the program is exited. Any other character may cause CYBER echoes and responses which will be written into the file.

Transmitting NOVA to CYBER

Flags currently available are:

- Automatic resumption of transmission. If the CYBER tries to send a message while the NOVA is transmitting, transmission stops and the CYBER is allowed to send the message. Transmission continues after 10 seconds if A=.T., otherwise the user must manually restart by striking any key.
- E Empty lines are sent if E=.T., otherwise a blank is inserted.
- T Horizontal tabs are blank-filled if T=.T., otherwise I is sent.

Filename: In response to "FILENAME?", a CR will open the previously used file at its last closing position. Otherwise the specified disk file is opened at BOF. (If it does not exist, then another is requested.)

Suspending transmission: Procedure is the same, except that striking any key will restart transmission (as no keyboard strikes are sent to the CYBER.)

End of transmission: When the EOF is reached: [EOF] is displayed on the console, the disk file is closed, and the program reenters Mode 1.

APPENDIX B

STEREONET PLOTTING ON THE HEWLETT-PACKARD 9830A CALCULATOR

Written by P.H.Cohen, June 1976

HARDWARE AND CONFIGURATION

The 9830A calculator has 5.8K 16-bit words of memory. It is connected to a 9866A printer (80 columns wide) and a 9862A xy-plotter. The calculator also has one cassette handler, and a one line display of 80 columns although only 32 are visible at any time. A "Matrix" ROM and a "String Variables" ROM are used.

Because of the small memory the program is divided into sections that are stored on different files of the program cassette. To keep the use of the cassette to a minimum, the sections are organised so that related functions are together on the one file.

The program is written in BASIC. Due to the slow speed of the machine, the small memory, and the objective of an interactive program, sophisticated and/or precision algorithms are not utilized when a more approximate algorithm that uses a fraction of the time and memory can be employed. More sophisticated and precise algorithms are available elsewhere.

INTRODUCTION

The program was primarily written for three purposes: 1) to plot field data on a stereographic net, 2) to convert field measurements into a standard form, and 3) to make available to the non-computing geologist an easy-to- use program that can process, analyse and plot field data.

The program uses three types of net: equal-angle (Wulff) net, equal-area (Schmidt) net, and orthographic projection. All plotting is done on the lower hemisphere.

All available program functions are listed in Table B.1.

The combination of small memory and large program means that only a small data set can be held in memory at one time. A limit of 100 points is set, where each point is associated with four values: the symbol and label with which it is plotted (Table B.5), and its trend and plunge (computed from the input data). Once a data set has been entered, it can be stored, retrieved, contoured, and otherwise analysed.

A serious consequence of the small memory is that the program is not very sophisticated. For example, once bad data have been entered they are difficult to rectify.

USAGE

Functions are activated by entering a string of eight numbers (V_1 to V_8), separated by commas. Where a number, V_n , is to represent two values then it is specified as $V_n \cdot V_n$. The values of these eight numbers (Tables B.2 to B.14) depend on the function to be performed.

 $^{\rm V}$ is the command which initiates the appropriate function. The numbers, $\rm V_n$, can be integer or floating point.

All angles are in degrees, and although they can be entered as either integer or floating point, the final value stored is integer.

RESULTS

The results of calculations are plotted, printed, and displayed. Only orientations of the first 100 point data are stored in memory. Extra data are processable but not stored. A 101st point datum exists in memory but contains the number of points in the data set, the file number that the data is stored in, the tape number, and the last is reserved.

Some functions are very slow. Fitting of circles and modes take a couple of minutes each. Contouring takes about 20 minutes irrespective of the data. Other functions may take a few seconds.

The algorithms for fitting great and small circles do not always produce reliable results.

Draw and Title Stereonet $(V_1 = 2)$

A stereonet can be drawn up with the centre and north marked, and titles given to the plot (Fig. B.1). The type of net to be used is also defined with this function. Table B.2 contains the list of values for V to V_8 .

Plotting Points (V₁=3,-3)

Table B.3 contains the values for V_1 to V_8 , expanded in Table B.4 which contains a list of the allowable data forms and their appropriate values of V_3 to V_8 .

All points entered during the run of the program are stored in a matrix until the maximum (100) is reached. Further points entered will be plotted but not stored.

Any point with a plunge of zero degrees is plotted twice, once in the calculated position, and the other 180° of trend away.

There are three ways in which data points can be plotted.

Single points: When plotting one point at a time, all eight values V_1 to V_8 must be entered (Fig. B.1).

Multiple points: When plotting many points, all eight values V_1 to V_8 must be entered for the first one, and only V_3 to V_8 for the following points (Fig. B.1).

Replotting points without rotation: Points already entered can be replotted by using the replot option (Table B.4). By specifying a symbol in V_1 ' and/or a label in V_2 only points with the matching symbols/labels are replotted. (If these are zero, then all points are replotted). If it is desired to change the symbol and/or label then use the rotation function ($V_1=7$) with a rotation of zero degrees.

Drawing Great Circles (V1=4)

Great circles can be drawn in a number of different line types (Table B.9). A variety of data input forms are available for plane orientation (Table B.8, e.g. Fig. B.3). Values for V_1 to V_8 are given in Table B.7.

Drawing Small Circles (V₁=5)

Small circles can be drawn in a number of different line types (Table B.9, e.g. Fig. B.2). Values for V_1 to V_8 are given in Table B.10. This is a fairly slow routine, and therefore, a fairly coarse angle of arc (the value of V_3 in the function $V_1=2$) is suggested for small diameter cones.

Contouring (V₁=6)

Titled contour plots of selected datum points can be produced on the plotter (Fig. B.4). Five contour levels (after Bridges and Etheridge, 1974) are used, where each contour level is half the value of the next highest level, with the highest level set at 92.5% of the maximum count (after conversion to % per 1% area).

The algorithm uses the standard manual technique of point counting in a 1% circle centred on the nodes of a 20×20 grid, where the points are projected onto an equal-area net.

Counting (Fig. B.4b) takes about 2 minutes and contouring (Fig. B.4c) takes approximately 20 minutes. Hence, if either an alternative sequence of contour levels, or merely a rapid guide to the contour shape, is required, a printout of the counts at each node can be produced.

Table B.11 contains a list of the V_{n} values.

Rotation of Data (V₁=7)

Selected data can be rotated clockwise around any orientation, and plotted with a new symbol (Fig. B.5) and/or label as desired. The rotated data replace the initial data in memory, and so the latter are lost as they

are rotated. Table B.12 contains the values for V_1 to V_8 . If more than one rotation is required (i.e. V_8 is not zero) then only V_4 to V_8 need be entered for each subsequent rotation.

Saving Data on, and Reading Data from, Cassette $(V_1=8)$

Data can be saved on, and read from, a cassette file. Data in memory can also be cleared. Table B.13 contains the values of $^{\rm V}$ to $^{\rm V}$ 8.

Fitting Planes, Cones, and Modes to Data Distributions $(v_1=9)$

Best fit great circles, small circles, and modes can be found for distributions of points stored in memory (Table B.14, e.g. Fig. B.6). A minimum of one point is needed for a mode, two for a great circle, and three for a small circle. The algorithms for fitting the circles are after Ramsay (1967, p.18ff). Although these algorithms are known to be unreliable, they work reasonably well for distributions which are fairly close to the ideal. Correct algorithms are too big for the calculator. The algorithm for determining modes uses the maximum count from the counting section of the contour routine. This gives an approximate result as there are only 314 counting nodes. Also, only one mode is recognized even if the distribution is multi-modal.

LIST OF TABLES

Table B.1 List of available functions and their appropriate V1 value.

	$\mathtt{Value} \ of \ \mathtt{V}_{1}$
Function	2
Set up stereonet and/or title the plot Plot new points (one or many), or replot points	3,-3
	4
Draw great circles	5
Draw small circles	6
Contour	7
Rotate data Store and/or retrieve and/or clear memory	8
Fit great and/or small circles and/or find mode	9

Table B.2 List of V_1 to V_8 values for setting up stereographic nets.

```
V_1 = 2
                      1 Wulff
                                  (equal-angle)
V_2 = type of net =
                      2 Schmidt (equal-area)
                      3 Orthographic projection
                      0 Default ( = Schmidt)
                                          0 = default (5^{\circ}).
V_3 = step size in degrees.
                                          5 is a useful value.
       This is the angular
                                          10 or 15 are better when
       increment when drawing
                                          drawing small diameter
       arcs (eg. stereonet
                                          small circles
       outline, great circles,
       small circles)
V_4 = number of characters in the title (\leq 50 char)
V_5 = number of characters in the subtitle (\leq 50 char)
v_6 = draw outline of stereonet
                                                    1 = yes
                                          0 = no
\vec{v_7} = tick and mark north with "N"
                                                    l = yes
                                          0 = no
                                          0 = no
                                                    1 = yes
V<sub>8</sub> = mark centre with "+"
```

Table B.3 List of V_1 to V_8 values for plotting points.

```
V_1 = 3 plot one new point only, or replot selected existing points.

-3 plot a series of new points using the same V_1' and V_2 for all.

V_1'= type of symbol (see Table B.5)

V_2 = label of point (see Table B.5)

V_3 to V_8 = data (see Table B.4)
```

Table B.4 Types of data for points.

Type of Data	Value of Input Variables $V_{ m n}$					
Type of Data	$\overline{v_3}$	<u>v4</u>	v_5	v_6	$\frac{\mathbf{v_7}}{\mathbf{v_7}}$	$\frac{v_8}{}$
Lineation	T	Pl	0	0	0	0
Planes One plane	DD	D	-9	0	0	0
one Passe	S	D	Q_2	0	0	0
Intersection of 2 planes	\mathtt{DD}_1	\mathtt{p}_1	0	DD_2	D ₂ *	0
	DD	D_1	0	S	D_2	Q_1
	S	$^{\mathtt{D}}\mathtt{1}$	Q_1	S	D_2	Q_1
Plane + Lineation	DD	D	0	Q	Pi	0
Pitch in plane	S	D	Q_1	Q_1	Pi	0
Trend in plane	DD	D	0	T*	0	0
-	S	D	$Q_{\underline{1}}$	T*	0	0
Plunge in plane	DD	D	0	Pl	$Q_{\mathbf{l}}$	0
	S	D	Q_1	Pl	Q_{1}	0
Extra Forms	-1	0	0	0	0	0
Replot points Return to "COMMAND?"	-1	-1	0	0	0	0

^{*} These values must not be zero (if either is zero then use 0.01 instead).

T=trend, Pl=plunge, Pi=pitch, DD=dip direction, D=dip, S=strike,

Qi=quadrant that D is in (and that Pl and Pi are measured from (see Table
B.6)). Range of T, S, DD is 0°-360°; Pl, Pi, D is 0°-90°. Subscripts on
symbols (except Q) are used to differentiate between them when more than
one appear on the same line.

Table B.5. Abbreviated list of symbols and their values (see the Hewlett-Packard manual on pen plotting for the full list).

Symbol	Value			
		0		
blank	**	01 -	34	
#		35		
÷		42		
+		43		
0 - 9		48 -	57	
A - Z		65 -	90	

Note: Values >99 will give incorrect symbols.

Table B.6. Values of Q_1 and Q_2 used in Tables B.4 and B.8.

0		Quadrant (Azimuth)090°) SE (090°-180°) SW (180°-270°) NW (270°-36			
×	NE (000°-090°)	SE (090°-180°)	SW (180°-270°)	NW (270°-360°)	
0,	~1	-2	- 3	-4	
Q_2	- 5	- 6	-7	-8	

Notes:

1. If the Q value refers to a strike (S) then use the quadrant that the dip direction of the plane lies in.

2. If the Q value refers to a pitch (Pi) then use the quadrant that

contains the strike of the plane from which the reading was taken.

3. If the Q value refers to a plunge (P1) then use the quadrant that contains the strike of the plane to which the lineation is closest.

Table B.7. List of V1 to V8 values for drawing planes.

 $\overline{V_2}$ = type of line (see Table B.9) V_3 to V_8 = data (see Table B.8)

Table B.8. Types of data for planes.

				**	V-	%7 _
Type of Data	v_3	$\mathbf{v_4}$	$\frac{v_5}{}$	$\overline{v_6}$	<u> </u>	$\frac{v_8}{}$
	DD	D	0	0	0	0
Plane	S	D	Q_1	0	0	0
D 1	T	Pl	-9	0	0	0
Pole Plane through 2 lineations*	\mathbf{T}_{1}	Plı	0	\mathbf{T}_{2}	Pl_2	0
Plane through 2 lineations	DD1	D_1	- 9	DD_2	$\mathtt{D_2}^-$	- 9
Plane through 2 poles	DD	D_1	- 9	ຣ້	D_2^2	Q_2
	S	\mathbf{p}_{1}^{-1}	Q_2	DD	D ₂	- 9
	\tilde{s}_1	D ₁	\overline{Q}_2	s_2	D_2	Q_2
man a /alama Ahmangh	T	Pl	0	DD	D [*]	-9
"N" plane (plane through	Tr.	Pl	0	S	D	Q_2
pole of plane and linea-	-	**	•	_		
tion contained within)						

T2 and Pl2 cannot both be zero. See Table B.4 for meanings of symbols.

Table B.9. Types of lines available (see Fig. B.2 for examples).

Value	Type of Line
0	no line
1	
2	8 121 - 1 11 0
3	
4	
5	
6	

Table B.10. List of V1 to V8 values for drawing small circles.

```
V_1 = 5

V_2 = \text{type of line (see Table B.9)}

V_3 = \text{trend of centre of small circle}

V_4 = \text{plunge of centre of small circle}

V_6 = V_7 = V_8 = 0 (not used)
```

Table B.11. List of V1 to V8 values for contouring data.

```
\overline{v_2} = symbol of points to be contoured
                                                      0 = no
                                                                  1 = yes
V_3 = \text{plot a title } (650 \text{ char})
                                                                  1 = yes
                                                      0 = no
V<sub>4</sub> = plot a subtitle (≤50 char)
                                                                  1 = yes
                                                      0 = no
V_5 = draw outline of net
                                                                  1 = yes
                                                      0 = no
V_6 = tick and label north
                                                                  l = yes
                                                      0 = no
V<sub>7</sub> = mark centre of net
V_8 = 0 contour plot
      1 print out the counts
      2 both the above
```

Table B.12. List of V1 to V8 values for rotating data.

```
v_1 = 7
                                                (if 0, then all points)
V_2 = symbol of points to be rotated
                                                (if 0, then no changes)
V_2' = \text{new symbol for rotated points}
                                                (if 0, then all labels)
v_3 = label of points to be rotated
                                                (if 0, then no changes)
V3'= new label for rotated points
V<sub>4</sub> = plunge of rotation axis
V_5 = trend of rotation axis
V_6 = angle of clockwise rotation (in degrees)
V_7 = type of line to join points (see Table B.9)
              - no more rotations,
     not zero - then another rotation to follow (in which case
                 only input V4 to V8 for the next rotation).
```

Table B.13. List of V1 to V8 values for data storage and retrieval.

Table B.14. List of V_1 to V_8 for fitting circles to data distributions.

 V_1 = 9 V_2 = symbol of points to be fitted V_3 = fit mode 0 = no 1 = yes V_4 = fit plane 0 = no 1 = yes V_5 = fit cone 0 = no 1 = yes V_6 = V_7 = V_8 = 0 (not used)

APPENDIX C

CODING GEOLOGICAL DESCRIPTIONS OF DATA STATIONS

Introduction

Geological structure data alone are inadequate for more than rudimentary analyses of geological structures. It is often necessary to extract structural data according to their geology (geological parameters, or combinations thereof), during analysis. Comprehensive geological data banks (such as described by Berner et al, 1972; Boullé, 1976a; Davidson and Moore, 1978) are not essential to the more immediate aims of this thesis, but simply-coded descriptions of those geological parameters which may be required during analysis are necessary. The more important geological aspects are: age, lithology, stratigraphic position, and mineralisation. Specific and exotic parameters can be incorporated as required.

For the sake of simple programming $^{\sharp}$, all possible geological parameters (for any one map) should be translatable into one computer word. Each data station thus contains one computer word (termed a "description" word, \underline{D}) which describes the geology for that station. Programming is further simplified if the mapping of the parameters into the \underline{D} word is performed by the user.

For ease of coding, geological parameters are structured into aspects, which are subdivided into classes (see Fig. C.1). A class may be either a single geological parameter (e.g., "Silurian", in an "age" aspect), or a group of parameters (e.g., "Mineralised with Cu and Zn, but not Pb", in a "mineralisation" aspect, with the three parameters: "Cu", "Pb" and "Zn").

Coding Methods

There are several ways in which coding can be done. The two most suitable methods make use of a 15 bit word* (represented as a five digit octal number).

(1) Each digit represents a geological aspect. As an octal number, the range of values the five digit-number can assume is 000008 to 777778.

[#] The extreme limitations imposed by small minicomputers (in this case a Nova2) in memory and processing speed make it essential that programs are kept as small and simple as possible, so that reasonable turnaround times can be maintained in interactive processing. Modern machines of similar class to the Nova no longer have such major restrictions. Furthermore, as this is a singlehanded attempt at a large project, program sophistication has been given low priority.

^{*} Programming is further simplified if the sign bit of the description word (Fig. C.1) is not utilised. For the Nova, this means 15 bits are available for coding the geology.

This is superior to other bases. For example, decimal numbers (with the range 00000₁₀ to 32767₁₀), are awkward and the range is best reduced to 29999₁₀. This is unsuitable as: a) some bits of the word are used by more than one digit (aspect) and so would be difficult to mask (see later), and b) testing the digits is more complex and slower than with direct use of an octal number. Other radices can be considered. For example, the range in a hexadecimal system is 0000₁₆ to 7FFF₁₆ (F=15), which limits the number of aspects to four, but allows 16 classes per aspect (except for one, which allows eight). The hexadecimal system is generally more awkward to use.

(2) A computer word that has its bits assigned to each aspect as are necessary. This is a general form of method (1). In (1), 3 bits are assigned to each aspect, allowing eight classes per aspect. If some aspects have more, and others less, then the coding can be performed more efficiently with method (2). However, a reasonable understanding of both octal and binary number systems is necessary.

The two methods were compared (Fig. C.1) with regard to employment procedures, and their differences in efficiency demonstrated. The first method failed to encode all the geological parameters, whereas the second method succeeded without utilizing the full word.

Assigning numbers to classes requires some consideration. This depends on the type of classes involved (i.e. single parameters or groups), and on how they are used. If classes are made up of groups of parameters, then the numbering sequence is immaterial; otherwise, the sequencing of the parameters within each aspect must be considered. For instance, age classes could be sequenced from youngest to oldest. The importance of a logical sequence arises when structural data are to be screened (i.e. selected) by particular geological properties consisting of more than one class from a single aspect. A class number of "0" is usually reserved for the class termed "aspect not applicable". (E.g., if a station is in igneous strata, then the class for describing the sedimentary aspect would be "0", i.e. "not sedimentary".)

Data Screening

Once the geology has been successfully coded, some means of instructing a program to screen for particular geological properties is required. For program simplicity, the particular geology required must be coded (termed a "match" word, \underline{M}), by method (2) above, by the user. It is a simple matter to compare \underline{M} and \underline{D} words. As not all aspects (or parts thereof) may be necessary to define a geological property, a third ("control", or \underline{C}) word is required to specify which aspects or bits are to

be considered and which to be ignored. \underline{C} is constructed by a process whereby for every bit of the \underline{D} word to be used in data screening the corresponding bit of the \underline{C} word is set to "1", and every bit to be ignored has the corresponding bit set to "0". Programs then check for the following relationship:

$$\underline{\mathbf{D}} \cap \underline{\mathbf{C}} = \underline{\mathbf{M}} \cap \underline{\mathbf{C}} \tag{C.1}$$

where \cap is logical multiplication in set notation (Maher, 1968).

The M,C word-pair is termed a condition throughout the text. Examples of these are given in Fig. C.2. Every datum point which satisfies (C.1) has the desired geology. All other points are ignored. Because of current limitations in defining geological properties, programs allow repetitive applications of (C.1), using different conditions, until all criteria are satisfied.

The above method of data selection is suitable provided that conditions only require one class per aspect (such as the condition: "Of Silurian age, Cu mineralised, and sedimentary" - provided that "sedimentary" is a class). Often, however, conditions may involve groups of classes (i.e. a property) per aspect, (e.g., the previous condition changed to: "older than Jurassic, Cu or Zn mineralised but no Pb, and sedimentary" - where "sedimentary" may be an aspect).

A limited amount of class grouping can be achieved with existing conditions usage provided that classes are correctly sequenced. Consider the following example:

Assuming it is desired to separate marine sediments from terrestrial sediments, then all marine classes could be assigned even numbers and terrestrial classes odd numbers (Fig. C.3a). To test for "all marine sediments", the bit pattern for the sedimentary aspect will be 000_2 for M, and 001_2 for C. Hence only those sediments with the rightmost bit = 0 will be processed. Alternatively, all marine sediments could be sequenced from 0 to 3 and terrestrial from 4 to 7, and the leftmost bit tested for "0" with the condition: "0002,1002" (Fig. C.3b).

Proposed Comprehensive Methods

More powerful and versatile methods for defining conditions would also be more complex, and there is more than one solution. The three discussed below are among the more acceptable.

Use one bit per class or parameter. This is already done for some classes (e.g., mineralisation in Fig. C.1, where Cu, Pb and Zn each have one bit). However, single parameter classes (e.g., age) would also be assigned one bit each (i.e., eight ages would use eight bits, as opposed to three.) The problem that arises (apart from binary/octal conversions) is that the \underline{D} , \underline{M} , and \underline{C} words will be longer (five aspects, each with eight classes, expands to forty bits, or three computer words), which is not

desirable. This solution is incomplete because it still does not allow for all possible conditions to be defined, (e.g., the condition: "mineralised with Cu or Zn, but not Pb", cannot be used.)

- Incorporate a "map" word (termed \underline{P}) and a "relations" word (termed b) \underline{R}). \underline{P} is a map of the bits in \underline{D} used for each geological aspect. \underline{R} is a list of the relations required for each aspect in all $\underline{M},\underline{D}$ comparison tests. \underline{P} and \underline{R} are not single computer words, but vectors (series of Each vector element of \underline{P} contains the mask for one aspect (Fig. C.4). A routine to formulate conditions (rather than this being done by the user) would require such a map word. Thus far, no significant complexity is introduced by attempting to group classes. -- The complexity arises from R_{\bullet} The "=" in (C.1) would need to be replaced with the relation conveyed in R. For some aspects the relation may be ">" (e.g., "older than Jurassic"), "≠" (for example, "sedimentary", i.e. "not not-sedimentary" where "not-sedimentary" is a class), " \langle ", " \leq ", " \rangle ", and "=". instead of relating the full word of $\underline{\mathtt{M}}$ to $\underline{\mathtt{D}}$ only once (after masking with C, as in equation C.1), each aspect must be tested separately. requires each aspect under consideration to be extracted from the \underline{M} and \underline{D} words and then compared. Data can be screened with (C.1) modified by the steps:
 - i) replace \underline{C} with $\underline{C} \cap \underline{P}$,
 - ii) replace "=" with \underline{R} , and
 - iii) repeat the equation for each aspect;
 to give the expression:

$$\sum_{i=1}^{n} \underline{R}_{i} \quad (\underline{D} \cap \underline{C} \cap \underline{P}, \underline{M} \cap \underline{C} \cap \underline{P}) \qquad (for n tests).$$
 (C.2)

That is:

All geological parameters per datum point ≤ geological properties desired.

where ⊆ is set notation (Maher, op. cit.) meaning "subset".

Equation (C.2) states: "if all tested geological parameters at a datum location satisfy the desired geological properties, then that point is accepted for processing". Data screening is only used if C is non-zero.

data set several times, each time with a different condition, is a relatively simple method to incorporate into existing programs, and this has been done for some.

Proposed Modification

Most of the problems and possible solutions have been discussed. A brief description of a proposal for improvement is given here.

Current problems associated with using geological descriptions and conditions are that the user is required to design and code geological information and control masks in octal and binary number systems. table of geological descriptions, their mnemonics and corresponding values, was available, then only mnemonics need be referred to when forming \underline{D} and $\underline{\underline{M}}$ words. (Programs could generate \underline{C} words.) By including the symbols > , < , =, # (# is used instead of \neq , as the latter is generally not available on computer terminals), conditions can be extended to include properties of aspects, as in (b) above. Programs would also handle \underline{R}_{ullet} By using the mnemonics table and an interpreter routine, conditions could be specified in mnemonic form. (For example, the condition: "older than Jurassic, mineralised but no Pb, and sedimentary" could be coded with such a " > JU MI #PB SD", where "JU" is the class mnemonic for Jurassic in an age aspect, "MI" is the aspect mnemonic for mineralisation, "PB" is the class mnemonic for Pb in the same aspect, and "SD" is a sedimentary aspect mnemonic.

By the same process, an interpreter routine could be used in a program that extracted data files from data banks such as those described in the literature. Hence data files for particular geological properties, as described for the NOVA system, could be created from these data banks.

Given such sophistication, the techniques employed need not be restricted to coding complete geological descriptions into single computer words.

APPENDIX D

AUTOMATIC MAPPING ON THE CYBER173

Introduction

There is a great need for a program package that can produce high quality structure maps. Such a package should have a large repertoire of symbols and manage all drafting situations, including stereoplot insets and suitable legends. A comprehensive package is beyond the scope of this thesis, but it is necessary to have some form of versatile mapping package that can access and plot data from a data bank, place stereonets on the plot, and produce some form of a legend. Although a basic mapping routine was written for program SLINE (Appendix K) it was too limited. A description of a program package that meets most of the specifications required follows.

Data Bank Creation

Both orientation data and reference data (points and lines) were to be used, but due to time constraints the latter were not incorporated (but were for the Nova (see Appendix R)).

The initial data file consists of up to 16 columns of 8 characters each (Fig. D.1), to fit on one line of a lineprinter. The first column is the station identification, the second is the coded geology description column (Appendix C), followed by one column for each structural element, and finally the X and Y coordinate columns. Coordinates are in grid units, not latitude and longitude, because some station locations in the research area are within a metre of each other. Any unused columns are ignored. Each map is headed with a relevent information card which contains the map scale, map units, and position and orientation of the map grid. Maps are separated from each other in the data file by a blank line.

Maps are digitised on a D-Mac digitiser (Economic Geology, University of Adelaide), which has a resolution of 200 microns. As each station location is digitised the relevent structure data is entered into a Sygnetics 2650 microprocessor (constructed by Willoughby, personal communication). The data is directly transmitted to the Cyber, via a terminal line, where it is received by program DIGIT (not described in this thesis) which formats the data for further use. No editing features are available on the Sygnetics, so DIGIT was designed to recognise a limited range of editing characters inserted in the data stream.

Coded sequential (card image) data files (e.g. as produced by program DIGIT) are not efficient as a data library (or bank). Program FDSUP was written to convert card image data files into random-access binary library

files, packing an integer number of stations into each 64 word random record. (For example, six 10 column (i.e. each station has 6 structural elements + station ID + conditions + X + Y columns) coded records can be stored in one random record). This is not the most efficient method for packing data, but is very efficient for searching and extracting data. Le Maitre and Ferguson (1978) described a more efficient method for packing data (which is machine independent) for their CLAIR system, but it is inefficient in searching and extracting data.

The library does not support reference data (e.g. XY files, Appendix R).

Data Bank Maintenance

If any updating is needed for card image files (e.g. using a system editor) then a new data library must be created and the old one deleted.

Program LOOKMS prints the contents of data libraries (e.g. Fig. D.1).

Data Extraction

The extraction of a map (which may be a composite from a number of maps or a subset of one map) for analysis differs from that described in Appendix R, because the required facilities are not available on the Cyber. Instead, all station ID's in the new map are specified in a data file (e.g. Fig. D.2). An extraction program then searches the library for the requisite stations and sets up a data file suitable for the analytical programs (e.g. program PLTMAP, below, and program CNTRFIN, Appendix H). As the various analytical programs cannot read the same data files there is more than one extraction program. This is awkward but acceptable because it takes less effort to produce a new version than to modify the analytical programs to read the same data files. Program MSETUP sets up a data file for stereonet analysis (program CNTRFIN, and program FIT, Mancktelow, 1979), and program MPSUP sets up data files for structure map production (program PLTMAP) and for use on the Nova (Appendix R).

Description of Program PLTMAP

PLTMAP uses an input data file similar to that used for CNTRFIN (see Bridges and Etheridge, 1974), except that each line of orientation data is followed by the data station coordinates. The program rescales and plots data on a CALCOMP drum plotter (25cm or 75cm) with appropriate symbol(s), optionally produces stereonets on the map, and provides a north arrow and scale bar (e.g. Fig. D.3a).

The program is capable of performing affine transformations, so that data from different source maps (with different scales and grid orientations) can be compiled onto the one map. The design of the input

file is similar to that used by program CNTRFIN in order to keep the inconsistency between data files to a minimum.

PLTMAP produces stereonet plots on the final map by calling CNTRFIN as overlays. (In actual use, it calls a version of CNTRFIN, as the first overlay of CNTRFIN is "OVERLAY (0,0)", which cannot be called by another program.) All the facilities of CNTRFIN are available to the mapping program. The sizes and positions of stereonet plots on a map are specified in the input files.

For this project the legend need only consist of a scale bar and north arrow. The scale bar is computed from the map scale and distance unit (kilometres, miles, etc.) (Fig. D.3a).

The plotting of station locations with their ID's (Fig. D.3b) is an alternative to plotting structural elements.

The program tessellates maps (e.g. Fig. D.3b), whether for triangulation and contouring (Appendix M) or for producing PY files for the Nova (Appendix R). It also produces the XY and PY files (Appendix R) used by the Nova programs.

Preprocessing Program PLTMAP Data Files

Data files can be preprocessed to extract information concerning the data contents (e.g. range of values covered). They can also be preprocessed to exaggerate data values, or to "window" (Newman and Sproull, 1973) the data range, i.e. discard all data outside a defined range of values. Data files can also be transformed. For example, single-valued data, such as rainfall, chemical concentrations, or whatever, can be processed by program PLTMAP provided that they are first converted to two-valued data which lie in the valid range recognised for orientation data. Low (1980) has successfully used PLTMAP and program TRICON (Appendix M), using the preprocessors PREPARE and PREWIND, to contour dustfall levels on a map. He used both total range and "windowing" (his Figs. 4.8 to 4.36, 4.39 to 4.48). A version of PLTMAP was used to plot wind velocities on a polar graph (his Figs. 5.3 to 5.8).

APPENDIX E

DERIVATION OF ISODIP LINES FOR AN ELLIPSOID

The parametric equation for an ellipsoid with principal axes A,B and C coinciding with the x, y and z axes, respectively (Fig. E.1), of a right-handed orthogonal Cartesian coordinate system is:

$$\underline{r} = A_{COS}V_{COS}U \hat{\underline{i}} + B_{COS}V_{SIN}U \hat{\underline{j}} + C_{SIN}V \hat{\underline{k}}$$
 (E.1)

where U is the trend of the vector \underline{r} with north along the +x axis, and V is the angle of declination from the xy plane.

The unit vector normal, \hat{n} , to the surface of the ellipsoid (Kreysig, 1967; p.322) is defined by the equation:

$$\frac{\hat{n}}{\hat{n}} = \frac{\underline{r}_U \times \underline{r}_V}{|\underline{r}_U \times \underline{r}_V|}$$
where \underline{r}_U and \underline{r}_V are the partial derivatives of \underline{r}_V of \underline{r}_V where \underline{r}_V and \underline{r}_V are the partial derivatives

Let
$$L = |\underline{r}_{U} \times \underline{r}_{V}|$$
 i.e. the length of the vector, $(\underline{r}_{U} \times \underline{r}_{V})$.

Now:
$$\underline{r}_{U} = -A\cos V \sin U \hat{\underline{i}} + B\cos V \cos U \hat{\underline{j}}$$
,

$$\underline{\mathbf{r}}_{\mathbf{V}} = -A\sin\mathbf{V}\cos\mathbf{U} \ \hat{\underline{\mathbf{i}}} - B\sin\mathbf{V}\sin\mathbf{U} \ \hat{\underline{\mathbf{j}}} + C\cos\mathbf{V} \ \hat{\underline{\mathbf{k}}}$$

$$\underline{\hat{L}}_{\underline{n}} = BC\cos^{2}V\cos U \quad \hat{\underline{i}} - AC\cos^{2}V\sin U \quad \hat{\underline{j}} + (AB\cos V\sin V\sin^{2}U + AB\cos V\sin V\cos^{2}U) \quad \hat{\underline{k}}$$

So
$$\frac{\hat{n}}{L} = \frac{BC_{\cos}^2 V_{\cos}U}{L} \frac{\hat{i}}{L} - \frac{AC_{\cos}^2 V_{\sin}U}{L} \frac{\hat{j}}{L} + \frac{AB_{\cos}V_{\sin}V}{L} \frac{\hat{k}}{L}$$

As $\hat{\underline{n}}$ is always perpendicular to the tangential plane at every point on the ellipsoid surface, to trace out any one isodip line we only need to set the inclination of $\hat{\underline{n}}$ as a constant value, say β (0° \leq β \leq 90°).

If we let
$$\underline{\hat{n}} = D\underline{\hat{i}} + E\underline{\hat{j}} + F\underline{\hat{k}}$$
 ,

then
$$\tan \beta = \frac{|F\hat{k}|}{|D\hat{j}| + E\hat{j}|}$$
;

where
$$|\underline{D}\hat{\underline{i}} + \underline{E}\hat{\underline{j}}| = (B^2C^2L^{-2}\cos^4V\cos^2U + A^2C^2L^{-2}\cos^4V\sin^2U)^{1/2}$$

= $CL^{-1}\cos^2V (B^2\cos^2U + A^2\sin^2U)^{1/2}$;

and
$$|\hat{F_k}| = ABL^{-1} \cos V \sin V$$

So:
$$\tan B = \frac{ABL^{-1}cosVsinV}{CL^{-1}cos^{2}V(B^{2}cos^{2}U + A^{2}sin^{2}U)^{1/2}}$$
$$= \frac{AB}{C} \tan V (B^{2}cos^{2}U + A^{2}sin^{2}U)^{-1/2}$$

Hence tanV =
$$\frac{\text{Ctanß}}{\text{AB}} (B^2 \cos^2 U + A^2 \sin^2 U)^{1/2}$$

As tanß is a constant, let $K = \frac{C \tan B}{AB}$

Therefore:
$$V = \tan^{-1} \left(K \sqrt{B^2 \cos^2 U + A^2 \sin^2 U}\right)$$
 (E.2)

Although V varies with the direction U the variation is deemphasized by the principal axes ratio C/AB . So, for a generally upright subhorizontal fold with C as the vertical axis (which is usually the intermediate axis for tight folds) V varies from $\tan^{-1}(C/A \tan\beta)$ at $U=000^{\circ},180^{\circ}$ (north, south) to $\tan^{-1}(C/B \tan\beta)$ at $U=270^{\circ},090^{\circ}$ (west, east). So with A>C>B, V is less than ß (i.e. lower in height) along the y axis. Because any one strike-line has a constant value for V for any direction U*, the strike-line associated with the angle ß can be superimposed on the $(90^{\circ}-\beta)$ isodip contour for comparison (Fig. E.2).

^{*} From the parametric equation (E.1), all height information is contained in the last term: $C\sin V = \sin^{-1}(H/C)$, which is a constant.

[#] Isodip contour values refer to the dips of the tangential surface to the ellipsoid surface, which is complementary to the inclination of the unit vector normal.

APPENDIX F

GRAPHICS AND UTILITY ROUTINES FOR THE NOVA2

Graphics Software

The graphics library, PLOT.LB, (Bielby, personal communication) for the Nova2 was extremely limited in order to keep its central memory space to a minimum. It did have two advantages that were made of use:- 1) It had a text and numeral plotting routine, and 2) all plotting by the library routine can be routed to either the colour display or the HP pen plotter.

There were three other routines already available that were utilized. Routine CLRECT (Fensom, personal communication) clears a rectangle from the display, and a pair of routines (Clarke, personal communication) that read the (X,Y) coordinate of the stylus on the data tablet (routine RDTAB) and plotted a cursor (routine CURSOR) on the display in the form of a "+" in "invert" mode (see below). RDTAB had a timing problem which was rectified.

Five different ways to plot screen-pixels (Fig. F.1) were developed for the display programs (Appendix R).

- i) "overwrite" the existing colour with the new one;
- ii) "add" the new colour to the existing one (Boolean addition);
- iii) "clear" the colour;
 - iv) "invert" the colour (Boolean complement) (i.e. change the
 pixel to its complementary colour);
 - v) "underwrite" only use the colour if the old one is black.

The graphics routines developed for Appendix R are mainly written in ASSEMBLY, although some are a mixture of FORTRAN and ASSEMBLY.

BITPD (BTPAD and BTPADSC are shortened versions) controls input from the data tablet, i.e. whether to draw or remove a cursor; draw, fix, or remove a rubberband line (see "Rubberbanding", Newman and Sproull, 1973); or pass the coordinates to the controlling program.

DOT is a routine to plot a screen-pixel on the display. Colour and plot mode are preset in global variables.

GLINE (JLINE, FLINE, and DLINE are entry addresses) is a vector generator (line drawing) routine using the DDA (Digital Differential Analyser) technique (Newman and Sproull, opecite). JLINE requires both end points to be specified, whereas DLINE (and the FORTRAN entry, FLINE) draw from the previous end point to the new end point.

PLTPT draws special symbols (see SYMBOL table in Fig. R.6b).

PLTCR displays a number.

DBND joins a sequence of points (optionally scaled) stored in labelled COMMON by straight lines. The colour, which can be two toned, is supplied by the calling program. (e.g. Appendix Q).

FRECT draws a rectangle.

DISPL displays one screen line using colour-pixels (see Appendix X).

SEGMENT (SEGMENTSC is a brief version) is a routine for windowing, i.e. to display only that part of a picture that lies within a defined area (or window).

DSPXY reads, scales and displays XY\$ files (see Appendix R). If the input file is ASCII (XY\$-.DT) then it creates a binary version (XY\$-.BN).

DSPRF is the same as DSPXY, but processes RF\$ files.

DSPPY reads, scales and displays PY\$ files.

SIZED transforms a coordinate from one map coordinate system to

TITLE displays text, left or right justified or centred and/or underlined.

DSPNM displays a subarea title.

LKUPT defines a colour chart look-up table.

FLLA (FFLLA is the FORTRAN entry address) is a polygon-fill routine (see Appendix Q).

TABLE displays a table as menu.

CHOICE selects a menu entry.

SHBOX colours in a menu entry.

The list does not include the multitude of routines imbedded (i.e. inline functions) in the applications programs.

Utility Routines

The following general purpose utility routines were written for this thesis, again not including inline functions.

GAXES computes an orientation of a location inside a stereonet.

TRIG computes forward/inverse trigonometric functions (see below).

MFNAM creates a data file name (see Appendix R).

FVFIL verifies that a file is available for use.

RENAM renames a file.

LSTSB lists all available subarea labels and titles.

XYBN converts ASCII XY\$ files (Appendix R) to binary.

RWBYTE read/writes a byte in memory.

MVBLK moves a block of memory from one location to another.

Alternative FORTRAN Routines

Alternative routines were written to replace particularly slow FORTRAN ones for trigonometric and square-root functions. Use was also made of alternative arithmetic operators (FLPT.LB, Bielby, personal communication). Trigonometry Not only were trigonometric functions slow, but the inverse functions, arc-sine and arc-cosine, did not exist. The latter can be computed from the equations:

$$\sin^{-1}(t) = \tan^{-1} [t/(1-t^2)^{1/2}]$$
 , $0 \le t < 1$ (F.1a)

$$\cos^{-1}(t) = \tan^{-1}[(1-t^2)^{1/2}/t]$$
 , $0 \le t < 1$ (F.1b)

These are very slow computations as all arithmetic is done by software (even using FLPT.LB). All angles must must be in radians although input/output (I/O) of angles is in degrees (for user convenience). Speed was obtained by using lookup tables in routine TRIG.

Routine TRIG Because I/O of angles are normally required only to the nearest degree, the lookup tables (sine and tangent, as coss=sin[90°-ß]) in routine TRIG have entries for every degree, with the degree being integer and the trigonometric value of that degree being in normalised floating point notation (Appendix C of Data General Corporation, 1970a). forward operation (sine, cosine, and tangent) the angle (in integer degrees) is reduced to a quadrant (0° \leq ß \leq 90°). (Permissable range of angles is from -32767° to 32767°). For an inverse function a search must be made in the table to find the closest match. As all integer angles (from 0° to 90°) can be expressed as a 7 digit binary number, a search sequence was devised to find the closest matching angle to the nearest degree in a maximum of seven tests. An extra test may be required to ensure an error of no more than 0.5°. Comparison of a given value with a table entry is done as if the values were integers, which breaks the rules for floating point arithmetic. Because of this, larger errors can occur between angles with differing exponents. For arc-sines (and arc-cosines) these are $0^{\circ}/1^{\circ}$ and $3^{\circ}/4^{\circ}$; and $0^{\circ}/1^{\circ}$, $3^{\circ}/4^{\circ}$, $45^{\circ}/46^{\circ}$, $86^{\circ}/87^{\circ}$, $89^{\circ}/90^{\circ}$ for arc-tangents.

Many equations in the application of the S.O.D.A. technique compound the errors, giving rise to very approximate results. For example, the equations for computing the plunge of a point in a stereonet, given an (X,Y) coordinate (GAXES above) are (for Wulff and Schmidt nets respectively):

plunge =
$$2 \tan^{-1} (r/R)$$
 (R = radius of stereonet) (F.2a)

plunge =
$$2 \sin^{-1} (r/2R)$$
 (r = distance of point from centre). (F.2b)

Square roots The FORTRAN library SQRT function for computing square roots is particularly slow and so was replaced with the single and double precision unsigned integer SQRT routines as described in the Relocatable Math Library File (Data General Corporation, 1970b), whenever it was feasible to do so. These algorithms are untitled.

Appendix G

TERMINOLOGY FOR THE HIERARCHY OF DOMAINS IN SUBAREA ANALYSES

In the subarea analysis of a mapped area, it may be necessary to subdivide subareas into smaller domains, which may further need to be subdivided, repeatedly. Accordingly, the terminology for describing levels of subareas is given here, based on the terminology developed for the computer package (Chap. 3) and described in Appendix R. The term area, or map, refers to the source area, or map, which encompasses the total region of interest for which the structural analysis is being conducted. The first division of the area, or map, into subareas gives rise to regions termed subareas or submaps. The subdivision of these into domains give rise to primary domains, which divide up into secondary domains, which can be further divided into tertiary domains. Although further divisions may be required, no particular terminolgy is assigned. (The logical extensions to the above (e.g quarternary domains, etc.) are recognisable and need not be explicitly defined.)

Terminology expressing the relationship of one domain to another is also required. Any domain or subarea may have <u>subdomains</u> and any domain may belong to a <u>superdomain</u>, irrespective of whether the superdomain is an area, subarea, or domain.

In Appendix R map has a label 'a0', submaps have the label '10', where 'l' is a letter (from b to z), and all levels of domains have the label 'lv', where 'l' is a letter and 'v' is a number. Domain labels do not differentiate between domain levels, and although a terminology could be devised (e.g. lv = primary, lv' = secondary, and lv'' = tertiary domains; or lv = primary, lv'' = secondary, and $lv''_{V} = tertiary domains$; or lv = primary, lvv = secondary, and lvv = tertiary domains; and so on), it is unnecesary to do so because it is generally unimportant to specifically know to which level a region belongs.

During the process of using the S.O.D.A. technique, subareas and domains may be generated which are later discarded. Hence, final solutions for subarea and domain boundaries may have labels that are neither consecutive, nor orderly.

Because subareas and domains identify regions on a map that can be referenced by their labels, regions of interest can be defined by the 'addition' and 'subtraction' (exception) of domains that are included (and excluded) from it (e.g. f7 = b3-b9+b5+e1, where b9 is a subdomain of b3).

APPENDIX H

STEREONET PLOTTING AND CONTOURING PROGRAM "CNTRFIN"

Program ORIENT (Bridges and Etheridge, 1974), written by Bridges, was chosen for use in this thesis as it was suitable and was already available on the CYBER173. The program contained a number of problems.

- It was not efficiently coded.
- 2) It did not produce scatter diagrams.
- 3) The counting grid was too coarse for the smaller allowable counting circle sizes.
- 4) Ambiguous plots arose when small counting circles were used;
- 5) It was incorrectly formatted for the current line printer train.

 The corrections to the problems are given below. The modifications required a complete restructuring of the program and changes in algorithms, giving rise to a new program, CNTRFIN.

Improved Efficiency

The central processor time was reduced by approximately 75% by using the following modifications:

- a) Reduce all multidimensional variables to vectors.
- b) Use a more efficient method of counting (Appendix Z). The method as used by ORIENT required five words of memory per grid node. It determined which nodes were inside the counting circle by computing the angle between each node inside the square (circumscribing the circle) and the circle centre (using cross-products; Mase, 1970). The more efficient method used here requires only one word per grid node (which could be further reduced by packing), and computes the range of grid nodes inside the counting circle directly from the circle. Although not much faster than the original method for the original grid size used, there is a two fold saving: i) a large reduction in memory, and ii) with a finer grid there is a large saving in computation time.

2) Scatter Diagrams

The ability to produce scatter diagrams was introduced as a subroutine. Line 1 of the input data file was modified so that column 43 of line 1 contains a one (1) for a scatter diagram or a zero (0) or blank () for no scatter diagram. It is produced on the same media as the contour plot. Points are plotted with "plus" (+) on pen plotters, and digits specifying the number of points plotted at each location (Fig. H.1) on line printers.

3) Improved Grid

The grid is of the correct form (polar) and superior to that used by Tocher (1967, 1978b) and Starkey (1969) (square), and Kalkani and von Frese (1979) (polar or rotated polar) because the simplest projection of a unit sphere onto the equatorial plane (i.e. stereographic projection) assumes a polar coordinate system. Kalkani and von Frese (op. cit.) did not modify their polar grid (Fig. H.2) to allow for increased distortion at greater dips, as was done by Tocher (op. cit.). A number of problems were encountered with the grid used by ORIENT.

- a) The grid was too coarse.
- b) At dips greater than 60° the grid was coarsened (because it becomes finer at higher angles) but did not take into account the distortion that occurs at high angles.
- c) With the larger counting circle sizes (6%) ORIENT failed to check all grid nodes inside the counting circle, and at the smaller sizes of counting circle ($\le 0.5\%$) some data points failed to register a count because the grid was too coarse (5° for dips ≤ 60 °, and 10° for dips ≥ 60 °).

The improved efficiency of CNTRFIN allowed the use of a grid that was twice as fine (i.e. 2.5°) and still required less memory and CPU time than the original. With a finer grid and an improved counting technique problems (a) and (c) were solved. Problem (b) was solved by considering only those grid nodes around each isodip line which had angular distances closest to the grid size (see below). In this way a semi-regular grid was maintained. This method may not be as good as smoothing (Tocher, op. cit.), nor as that suggested by Starkey (1977), but is adequate for the study's purposes.

The choice of a 2.5° grid appears cumbersome but is in fact an ideal The angular distance between grid size for the contouring method used. nodes around an isodip line must be constant, and there must be an integer number of them for the grid to be regular (Fig. H.3). To allow for the changing grid as the dip increases there has to be a smooth transition between two isodip lines which have differing numbers of nodes (described below). The transition is achieved by successively halving the number of nodes at each transition (isodip) line. Hence, the maximum grid size for the number of transitions desired, n, is $360^{\circ}/2^{n+1}$ (as the minimum number of grid points that are desirable around an isodip line is 4, not 2, excluding the special case when the dip is vertical, 90°). So, for n=5, the grid size is 5.625°. Because the dips at which transitions take place will not necessarily occur at grid lines (Fig. H.4), the actual number obtainable will be, if anything, fewer. (The grid of 5.625° can only achieve four transitions as the fifth occurs between the 84.375° dip line and the vertical). Transitions occur at those grid isodip lines where the angular distance between two consecutive usable grid nodes (i.e. excluding the nodes not used) on an isodip line is less than half the angular distance between isodip grid lines. (This allows a maximum distortion of grid cells as a "polar" rectangle with an isotrend to isodip angular ratio of 2:1, excluding the cells adjoining the vertical as they become triangular due to the loss of one side.) As the grid size of 5° also gives four transitions, this simple angular size is preferred to the more awkward 5.625°. As mentioned earlier, a 5° grid size is too coarse, so this is halved to 2.5°, which is preferred to 2.8125°. The change in grid size is accommodated by a shift in the transition dip value, and therefore a change in the distortion of the grid cells.

The disadvantage of the 2.5° grid over, say, a 1° or 2° grid (Fig. H.2) is that data points are often not symmetrically positioned with respect to the grid. As data are usually measured to the nearest degree the points will fall exactly on a grid node (for a 1° grid) or exactly on or halfway between two grid nodes (in either direction) for a 2° grid. Hence the point count caused by any one datum point is symmetrical, whereas a 2.5° grid is often asymmetrically disposed to a datum point, and so can give asymmetric results for what ought to be symmetrical (Fig. H.5).

4) Unambiguous Plots

Program Okient contoured data by the simple method of interpolating between consecutive nodes along grid lines and plotting (or printing) the contour level number in the appropriate position (Fig. H.6). The numbers were then joined manually. At counting circles of about 2° and greater this method was acceptable, but with a finer resolution (finer grid and/or smaller counting circle sizes), ambiguous plots arose as the contour edges became increasingly irregular.

The problem has been solved by having the computer draw the contours. This required a modification and an addition to the program.

- (a) Ambiguity caused by saddles and ridges (Fig. H.7) can be removed by dividing each grid cell into four "isosceles" triangles, with the centre node being the average of the four surrounding grid nodes. Transitions at isodip lines cause problems (see Fig. H.8a) and so the modification shown in Fig. H.8b was used. Nine grid nodes are used for each cell and are divided into eight "isosceles" triangles. In this case, all apices of the triangles are grid nodes. The advantage of this version is that transitions can be accommodated by merging the two triangles that share the common redundant (skipped) node into one larger triangle.
- (b) A routine to draw the segments (Appendix J) was required. It is not needed if the contours are drawn in one colour and no smooth lines are

The line drawing routine was written as it was simpler than attempting to write a contour-following routine (Tocher, 1979; Dayhoff, 1963; Armbrust, 1968) that was as fast, or as efficient, as the combination of the above contouring with accompanying line drawing. Two advantages of using a routine that sorts and draws line segments over contour-following routines are: 1) it is independent of the grid, and 2) all contour levels in each cell are calculated only once, so grid cells are only processed once. Hence the same routine can be used on polar, cartesian, hexagonal or user defined grids without requiring modification. The advantages of using the sort-and-draw routine over direct plotting of line segments as they are calculated are: 1) the contours can be plotted in colour, as there are only five contour levels (see Bridges and Etheridge, 1974); 2) the contours are more efficiently plotted as the segments are sequential; 3) smooth lines can be drawn instead of the straight line segments, if desired; and 4) the program can determine if the contour loop is open or closed, for two reasons: a) high quality smooth line drawing routines require that the loop be known whether it is open or closed, and b) when shading inside a closed loop by automated means (such as by program SHADL, an overlay for polygonfilling, developed by the writer but not described in this thesis), the boundary of the plot need not be considered if the loop is known to be closed, thus increasing the efficiency of an otherwise difficult routine.

6) Updated Line Printer Output

ORIENT was originally written to produce plots on a printer of 6 lpi (lines per inch) and 10 cpi (characters per inch). This has been updated to plot on the current printer of 8 lpi and 10 cpi.

Conclusion

The modifications above required a complete rewrite of program ORIENT, except for the subroutines that read in, standardised, and rotated data. The program was restructured to work in overlays (Fig. H.9). In this form, extra functions, such as program FIT (Mancktelow, 1979), can be added with minimal modification to programs and with no significant increase in central memory usage.

APPENDIX J

AN EFFICIENT ALGORITHM FOR SORTING LINE SEGMENTS

INTRODUCTION

Developing efficient computer programs that use segmented lines (particularly computer-generated ones, e.g., contours) for the purposes of fitting smooth lines through them (e.g., Ahlberg et al., 1967; Ahuja, 1968; 1970; DeBoor, 1969; Holroyd and Bhattacharyya, Bhattacharyya, Nutbourne, 1973; Adams, 1974) or drawing them on a plotter (in colours or patterns, labelling, and shading of polygons) is a common problem in computer applications to draughting. This often requires computer programs to have in sequence all line segments making up each line and has already "contour-following" algorithms. been achieved for programs that use However, program development is often much simpler if all contour segments Such a program is then faced for each grid cell are computed together. with the task of sorting the segments into line sequences. A simple but very inefficient method is to match coordinates against all others until a match is found (e.g., program CMPP2, Yamamoto and Nishiwaki, 1976). is not only computationally slow, but requires a very large amount of memory if there are many line segments (e.g. hundreds or thousands). An alternative method for sorting line segments was developed and is described below.

THE TECHNIQUE

The technique is based on a method whereby, for each contour level, the segments are first sorted into a set of line sequences such that the end of each sequence increases in positive X value with each segment added, and then the end points of each sequence are matched with each other to find how they are connected. Multi-valued X values do not pose a problem as each value will have its own sequence of segments (e.g. see Fig. J.3). Neither do crossed contours (e.g. in "caves" and overturned surfaces, Morse, 1969) and contours that meet (saddles) pose problems, as only two sequences are ever matched together. Therefore three sequences meeting at a point are considered as one closed and one open pair of contours, and four sequences meeting at a point are considered as two contours (Fig. J.4).

The algorithm uses an extremely efficient Cyberl73 system SORT program (Control Data Corporation, 1977) to first sequence segments into a known position, and then to use a method of indirect addressing (e.g. Pro-Log Corporation, 1979) to keep control on the locations of segments that are consecutive in line sequences. This makes it unnecessary to continually shunt coordinates about in memory. As the SORT program can operate on data

files, only those coordinates that belong to one contour level need be stored in memory at any one time. Furthermore, as sorting is primarily based on contour level values, the sorted data file need be read sequentially once only.

This algorithm is described in three parts: sorting, sequencing, and plotting.

Sorting

The aim is to have all line segments residing on one data file in an order such that all segments for each contour level are in a contiguous block; and within each block the segments are ordered in a way that allows rapid determination of the situation of each segment's coordinates with regard to all others.

A data file to be sorted is generated by writing all data for each segment as one file record. This includes line number (e.g., contour value), and the two end-point coordinates. The file is then sorted into ascending order by the three keys (in decreasing importance): 1) line number, 2) end-point with smaller X coordinate value, 3) end-point with smaller Y coordinate value.

Sequencing

Four arrays are required to sequence a line: 1) for storing each segment as it is read from file (Array IV, Fig. J.3), 2) a vector (Array LAR) whose consecutive elements contain the locations in (1) of segments that are consecutive in a line sequence, 3) a vector (Array LPOS) to record the location in (2) of the starting element for each sequence, and 4) a vector (Array LJOIN) to record which sequences are combined together.

As each segment is read from the file, it is first checked to see if it is identical to the previously read segment, within a predetermined tolerance. (For instance, it may be pointless in considering a segment whose end-points only differ by a thousandth of a centimetre from a previous one if the plotting medium is only accurate to one hundredth of a centimetre.) If unique, it is stored in the next available position in The coordinate of key (2) is then matched against the last coordinate of each existing line sequence until one is found. If one is found, then the location of this segment is inserted into the appropriate position in (2). Values in (3) are then updated to record the shift in location of the Insertions are made in (2) by shifting all higher sequences in (2). The procedure is continued until positioned elements up by one element. all segments for one contour level are processed. Finally, all starting coordinates for each sequence are compared with one another, and all

matches recorded. The same is done for finishing coordinates.

Plotting

Lines can now be plotted in any form desired. Firstly, all openended sequences (i.e. those terminating at the boundary of the plot) are plotted. As each sequence is plotted its record is cancelled from (4). All remaining records are closed loops, and plotting of these may start in any sequence.

THE ALGORITHM

The algorithm written for this thesis (program DRAWER) follows closely the method outlined above, but there are slight departures due to the way in which it was coded. These do not affect the method.

Sorting

The algorithm was developed for drawing contour lines on a stereonet with a maximum diameter of 20cm, on a plotter with a resolution of .01 inches. This meant that all possible coordinate values could be comfortably mapped into a 13 bit byte. As only five contour levels are computed only 3 bits are required to store the contour level. Consequently, the contour level and all segment coordinates could be packed into a single 60 bit computer word (Fig. J.la). Hence, each (binary) file record consisted of a single word. The SORT program could then sort the records using only one key, i.e. the full record.

Sequencing

Each unique record, as it is read, is stored in a vector (Array IV, as shown in Figs. J.1b and J.3). End-point coordinates are matched by using Boolean algebra and SHIFTing functions (Control Data Corporation, 1978) to compare values stored in different portions of computer words. Whilst checking for the continuation of a line sequence (Fig. J.2b), the algorithm also checked for sequence terminations (Fig. J.2c), described in (4) above. Data in vector (4) (Array LJOIN) are also packed (Fig. J.1c). When all records for a contour level are read, all starting coordinates are checked and matching sequence numbers (i.e. Fig. J.2a) recorded (Fig. J.1c).

Plotting

Once this has been done, the program then extracts one complete contour line at a time and stores it in an array (Array JVC, Figs. J.ld and J.3), ready for plotting or further processing.

EXAMPLE

An example of a simple closed loop is shown in Fig. J.3 in order to demonstrate the roles of files and arrays in sorting, sequencing, and plotting.

DISCUSSION

A number of features of the algorithm appear to flout the simpler and more usual program writing techniques and styles (Kernigham and Plauger, 1978).

- (1) The generally complicated nature of sorting and sequencing using indirect addressing is quite confusing and tends to look inefficient compared to the elegantly simple algorithms that were mentioned earlier. However, an indirect addressing technique is in fact essential for computers to function at all at the ASSEMBLY and machine code programming language levels. Higher-level programming languages, such as FORTRAN, ALGOL and BASIC, afford programmers the luxury of avoiding the confusing addressing method, but they do have their place in programming techniques, as is found here.
- (2) Much of the apparent complication in the actual program coding is due to the packing of several items of information into one computer word. Hence, every time one of these items are required, it must be extracted by a combination of Boolean algebra and SHIFT functions. This complication has no real effect on the speed of the computations as Boolean algebra and SHIFT functions are among the simplest of computer operations and form the basic ingredients for almost all other operations. Hence, the complication is only apparent to the inexperienced programmer. On the other hand, the saving in memory space is substantial (halved).
- (3) The use of packing information tends to make the algorithm machine-dependent. (There are not many machines that use 60bit words.) This means that it has to be modified for each new machine. Packing is also based on each coordinate axis value having a resolution not greater than 1 in 2¹³. This also means rewriting is necessary if the requirements of resolution change.
- (4) The saving in memory means that the program will generally have a higher priority in a multi-user queue, and can thus be used interactively, where speed and high turn-around times are essential.
- (5) In applications to three different programs (modified wherever necessary, (3) above), the algorithm has shown itself to be very fast (several times the speed of that technique commonly used by such programs as CMPP2), and easily adaptable to various plotting requirements (from coloured lines and dot-dash patterns, to labelling and polygon shading).

APPENDIX K

TYPE I TREND SURFACE ANALYSIS PROGRAM PACKAGE

Introduction

Three programs of a program package for conducting Type I trend surface analyses (Chap. 2) were obtained from Yamamoto and Nishiwaki (1976), along with their test data. These programs read sets of orientation data (with their locations) and produced trend surfaces that were facsimiles of original geological surfaces (strata, layers, or bedding). (Program SLINE converts irregularly spaced orientation data into regularly gridded gradient data, as well as optionally producing structure maps (e.g. Fig. K.1), strike-line and isocline maps; program RECON fits surfaces to regularly gridded gradient data; and program CMPP2 produces pen plotted contour maps of the surfaces). Modifications and corrections that had to be made to the programs beyond those necessitated by the differences in machinery are described below. Generally, the programs required very large amounts of CM and CP time, due to some very inefficient algorithms. The versions developed here require a fraction of that used by the originals, whilst extending the capabilities of the programs.

Modifications and Corrections to Program SLINE

The program as supplied was not only inefficient in memory and CP time but was also missing functions that were described in their 1976 paper (e.g. the ability to produce strike/dip structure maps, Fig. K.1). Routines were written to correct these shortcomings.

 $175\mathrm{K}_{8}$ words of CM and approximately 20 to 30 minutes of CP time was required to run the original program. Two sections of the program were found to be causing the time problem.

- 1) When finding the "best-fit" gradient to all (gradient) data points inside a grid cell, the routine checked every point to see if it was inside the cell or not. The algorithm was modified by presorting data before processing it (program PRES, see below). Not only did this procedure eliminate the time-consuming testing algorithm (which can be on the order of several million FORTRAN statements for large data sets), but it had the added advantage of greatly reducing the plotting times for structure maps, as the symbols are plotted in an orderly fashion rather than at random.
- 2) The program called a general purpose polygon-fill routine to shade the cells when producing strike-line maps. Such a subroutine is very inefficient when a simple polygon such as a rectangle is to be shaded. By replacing the general subroutine with a specific one (subroutine)

SSHADE, not described in this thesis) the CP time was greatly reduced (by 10 to 15 minutes).

CM was markedly reduced by making use of binary files created by program PRES. (Program PRES sorts (using a system SORT program, Control Data Corporation, 1977) all orientation data locations according to their associated grid cell, and writes them onto binary files with each binary record consisting of all data for each grid cell. Reference, or geographic, data are written as one or more lines and one or more points per record.) Therefore instead of storing all data, and their derivatives, in CM (which restricted the maximum possible size of a data set), only the data for one cell is ever stored in CM at any time. Although this increases input/output (I/O) time the program can process extremely large data sets (tens of thousands of points) in the reduced space of 110K₈ words, whereas the original program processed a maximum of 2000 data points in 175K₈ words, and took 30 times as long.

The original program also contained programming errors. In subroutine NORVCT the statement: "DO 280 I = 1, NUNITY" should be "DO 280 I = 1, NUNITX".

Modification to Program RECON

MRECON. CM requirements for the program were related to the square of the size of the grid (number of grid cells squared). The program would not fit into allowable memory because of this, so the largest grid size was reduced by two-thirds. However, large grids can be processed by dividing them into smaller ones (with overlap). Each small grid is individually processed and printed (Fig. K.2), but is adjusted to conform to those already processed.

Modifications and Corrections to Program CMPP2

The program listing contained both inefficient algorithms and programming errors, and the latter made the program unworkable. CMPP2 contours data values at the nodes of a regular grid (or of a pre-defined network of triangular cells) by computing and drawing all contour levels in each triangle stored in memory (where cells of a regular grid are divided into triangles).

Storing all triangle definitions (i.e. the three nodes defining each triangle) simultaneously in CM is inefficient, and limits the maximum allowable size of the data set. Instead, triangles can be individually processed (with some increase in the I/O time for pre-defined networks). For regular grids there is no necessity to store their triangle definitions.

As this makes the contouring section of the program dependent on the source of the triangles, CMPP2 was separated into two programs: CMPPI for

irregular data (i.e. pre-defined networks of triangles); and CMPPR for regular grids. An alternative to CMPPI was already available (Appendix M) and so CMPPI is not considered further. CMPPR is more efficient in terms of memory usage as only one cell is ever divided into triangles at any one time.

Program CMPP2 contained two errors that had to be corrected. divided each cell into two triangles by inserting a NE/SW diagonal. Firstly, only one of the two triangles was saved. Hence, half the grid was Secondly, this method introduced a definite, not considered. fictitious, NE/SW structure trend. As the test data used by Yamamoto and Nishiwaki has a real NE/SW trend, this error was not detected in their Their method also fails to recognise such geometries as saddle points (see Fig. K.3b). Other contour programs (e.g. Starkey 1977; personal communication) employ a method of dividing grid cells into triangles using only one diagonal, but they alternate the diagonal used between consecutive cells (Fig. K.3c). This is suitable only if the grids are so fine that saddle points are never contained in a single cell. CMPPR uses both diagonals to divide each cell into four triangles, with the centre value being the average of the four corner values (Fig. K.3d). Hence saddles are recognizable, irrespective of the coarseness of the grid.

Subroutine VPRINT (in program CMPP2) employs an inefficient technique of sorting line segments for labelling contours. CMPPR uses the sort-and-draw routine, DRAWER (Appendix J) to allow smooth contour lines to be drawn and labelled (Fig. K.4).

Discussion

With modern trends in computer architecture, some of the limitations of the programs caused by memory size become redundant. For example, virtual memory would allow grids of any size to be processed.

The division of a grid into a number of smaller grids for processing by program MRECON introduces the possibility that dislocations may occur (Chap. 1) because independent paths are followed to the same point. In most practical applications of this program package, the discrepancies would be quite small, and so an average value is used at subgrid boundaries as a first approximation.

The trend surface analysis program package described by Yamamoto and Nishiwaki (op. cit.) was found to be unnecessarily expensive to use and limited in its application. The modifications and corrections described above have rendered them cheaper and more accurate to use. The package is limited by the problems outlined in Chap. 1, although it is possible to take steps to overcome some of these (e.g. overturned data).

APPENDIX L

ALGORITHMS FOR SPHERICAL PROJECTIONS OF ORIENTATION DATA

Although many stereographic, and other spherical, projection programs exist (both published and unpublished), they are generally rigid in data format and/or inefficient in their algorithms and coding. This is an important point when attempting to program small computers or desk-top calculators. A number of algorithms are developed here that are computationally superior, although perhaps not as mathematically elegant.

A number of variables are defined in Fig. L.1. A plane has dip direction, DD, with a dip of D, a strike of S (two possible values, anticlockwise from DD, Sa, and clockwise from DD, Sc). Vectors (lineations, poles to planes) have trends, T, and plunges, P. They may alternatively be measured as angles of pitch, PCH. The four quadrants of the compass, Q, (Table B.6) are used, although other methods of defining rotational relationships between trends or general trend directions are possible.

All angles are in degrees.

A. Pole to plane

Given DD/D, the pole, T_p/P_p can be found by:

$$T_{p} = DD + 180 .$$

$$P_{D} = 90 - D$$
.

B. Pole to plane

Given S/D and Q:

1. Find the larger value of S: If S 180 then
$$S = S + 180$$
. (L.1)

- If S is southerly then go to step 4;
- 3. northerly:

if DD westerly (Q=3 or 4) then
$$T_p = S - 090$$
; (L.2)

else easterly (Q=1 or 2) then
$$T_p = S - 270$$
. (L.3)

Go to step 5.

4. southerly:

if DD southerly (Q=2 or 3) then
$$T_p = S + 090$$
; (L.4)

else northerly (Q=1 or 4) then
$$T_p = S - 090$$
. (L.5)

5.
$$P = 90 - D$$
. (L.6)

The remaining algorithms require the use of the spherical trigonometry equations (after Selby, 1971):

$$sin B = tan(90-D) \cdot tan P$$

$$= \frac{\tan P}{\tan D}$$
 (L.7)

$$\sin P = \cos(90-PCH) \cdot \cos(90-D)$$

= $\sin PCH \cdot \sin D$ (L.8)

C. Intersection of two planes

This requires the use of a more general algorithm which fits a plane to two lineations, T_1/P_1 and T_2/P_2 . This method has not previously been used, probably because it is more involved to derive a solution than the simple method of cross-products (Mase, 1970). Both methods are given here for comparison. The fitting of a plane to two lineations is preferred as the final solution is computationally simpler and twice as fast.

Using the method of cross-products.

Given two planes, DD_1/D_1 and DD_2/D_2 , find intersection, T'/P'.

- Find poles to planes T_1/P_1 and T_2/P_2 .
- Find vector representation, [1,m,n], (direction cosines) of 2. the poles:

$$1 = \cos P \cdot \cos T$$

$$m = \cos P \cdot \sin T$$

$$n = \sin P$$
(L.9)

If we represent the two vectors by \underline{a} and \underline{b} , and the desired intersection by c, then:

$$\underline{\mathbf{c}} = \underline{\mathbf{a}} \times \underline{\mathbf{b}} \quad (L.10)$$

which is computed by:

$$T' = \tan^{-1} \left\{ -\frac{1_2 \cdot n_1 - 1_1 \cdot n_2}{m_2 \cdot n_1 - m_1 \cdot n_2} \right\} , \qquad (L.11)$$

and

$$P' = \tan^{-1} \left\{ - \frac{1_1 \cdot \cos T' + m_1 \cdot \sin T'}{n_1} \right\} . \quad (L.12)$$

This requires 5 sines, 7 cosines, 2 arc-tangents, 10 multiplications, and 2 divisions.

Using the method of finding the pole to a plane fitted to the poles of two intersecting planes:

- Find the poles as before. 1.
- To find T'/P' we first need to find the plane DD'/D' (the plane to the pole T'/P'). We therefore need to find either B₁ or B₂.

Consider the ratio:
$$\frac{\sin \theta_2}{\sin \theta_1} = k \text{ (a constant)} \cdot \text{ (L.13)}$$

If we assign
$$\beta_1 \leq \beta_2$$
 then $k \geqslant 1$.
Let $\beta_s = \beta_1 + \beta_2$, (L.14)

$$\frac{\sin (\beta_s - \beta_1)}{\sin \beta_1} = k .$$

Expanding:
$$k = \frac{\sin \alpha_{s} \cos \alpha_{1} - \sin \alpha_{1} \cos \alpha_{s}}{\sin \alpha_{1}}$$

$$= \frac{\sin \alpha_{s}}{\tan \alpha_{1}} - \cos \alpha_{s} .$$

Therefore:
$$\beta_1 = \tan^{-1} \left\{ \frac{\sin \beta_s}{k + \cos \beta_s} \right\}$$
 (L.15)

To find k we can use (L.7) and remove the unknown value D'.

As
$$\sin B_2 = \frac{\tan P_2}{\tan D}, \qquad (L.16)$$

and
$$\sin \beta_1 = \frac{\tan P_1}{\tan D^*}$$
 (L.17)

dividing (L.16) by (L.17) we obtain (L.13):

$$k = \frac{\sin B_2}{\sin B_1} = \frac{\tan P_2}{\tan P_1} \qquad (L.18)$$

The second value to find is \mathfrak{B}_{s} , which can be derived from \mathbf{T}_{1} and \mathbf{T}_{2} by:

$$\Delta T = | T_1 - T_2 | ,$$
 (L.19)

and
$$B_{S} = |180 - \Delta T|$$
 (L.20)

As $k \geqslant 1$ and $0 \le B_s \le 180$, then $0 \le B_1 \le 90$.

3. Compute DD' and D'.

If T_1 is clockwise from DD', then:

$$DD' = T_1 + B_1 - 90$$
 , (L.21a)

if it is anticlockwise then:

$$DD' = T_1 + 90 - B_1$$
 (L.21b)

The direction is verified by also calculating DD' using the second vector (and incorporating (L.14)):

$$DD' = T_2 + A_s - A_1 - 90$$
, (L.21c)

provided 0 < DD' < 360 for all equations.

The dip is computed by rearranging (L.7):

$$D' = \tan^{-1} \left\{ \frac{\tan P_1}{\sin B_1} \right\} \qquad (L.22)$$

4. Compute T'/P' from DD'/D'.

In total this method requires: 2 sines, 1 cosine, 3 tangents, 2 arctangents, and 2 divisions.

As in all cases of programming, checks must be made for indefinite calculations (eg. dividing zero by zero) and division by zero. This has not been considered for the method of cross-products because it is not of interest. Three situations may arise in the second method:

- i) T =180. This leads to $P_1 = 0$.

 If $P_1 = P_2 = 0$ then D' is indefinite.

 If either P_1 or P_2 not zero then D' = 90.
- ii) $P_1 = P_2 = 0$ and $\Delta T \neq 180$, then D' = 0 and DD' is indefinite.
- iii) P_1 = 0 only. This leads to B_1 = 0 . If (i) and (ii) are not valid then D' can be computed by substituting B_s (= B_2) and P_2 in (L.22).

D. Convert pitch to plunge

Given pitch, PCH, measured from strike, S, of the plane, DD/D, containing it, find trend and plunge, T/P, of the lineation.

Plunge is determined from equation (L.8):

$$P = \sin^{-1} (\sin PCH \cdot \sin D) \qquad (L.23)$$

We can find T by first computing B, using equation (L.7):

$$B = \sin^{-1}\left\{\frac{\tan P}{\tan D}\right\} ; \qquad (L.24)$$

and
$$T = S + B$$
 (L. 25)

-B is used if S is clockwise from DD (Sc), and +B if S is anticlockwise (Sa). Q can be used to solve the direction (with algorithm B) instead of S.

E. Find trend of lineation

Given plunge, P, of lineation nearest strike, S, lying in plane, DD/D, determine the trend, T.

This is solved by using (L.24) and (L.25) above.

F. Find plunge of lineation

Given a trend, T, of a lineation lying in a plane, DD/D, find the plunge, P.

1. First find B.

Let
$$\Delta T = |DD - T|$$
, where $\Delta T \le 90$, (L.26)
then $B = |90 - \Delta T|$.

(If $\Delta T > 90$ then regard the lineation as being in the upper hemisphere, and so find the lower hemisphere equivalent.)

2. Plunge is found by rearranging (L.7):

$$P = \tan^{-1} (\sin \beta \cdot \tan D) \cdot (L.28)$$

G. Other equations

All other algorithms used in the program consist of standard equations Produced here are equations for the three found in text books. stereographic projections available (see Appendix A of Hobbs et al, 1976).

1. Wulff net:
$$d = R \tan \frac{90 - P}{2}$$
; (L.29)

2. Lambert:
$$d = R\sqrt{2} \sin \frac{90 - P}{2}$$
; (L.30)
(Schmidt net)

where d is the distance from the centre of the net to the projected point, R is the radius of the sphere, and P is the plunge of the point.

APPENDIX M

AUTOMATIC CONTOURING OF IRREGULARLY DISTRIBUTED DATA

The sequence for producing a contoured map by automated means, program TRICON, is shown in Fig. M.1. First a map is defined (Appendix D), which is then tessellated (Appendix D) with Thiessen polygons (Rhynsburger, 1973) and a list of neighbours for each data point is found. The map is triangulated (using the list of neighbours) with data points forming the vertices of the triangles (Fig. M.2). The triangles are then contoured in a method similar to that described by Harbaugh and Merriam (1968) and Yamamoto and Nishiwaki (1975), among others. The contours are finally processed by a version of a sort-and-draw routine, program DRAWER (Appendix J), with an accuracy of 1 in 2²¹, instead of 1 in 2¹³.

The triangulation and contouring of data provides a fast and versatile trend surface analysis program that is simpler to use than the CMPP2 of Yamamoto and Nishiwaki (1975, 1976), as input data need only consist of station coordinates and their readings, and triangulation is done by computer. Although triangulation by automated means may not be the best (Crain, 1978) it is generally suitable for the level of accuracy required.

A recent publication of a program description to perform a similar function, program ACORD, is described by Watson (1982). His program has a similar performance to TRICON except on two points. The triangulation algorithm is more efficient than the method used by TRICON as it uses a different procedure, and may subsequently derive a different set of triangles for the same data set. Program ACORD does not have independent techniques for sorting and drawing contours (Appendix J) which is very useful for versatile line plotting.

APPENDIX N

SOME STRUCTURAL ASPECTS OF THE LINCOLN COMPLEX FROM TUMBY BAY TO PORT NEILL

A paper presented at the Symposium on The Gawler Craton

Organised by the Geological Society of Australia Inc.
South Australian Division

Adelaide, December 1979

Some structural aspects of the Lincoln Complex from Tumby Bay to Port Neill

P. Cohen & P. R. James

Department of Geology & Mineralogy, University of Adelaide.

A well exposed coastal section of the Lincoln Complex extends in a north-northeasterly direction from Tumby Bay to Port Neill. This section cuts obliquely across the regional northeast structural trend and displays a complex morphology, geometry and history. The Lincoln Complex is an interlayered sequence of granitic gneisses and minor amphibolites. Four periods of deformation are recognized, D₁, a fabric-forming deformation producing few folds, formed well developed fabrics of varying style (S \rightarrow SL \rightarrow L) and intensity. The foliation (S1) is always parallel to the gneiss/amphibolite contacts. D2 does not appear to have been an intense deformation in this area, though D2 folds are recognised in interference structures. D₃ was a major fold-forming event of variable strain intensity and orientation. Structures formed during D3 control the regional northeast trend. Dia, the mylonite-forming event, appears to have been associated with D3 - mylonite zones are regionally parallel to D3 structures. D4 was a weak event that is recognised by kink folds and crenulations. The regional structure can be separated into three zones of differing D3 deformational style. The Lipson Cove transition zone (Zone 2), which is an area of very complex strain variation and fold style, separates a southern zone (Zone 1) extending to Tumby Bay, from a northern zone (Zone 3) extending to Port Neill. In Zone 1, D₃ produced asymmetric, steep northerly plunging folds in S₁, and local proto-mylonites. In Zone 3 D₃ folds plunge shallowly to the northeast and southwest, with less intensely deformed S₁ fabrics than Zone 1. Strain intensity increases towards the north and a mylonite zone forms the northern boundary at Port Neill. D₁ and D₂ folds and complex interference folds are recognized in Zone 2.

Appendix O

GEOLOGY OF THE TUMBY BAY TO PORT NEILL REGION

Overview

A cursory examination is made of the geology from Tumby Bay to the last outcrop north of the Dutton River, and the key localities marked (Fig. O.1), to obtain general information on the structural geology in which the area of Lipson Cove is contained. An important locality, W, at Waterfall Creek (also known as Mine Creek) a few kilometres west of Tumby bay is also examined. Clarke (1976) has described aspects of the structures from Cape Hardy northwards. Geophysical and digital terrain models (DTM) of the area are presented in Appendix P. The aeromagnetics of southeast Eyre Peninsula are of general interest because it is an iron-rich province, and may be very useful in interpreting the geology.

A constant northeast-southwest trending foliation is the only structure that appears on aerial photographs both to the south and north of Lipson Cove. Ground reconnaissance revealed apparently fewer, smaller and simpler structures (folds), which usually did not show interference effects. The strains appear to be as strong to the south of Lipson Cove as in the mapped area. To the north (north of locality D), and south of Port Neill, the strains appear considerably lower, except where subsidiary shear zones occur (e.g. locality F). The mylonite zone crosses the coast north of Port Neill (locality I), and high strains related to this zone can be seen along the coast to the extreme northeast (Appendix N).

South of Lipson Cove

The geology is described with respect to a southward traverse.

Lipson Island consists of massive and layered granitic gneisses and amphibolites. No significant folds or complex interference effects occur. Thin iron-rich veins can be found, which are two or three centimetres wide and low- to non-magnetic, consisting mainly of hematite and limonite. The veins contain up to 90% of the iron minerals, which are fine-grained.

On the coast (locality B_1) the amphibolites and granitic gneisses have been heavily altered, with epidote and limonite appearing. Alteration has generally masked the structures and partially destroyed the foliation. The rare occurrences of boudinage are found here (Fig. 0.2a). Narrow veins of malachite and minor azurite are associated with iron-rich veins as described above.

A beach at the south end of the alteration zone separates this zone from the rest of the geology to the south (locality \mathbf{B}_0), which is

characterised by a strong L to SL fabric in fresh, generally pink granitic augen gneisses (Fig. 0.2b). The augen are uniformly prolate and plunge steeply $(60^{\circ}-70^{\circ})$ to the northeast. The outcrop to the south consists totally of this rock type until it nears the extreme southerly exposures (locality A), where the geology appears remarkably similar to that observed in the north end of submap M13 (locality C_1 , and Chap. 7), except that the folds have a dextral asymmetry.

Lipson Cove to Port Neill

At the northern end of Rodger's Beach (see Geology Sheet 1), the rocks are similar to those of submap M13. The folds are predominantly horizontal, generally with double plunges. Between this headland and a pronounced fault (locality D, Fig. O.1) the wavecut platforms show no fold structures and the headland near the fault is strongly altered.

A variety of rock types occur between the fault and Cape Hardy. Some are augen gneisses, with augen generally oblate (Fig. 0.3a) in a mafic (biotite + hornblende) assemblage, and some appear to be metasediments. Folds are small and are not common. They have variable plunges, from shallow to steep, characterised by an elongation lineation (Fig. 0.3b) plunging in either a northeast or southwest direction. Relatively undeformed amphibolites occur, some folded and some boudinaged (Figs. 0.3c and 0.4). The amphibolites vary in appearance from homogenous grey to black <u>+</u> megacrystic feldspars. Clarke (op. cit.) described the amphibolites as only being boudinaged in a horizontal direction, with vertical effects being rare. However, all amphibolites examined that were horizontally boudinaged also showed some vertical effects of boudinage (e.g. Fig. 0.4c).

At Cape Hardy (locality E) the predominant rock type is a massive megacrystic granite gneiss showing quite low strains (Fig. 0.5b), which could alternatively be described as a megacrystic gneissic granite. A small outcrop approximately 100 metres in size of relatively undeformed megacrystic granite occurs here (Fig. 0.5a), surrounded by more intensely strained rocks at its boundaries. Some amphibolites are interlayered with the gneisses.

The dominant foliation at Cape Hardy is more reclined than those occurring elsewhere.

The strains increase rapidly north of Cape Hardy, with the regional foliation becoming increasingly intense and upright. The mesoscopic folds (e.g. Fig. 0.6) are tight to isoclinal, generally upright with shallow to moderate plunges, and become more horizontal to the north (Pt. Neill). An intense $S_{\rm m}$ fabric (Fig. 0.5c) forms in the granitic

gneisses at locality F.

Boudins are commonly found in the Lincoln Complex north of Cape Hardy.

North of Port Neill - The Mylonite Zone

The Kalinjala mylonite zone crosses the coast at locality I. A shear zone occurs at locality H, where the gneisses end and granulites and tectonites begin. Amphibolites at locality H have been tightly folded and boudinaged.

A slaty mylonite occurs at locality I, marking the centre of the mylonite zone, where quite coarse materials can also be found. The mylonite fabric (Fig. 0.7a) has rotated itself (Fig. 0.7b) in places.

North of the Dutton River (0.5 km north of locality I) the tectonite fabrics (Fig. 0.7c,d) demonstrate features of boudinage (mainly rhombic with some 'pinch-and-swell') and fabric rotation, as well as D_4 crenulations.

Waterfall (Mine) Creek

This locality occurs seven kilometres WNW of Tumby Bay (locality W on Fig. 0.1). Both the Hutchison Group and the Lincoln Gneisses are exposed here, although the contact itself is not. The units of the Lincoln Complex are similar to those described elsewhere (Coin, 1976; and §6.3), and also include layered gneisses. The amphibolites appear younger (syn-orogenic), similar to those occurring north of Lipson Cove. The augen gneisses affected by the mylonite zone (Fig. 0.8a) appear morphologically different to those that were unaffected. (Although they appear similar to Fig. 7.20a, the latter has not developed the $S_{\rm m}$ fabric.) The structures revealed in the Lincoln Complex east of the mylonite zone appear simple because of the strong mylonite overprinting, but away from the mylonite zone upright D_3 folds and reclined D_2 folds occur (Figs. 0.8b,c), similar to those described by Parker (1978).

APPENDIX P

A GEOPHYSICAL STUDY OF THE TUMBY BAY TO PORT NEILL REGION

Introduction

In order to obtain an understanding of how the area of Lipson Cove (Chaps. 6 and 7) fits in with the regional geology, both as an aid to understanding the geology of Lipson Cove and to enable an integration of this study with other studies made in the Gawler Craton (see Fig. 6.1), geophysical (aeromagnetic and gravity) and topographic data (DTM - Digital Terrain Model, see for examples Moore and Simpson (1982) and Harrington et al (1982)) are collated and interpreted where possible, and compared to field observations. Key localities refer to those marked on Fig. 0.1, and the geology for the region is presented in Appendix O.

Aeromagnetic Interpretations

Overview

A low-level (average height of 80 metres) aeromagnetic survey was conducted in 1976 for Broken Hill Prop. Ltd. (B.H.P.) over the coast from Tumby Bay to Cowell. Stacked profiles (Fig. P.1), produced by B.H.P., of the southern portion (Fig. 6.1) were compiled to portray the aeromagnetic topographical surface. Two particular aspects of the magnetic topography are of interest in the interpretation of features of the structural geology; magnetic ridges (or highs) and magnetic valleys (or lows)*. They occur on and to the east of the Kalinjala mylonite zone, which is the dominant curvilinear magnetic high shown extending the length of Fig. P.1. The Kalinjala mylonite zone separates the Hutchison Group from the Lincoln Complex in this part of southeast Eyre Peninsula.

Magnetic Ridges

A number of parallel ridges trend in a northeast-southwest direction. The dominant ridge is associated with the Kalinjala mylonite zone but is not coincident with it. (The magnetic ridge is approximately one hundred metres to the west of the mylonite zone. Such discrepancies have also been described for mylonite zones elsewhere - D. Boyd, personal

^{*} The terms "ridges" and "valleys" are used because the highs and lows have these topographical forms on the magnetic topographical surface (Fig. P.1). By treating aeromagnetic survey values as being the "height" values of a topographical surface, it is made homologous to a trend surface. Thus the two surfaces are compatible and can be integrated for combined analyses (see §8.4).

communication.) The mylonite zone, although regarded as vertical (e.g. by Coin, 1976), is interpreted by computer interpretation of magnetic profiles (e.g. Fig. P.2), using a computer program developed by Ukaigwe (personal communication) to have a hade of 20° to the northwest and centred 65 metres east of the magnetic ridge centre. The hade is rather large and the interpreted value would be lessened considerably if the program took into account remanent magnetism (which is unknown). The effective width, i.e. the width contributing to the magnetic signature, is interpreted to be approximately 253m, with oxidation to a depth of 258m. The proposal of a northwest hade is supported by rotation fabrics such as those found at locality J (no figure available but similar to Fig. 0.7b).

Two other shear zones have been inspected (localities F and H). The ridge at locality F can be matched to the rock type (Fig. 0.5c). The ridge at locality H is very weak and this corresponds to a rock type of very low mafic content (Fig. 0.7b), even though the intensity of the strains at the latter location is greater than that at the former. The other ridges are not associated with outcrops.

In the southern portion of the magnetic topography, the minor parallel ridges disappear, leaving two dominant ridges that converge towards each other before becoming parallel. Although the fabrics in the easterly ridge approach protomylonite with associated intense strains (Cohen and James, 1980), the major cause of the magnetic ridge is the high magnetite content of the rocks along the coast. A major difference between the two ridges is the cause of the magnetic highs. In the northern shear zones, the higher magnetite content was probably caused by an influx of magnetic material, which occurred during D_3 (Table 6.1), as well as some retrograde alteration releasing magnetite from mafic minerals; whereas in the ridge from Tumby Bay to locality C_{Ω} , much of the magnetite has been derived from amphibolite facies retrogressive metamorphism (Table 6.1). (One example of magnetic influx is the anomalous magnetite grains discussed in §6.3.4. These are interpreted as having once been a system of very thin "stringy" magnetite-rich veins.) Marked variations in the magnetic values over short distances in the vicinity of locality B are caused by oxidation and alteration of magnetite to hematite and limonite (which have much weaker magnetic properties (see Nettleton, 1971)).

A small ridge trending northwest-southeast between the two dominant ridges provides evidence of a granitic intrusion (see Fig. 0.1) that carried magnetic material. It was probably the same event that supplied magnetic material to the eastern ridge. There is a drop in magnetic intensity where the intrusion intersects the mylonite zone, suggesting that the associated fluids have removed or altered much of the

magnetic material. It is not knwon whether the mylonite zone was a source of magnetic material for the intrusion. This ridge coincides with a small gravity low (Fig. 0.1), which suggests an intrusion of lower density rocks, such as very silicous minerals. As the country rock is predominantly granitic gneiss with some interlayered amphibolites, the intrusion must be fairly significant to enable the small change in densities to be recorded. (It is possible that the one gravity data point measurement which indicates a gravity low is in error. The original data are no longer available for verification (Dept. of Mines and Energy, personal communication).) Further evidence for the intrusion is provided by the large amount of silicous, simple (quartz and feldspar) veining in the vicinity of the area extending from locality A to locality B, which may in places contain minerals uncommon to the area (Fig. 0.2c). These veins become simple, with minimal amounts of limonite, towards locality C.

Magnetic Valleys

Lines of magnetic lows are interpretable as faults (Nettleton, 1971; Telford et al, 1976; Parasnis, 1979). Three faults can readily be detected between localities D and E, and there is a fourth near Port Neill (Fig. O.1). They all trend ENE-WSW. Coin (op. cit.) has described one of these faults (see Fig. O.1) which has quartz veining associated with it. The faults appear to post-date the Kimban Orogeny, whereas the large dextral warp in the aeromagnetics between the townships of Tumby and Lipson (described by Coin (op. cit.) as a Wartaken (D₄) event) can be inferred to represent a strike-slip fault (Thomson, 1980), although the timing need not differ from that proposed by Coin (op. cit.).

Gravity Data

The most striking feature of the bouguer anomalies (Fig. 0.1) is the linear gradient that parallels the trend and approximate position of the mylonite zone. This trend is the alignment of two gradients, one to the south, and the other to the north, of locality B. The gradients differ in that the southern one increases westwards towards a positive anomaly, whereas the northern one increases eastward. The cause of the increase in anomaly from Tumby Bay to Port Neill is not known. Again, there are too few data to generate a reliable model. The data stations, on average, are spaced seven kilometres apart, giving results that are too general for specific interpretations.

Digital Terrain Model (DTM)

Topographic features (i.e. streams, valleys, and uplands) which

correlate with the geophysical anomalies described above can be located, but equally-developed features may not be associated with any anomaly. Those topographic lineaments that appear to be related to structures that have been observed, or are inferred to exist, are also noted (Fig. 0.1). Of interest here are those occurring south of locality D.

A small structure has been located between localities D and C_1 , from aerial photographs. Its significance is tenuous, but it is of interest because the structures on either side of it vary. The south side is represented by submap M13 (Fig. 6.2, Sheet 1) and the north side is described in Appendix O. The northernmost outcrop shown on submap M13 is a massive simple pegmatite/granite vein. The fold structures shown in submap M13 are predominantly F_3 folds plunging steeply to the southwest (Chap. 7). The dominant folds in the next outcrop to the north are generally horizontal.

A second feature is noticeable between localities ${\rm C_0}$ and ${\rm B_1}$. This feature separates the complex structures and asymmetric sinistral folds of Lipson Cove North from an upright foliation that has few folds, some boudins, and many thin iron-rich veins associated with country rock alteration.

Between localities B_1 and B_0 , a linear feature occurs that separates the altered and mineralised rocks (Appendix O) from a massive fresh granitic augen gneiss that has a strong L fabric plunging steeply to the northeast (Fig. 0.2b).

There are three well-defined lineaments trending SSE immediately south of locality A (Fig. 0.1). Not only do these (combined) lineaments coincide well with breaks in the mylonite zone magnetic signature, but they also mark the end of a line of hills that occur to the north. To the south are marshes. The last coastal outcrop occurs just south of locality A.

As the geology tends to change markedly across all these lineaments (which are expressed as streams, and end in beaches) they can be inferred to be faults.

Conclusions

The mylonite zone is associated with marked magnetic and gravity anomalies. An incipient mylonite zone was formed to the east, and is the easternmost shear zone noted (Fig. 0.1). The faults interpreted from the aeromagnetics and topographic lineaments all contributed to an upthrowing of the south side and the downthrowing of the north side (evidenced by the decrease in magnetic signature of the minor shear zones as they cross the three faults described earlier). Although there may also have been horizontal movement (such as in the fault through locality D) the sense and

displacement of any such movement have not been determined.

The upthrowing of the southern side of the faults (and hence from a deeper level in the crust) possibly explains why the general strains of the rocks are higher than those to the north (see Appendix N).

APPENDIX Q

POLYGON-FILL ROUTINES FOR DISPLAY ON COLOUR MONITORS

Introduction

Two situations were encountered for shading polygons (or polygon fill, Fig. Q.1). One was with a known internal point and the other without a known internal point. The latter can be converted to the former by a routine to compute such a point. For the purposes to which these polygon fill routines were applied, the two separate situations were kept separate (programs SUBMAP and SHADEMAP, Appendix R).

A number of restrictions apply to both routines. They must be fast and as small as possible. The speed requirement eliminates techniques that calculate the intersections of each shade line with the polygon boundary, irrespective of how efficiently the polygon is arranged in memory (Burton, 1977), particularly as the polygons in use may be very complex with a large number of sides (up to 200).

Both methods read the display memory to determine where the polygon boundaries are.

Polygon-Fill Without an Internal Point

A restriction on this routine is that there must be no other polygon contained within the rectangle that circumscribes the polygon to be filled, except for polygons that are to be left unshaded within the polygon. This can be avoided if the other polygons to be filled are done at the same time, and the circumscribing rectangle includes all of them. A second restriction is that the polygon must not have been already shaded (unless with the colour black).

The algorithm (Fig. Q.2) first clears the display (routine CLRECT, Appendix F) within the rectangle circumscribing the polygon and then draws the polygon boundary in two colours using routine DBND (Appendix F). Areas to be filled have their boundaries drawn clockwise, and (internal only) polygons to be left unfilled have their boundaries drawn anticlockwise. Each side of the polygon is coloured green if it is drawn in a zero or ty direction, and red if drawn in ty direction. As these polygons are only filled in blue, and the boundary is included, blue is added to the boundary. The rectangle is scanned from left to right starting at the bottom. When green is encountered polygon filling commences and when red is encountered the filling ceases.

Problems arise at vertices as all oblique lines are made up of short horizontal or vertical lines. All vertices consist of red and green, and if the internal angle at a vertex is small enough, a portion of the two

lines approaching the vertex will also contain both green and red. All problems arising from this complication can be overcome if the screen-pixel immediately prior to the complication is included in the considerations. If it was i) red, or ii) black and filling, then green prevails; if it was iii) green, or iv) black and not filling, then red prevails.

If the colouring for the polygon filling is not to be as simple as described, then the algorithm must be modified to a structure more like that of the second method (below), where all the end points of each shading line are found and stored and then the polygon is filled later.

Polygon-Fill With an Internal Point

The technique consists of two parts. The first part finds the end points of each shade line and stores them, and the second part fills the polygon using the stored coordinates.

Starting with a known internal point (x_i, y_i) the routine scans to the left (-x direction) until a boundary point (x_0, y_i) is found. then scans to the right to find the matching end point of this first shade The two x and one y values are stored (packed into two words). From (x_{o}, y_{i}) , the routine tracks around the boundary in a direction (Fig. Q.3c). It determines whether each boundary is on the left of a shade line (Fig. Q.3d). If it is, then its matching end point is found and the coordinates stored. If it determines the boundary to be on the right of a shade line (Fig. Q.3d), then the coordinate is checked with stored values to see whether the shade line was found before. every end point of shade lines is checked, when the tracking arives back at the starting point (x_0, y_i) it is possible to determine where internal polygons have obstructed the left-to-right shading. The shadows can then be appropriately filled by a similar procedure, except that the tracking of internal polygon boundaries is anticlockwise (but using Fig. Q.3a as now on the outside of polygon boundaries).

Open polygons (polygons that intersect display windows, which is usually the edge of the screen) are also accounted for in the tracking procedure.

Polygons can be coloured from the colour chart (Appendix X), which uses 3x3 bit colour-pixels. Polygon boundaries have only 1 bit and so colour-pixels can be split by the boundaries. For each shade line, the start, or left, coordinate must be located within the colour-pixel (as colour-pixels are always positioned relative to the screen origin), and the shade line then drawn accordingly.

The subroutine FLLA (Appendix F) uses about 600 ASSEMBLY instructions and uses red for the polygon boundaries.

APPENDIX R

DESCRIPTION AND USE OF STRUCTURAL DATA ANALYSIS PROGRAMS ON THE NOVA2

Once data files are created, they can be analysed by the sequence outlined in Appendix S. The programs described are some of those developed for the analysis of structural data on interactive computer graphics facilities. They are experimental and involve much developmental work in both applications and methodologies. Some of the more sophisticated techniques available for some functions are not used because the Nova has a prohibitively small memory (64K bytes). This restriction does not apply to more modern or larger computers, and so recommendations are suggested for the programs.

Types of Data Files

All programs use the same data files. The designing and coding of programs that interact with one another are thus simplified. This ensures that there is no unnecessary duplication of data, which is essential if the amount of disc space used is to be kept to a minimum.

For an initial geological source map there can be one, two, or three source data files, as follows:

- 1) Structural data (with geological description) and their coordinates;
- 2) reference (geographical, geological) data; and
- 3) tessellation outline coordinates (see Appendix S).

The files are referred to by their prefixes, "XY", "RF", and "PY" respectively. The XY file is essential, but the others are optional. These source files are in ASCII (card image) and contain all information (Figs. R.la,b). They are distinguished from other files by the file name extension ".DT". For increased speed of processing, binary versions of XY and PY files (Figs. R.lc,d) are used, and have the file name extension ".BN".

Subarea files (Figs. R.2a,b,c) are binary and have the file name extension ".BN". To minimise data duplication, the XY files contain pointers to data held in the source XY files, rather than data itself.

File Name Nomenclature

Two formulas were devised to standardise file names, one for source files and one for subarea files. They are:

source filenames = type\$key.DT and type\$key\$type.BN

subarea filename = type\$key\$lv.BN

where type refers to the type of data (XY, RF or PY); key is an identifier of source maps; and lv is a letter-digit label assigned (by the programs)

to subareas as they are created. There are three rules for generating <a href="https://linear.com/l

Data File Content and Format

"XY\$key.DT" files (Fig. R.la) contain all structure data and pertinent map information. All data (including the geological description) are stored as three and two digit numbers. Missing data are stored as "999,99". Orientation data can be stored as "trend,plunge", "dip direction, dip" or "strike,dip". Each data location is assigned a colour (for display purposes). Card image files are converted to binary images (Fig. R.lc) for actual usage.

"RF\$key\$.DT" files (Fig. R.lb) contain all reference (non-structural) data, consisting of each item's colour (Fig. R.6b, "COLOR" menu), symbol (Fig. R.6b, "SYMBOL" menu numbers 01 to 12), and name. Lines have a symbol of "00".

"PY\$key.DT" files (Fig. R.lb) are identical in structure to RF files but are used to contain S.O.D.A. plot boundaries (e.g. grain boundaries, map tessera). Card image files are converted to binary images (Fig. R.ld) for actual usage.

Creation of Data Files

Data files can be created either by the transfer of data from the Cyber (or from elsewhere), or by digitising maps on the data tablet. The former method has been used to process the thesis field data, and the latter has been used to generate test data.

Transfer from the Cyber. Program PLTMAPNOVA (Appendix D) can generate both XY-.DT and PY-.DT files. Program CYBER (Appendix A) was written to achieve the transfer.

Digitising on the Data Tablet. Any map to be digitised must be no greater than the data tablet (28cm x 28cm) as there is no program for concatenating maps. Program MAKEMAP (Fig. R.3) creates and extends data files.

Table R.1 contains digitising commands, other than for standard stylus control, written for program MAKEMAP. As the program has no facility for correcting errors, these must be corrected with a system editing program.

Lines are drawn in <u>rubberbanding mode</u> (Newman and Sproull, 1973). There are three main problems with direct digitising and storing of coordinates.

i) The tablet can generate as many as 64 coordinates per second with an accuracy of + .lmm in both the X and Y directions. This leads to very large and over-accurate data files. ii) Tilting of the stylus from vertical causes a shift in coordinates although the stylus point is not moved. This gives rise to knotted lines. iii) While coordinates are being stored in a buffer there is no loss of data, but as the program is suspended while the buffer is written to a disc file, any points digitised during this time are lost. To overcome these problems without resorting to lengthy line characterisation algorithms (see modification 5), it was simpler to incorporate the condition that no new point would be recognized unless the stylus had been raised from the tablet since the selection of the previous point.

PY files are created as RF files and then renamed.

Proposed Modifications

- 1) Editing structural data. As station locations do not have labels (in XY files at least), finding a station using a system editor can be difficult. The ideal way to edit a mistake would be to point the stylus at the offending station (on the display), and the program would then open the nearest station to the stylus coordinate by printing its data. The data can then be changed if necessary. Two extra options would be: i) the ability to move the station, and ii) the ability to delete the station. This latter would cause problems if subareas had already been created (with program SUBMAP below). Thus station deletion would consist of changing the colour to black and replacing all data by "no data". (A program could be used to "clean up" edited files (i.e. remove deleted records) and also to modify all subarea file pointers to correspond to the "cleaned" data file.)
- 2) Naming data stations. It would be beneficial to have a label for each station in XY files, as this makes for easier use of system editing and allows data stations on maps to be labelled.
- 3) Editing reference points. This process would be similar to (1), except that points could be deleted as subarea files make no reference to the source file. (However, subarea files would not be updated. This too could be overcome by writing a program for that purpose.)
- 4) Editing reference lines. Process (3) could be used to change the colour or name of a line, but to replace parts of a line further

programming is required. There are two possible ways: i) delete portions and redraw, and ii) hook the stylus onto the line, stretch it to a new position, and then pin it in place, repeatedly, until the new line is achieved. Other modifications would be the ability to extend or to (partially or wholly) delete a line.

- 5) Line characterisation. A point on a line within a certain distance of its previous point is rejected. This is a crude form of line characterisation (Douglas and Peucher, 1973) to keep the size of RF files to a minimum. However, it would be more correct if, after a line is drawn, a line characterisation routine is employed to remove unnecessary points.
- 6) Arc drawing is an alternative method to using a series of digitised points to draw curved reference lines (thus avoiding an unnecessarily large number of coordinates). Methods are described in the literature (Ch.4 of Rogers and Adams, 1976). This would require modifications to RF file structures to specify whether arcs or straight lines are to be drawn. Apart from keeping reference files small, arc drawing enables smooth arcs to be drawn at all scales.

Housekeeping Routines

Often it is necessary to modify data files by affine transformations as more information becomes available. Such programs would allow concatenation of maps, or portions thereof, which have been created at different scales, coordinate systems, and so on. Only a rescaling program ("RESCALE") is available at present.

The ability to mark coordinates (Table R.1) requires that marked coordinates be flagged in the data files. These flags must be removed if data files are to be rescaled such that coordinates can have negative values. Program "UNMARK" was written for this purpose.

Extraction of Subareas

Program SUBMAP (Fig. R.4) creates subareas, or domains, by enabling the user to draw the boundaries on a displayed map. Some of the computational techniques make use of the fact that the graphics is a raster type display.

Maps to be subdivided can be source maps or subareas. Any missing binary files (source files and base subarea "a0") are automatically generated. A list of all available subareas can be requested.

Two guides may be necessary in order to determine the locations of subarea boundaries. i) The data itself. Two types of data can be employed: geological/geographical boundaries and S.O.D.A. plots (see program SHADEMAP below). All can be displayed simultaneously. ii) The boundaries of existing subareas must be displayed to avoid overlap or data exclusion.

Only higher level subarea boundaries are displayed (for example, secondary subarea outlines if a primary subarea is on display.)

Subarea labels are automatically created. The program makes the last point of a subarea boundary equivalent to the first to obtain an exact closure. The program extracts subareas from the map on display (creating new XY and RF files), by shading the subarea polygons in blue (Appendix Q), and replotting the map. That part of the map which plots in blue belongs to the new subarea and its relevant information is stored. RF and PY files are similarly treated, but due to scaling problems associated with line drawing, the full screen rather than just the blue portion is used as a window.

New subareas can be displayed, analysed (programs STEREO and SHADEMAP, below), modified or rejected, with as many iterations as required (Appendix S). To modify a subarea without saving it requires the use of two temporary files: TX\$key\$00.BN (for the XY file) and TR\$key\$00.BN (for the RF file). These files are invisible to the user, but an abnormal program termination may leave these files residing on disc. The subarea label, "00" is used to ensure that only a maximum of two temporary files can exist for any map key, to keep unwanted files to a minimum.

Proposed Modifications

- 1) Improve layout of displayed maps. A portion of the screen could be reserved for a legend and menu. Legends would display such items as a scale bar, north arrow, and meanings of symbols. The menu would consist of options available at current program status (e.g. see program STEREO).
- 2) Pass parameters between programs. The only two ways to pass parameters from one program to another is via a disc file, and via the user. The system communications file, COM.CM, could be used instead of the (current) latter method. Only key and lv are passed at present, but shared information will increase with increased program sophistication.

Stereonet Analysis

Program STEREO (Fig. R.5) is a general purpose stereonet plotting program similar in function to the Hewlett-Packard program HPNET (Appendix B), but is more powerful, much faster, and can process unlimited data sets. As yet, only basic functions are available. There are no programming similarities between programs STEREO and HPNET program (although the algorithms detailed in Appendix L are used).

Layout of the stereonet can be seen in some of the colour plates (Appendix CP). Source map titles are displayed in the top centre with large letters and subarea titles with smaller letters. The stereonet is centred

with the type of projection displayed below it (lower hemisphere only). A functions menu (Table R.2 and Fig. R.6a) is displayed at upper right, and all options submenus (Fig. R.6b) are displayed at lower right. The stereonet legend (LEGEND table) is displayed at upper left.

Stereonet analysis is controlled by the data tablet, and the console is used only when necessary. A cursor in the form of a "+" (controlled by the tablet), has a two-fold function. The first is to act as a pointer (e.g. to point to an entry in a menu), and the second is to act as a positioner (e.g. to position a great circle on a net). There is no ambiguity between these two functions. When the cursor is inside the net, its orientation (trend and plunge) is displayed left of the north mark in blue.

As each function is selected from the function menu the actions taken next depend on the function. In most cases more information is required, and so "options" submenus, and/or the console, are used. Some functions terminate automatically whereas others terminate only when another function is selected.

SUBAREA A new subarea (lv) or map key can be opened for stereonet analysis.

NET The type of net (stereographic projection) can be selected. The default net is "WULFF". An "options" submenu ("NETS", Fig. R.6b) is used.

There is no automatic replotting of plotted data when the net is changed. As a consequence, a change of net type will cause any plotted points to be unrepresentative of the initial data.

COLUMN The structural elements to be plotted can be selected. A submenu ("COLUMN", Fig. R.6b) is used which contains the names of all available data columns. Any elements already plotted (i.e. their names are in the legend) will not appear in the submenu. This can only be avoided by immediately using the SUBAREA function after plotting. A chosen element is written into the legend, but remains temporary until another menu or submenu action is taken, when it becomes permanent.

COLOUR The colour of the next set of data points to be plotted can be selected. A submenu of colours ("COLOR", Fig. R.6b) is used. The colour, "MATCH", is a special entry, which causes data to be plotted in the colours specified in the source file, XY. "MATCH" is the default colour.

SYMBOL The symbol of the next set of data points to be plotted can be selected. A submenu of symbols ("SYMBOL", Fig. R.6b) is used. This function has the same characteristics as COLOUR. Once a symbol has been selected, it is assigned to all legend entries without symbols and is displayed beside the legend entry names in colour of COLOUR. The default symbol is "+".

CONDS. The (geological) conditions by which data is screened can be defined (Appendix C).

indicates data is to be plotted. A submenu ("DATATYP", Fig. R.6b) is used to select the way in which data are to be interpreted. Data of only one form can be plotted at a time. The number of data points plotted is displayed in yellow near the southeast quadrant of the net. The variables used by the FIT function are computed as the points are plotted.

variables used by the FIT function are computed as the points are plotted. Once data have been plotted, a great and/or small circle girdle FIT fit and/or mode to a point distribution may be requested. ("CIRCLES", Fig. R.6b) of possible distribution forms is used. When all forms have been chosen the result(s) are displayed in red near the southeast quadrant. The algorithm used is that of Ramsay (1967, p.18ff) which is known to be erroneous, but as for the HP stereonet program (Appendix B), lack of machine memory and shortage of time did not allow the methods described by Hamilton (1961), Mardia and Gadsen (1977), or Gray et al (1980) to be incorporated. Consequently, the results may be inaccurate. This function is used to draw great and small circles on the TRACE The submenu of "CIRCLES" is used, with entry, "MODE", ignored. stereonet. When an option is chosen the submenu is replaced with the "COLOR" submenu,

When an option is chosen the submenu is replaced with the "COLOR" submenu, and "MATCH" is ignored. This submenu acts as an inkwell whereby the cursor is dipped into the appropriate colour. The routine interprets the cursor position (when inside the stereonet) as being the dip vector (see Chap. 2) of the desired plane. Once it has been correctly positioned the coloured great circle is drawn. With dips greater than 45° the exact orientation is entered via the console.

DRAW Similar to TRACE, this function will enable coloured symbols and labels to be plotted and coloured lines to be <u>inked</u>, but will not necessarily be restricted to the net. Thus, diagrams and labels could be placed on the plot. The function is not yet available.

CONTOUR A function to contour plotted data is not yet available.

To implement this function, the present program would have to be restructured, as well as include some of the modifications suggested below.

LAYOUT The screen can be cleared of redundant information (e.g. menus).

CLEAR This function is used to start a fresh plot. The stereonet and legend table are cleared, and the "COLUMN" submenu is refreshed.

FINISH causes the program to stop.

Proposed Modifications

In its current state program STEREO is a basic model, requiring much modification and extension before it can utilise the full potential of the equipment. The list of suggestions below is by no means exhaustive.

1) Change the FIT routine to use correct algorithms. It could be further extended to incorporate population analysis (e.g. Shanley and

Mahtab, 1976; Sneath, 1977).

- Incorporate modification (2) of program SUBMAP.
- 3) Include the ability to reaccess structural elements (data columns). As the conditions by which data is to be screened may not be expressable in one "match/control" word pair (Appendix C), it may be necessary to access the same data elements more than once. It may also be desirable to compare data subsets from the same data column, by using different conditions or subareas. The generation of each of these populations may require several conditions.
- 4) Allow functions to be subordinate to START. Because FIT variables are computed in START, the ability to screen the same data columns with different conditions would require CONDS to be subordinate to START. The same applies to other functions (e.g. SUBAREA).
- 5) Merge TRACE and DRAW. The similarity between the two suggests that they should be made one function. The first submenu (Fig. R.8a) would call other submenus (Fig. R.8b,c,d). A number of improvements can be made (below).
- 5a) Lines, whether circles or <u>inked</u>, could be drawn in a variety of line styles (Fig. R.8b,d).
- 5b) Positioning of great and small circles could be improved. The cursor indicates the positions of dip vectors of great circles, and cone axes of small circles. A circle is not drawn until the cursor is correctly positioned, and once drawn cannot be erased without the use of CLEAR. Useful modifications would be: i) Have the cursor indicate the pole of a great circle (which is the cone axis of a small circle of 90° radius). ii) Use dragging to position circles. This technique (Newman and Sproull, 1973) allows the circle to be moved about. The temporary (unfixed) circle would be merely outlined by a number of computed points (e.g. Smith, 1971) to keep time lag to a minimum.
- 5c) Defining great circles is relatively simple, but defining and positioning small circles require further consideration, i.e. i) What to do with that part of a small circle (if any) in the upper hemisphere? ii) Choosing the size and position of small circles. Circle size could be specified either via the console or by zooming. The former method is simple but primitive. The latter could be implemented by using extra submenu entries, "MOVE", "ENLARGE", and "SHRINK". The growth (or shrink) rate should be exponential.
- 5d) Labelling items on a plot. The plot's title and/or subtitle may not be appropriate if data have come from more than one map or subarea. The user may also wish to label items or to place notes on the display. There are three ways of entering text and numbers using a data tablet,

apart from the console keyboard: i) Ink the characters (if good print is required then a character recognition routine is needed, which is not feasible). ii) Use a keyboard menu (i.e. reproduce the console keyboard as a menu on the display). This has the advantage of defining extra keys that are not available on the console, while excluding those keys that are not desirable. iii) Use a potentiometer for entering numbers (Newman, 1968). This has the advantage that it would be impossible to enter illegal or ambiguous numbers.

By using "LABEL" and "TITLE" entries, among others, in a submenu, the routine could obtain text from the console (or keyboard menu as in (ii) above), which would then be positioned with the data tablet. Text parameters such as size and colour are also required, and can be obtained either via the console or a submenu entry. The difference between "LABEL" and "TITLE" is that labels can be placed anywhere, whereas titles replace existing titles.

- 6) Change of net type. When a new net type is selected all plotted data, circles and points will no longer be correct, and cannot be corrected without using picture files (see (7)). For completeness, automatic replotting on a change of net should be an available option.
- 7) Construction of picture files. The need for picture files was recognized before STEREO was written, but because of the size of the task, it has been postponed until those functions which can be written without picture files are developed. As many of the functions would reference the picture files, their detailed design was not attempted until the functions and structure of the program had been developed.

Picture files (Fig. R.7) need only contain information pertinent to the inside of the stereonet and some extra items such as map key and subarea label. They would reside on disc, as do data files. Also like data files, the file names would be automatically generated, but their nomenclature would be different as information on one picture file may come from a number of subareas and/or maps.

A well designed picture file would consist of sub- and subsub-pictures. The use of a picture file has a number of advantages. a) A program run could be interrupted and then continued at a later time. b) Corrections and alterations could be selectively made via a CLEAR submenu (Fig. R.9) that allows deletion of the last operation, subpicture, or total picture. This could be extended to allow selective erasure of any part of a picture. c) Different stereonet plots can be compared. This could be done by superimposing two or more plots on the one net with each displayed in a different colour and/or symbol. This may not be satisfactory, but there are two other possible solutions:- i) Shrink plot sizes so that several

can be displayed simultaneously. Because only picture files are required, and the layout could be designed interactively, the comparison function could be a separate program. ii) Obtain hard copies of each plot either by photographing them or with function (d). d) It would be advantageous to be able to display stereonet plots on other devices such as other graphics terminals and hard copy devices (usually pen plotters and printers). As for (c), the display of stereonet plots on other devices is preferably done using a separate program. e) If data are not to be plotted more than once, then either different screening conditions must be mutually exclusive, or no data station must satisfy more than one condition. As neither situation is satisfactory, a picture file can be used to check for data duplication.

8) Display the meanings of the <u>conditions</u> column. It would be convenient if a table of the geological aspects, classes and/or parameters, and properties, with their corresponding values (and mnemonics if the programming is sufficiently advanced) could be listed.

Application of S.O.D.A.

Analysis of spatially distributed data can be made with program SHADEMAP (Fig. R.10) using a method similar to the A.V.A. technique (Sander, 1970; Turner and Weiss, 1963). All interaction is done via the console. The program requires maps to be tessallated (grain boundaries if maps of thin sections; Thiessen polygons (Rhynsburger, 1973) for field maps), i.e. there must be a PY file. The program is in four stages:-

- i) Select a subarea to analyse. As for program SUBMAP, all required data files are automatically created if they do not already exist. A list of all subareas can be requested.
 - ii) Define a colour chart (see Appendix X).
- iii) Produce a S.O.D.A. plot. The data elements to be plotted, their form, plotting specifications (pole or dip vector), and the conditions for screening data are required. The program then generates a S.O.D.A. plot by shading the tessera around each data station with the colour found from plotting its data on the colour chart. This procedure is iterative so that a number of conditions or data formats can be used for the one S.O.D.A. plot.
- iv) Repeatedly modify the analysis using a list of options (Table R.3). The simultaneous display of the subarea's reference map (RF) is optional.

Proposed Modifications

Modifications (1) and (2) of SUBMAP should be implemented here.

3) As for modification (8) of program STEREO.

4) Due to the iterative nature of screening data according to different geological conditions and data forms, reshading of shaded tessera often occur. The algorithm for shading polygons (FFILA, Appendix Ω) assumes that the boundary contains red, so provided there is no red in the shading of a polygon, it can be reshaded correctly. (In display systems that have many (eight or more) memory planes, one plane can be reserved for the tessera and the problem will not arise.) Apart from using a shading routine that does not make use of display memory, there are few measures that can be taken to lessen the problem. Some suggested measures are: a) Keep the use of red to a minimum. b) Keep a list of plotted data points to prevent duplication. c) Restructure SHADEMAP so that tessera are not shaded until all data have been scanned by all conditions and forms and a list of data to be plotted has been compiled; then each tessera is accessed only once, irrespective of how many times it is to be shaded. However, intermediate results cannot be compared during construction of the S.O.D.A. plot.

LIST OF TABLES

```
Table R.1 Console commands for cursor control.
                          Function
Command
         Set FACTR (a variable) to this value.
 0 - 9
         Kill tablet; ignore data tablet, use console instead.
  K
         Pen; cancel K.
   P
         Only use x of cursor, use y of last selected point.
   X
                         ", "х"
               " У
   Y
         Move cursor left (-x direction) by FACTR.
   L
                                       )
                    right (+x
   R
                                               99
                                          11
                91
                                       )
                      up (+y
   U
                                          99
                                       )
                     down (-y
   D
         Fix; select current position as new point.
   F
         Erase; cancel F.
   E
         Mark last selected point.
   М
         Make nearest marked point the next selected point.
   N
         Close; make first selected point the next selected point.
   С
         Read next selected point's coordinates from the console.
   I
         Grid the display according to FACTR.
   G
         Display various relevant coordinates, according to FACTR.
   Т
         Change state of homing bell flag. Bell rings when cursor is
   В
         horizontally or vertically aligned with the first selected point.
         Change method of reading data tablet, according to FACTR.
   J
         Show state of flags (B, G, FACTR, etc).
         Start cursor control from console, not data tablet.
   ^s
                                 " data tablet, not console.
   ^T*
   ^z
         All other characters are invalid and are ignored.
   else
 This command operates by default.
```

```
List of functions.
Table R.2
             define data conditions (Appendix C).
CONDS.
             select the type of stereographic projection.
NET
            plot data on the net.
START
             end of program run.
FINISH
             select another subarea lv and/or map key.
SUBAREA
             clear the plot and start again.
CLEAR
             select the data column(s) to be plotted.
COLUMN
             select the symbol with which data is to be plotted.
SYMBOL
                     " colour " "
                                           E1 U1 U1 EE
COLOUR
             draw on display, i.e., ink in lines, points, and labels.
DRAW
             draw great and/or small circles.
TRACE
             fit a great, and/or small, circle and/or mode to plotted data.
FIT
             contour plotted data.
CONTOUR -
             remove all extraneous information from the display.
LAYOUT
```

Table R.	3 List of options for modifying current analysis results.
Option	Function
1	End of program run.
2	Get new map (key).
3	Get new new subarea (lv).
4	Display the reference chart, and allow modifications.
5	Select new structural elements.
6	Modify the lookup table for the colour chart.
7	Modify the reference list (without displaying the chart).
8	Modify the interpretation of how data is read and plotted.
9	Modify the conditions by which data is screened.
10	Swap in program STEREO.
11	Replot the S.O.D.A. plot using all modifications (if any).
12	Overlay the reference map, RF, if any.

APPENDIX S

APPLICATION OF INTERACTIVE COLOUR GRAPHICS TO THE DISPLAY AND INTERPRETATION OF STRUCTURAL DATA

Paper presented at the

International Conference on Deformation Processes in Tectonics

Alice Springs, Australia, 1981

APPLICATION OF INTERACTIVE COLOUR GRAPHICS TO THE DISPLAY AND INTERPETATION OF STRUCTURAL DATA

P.H. Cohen

Geology Department, University of Adelaide, S.A., 5000, Australia

The analysis of the structural geometry of an area includes a number of time consuming processes: (1) the compilation of a structure map, (2) stereographic plotting and analysis of structural data, (3) subdivision of the map into subareas, with modifications based on the results of (2) above, and (4) presentation of diagrams. These processes have been automated to greatly speed up structural analysis. This paper describes part of the automated process - which is the ability to rapidly define subareas in a map, analyse these subareas using both stereographic plots and a technique modified after Sander's A.V.A. process (Sander, 1970), and finally to be able to alter at will the subarea boundaries, based on these analyses (see Fig. S.1).

The method of analysing areas by subdivision is conducted by the user interactively controlling the flow of the analytical process. This is achieved by using a "light pen" coupled to a colour graphics display unit. The system is run on a minicomputer.

Defining a subarea boundary on a displayed map is achieved by drawing the boundary on the display with the use of the light pen. Data files for the subarea are made from the map's data files, and these can then be analysed using the stereographic plotting program and a technique, described below, termed SODA (Spatial Orientation Distribution Analysis). The subarea boundary can further be modified with the light pen and the process repeated until the user is either satisfied with or rejects the subarea. Any map or subarea can be used as a source map for subdivision.

The choice of subarea boundaries is made by using the SODA technique, of which the A.V.A. process is a subset. This technique firstly polygonises teh map with regular (Thiessen) polygons so that there is only one station location containing orientation data within each polygon. These polygons are then shaded in colours according to the orientations of the structural elements contained within them. The colours used can be chosen by the user. In this way regions of orientations (e.g. different fold limbs) can be distinguished by different colours.

The result of the application of interactive colour graphics in the way described above is that structural analyses which may have taken days to carry out can be achieved in a few hours.

REFERENCE

Sander, B., 1970: An Introduction to the Study of Fabrics of Geologic Bodies. Authorised translation by F.C. Phillips and G. Windsor, (Oxford Pergammon Press) 641 pp.

APPENDIX U

GENERAL FABRIC ANALYSIS TECHNIQUES WITH COMPUTER-AIDED S.O.D.A.

A paper presented at the

International Conference on Planar and Linear Fabrics of Deformed Rocks

Zurich, Switzerland, 1982

GENERAL FABRIC ANALYSIS TECHNIQUES WITH COMPUTER-AIDED S.O.D.A.

Peter H. Cohen

Geology Department, University of Adelaide, Adelaide, 5000, South Australia

A general technique for analysing spatially distributed orientation data has been devised by the author, and is termed S.O.D.A. (Spatial-Orientation Distribution Analysis; Cohen, 1981a and in prepa). The technique is the application of trend surface analysis to structural geology, particularly where data are orientations of structural fabric elements.

There are two types of trend surfaces, viz. structural surfaces i.e. orientation data which are gradient values of the structure (trend) surface (type "I"), and functions, $f(\emptyset,\theta)$, of properties of orientation data (type "II"). The latter type is presented in this paper.

Type II analyses encompass such domain analysis methods as the A.V.A (Sander, 1970) (fig. U.2), strike-dip maps (fig. U.3), two dimensional fold classifications (Ramsay, 1967) (fig. U.4), three-dimensional fold classifications (Cohen, in prepa), and correlation with other geological and geophysical data (under development). S.O.D.A. was developed to include all of the above.

Four procedures are used in analysing for structural domains once maps have been digitised and tessellated, and orientation and geological data have been filed in the computer. These are: 1) stereonet plotting (with associated distribution analysis routines), 2) stereonet sectioning (i.e. defining $f(\emptyset,\theta)$), 3) S.O.D.A. plotting (domain plotting), and 4) map sectioning (domain extraction for analysis).

The equipment consists of a mini-computer (Nova2), a display processor (with 3 bits/pixel), a colour monitor for (raster) picture displays, a data tablet for alternative efficient interactive processing (digitising, modifying display, controlling program flow), mass storage (a 2Mbyte disk), a magnetic tape drive for program backup, and a console for user control. A link to a Cyberl73 (Cohen, 1981b) enables high powered computing and alternative data sources to be available to S.O.D.A.

Domain analysis is performed by defining primary domains with a coarse analysis, segmenting the map into these domains, and then analysing for secondary domains and relationships between the structures and the geology. The basic sequence follows the procedures as numbered above, although analytical flow is flexible enough to allow temporary and permanent modifications and alterations to the process.

- 1) Stereonet plotting is highly flexible with a variety of nets, fitting of girdles and points to distributions, and selectivity of plotted data according to geological conditions.
- 2) Sectioning the stereonet (defining $f(\emptyset,\theta)$) is a simple process of choosing from one of three basic functions and then modifying and rotating as desired (fig. U.1). The three functions are: a) $f(\emptyset)$ or isotrend chart (fig. U.1E) (i.e. contours of constant trend represented by radial lines on a polar net), b) $f(\theta)$ or isodip chart (fig. U.1F) (i.e. contours of constant dip represented by concentric rings on a polar net), and c) $f(\emptyset)+f(\theta)$ or "standard" chart (fig. U.1D) represented by a polar net. Charts may be unidirectional (i.e. opposing trends are different) or bidirectional (opposing trends not distinguished). The resolution (number of contours) is variable, as is the colouring of segments and the contrast between colours of adjacent segments. Two other basic functions (user definable) can be used to mask out portions of the stereonet not desired

for analysis (fig. U.1). A number of mask combinations can be employed for the sectioning of one net, allowing quite detailed segments to be defined.

3) A S.O.D.A. plot is similar to an A.V.A. i.e. an area of the map encloses only one data point, and that area is coloured according to its datum. For the A.V.A. the areas are defined by grain boundaries, and for mesoscopic fabric data the areas are Thiessen polygons (Rhynsberger, 1973). Data to be analysed can be selected according to geological criteria thus allowing correlations between structure and other geological parameters.

4) Map (including S.O.D.A. plot) sectioning is performed by outlining the domain to be extracted (using the data tablet) and labelling it. The extracted domain then becomes a map available for analysis and sub-

division.

A number of examples are presented to demonstrate the use of S.O.D.A. The A.V.A. technique is not included here as it is presented elsewhere (Cohen, 1982).

Example 1. Small F₃ folds in a planar fabric were measured on a strip of coastline at Lipson Cove, South Australia. The stereonet plot of the fabric elements shows the folds to define a complete axial plane girdle parallel to the weakly developed axial plane fabric. A rotated bidirectional isotrend chart is used to section the girdle into a series of segments. The resulting domain analysis determines that the area consists of two primary domains, dividing the area in two, and each of these contain distinct subdomains.

Example 2. In a theoretical example a subhorizontal planar fabric was synthesised for two situations. The pole plot figures of both are identical and are well defined vertical maxima. However the S.O.D.A. plot shows that one of the areas is an open domic structure, and the second is an undulatory plane. A detailed analysis of the latter shows a dislocation that rotates the fabric on one side by a few degrees from that of the other. By sectioning the S.O.D.A. map the two domains can be demonstrated on a pole figure. (Plotting dip vectors rather than poles produces a better distinction of the two domains.) The orientation of the dislocation suggests that the structure would either be a scissor fault or a refraction (if the planar fabric was a schistosity), rather than an open fold.

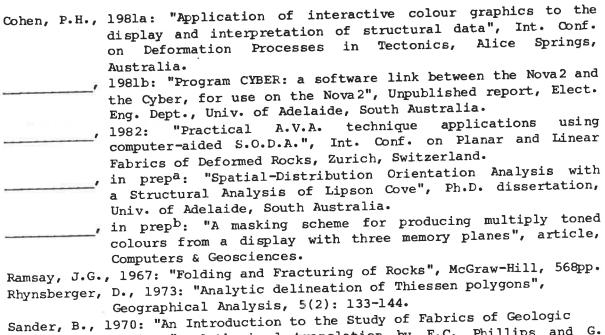
Example 3. Bedding is the only fabric data available for a test analysis of a mineral lease in Western Australia. The pole figure describes a poorly defined profile plane girdle dipping steeply to the southeast. The S.O.D.A. plot defines three primary domains, when a standard chart is used, which represent the three limbs of an upright, shallow northwest plunging syncline/anticline pair. Subdomains can also be recognised. A S.O.D.A. plot using a rotated isodip chart describes the limbs to be planar (with small folds contained within) and the hinges to be angular, hence defining a megakink.

Separate analyses of the three primary domains reveal these domains to be more tightly folded in the southeast, and open towards the north-west. Therefore the open "cylindrical" fold system is constructed of tighter conical folds and more open cylindrical folds, the former causing the scatter in the overall pole figure.

A "finely tuned" analysis reveals two other trend directions, NNE-SSW and NE-SW. This suggests that another deformation episode may have occurred (which is the case) and/or the effect is due to trends in the original sedimentary basin.

An analysis of the structures in the mineralised areas does not significantly vary from those in unmineralised areas of the same formation. However, if the location of drill holes is an indicator of possible economic grade, the S.O.D.A. plot demonstrates that the higher grades are structurally controlled and occur in one limb of the megakink.

References:



Bodies.", Authorised translation by F.C. Phillips and G. Windsor, Oxford Pergammon Press, 64lpp.

Wilson, C.J.L., 1973: "The prograde microfabric in a deformed quartzite sequence, Mount Isa, Australia", Tectonophysics, 19: 39-81.

APPENDIX V

PRACTICAL A.V.A. TECHNIQUE APPLICATIONS USING COMPUTER-AIDED S.O.D.A.

A paper presented at the

International Conference on Planar and Linear Fabrics of Deformed Rocks

Zurich, Switzerland, 1982

PRACTICAL A.V.A. TECHNIQUE APPLICATIONS USING COMPUTER-AIDED S.O.D.A.

P. H. Cohen

Geology Department, University of Adelaide, Adelaide, 5000, South Australia

The manual application of the A.V.A. technique (Sander, 1970) is very slow, tedious and hence not often used. However with modern technology A.V.A.'s can now be performed rapidly and efficiently. With the common use of mini-computers and the more recent involvement of colour monitors and display processors as computer peripherals, an automated means for manipulating, modifying, and displaying of analytic results of geological data can be achieved. The general technique developed by the author, S.O.D.A. (Spatial-Orientation Distribution Analysis; Cohen, 1981, 1982, and in prep.a), which incorporates the A.V.A., is just such a technique using interactive computer graphic processing. This paper exemplifies the use of S.O.D.A. for the axial distribution analysis of microfabrics.

Example 1.

A sample of amphibolite was collected from Lipson Cove, South Australia, and a large thin section prepared (fig. V.1). Sections were cut from it for microfabric analysis, and photographic prints were made by placing them in a photographic enlarger. These formed base maps for recording measured grains and for digitising for computer analysis. As each grain was orientated on the universal stage, the four angles were entered into a HP 9830A calculator for computing, printing and stereonet plotting of the three crystal axes, [100], [010] and [001] (Cohen, in prep.b).

The large thin section (fig. V.1) shows an S_1 fabric tightly folded by F_2 , and crenulated by D_3 (Cohen, in prep. a). In plane polarised light the hornblende pleochroism dramatically demonstrates that the D_3 crenulations are well developed in one limb of the F_2 fold but is very weak in the other.

 F_2 Hinge Region. (fig. V.2) The stereonet plots of [100] and [001] axes show point maxima with some spread along orthogonal great circle girdles. Much of the scatter being attributed to the overprinting crenulations. An A.V.A. plot (fig. V.4A) using a bidirectional isotrend chart shows two primary domains, representing each limb of the F_2 fold. The stereonet plots of the two domains show distinct differences in orientation and scatter.

The north limb shows the [100] girdle dipping very shallowly WNW with a NNE-SSW horizontal point maximum, and an orthogonal [001] girdle with a subvertical point maximum. The south limb [100] girdle dips very shallowly ENE with a NNW-SSE horizontal point maximum, and an orthogonal [001] girdle with a subvertical point maximum. The north limb [001] girdle is better defined than that of the south limb, due to the crenulating effects in the latter being more pronounced than in the former, and the hornblendes in the north limb tend to have a higher proportion of subhorizontal grains than those of the south limb. The scatter in the [001] of the south limb can be resolved into two weakly defined girdles representing the two limbs of the D3 crenulation.

 $\underline{D_3}$ Crenulation. The distribution of [100] axes forms a very shallowly east dipping girdle with a horizontal north-south point maximum. The [001] axes form a point maximum plunging subvertically but towards the southwest. Asymmetry of the distribution defines a weak partial girdle (or cone) with the dip vector corresponding to the point maximum. With the use of a bidirectional isotrend chart (RES=45) an A.V.A. plot (fig. V.4B,C) can

be produced to show that the [100] generally defines the crenulation (limb orientations), but many hornblende grains of the S_1 fabric orientation persist throughout the crenulation. The [001] show a very poor to non-existent relationship to different areas of the crenulation.

It appears from the above that the orientation of hornblende [001] axes have a strong bearing on the crenulating effects of the D3 stresses. The alternative argument is that [001] may or may not be more easily rotated depending on the orientation of [100] to the stress field. The latter is unlikely as hornblendes are more easily twinned than they are rotated. The differing [001] orientations across the F_2 fold would have been caused by

Example 2.

Quartz fabric analyses were made on specimens from Wilson (1973). The stereonet plot of a sample of polygonal grains shows a random scatter in Z orientations (fig. V.3A). The A.V.A. plot (fig. V.4D) shows that this randomness is also seen in the grain distribution. No region of more than a couple of grains in the section could be found to have correlative orientations. The stereonet plot for a section with exaggerated grain growth (fig. V.3B) show better defined orientation distributions. A corresponding increase in grain relationships can be found in the A.V.A. plot (fig. V.4E), whereby adjacent grains can be seen to have related orientations. By assigning related grains with the same colours, domains can be defined that demonstrate a strong grain and domain boundary orientation that diverges from the schistosity by 30°, which is a physical comparison to the 30° variation between the Z axis girdle and the schistosity (vertical, north-south) shown in the stereonet plot.

References:

- Cohen, P.H., 1981a: "Application of interactive colour graphics to the display and interpretation of structural data", Int. Conf. on Deformation Processes in Tectonics, Alice Springs, Australia. , 1982: "General fabric analysis techniques with computeraided S.O.D.A.", Int. Conf. on Planar and Linear Fabrics of Deformed Rocks, Zurich, Switzerland. , in prepa: "Spatial-Distribution Orientation Analysis with a Structural Analysis of Lipson Cove", Ph.D. dissertation, Univ. of Adelaide, South Australia. in prepb: "A BASIC program for desktop calculators for computing hornblende axes orientations from universal stage readings", article, Computers & Geosciences. Ramsay, J.G., 1967: "Folding and Fracturing of Rocks", McGraw-Hill, 568pp. Sander, B., 1970: "An Introduction to the Study of Fabrics of Geologic Bodies.", Authorised translation by F.C. Phillips and G. Windsor, Oxford Pergammon Press, 641pp. Wilson, C.J.L., 1973: "The prograde microfabric in a deformed quartzite
- sequence, Mount Isa, Australia", Tectonophysics, 19: 39-81.

APPENDIX X

DESIGN AND USE OF COLOUR CHARTS FOR S.O.D.A. TECHNIQUE APPLICATIONS

Description

The division of a stereographic net into groups can be done in a number of ways, each with their particular merits. There are four which have immediate applications: 1) divide according to structural geometry, 2) divide manually, 3) divide according to contour levels, and 4) divide according to results of cluster analysis programs. Only method (1) has been implemented as time and hardware constraints have excluded the others.

The programming of method (1) is contained within the main subroutine ARSS (Fig. X.1), which uses two other subroutines, DISPL, and LKUPT.

The technique uses two masks (labelled "Q" and "R") to define regions. Reference mask R (Figs. X.2b,c) is based on the geometry of cylindrical folds. A referential great circle can be defined by the variables STR (strike) and DIP (measured from a dip direction 90° clockwise from STR). Two other variables are used to complete the definition of the mask: PCH (pitch of a referential point on the referential great circle) and TOL (tolerance— the maximum angular displacement that a point can be from the referential great circle and still be considered to belong to it). Quadrant mask Q (Fig. X.2a) defines quadrants (Table X.1). The mask can be rotated about the vertical by STR (of mask R). A single combination of the two masks is termed a reference. Up to ten references can be used to define a single reference chart.

There are three types of colour charts (Figs. X.2d,e,f) from which to select for operation upon by references. These are: a) the standard colour chart, b) isotrend contour charts (u- or b-) (Chapter 2), and c) isodip contour charts (u- or b-). If either (b) or (c) is used, then contour resolution, RES, can be defined. (The standard chart is a combined chart of (2) and (3) with RES of 30° and 18° respectively.)

Charts can be rotated about the vertical (by ROT, see later) prior to rotation by Mask $\ensuremath{\text{R}}_{ullet}$

There are two basic colour schemes for charts, shown in Figs. CP.2a,o. The first is generally more useful. The colour schemes can be modified by: a) changing the row length of the colour matrix (the default length is 12), and b) specifying a contrast factor (low, medium, and high). The latter modifies the former by a factor based on the type of chart and the value of RES.

An overriding colour can be specified for each reference, giving the option of using portions of a colour chart for some references

(combined with the ability of colour gun selection), and using single, "solid", colours for others.

Reference charts can be displayed by one of three stereographic projections (equal-area, equal-angle and orthographic, shown in Figs. CP.2a,b,c).

The Colour Matrix

The display processor, ULOS (Universal LayOut System; Bell, 1978; Davis, 1979), contains only one memory plane per colour gun. Therefore, each screen-pixel is capable of having only one of eight hues (Fig. X.3). (The term "hue" is defined in the Munsell system, Eastman Kodak, 1972). Many more colours are required for S.O.D.A. to be successful as a general purpose technique and therefore a more complex approach had to be developed in order to obtain toning. (The term is used here as an alternative to chromaticity (Eastman Kodak, op. cit.) as it also includes reflectance (or transmittance) to some degree.) This precludes the accurate colour generation techniques (for both visual and photographic uses) described in the literature (e.g.: C.I.E., 1978; Fangeras, 1979; and O'Callaghan et al., 1981).

Colour-pixel masks (Figs. CP.lf,g,h,i,j) were designed to simulate toning (C.I.E., op. cit.). They consist of 3x3 arrays of screen-pixels. By varying the number of screen-pixels (0, 1, 3, 5, and 9) within an array, multiple toning is obtained. Due to the asymmetry of screen-pixel distribution, either within the colour-pixel or over a group of colour-pixels, patterns occur within the resulting colours.

The effective display resolution of a picture using colour-pixels is 172x172. However, the polygon-fill routine, FFLLA (Appendix Q), is capable of splitting colour-pixels, keeping the original 512x512 display resolution intact.

With five colour-pixel masks and three colour guns a total of 5^3 colours are possible. Every hue can be expressed as a three digit quaternary number (i.e., to base 4) by numbering the masks from 0 to 4, giving a colour range from 000_4 (black) to 444_4 (white). (The three digits refer to (from left to right) red, green, and blue.)

Although a digit requires only two computer bits, for practical reasons each is converted to an octal digit (except in routine FFLLA).

The alternative colour matrix (shown in Fig. CP.20) uses the full colour scheme from 001_4 (dark blue) to 444_4 . This sequence is not generally useful, and so an optimum set was extracted and rearranged in a logical sequence. The resulting matrix consists of four rows, twelve columns long. Each column represents a different hue and each row

represents a tone of that hue. Two further rows are set at white. This colour matrix can be presented in a colour wheel (Fig. CP.ld), which also defines the standard colour chart. The logic of the colour chart is demonstrated in the arrangement of the colour-pixel masks for the three colour guns (Figs. CP.la,b,c).

Reference Chart Display Procedures

To Display references, compute the orientation of every point within the stereonet, determine within which references it lies, and then shade it according to the chart selected and colour specified. Each point in the stereonet is defined as one colour-pixel.

The stereonet has a diameter of 91 points. In an array of 91x91 points, those that occur outside the primitive circle must be rejected. This is done by comparing the square of the distance (d_1^2) of point i from the circle centre (defined as the origin of a Cartesian coordinate system (x,y)), to the square of the radius (45.5^2) . An efficient method is to compute d_{i+1}^2 in terms of d_i^2 by the following procedure. Given: $d_i^2 = x^2 + y^2$,

Given:
$$d^2 = x^2 + y^2,$$

$$y_{i+1}^2 = y_i^2 \text{ (progressing in the x direction),}$$

$$x_{i+1}^2 = (x_i + 1)^2$$

$$= x_i^2 + 2x_i + 1.$$
If we define
$$\Delta d^2 = d_{i+1}^2 - d_i^2$$
then
$$\Delta d^2 = 2x_i + 1.$$
Therefore
$$d_{i+1}^2 = d_i^2 + 2x_i + 1..$$

$$(X.1)$$

 $2x_{i}$ is derived from the previous point, $2x_{i-1}$, by:

$$2x_{i} = 2x_{i-1} + 2$$
 (X.2)

A change in y at the start of each row of points can be similarly treated. Therefore, the square of the distance of every point from the centre can be computed by an addition, provided a starting point is provided.

Once a point is determined to be within the primitive circle, its distance (d) is found*, and its direction cosines computed (according to choice of projection). It is then rotated such that Mask R assumes its default position (STR=0, DIP=90, PCH=90), by the sequence: STR about the

^{*} In order to limit computing time, d is a single precision (unsigned) integer that can be rapidly computed (Data General Corporation, 1970b) from d^2 . As $d^2 < 4095$, it uses 12 bits of a 16 bit word. By multiplying d^2 by 16 (a binary shift of 4 bits), a distance of 4d is obtained. (I.e., d is calculated to two binary places, which is a fourfold increase in accuracy).

vertical axis, DIP-90 about the north axis, and PCH-90 about the east axis (where positive rotation is anticlockwise). It is then a simple matter to determine in which regions of Masks Q and R the point lies; as the masks are coded so that testing reduces to a single Boolean multiplication (a logical .AND. test).

Points within each <u>reference</u> must have their colours determined according to the type of chart and other specified parameters. This is a relatively simple procedure unless the colour chart is not centred on the vertical (Table X.1), in which case, intermediate results used in the above rotations are used, instead of the final results.

Designing Reference Colour Charts

Designing colour charts for any given structure is generally simple. The normal procedure is to maximize the number of colours that a data set will display. However, any design will ultimately depend on the data property to be determined.

Because many variables are used to define a chart, a simple nomenclature is required. The values of variables are written in the following sequence (see the colour plates for examples):

RES is omitted if chart=1. If any of the next three variables are omitted, their default values are assumed (ROT=0, row length=12, and contrast=1). If QR is omitted (and hence colour) their defaults are assumed (QR=00, colour=7). Omitting colour assumes the default value.

Suggested Modifications and Recommendations

- 1) Replace the single precision SQRT function for calculating the distance of a point from the centre (accuracy of 0.5% of the radius) to a double precision SQRT function.
- 2) Undesirable results may occur when mask R has either a PCH = 90° or a DIP = 90°. When PCH = 90° the E and W regions of Mask R also rotate. Although this can be overcome by specifying four references separately (use the desired PCH for the N and S regions, and a PCH of 90° for the E and W), it could be programmed so that, say, a colour of "40" would do what the program does now, and a colour of "20" would only rotate the reference great circle, not the two regions off it. When DIP = 90° some of the N region accompanies the S and vice versa. This can be solved by programming, so that by adding 5 to the colours of "20" and "40", to give colours of "25" and "45", the problem may be bypassed.

- 3) Increase the versatility of the masks.
- W region of mask R rotates into the upper hemisphere) in a different colour, e.g. magenta, then this could be requested by adding "10" to the above colours, giving colours of "30", "35", "50", and "55".
- b) In areas of either conical or complex folding, mask R does not relate well to the geometry of the structure. In this case it may be possible to use a reference small circle mask "S" (similar in design to mask R). Limited applications of this option are already available as the boundaries between regions on and off the reference great circle are small circles, as are the regions in isodip charts.
- 4) A limiting factor in applying S.O.D.A. is the subdivision of stereonets. Design of the references ought to be in program STEREO (Appendix R), where the exact relationship between data and references can be displayed. (Mask outlines could be displayed on stereonet plots.)

 Reference mask parameters could be returned to subroutine ARSS via the COM.CM file (a systems communication file), where colours can be assigned and the reference chart displayed as before.

Table X.1 Tables for defining references and charts.

Mask Q	Quadrant	Mask R	Region	Col	lour	(Guns)	
0	All	0	All	0	Black/ne	ew refs.	chart
1	NW	1	E	1	Blue	(B)	
2	NE	2	W	2	Green	(G)	
3	SE	3	N	3	Cyan	(B+G)	
4	SW	4	S	4	Red	(R)	
5	w (sw+nw)	5	E+W	5	Magenta	(B+R)	
6	N (NW+NE)	6	N+S	6	Yellow	(G+R)	
7	E (NE+SE)			7	White	(B+G+R)	
8	S (SE+SW)			+			
	,			40	Mask R	Colour	
Chart	Туре	C	ontrast		3	-1	
1	Standard	1	Low		4	- 6	
2	U-isotrend	2			1	-4	
3	B-isotrend	3	High		2	-2	
4	B-isodip		•				
5	U-isodip						
9	<u></u>						

Variable	Positive Value	Negative Value
STR	Rotate Mask Q	no rotation of Mask Q
DIP	Chart centred on vertical	centred on pole to ref. great circle
PCH	" by DIP	centred on reference point
Colour	Use colour guns specified	use "solid" colour
Chart	Use default colour matrix	use alternative colour matrix
RES	Use total colour matrix	use second half of colour matrix

Note: In calculations the signs of the above variables are removed so that the variables are always positive.

APPENDIX Z

AN EFFICIENT ALGORITHM TO POINT COUNT FOR CONTOURING STEREONETS

INTRODUCTION

The standard, and simple, technique for determining whether a point and a grid node are within the same counting circle, for the purposes of contouring, is to use dot-products. That is:

$$a \cdot b = ab \cos \theta$$
 (Z.1)

In this application, a and b both have length 1, and so (Z.1) simplifies to:

$$\cos\theta = \underline{\mathbf{a}} \cdot \underline{\mathbf{b}} = \mathbf{a}_{\mathbf{x}} \mathbf{b}_{\mathbf{x}} + \mathbf{a}_{\mathbf{y}} \mathbf{b}_{\mathbf{v}} + \mathbf{a}_{\mathbf{z}} \mathbf{b}_{\mathbf{z}}. \tag{Z.2}$$

(The RHS terms are direction cosines.) As the half-apical angle for the counting circle is fixed, (Z.2) can be compared against the cosine of the half-apical angle to determine if a grid node count is to be incremented.

Equation (Z.2) requires the direction cosines to be calculated (five trigonometric functions and two multiplications per vector). The number of calculations can be reduced if the direction cosines are computed once for all data points and/or grid nodes and then stored in memory. Computation time is greatly reduced but the size of the program increases significantly. Program ORIENT (Bridges and Etheridge, 1974) does this for grid nodes, but not for data points. For this to be practical the grid must be coarse (5°). The short cut must be abolished if a finer grid is used, as the number of grid nodes increase by the square of the increase in resolution. Hence the 2.5° grid used in this thesis requires four times the number of grid nodes used by program ORIENT.

To avoid comparing every grid node with every data point, a simple test is required to delimit that portion of the grid that contains all possible nodes that lie within the counting circle centred on a data point.

Although mathematically elegant, computer coding for the above method is inefficient. A better method is described below.

METHODOLOGY

The concept of the method used here is quite simple: every grid node that lies in the counting circle is directly computed. This proves to be efficient as grid nodes are simply related to each other in position. The steps involved are: 1) divide the counting circle into two portions if necessary (i.e., simplify the process), 2) find the range of isodip grid lines lying within each portion of the counting circle, 3) for each isodip grid line find the range of isotrend grid lines within the counting circle, and 4) increment the count of these grid nodes.

TERMINOLOGY

The following terminology is geometrically expressed in Fig. Z.1.

```
= area of counting circle expressed as a fraction of the net area.
area
COSRAD = 1 - area = cos \theta_b.
          \cos^{-1} \text{ COSRAD} = \Theta_h.
HTH
       = trend of data point.
          plunge of data point.
          dip value of current isodip grid line being considered.
                   = 90^{\circ} - \Theta_{p}
        = CONST
           CONST2 = \cos C = \sin \theta_{D}
       = CONST3 = \sin C = \cos \theta_{p}.
C3
           CONST4 = 90^{\circ} - \Theta_{d}.
C4
           maximum dip value obtainable in counting circle in portion a.
GD1
GD2
        = minimum declination of circle circumference in portion a.
SDl
SD2
        = maximum
SD3
SD4
        = Number of portions counting circle divided into (1 or 2).
NL
                                                             " , due to trend
           values crossing the 000^{\circ}/360^{\circ} boundary (1 = no, 2 = yes).
```

HSTR = β = range of trend values subtended between $\phi_{\rm p}$ and trend of intersection of $\theta_{\rm d}$ with counting circle circumference.

The process must consider which of three possible situations (Fig. Z.1) the current data point causes: counting circle includes the vertical (b), includes the primitive (c), or neither (a).

Situation a

Values that must be set are:

GD1 =
$$\theta_p + \theta_h$$
.
SD1 = $\theta_p - \theta_h$.
NL = 1.

Situation b

GD1 = GD2 = 90°.

SD1 =
$$\theta_p - \theta_h$$
.

SD2 = SD3 = 90 - $\cos^{-1} [\cos(\theta_h)/\sin(\theta_p)]$.

This can be computed from spherical trigonometry (Fig. Z.1b):

$$cos(c) = cos(b) \cdot cos(a)$$

$$i.e. \quad cos(\theta_h) = cos(\theta_0 - SD2) \cdot cos(\theta_0 - \theta_p) .$$

$$cos(\theta_0 - SD2) = cos(\theta_h) / sin(\theta_p) .$$

$$SD4 = \theta_0 - (\theta_p + \theta_h) .$$

$$NL = 2 .$$

Situation c

GD1 =
$$\Theta_p + \Theta_h$$
 .

GD2 = $\Theta_h - \Theta_p$.

SD1 = SD2 = 0 .

NL = 2 .

The final equation that must be determined is for ß (Fig. Z.lc). From the law of cosines for oblique spherical triangles:

$$\cos(a) = \cos(b) \cdot \cos(c) + \sin(b) \cdot \sin(c) \cdot \cos(a) ,$$

$$\cos(a) = [\cos(a) - \cos(b) \cdot \cos(c)] / [\sin(b) \cdot \sin(c)] .$$

$$As: a = \theta_h , b = 90 - \theta_d , c = 90 - \theta_p .$$

$$a = \cos^{-1} [\cos\theta_h - \sin\theta_d \cdot \sin\theta_p] / [\cos\theta_d \cdot \cos\theta_p] .$$
(Z.4)

DISCUSSION

Equation (Z.3) is calculated once for each data point (involving three trigonometric functions and a division), and (Z.4) once for each isodip grid line in the counting circle (involving six trigonometric functions, two multiplications, and a division). Compared to (Z.2) (which requires ten trigonometric functions and seven multiplications for each grid node in an area large enough to contain all nodes that may be included in the counting circle (reduced to five trigonometric functions and five multiplications if the direction cosines for each data point are saved as constants after being calculated once)), the method developed here is more efficient.

The algorithm used by program ORIENT was compared to this one. For a coarse grid of 5° the run time was equal, but this algorithm reduced memory by 4104 words. (The saving is not quite that great as the new algorithm is slightly longer.) With a finer grid of 2.5° the algorithm was half again as fast as an equivalent of ORIENT. (The latter also required an extra 16400 words of memory. A version that did not use this extra memory had run times two to three times longer.)

APPENDIX CP COLOUR PLATES

Pictures produced on the colour graphics display equipment used in this thesis have been reproduced as colour plates (Figs. CP.1 to CP.19). These plates contain a number of pictures, each representing one full display screen. The plates were first designed with respect to final layout and size of the pictures that they contained. They were then scaled down to the maximum size that the colour enlarger (for printing) could manage. Each picture was then photographed so that it would appear to the correct, scaled down size on a slide (or negative). The slides were combined, and masks containing labels, scale bars, and other accessories were overlayed, resulting in super slides (or negatives).

There are a number of points to note concerning the figures.

- 1. In the stereonet figures, data points are plotted in "add" mode (see Appendix F) and therefore overlapping points of different colours give rise to new colours. For example, the overlapping green and red data points of Fig. CP.16b combine to give yellow (see Fig. X.3). The figure captions refer only to the primary colours concerned and not to possible variations due to overlap. Although this appears as a problem, it has its advantages, viz., a) different data sets are distinguishable even though they may overlap, and b) with most colour display processors (including ULOS) individual memory planes can be switched off by the program, and hence individual data sets may be switched on or off the display as desired.
- 2. There will be some colour variation between S.O.D.A. plots and the colour chart from which they are derived. These are due to changes in colour monitor performance with time, and variations in exposure during photography because of change in scale for the different sized figures. However, variations will be small and confusion should not arise.
- a falling off of intensity away from the centre of the monitor, and because of stray magnetic fields causing one colour gun to overspill into another colour's mask. The colour most badly affected by overspill is red, which tends towards pink and orange in various places.
- high costs. This causes the infrequent occurrence of portions of diagrams (particularly text in stereoplots) to be very small in size, thus requiring a magnifying lens to read them. The author apologizes for any inconveniences. In most cases the stereoplots are repeated at a larger scale in the black and white diagrams.